



Universidad de Oviedo

Programa de Doctorado “Investigación en Cáncer”

**“MOLECULAR MECHANISMS INVOLVED IN THE
PATHOGENESIS OF HEAD AND NECK
PARAGANGLIOMAS”**

TESIS DOCTORAL

ANNA MERLO

23/06/2014



Universidad de Oviedo

Programa de Doctorado “Investigación en Cáncer”

**“MOLECULAR MECHANISMS INVOLVED IN THE
PATHOGENESIS OF HEAD AND NECK
PARAGANGLIOMAS”**

TESIS DOCTORAL

**ANNA MERLO
23/06/2014**



RESUMEN DEL CONTENIDO DE TESIS DOCTORAL

1.- Título de la Tesis	
Español/Otro Idioma: MECANISMOS MOLECULARES IMPLICADOS EN EL DESARROLLO DE LOS PARAGANGLIOMAS DE CABEZA Y CUELLO	Inglés: MOLECULAR MECHANISMS INVOLVED IN THE DEVELOPMENT OF HEAD AND NECK PARAGANGLIOMAS.
2.- Autor	
Nombre: ANNA MERLO	DNI/Pasaporte/NIE:
Programa de Doctorado: Investigación en Cáncer	
Órgano responsable: INSTITUTO UNIVERSITARIO DE ONCOLOGÍA	

RESUMEN (en español)

Los paragangliomas abdominales y feocromocitomas (PGLs/PCCs) y los paragangliomas de cabeza y cuello (HNPGLs) son tumores que surgen, respectivamente, de los paraganglios (PG) simpáticos y parasimpáticos. Son tumores raros, generalmente benignos con una incidencia de 1:1.000.000 de habitantes por año. La mayoría son esporádicos, pero se estima que 1/3 son hereditarios debido a mutaciones germinales en genes de predisposición. Hemos analizado la frecuencia de mutaciones en el gen de predisposición MAX en 1694 pacientes con PGL/PCC y HNPGLs. Se encontraron 16 mutaciones patogénicas en 23 pacientes con PCC, pero no en los pacientes con HNPGLs. El mecanismo patogénico implicado en el desarrollo de los HNPGLs esporádicos no es conocido. Para profundizar en las bases moleculares involucradas en el desarrollo de los HNPGLs se intentaron definir los perfiles de expresión de genes, miRNAs y HIF-1 α que distinguen los HNPGLs de los PG normales. Los resultados mostraron que los HNPGLs comparten un perfil de expresión génica común que difiere del de los PG normales y es independiente de la presencia de mutación en genes SDH o de las características clínicas de los pacientes. No se encontró enriquecimiento en los genes implicados en la respuesta hipóxica en contra de estudios publicados sobre PGL/PCCs. Se encontró que los HNPGLs tienen alteradas la expresión de genes implicados en locomoción, respuesta inmune e inflamatoria y morfogénesis. Encontramos activación de los genes relacionados con HIF-1 α solo en 3 de 17 HNPGLs esporádicos. La firma pseudohipoxica (pHx) consistía en la sobreexpresión de HIF-1 α , su miRNA diana, miR-210, y represión de ISCU1/2 (IFe-S Cluster Scaffold Protein1/2), diana de miR-210. Tras la validación de los resultados en una serie independiente de 12 HNPGL encontramos otra muestra que presentaba activación de la vía de pHx y que además tenía una disminución de los niveles de la proteína SDHB, que contiene 3 centros Fe-S en esta muestra. Este estudio desveló la existencia de una nueva vía de señalización (HIF-1 α /miRNA-210/ISCU) que podría afectar la estabilidad de la proteína SDHB por un mecanismo independiente de mutaciones en SDH. Encontramos mutaciones somáticas en el gen VHL en 2 de los 4 pHx-HNPGLs y se identificó pérdida de heterocigosidad (LOH) de VHL en uno de ellos. No se encontraron mutaciones en VHL en una serie de 29 HNPGLs esporádicos que carecían de la activación de la vía de pHx. Por lo tanto, las mutaciones somáticas del gen VHL pueden ocurrir en alrededor del 6% de HNPGLs esporádicos y podrían ser responsables de la activación de pHx. El estudio del número de copias del gen VHL reveló que el 12% de los HNPGLs esporádicos tienen delección y tienden a expresar niveles de mRNA de VHL inferiores respecto a muestras con número de copias normales. Además encontramos que el 22% de los HNPGL mostraban silenciamiento o niveles más bajos de pVHL. Esto se observó en HNPGLs con y sin mutación en SDH. A diferencia de los resultados de expresión génica hallados en pHx-HNPGLs con mutaciones en VHL, los tumores con delección del gen o expresión baja de proteína no presentaban sobre-expresión de genes de hipoxia pero, a diferencia de HNPGL con mutación en VHL, mantenían niveles normales de expresión de genes de la fosforilación oxidativa. Por lo tanto, el gen VHL, que participa en la tumorigénesis de algunos PCC y de los carcinomas renales de células claras (ccRCC), puede tener un papel importante en la patogénesis de los HNPGLs, y es la diana más frecuente de alteraciones somáticas hasta ahora encontrada en HNPGLs. Mediante el uso de líneas celulares que no expresan VHL (RCC4-) o que no expresan VHL y HIF-1 α (782_OpRV-) y tejidos de ratones knock-out para HIF-1 α , hemos puesto de manifiesto que la expresión de miR-210 requiere HIF-1 α (no HIF-2 α) y la forma nativa de VHL. Además, la expresión de miR-210 se incrementa por sobre-expresión de la mutación de VHL, p.F76del. Sin embargo, el descenso de los niveles de

Anna Merlo



UNIVERSIDAD DE OVIEDO

Vicerrectorado
de Internacionalización y Postgrado



CENTRO INTERNACIONAL
DE POSTGRADO
CAMPUS DE EXCELENCIA
INTERNACIONAL

expresión de pVHL no parece ser suficiente para activar la respuesta pHx. El estudio del perfil de expresión de miRNA en HNPGLs versus PG normales reveló que 15 miRNAs se encuentran reprimidos en los HNPGLs. Además identificamos 2 grupos de tumores con perfiles diferentes de expresión de miRNAs. La mayoría de los HNPGLs sobre-expresaban el cluster miR-379/miR-656, además de los genes DLK1 y MEG3 adyacentes al cluster de miRNA. Estos miRNA ejercen papel importante en la regulación de la diferenciación neuronal, embriogénesis y mantenimiento de las células madres.

RESUMEN (en Inglés)

Paragangliomas, pheocromocytomas (PGL/PCC) and head and neck paraganglioma (HNPGLs) are tumors arising from sympathetic and parasympathetic paraganglia (PG), respectively. Are rare, generally benign tumors, with an incidence of 1:1000000 people per year. Most of them are sporadic but about one-third are hereditary, due to a germinal mutation in susceptibility genes. We analyzed MAX mutations frequency in 1694 patients with PGL/PCC and HNPGLs. We found 23 patients with PCC that carry pathogenic mutation, but no in patients with HNPGLs. The pathogenic mechanisms involved in the development of HNPGLs are unknown. To get some insights into the molecular basis of HNPGLs, we attempted to define the gene, microRNA and HIF-1 α expression patterns that distinguish tumors from healthy PG. Results show that the HNPGLs share a common expression profile that differ from normal PGs and is independent from SDH mutation or the clinical characteristics of patients. We did not find enrichment in the hypoxia- regulated genes in contrast to previously publication on PGL/PCC. We found deregulation in genes involved in locomotion, inflammation and morphogenesis. We found activation of a canonical HIF-1 α -related gene expression signaling only in 3 of 17 HNPGLs from patients that did not harbor germline or somatic SDH mutations. The pseudohypoxic (pHx) signature consisted in the over-expression of both, HIF-1 α -target genes and the HIF-1 α -inducible miRNA, miR-210, and downregulation of the miR-210 target gene, ISCU1/2 (Fe-S cluster scaffold protein1/2). We validated the results in a independent series of 12 HNPGLs and we found another sample carrying the pHx activation and furthermore presented lower levels of SDHB protein which carry 3 Fe-S centers. Collectively, this study unveiled a putative signaling axis of HIF-1 α /microRNA- 210/ISCU in a subset HNPGLs that could impact on SDHB protein stability by a mechanism independent on SDH mutations. We found somatic VHL gene mutations in 2 of 4 of the pHx-HNPGLs and concomitant LOH of VHL in one of them. We did not find VHL mutation in a series of 29 HNPGL that lack pHx activation. Therefore, somatic VHL gene mutations may occur in about 6% of sporadic HNPGLs and may be responsible of pHx activation. The analysis of VHL copy number revealed that the 12% of HNPGLs present deletion y tent to express lower mRNA levels of VHL. Furthermore we found silencing or lower levels of pVHL in the 2% of HNPGLs. This was observed in HNPGL with or without SDH mutation. In contrast to the data of gene expression found in pHx-HNPGLs carrying VHL mutation, tumors with deletion in VHL or lower protein expression do not present over-expression of hypoxia-related genes and maintain normal levels of oxidative phosphorylation in contrary to what observed in presence of VHL mutation. So VHL that is involved in the pathogenesis of PCCs and clear cell renal cell carcinomas (ccRCC) could be important also in the tumorigenesis of HNPGLs and is the most frequent somatic alteration so far know in HNPGLs. Using a cell lines which do not express pVHL (RCC4-) or pVHL and HIF-1 α (786_OpRV-) and tissues from mice knock-out for HIF-1 α , we showed that miR-210 expression required HIF-1 α (no HIF-2 α) and native form of pVHL. Furthermore miR-210 is over-expressed in presence of the VHL mutation p.F76del; however lower levels of pVHL seem to be not sufficient to activate the pHx pathway. The analysis of the miRNA expression profile in HNPGLs versus normal PG revealed 15 miRNAs to be downregulated in HNPGL. Furthermore we found two groups of tumors with different miRNA profiles. The majority of HNPGLs over-expressed the cluster miR-379/miR-656, in addition to DLK and MEG3 that map in the same chromosome region. These miRNA are involved in the regulation of stemness, embryonic development and neuronal differentiation.

SR/A. PRESIDENTE/A DE LA COMISIÓN ACADÉMICA DEL PROGRAMA DE DOCTORADO EN Investigación en
Cáncer

INDEX

1. INTRODUCTION.....	2
1.1 The neural crest.....	2
1.2 The paraganglion system.....	3
1.2.1 The carotid body.....	5
1.2.2 Adrenal medulla.....	7
1.3 Paraganglioma and pheocromocitomas.....	7
1.4 Genetic background of HNPGLs and PGL/PCC.....	8
1.4.1 Von Hippel Lindau disease.....	9
1.4.2 Neurofibromatosis Type 1.....	10
1.4.3 Multiple Endocrine Neoplasia Type 2.....	10
1.4.4 SDH mutation.....	10
1.4.5 Transmembran protein 127 (TMEM127).....	13
1.4.6 1.4.6. Myc-associated factor X (MAX).....	13
1.4.7 Hypoxia inducible factor 2 alpha (HIF-2 α).....	13
1.4.8 1.4.8. Fumarate Hydratase (FH).....	14
1.4.9 1.4.9. Prolyl hydroxylase domain 2 and Kinesin family member 1B.....	14
1.5 Genetic testing.....	14
1.6 Hypoxia and tumorigenesis.....	15
2. OBJECTIVES.....	18
3. MATERIALS AND METHODS.....	19
3.1 Biological sample.....	20
3.2 Tumors and normal paraganglia samples.....	20
3.3 Cell culture.....	22
3.4 Chemical treatments.....	23
3.4.1 DMOG treatment.....	23
3.4.2 TTFA treatment.....	23
3.5 SiRNA treatment and transient transfection.....	24
3.6 In situ mutagenesis.....	25
3.7 Plasmid isolation.....	27
3.8 Bacterial culture medium.....	27
3.9 DNA extraction.....	28
3.10 RNA extraction.....	29
3.11 cDNA synthesis.....	30
3.12 Real Time q-PCR with Syber Green® Master Mix (Life Technologies).....	30
3.13 cDNA synthesis “RT-PCR TaqMan MicroRNA Assay Kit” (Applied Biosystem).....	31
3.14 Real Time q-PCR with TaqMan 2X Universal PCR Master Mix.....	32
3.15 Multiplex Ligation Probe-dependent Amplification.....	32
3.16 Real time q-PCR method to confirm results from MLPA.....	35

3.17 Western blot.....	36
3.18 Bisulfite Conversion and Pyrosequencing.....	36
3.18.1 Bisulfite Conversion.....	37
3.18.2 Bisulfite Pyrosequencing.....	37
3.19 Mutation analysis.....	38
3.20 Polymerase Chain reaction (PCR).....	38
3.21 Purification of PCR products.....	42
3.22 Immunocitochemistry.....	42
3.23 Immunofluorimetry.....	43
3.24 Immunohistochemistry.....	43
3.25 Microarrays and TaqMan Low-Density Array (TLDA).....	44
3.26 Vascular Density.....	44
3.27 Statistical Analysis.....	45
3.28 Microarray data analysis.....	45
3.29 Bioinformatics Analysis of Oncomine Cancer Gene Microarray Database.....	45
4. RESULTS.....	47
4.1 Expression profiles analysis of HNPGLs vs normal samples.....	48
4.2 Validation of microarrays data.....	56
4.3 Relationship between the pseudohypoxic gene signatures of HNPGLs and the <i>SDH</i> mutation status.....	57
4.4 C1-tumor analysis for somatic mutation in <i>SDH</i>	58
4.5 Vascular density of C1-C2-HNPGLs and normal paraganglia.....	58
4.6 Analysis of HIF-1 α and HIF-2 α protein expression in HNPGL.....	59
4.7 Hypoxia related miR-210 is overexpressed in C1-HNPGL.....	60
4.8 Link between hypoxia/HIF-1 α and <i>ISCU</i> and miR-210 expression.....	62
4.9 Identification of negative SDHB immunostaining in association with deregulation of HIF-1 α , miR-210, and <i>ISCU</i>	65
4.10 Validation of the data on HIF-1 α /miR-210/ <i>ISCU</i> /SDHB pathway in HNPGLs.....	68
4.11 Mecanismos of HIF-1 α upregulation in non- <i>SDH_x</i> HNPGLs.....	70
4.12 Somatic <i>VHL</i> mutations in HNPGLs in association with HIF-1 α /miR-210 gene signature.....	72
4.13 Oncomine meta-analysis reveals similarities of pHx-HNPGL with ccRCC.....	77
4.14 <i>VHL</i> mutation is involved in the activacion of the hypoxia signaling via HIF-1 α	80
4.15 pVHL loss of expression and <i>VHL</i> deletion do not activate HIF-1 α /CAIX pathway in HNPGL.....	81
4.16 HIF-1 α is required for miR-210 over-expression.....	82
4.17 <i>VHL</i> mutation F76del activates HIF-1 α /CAIX/miR-210 pathway.....	83
4.18 Loss of <i>SDH</i> does not activate the hypoxic pathway.....	86
4.19 Analysis of <i>VHL</i> gene alteration in HNPGLs.....	87
4.20 miRNA expression profiling of HNPGLs.....	93

4.21 PGL2, PGL3 and PGL7 differ from the rest of HNPGLs in the expression of genes involved in differentiation and energetic metabolism.....	96
4.22 “Cluster reverse”.....	98
5. DISCUSSION.....	100
5.1 Sporadic and <i>SDH</i> - HNPGLs show a common gene expression signature.....	101
5.2 Pseudohypoxic gene signature is driven by HIF-1 α activation in a subgroup of HNPGLs.....	101
5.3 A robust and distinct pseudohypoxic HIF-1 α -related miRNA profile defines a subset of sporadic HNPGLs.....	102
5.4 Comparison of the pseudohypoxia/hypoxia transcriptome common to all parasympathetic HNPGLs with that of sympathetic PGLs.....	107
5.5 C1-HNPGLs share a common hypoxic profile with ccRCC.....	109
5.6 Identification of somatic <i>VHL</i> genes mutation in sporadic HNPGLs with psuedohypoxic gene expression profile.....	110
5.7 Somatic <i>VHL</i> deletions are common in sporadic HNPGLs.....	113
5.8 <i>VHL</i> mutation p.F76del led to the activation of HIF1- α /CAIX/miR-210 pathway.....	115
5.9 MAX mutation analysis in HNPGLs.....	115
5.10 miRNA expression profiling of HNPGLs.....	115
5.11 Part of the cluster mir-379/mir-656 is found downregulated in PGL2, PGL3 and PGL7.....	116
5.12 miRNAs founded down-regulated in all NPGLs but not in PGL2, PGL3 and PGL7..	119
6. CONCLUSIONES.....	118
7. BIBLIOGRAPHY.....	120
8. SUPPLEMENTAL MATERIAL.....	141

1.INTRODUCTION

1. INTRODUCTION

Parangliomas and pheocromocytomas are rare tumors arising from parasympathetic and sympathetic paraganglia through the body. Paraganglia are part of the autonomic nervous system that derives from embryonic neural crest.

1.1 The neural crest.

The neural crest is an embryonic stem cell population unique to vertebrate that contribute to a wide variety of cells derivatives like sensory and autonomic ganglia of peripheral nervous system, adrenomedullary cells, cartilage and bone of the face, and pigmentation of the skin **(1)**. During its formation, in the embryonic development, neural crest undergoes an extensive morphogenetic movement (Fig.1). Initially the cells that will form neural crest are located in the neural plate border, at the edges of the neural plate which is the embryonic region that will form the central nervous system. During the neurulation, the neural plate invaginates by elevation of the edge forming a cylindrical structure called neural tube which will later form the brain and spinal cord. The premigratory neural crest cells, during the process of neural tube closure, converge toward the midline and are located in the dorsal part of the neural tube. Then, they lose the intercellular connection and undergo an epithelial to mesenchymal transition (EMT), and acquire the ability to migrate and leave the neural tube **(2, 3)**.

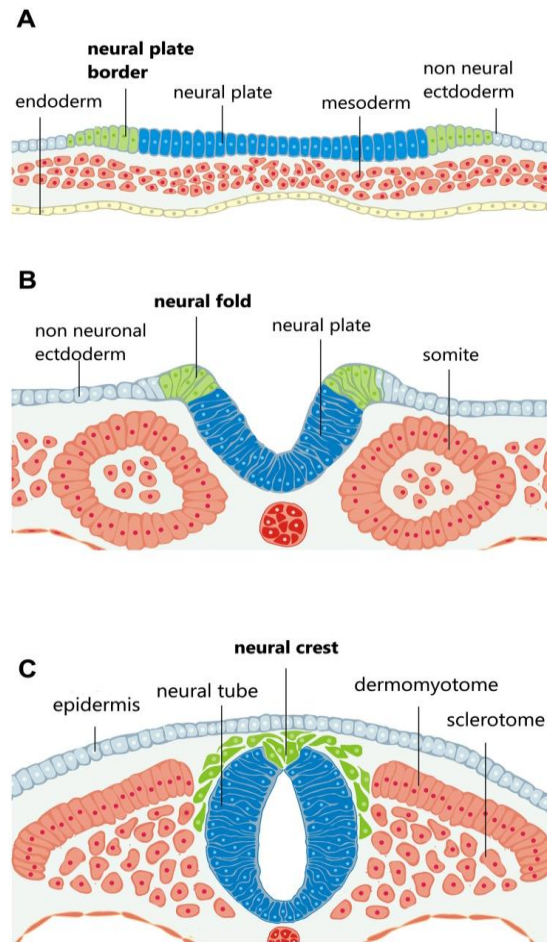


Figure 1. Neural crest formation. (A) Schematic diagram of transverse sections through embryo during neurulation. Cells that will form neural crest are located in the neural plate border (green), a territory between the neural plate and the non-neural ectoderm. (B) The neural plate invaginates, resulting in the elevation of the neural folds, which contain neural crest precursors. (C) After neural tube closure, neural crest cells lose intercellular connections and undergo an epithelial to mesenchymal transition and acquire the capacity of migrate. (Image taken from reference 1).

Neural crest cells emigrate and populate different niches throughout the embryo giving rise to different cell types and contribute to the formation of a variety of tissues and organs.

1.2 The paraganglion system.

Some of the neural crest cells migrate beyond the pre-vertebral and para-vertebral parasympathetic chains or beyond the sympathetic chains and take on glandular character resulting in the paraganglion system. Paraganglia are dispersedly diffuse from

the middle ear and the skull base to the pelvic floor and are classified as either sympathetic or parasympathetic (4).

Sympathetic paraganglia are located along the prevertebral and paravertebral sympathetic chains and sympathetic nerve branches of pelvis and retroperitoneum; they usually secrete catecholamines. The most representative paraganglia of this category is the adrenal medulla. The parasympathetic paraganglia are located almost exclusively along the cervical and thoracic branches of the glossopharyngeal and vagus nerves. The typical representative is the carotid body (Fig.2).

At birth, small patches of paraganglionic cells are located internally and centrally around major arteries and nerves; however, during the development, they are mostly obliterated. The organ of Zuckerkandl (OZ), located around the origin of the inferior mesenteric artery, is the major paraganglionic organ that secretes catecholamines in the fetal and new born period. As the OZ regress the carotid body and the adrenal medulla take over as the major paraganglionic organs (5).

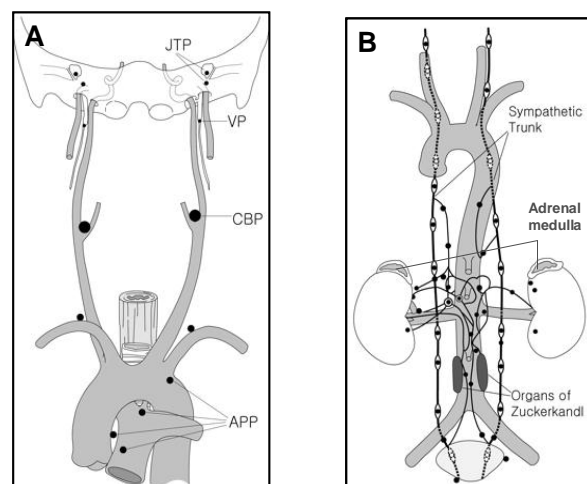


Figure 2. Anatomic distribution of paraganglia. (A) Parasympathetic paraganglia are located along the cervical and thoracic branches of the glossopharyngeal and vagus nerves. APP, aortic-pulmonary paraganglia; CBP, carotid body paraganglia; JTP, Jugulo-timpanic paraganglia; VP, vagal paraganglia. (B) Sympathetic paraganglia are located along the prevertebral and paravertebral sympathetic chains and sympathetic nerve branches of pelvis and retroperitoneum. The most important sympathetic paraganglia are the organ of Zuckerkandl and the adrenal medulla. (Image modified from reference 6).

Microscopically all paraganglia have a similar morphologic appearance characterized by two types of cells (Fig. 3):

- Glomus cells, or type 1 cells, are large and spherical shaped organized in well defined rounded nests; they are electrically excitable and sensitive to oxygen delivery, arterial oxygen and carbon dioxide levels, blood pH, reduced blood flow, inorganic phosphate and sodium cyanide (7);
- Sustencular cells, or type II cells (analogous to astrocytes), are tiny enlarged cells that encircled type 1 cells and are characterized by S-100 positive staining. They are not excitable and maintain stem cell proprieties with the ability of self-renewal and differentiation into type 1 cells and muscle cells (8).

Paraganglia are rounded by a fenestrated endothelium and a basal membrane and play an important role in maintaining the homeostasis of the organisms. They produce catecholamines and other neuroendocrine markers (9)

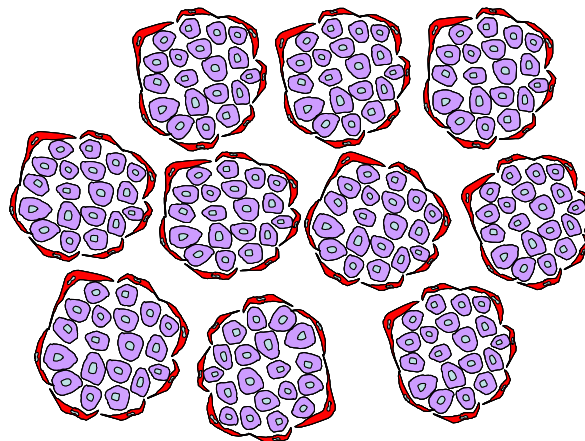


Figure 3. Representation of the parenchyma of paraganglias. Type 1 cells are in purple, while type 2 cells are in red.

1.2.1 The carotid body.

Carotid bodies are sensory receptors that detect changes in oxygen concentration in arterial blood and release sensory information to the control centre of breath in the brain. They are located in the carotid bifurcation (Fig. 4) (10). This is crucial for mammalian life and may play a life or death role in situations of acute hypoxia. The sensory complex of carotid body is formed by a branch of the glossopharyngeal nerve that innervate clusters of glomus cells that are the primary oxygen-sensing cells (11, 12, 13). The mechanisms of sensory transduction are still unclear. There are two major

hypotheses that try to explain this event: first a heme or a redox-sensitive enzyme is the oxygen sensor and a biochemical event associated with heme triggers the transduction cascade. The other hypothesis suggests that a K^+ channel protein is the primary oxygen sensor. According to this hypothesis, low oxygen level is detected by molecular sensors in the carotid body that inhibit K^+ channels in the cells membrane. Then the depolarization of the cell activates voltage-dependent- Ca^{++} channels, resulting in a Ca^{++} influx and neurotransmitters release (10). There are evidences that reactive species of oxygen (ROS) could function as signaling molecules to activate the response to hypoxia (14). Carotid body cells synthesize and store a variety of neurotransmitters (Table 1) that are released under hypoxic conditions (15, 16).

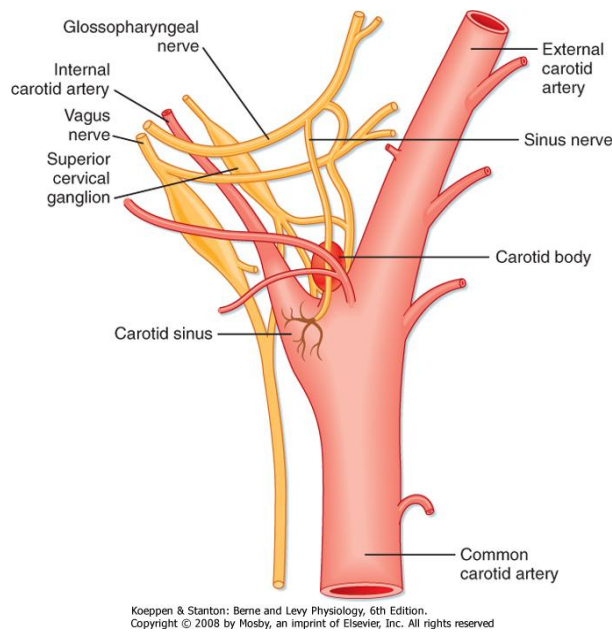


Figure 4. Representation of the carotid sinus and carotid body and their innervation (17).

Table 1. Neurotransmitters in carotid bodies cells.

Biogenic Amine	Neuropeptides	Gas Molecules
Acetylcholine	Enkephaline	Heme
Dopamine	Substance P	Oxygenase-2
Norepinephrine	Atrial Natriuretic peptide	NADPH-cytochrome c
5-Hydroxytrptamine	Endotheline	Oxidoreductse

1.2.2 Adrenal medulla.

The adrenal glands are two triangulated organs located in the inner part of the kidneys (Fig. 2) and are formed by two type of tissues: the adrenal cortex that is the exterior part of the gland, produce vital hormones like cortisol and aldosterone that regulate blood pressure and stress response and the adrenal medulla, that is the interior part of the adrenal gland.

The most abundant cells in the adrenal medulla are the chromaffin cells; so called because, if adrenal gland is fixed in a solution containing chromium salts, it takes on a brownish appearance due to oxidation of catecholamines to melanin.

In the adrenal medulla the chromaffin cells, that have differentiated from the neural crest-derived simpthoadrenal (SA) progenitor cells, acquire an endocrine phenotype and the capacity of synthesize and secrete catecholamines, furthermore these cells produce and secrete a variety of substance like neuropeptides, cytokines, enkephalines and neurotrophic factors (**18, 19**). They are also characterized by plastic proprieties as they can proliferate through life and acquire neural-like phenotype in response to neurogenic stimulation (**20, 21**). Adrenal medulla contributes to maintain body homeostasis in presence of stress signals from the environment by releasing catecholamine into the blood circulation in response to splanchnic nerve activation. Once delivered into the blood circulation, catecholamines act on the cardiovascular system, leading to appropriate adjustments of blood pressure and cardiac rhythm, and on the energy metabolism (**22**).

1.3 Paraganglioma and pheocromocitomas.

Pheochromocytomas and paragangliomas (PCC/PGL) are tumors of the autonomic nervous system that arise from chromaffin tissue in the adrenal medulla or extra adrenal ganglia along the sympathetic system many of those tumors have catecholamine hypersecretion (**23**). According to the 2004 World Health Organization classification, the term "pheochromocytoma" should only be used for adrenal tumors. Head and neck paragangliomas (HNPGs) are referred to the tumors that originate from the parasympathetic paraganglia in the cranial region (Table 2), the vast majority are non-secretory (**23, 24, 25, 26**). HNPGs are rare tumors, representing less than 0.5% of all head and neck tumors. Approximately 3% of paragangliomas occur in the head and neck area (**27**) being carotid body tumors the most common; other frequently HNPGs are vagal (Table 2) (**28, 29**). HNPGs in the nose or the paranasal sinuses,

the parotid gland, cervical sympathetic chain, larynx, thyroid gland, parathyroid gland, esophagus, or the orbit are extremely rare (30).

HNPGLs, PGL/PCC have an incidence of 2–8 per million people per year, with a peak incidence in the third to fourth decade of life (31). They are usually benign, but in rare cases they could metastasize; metastases can occur at initial diagnosis, or even 20 years later and this is not predictable by histology, The only evidence of a malignant HNPGL is the presence of local or distant metastases (i.e., PG cells in non-neuroendocrine tissue) (23, 26, 32, 33, 34). These tumors are treated by radiotherapy and/or complete resection depending on the location, extent of the tumor and the morbidity associated with treatment (35, 36).

They are associated with high morbidity and mortality secondary to mass effects, high circulating catecholamines (in the case of PGL/PCC) and surgical complications. Classical symptoms of PGL/PCC are episodic headaches, palpitations, diaphoresis, and anxiety, but they could also be asymptomatic (37). HNPGLs are space-occupying tumors that normally are not vasactive and do not secrete catecholamine. Thus, symptoms as tachycardia, hypertension and sweating attacks are not frequent (34).

Table 2. HNPGL main location.

Carotid body	Largely asymptomatic except for a mobile, non tender growing lateral neck mass. Mass effect may cause hoarseness, dysphagia, vertigo and/or paresis resulting from cranial nerve compression.
Jugular bulb	Jugular tumors grows in the jugular foramen where the jugular vein and several important nerves exit the skull.
Middle ear cavity	Glomus tympanicum tumors arise with the tympanic branch of the glossopharyngeal nerve. Jugular and tympanic glomus have similar symptoms that are pulsates tinnitus, conduction earring loss, aural pain, vertigo and hoarseness. When these tumors cannot be differentiated, they are referred to as jugulotympanic paragangliomas.
Cervical vagus nerve	Typical slow growing mass in the peripharyngeal space.

1.4 Genetic background of HNPGLs and PGL/PCC.

Although HNPGL and PGL/PCC are rare tumors they are more commonly associated with an inherited mutation than any other cancer type (23). Various studies on population have shown that about 1/3 of patients with apparently sporadic PCC/PGL

carry a germline mutation in a known susceptibility gene (38–40). However this number could rise to 79% of cases if we consider the presence of family history and it can be 54% in the case of HNPGLs (41, 42).

In the last years the number of genes that predispose to PCC/PGLs and HNPGLs has raise exponentially also thanks to the new techniques of massive sequenciation, being the tumors with more genes of predisposition known to the date. Furthermore there are a certain percentage of clearly familial PCC/PGLs and HNPGLs that do not seem to be associated with any of the germline mutations described so it is possible that other genes may be involved in the development of these tumors (43)

To the date 12 genes of susceptibility are known. Three of them are associated to well known syndromes as: *VHL* for the Von Hippel Lindau disease, *NF1* for the Neurofibromatosis Type 1 and *RET* for the Multiple Endocrine Neoplasia Type 2. The *Succinate Dehydrogenase (SDH)* complex subunit genes (*SDHA*, *SDHB*, *SDHC*, *SDHD*); one of the SDH complex cofactors, *SDHAF2*; *TMEM127*, *MAX*, *KIF1B*, *HIF-2 α* and two recently recognized susceptibility genes *FH* and *PHD2* are involved in PGL development.

1.4.1 Von Hippel Lindau disease.

VHL is a tumor suppressor gene that encodes for a protein involved in the regulation of the hypoxia-inducible factors (*HIF-1 α* and *HIF-2 α*). In normoxic conditions pVHL binds a residue of hydroxyproline on the α subunity of HIFs targeting it to ubiquitization and subsequent degradation in the proteasoma (44). In hypoxic conditions the proline residue of HIF-1 α can not be hydroxylated so pVHL can not bind it leading to a stabilization of HIF-1 α that can bind HIF-1 β subunity and activate the transcripcion of hypoxia inducible genes (45).

Von Hippel-Lindau disease (VHL) is a syndrome characterized by a variety of benign and malignant tumors including PCC (10–20%), hemangioblastomas of the central nervous system, renal cysts, clear cell renal cell carcinoma (ccRCC), pancreatic cysts, pancreatic neuroendocrine tumors, endolymphatic sac tumors and epididymal cystadenomas (46).

Type 1 VHL disease is usually associated with *VHL* truncating mutations or exon deletions and show lower penetrance for PCC and a higher penetrance for ccRCC. Type 2 VHL disease is frequently associated with missense mutations in the *VHL* gene

and higher penetrance for PCC. It has been shown that mutations around the site of the VHL-HIF protein interaction tend to lead to ccRCC development, whereas mutations in other parts of the VHL protein tend to lead to PCC development (47, 48). This suggests that PCC formation is independent of HIF regulation (23). Patient with VHL syndrome can develop HNPGLs in rare cases (0,5%) (34).

1.4.2 Neurofibromatosis Type 1.

NF1 encodes for neurofibromin that is a GTPase protein involved in the inactivation of Ras and the inhibition of the MAPK signaling pathway. *NF1* mutations cause the activation of Ras and hence, the downstream MAPK, PI3K and mTOR pathways (49, 50). The estimated rate of PCC in *NF1* is 5–7%, whereas HNPGLs are extremely rare.

1.4.3 Multiple Endocrine Neoplasia Type 2.

RET is a proto-oncogene that encodes for a transmembrane tyrosine kinase protein. When ligand binds to the RET receptor, or there is an activating mutation, a cell signaling cascade is triggered through the PI3 kinase pathway to regulate cell proliferation and apoptosis (51). Multiple Endocrine Neoplasia Type 2 (MEN 2) is an autosomal dominant syndrome. The risk of PCC in MEN 2 syndrome is associated with specific *RET* mutations. HNPGLs have been very rarely described (40).

1.4.4 SDH mutation.

SDH, also known as complex II, is an enzymatic complex involved in Krebs cycle and in the respiratory chain in the mitochondria, associates the oxidation of succinate to fumarate with an electron transport to ubiquinone as the final acceptor (Fig. 5). It is composed by 4 subunits, SDHD and SDHC that anchor the complex to the mitochondrial inner membrane, SDHA and SDHB that are the active core of the complex located in the mitochondrial matrix. The SDHA subunit has a FAD molecule covalently bonded. (52).

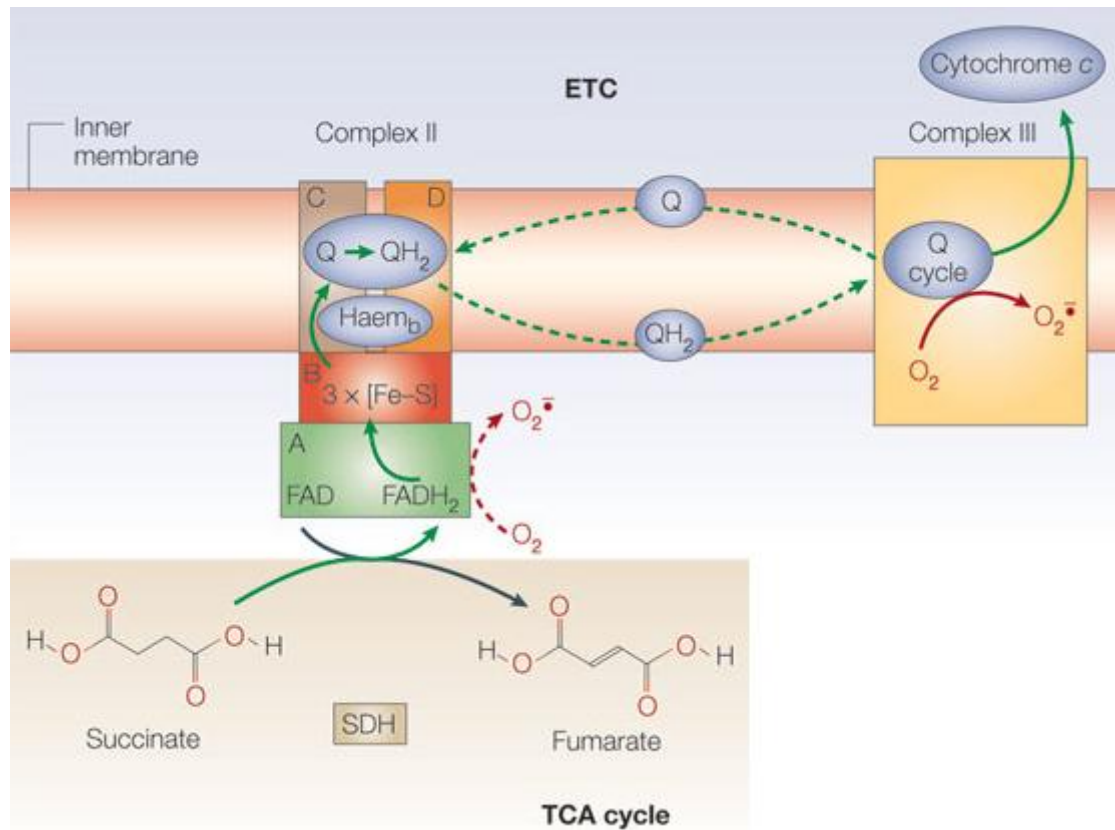


Figure 5. Representation of SDH complex. The enzymatic complex associates the oxidation of succinate to fumarate with the transport of an electron (represented by green arrows) to a final acceptor ubiquinone. During succinate oxidation to fumarate by SDHA, a two-electron reduction of FAD to FADH₂ occurs. Electrons are transferred through the iron–sulphur centres on SDHB and to ubiquinone (Q) bound to SDHC and SDHD in the mitochondrial inner membrane, reducing it to ubiquinol (QH₂). Quinones are mobile redox centres of the ETC (dotted green arrows). Ubiquinol transfers its electrons through complex III, in a mechanism called the Q-cycle, to cytochrome c. (Image modified from reference 53).

Mutations in any one of the subunits can lead to the development of PCC/PGL or HNPGL.

- *SDHD* mutations give rise to PGL syndrome type 1, that is the most common PGL (24, 30, 40), the gene is formed by four exons and maps on chromosome 11q23 (54, 55). It encodes for an anchor subunit with a ubiquinone binding site to which the electrons are transferred from the iron sulfur clusters within the SDHB subunit (23). About 91-98% of patients with SDHD germline mutation are at high risk for the development of HNPGLs (42, 4). Typically they present multiple HNPGLs (60% to 79% of the patient) that could arise at the same time or even many years later of the first tumor. There is also a risk of developing PCCs and extra-adrenal PGLs (16% to 21%) (4, 42, 40, 56). These mutations

are inherited in an autosomal dominant manner and disease susceptibility occurs when the mutation is inherited from the father (42, 57).

- *SDHAF2* mutations cause PGL syndrome type 2 that was the first PGL syndrome to be described in 1982 (58), although the gene was identified in 2009 (59). *SDHAF2* maps on chromosome 11q13 and encodes for a matrix protein involved in the flavination of *SDHA* (59). *SDHAF2* mutations are very rare, only a Spanish family and a Dutch family that carry *SDHAF2* mutation have been described to the date and are associated with the occurrence of multiple HNPGLs, but not extra-adrenal PGLs or PCCs. Transmission occurs exclusively via the paternal line; penetrance has been described to be very high in both the Dutch as well as the Spanish family (88% to 100%), and the average age at diagnosis is 33 to 34 years (59, 60, 61).
- *SDHC* mutations are cause of PGL syndrome type 3. The gene has 6 exons, maps on chromosome 1q23.3 and encodes for an anchor subunit (4). Mutations in this subunit are less frequent than *SDHD* and *SDHB* mutations and occur in only 0-6.6% of PCC/PGL patients (42, 62-65). The average age at diagnosis is higher than for the other PGLs (range: 38-46 years) (42, 65). In contrast to patients with PGL1 and PGL4, *SDHC* mutation give rise to mostly benign, single HNPGLs (35) Multiple HNPGLs are found in 19% to 31% of patients and PCCs, extra-adrenal PGLs, malignant PGLs are very rare (65, 42, 40, 66, 67).
- *SDHB* mutations are involved in the PGL syndrome type 4 described for the first time in 2001 (68). The gene contains 8 exons, maps on chromosome 1p36.1–p35 and encodes for a subunit with 3 iron sulfur centers.

Patients with *SDHB* mutation mostly develop extra-adrenal PGLs (52-84%) and PCCs (18-28%), while HNPGLs are less frequent (27-31%) (57, 40, 4, 69). The average age at diagnosis is reported to be between 30 and 37 years (57, 42, 4) *SDHB* mutations are inherited with an autosomal dominant manner. Tumor penetrance is somewhat lower than that seen in *SDHD* mutation carriers. Bennett et al (70) estimated the tumor penetrance in *SDHB* mutation carriers to be 29% at age 30 rising to 45% at age 40. The risk of malignant PGLs is higher in *SDHB* than in *SDHD* mutation carriers with an incidence of 17% (71). Recently it has been shown that p16INK4A promoter was heavily methylated in extra-adrenal PGLs with *SDHB* mutation and malignancy (72). *SDHB* mutations are associated to other type of cancers like gastrointestinal stromal tumors (GIST), papillary thyroid cancer, neuroblastoma and various types of renal cell carcinoma, including clear cell and papillary RCC (57, 24, 73-76).

- *SDHA* gene contains 13 exons, maps on chromosome 5p15 and encodes for a flavoprotein and the major catalytic subunit of SDH complex. The Leigh's syndrome is associated with *SDHA* biallelic mutation (**77, 78**). Germline *SDHA* mutations have been founded only in few cases of PCC/PGL (**79, 80**). Moreover it is quite difficult to analyze *SDHA* mutations due to the presence of two pseudogenes on chromosome 3 and 5. Only two cases of HNPGL with *SDHA* mutation have been described to date (**80**).

1.4.5 Transmembran protein 127 (*TMEM127*).

TMEM127 mutation was first described in 2010 in a patient with familial PCC. The gene is located in chromosome region 2q11 and encodes for a transmembrane protein that is probably involved in the mTORC1 signaling pathway (**81**). *TMEM127* mutations are rare and are mostly associated with PCCs. Only two cases of HNPGLs patients carrying *TMEM127* mutations have been described to date (**82**).

1.4.6. Myc-associated factor X (*MAX*).

MAX mutations were identified in association with PCC/PGL (**83**), the gene is formed by 5 exons and is located in chromosome 14q23 and codifies a protein which heterodimerizes with *MYC* to act as a transcription factor for genes involved in cellular proliferation, differentiation and apoptosis.

1.4.7 Hypoxia inducible factor 2 alpha (*HIF-2 α*).

HIF-2 α mutations were recently identified in PCC/PGLs (**85, 86, 87, 88, 89**). The gene is constituted by 16 exons and is located in chromosome 2p21 and codifies for the subunit 2 alpha HIF complex. Mutations predominately occurs in proximity of the HIF-2 α -stabilizing prolyl sites and led to stabilization of the protein (DAHIA 2014). Intriguingly, despite the somatic nature of the pheochromocytoma and paraganglioma mutations, a substantial proportion of patients also developed somatostatinomas that carried the same *HIF2A* variant (**89, 90**). Approximately 50% of the patients with *HIF2A*-mutant tumours developed early onset or congenital polycythemia (**85, 87, 90**).

1.4.8. Fumarate Hydratase (FH).

FH encodes for an enzymatic protein involved in the Krebs cycle and catalyzes the formation of L-malate from fumarate. Recently *FH* mutations were found in patients with PCC (**91**).

1.4.9. Prolyl hydroxylase domain 2 (PHD2) and Kinesin family member 1B (KIF1B).

PHD2 encodes for the main oxygen sensor responsible of HIF-1 α regulation. Germline mutations in this gene have been described in patients with familial erythrocytosis and recurrent paraganglioma (**84**). *KIF1B* functions as a tumor suppressor that is needed for apoptosis. *KIF1B* mutations were described in two patients with PCCs (**92**). Currently, it is too early to predict the role *KIF1B*, *PHD2* mutations in the pathogenesis of hereditary paraganglial tumors.

1.5. Genetic testing

The genetic screening of all the genes described above in patients with PCC/PGLs and HNPGLs would be unaffordable due to the high cost of Sanger sequencing. Based on the known genotype-phenotype correlation, there are several recommendation for genetic screening. In patients with PCC screening for mutations in *SDHB*, *SDHD*, *VHL*, and *RET* are recommended (**38, 93**).

For HNPGLs Carsten et al recommended testing first *SDHD*, followed by *SDHB* and *SDHC* in the cases of patients with multiple HNPLs; or solitary HNPGLs but positive family history; or in the case of concomitant HNPGLs and PCC. They recommend testing first *SDHB* followed by *SDHD* and *SDHC* in patients with solitary HNPGL and negative family history or in case of malignant HNPGLs.

A routine screening of patients with HNPGLs for mutations of the genes *SDHAF2*, *VHL*, *TMEM127*, *SDHA*, *RET*, *NF1*, *MAX*, *KIF1B*, and *PHD2* does not seem to be useful, as mutations in these genes are very rare (**43**). Nevertheless, next generation sequencing will offer the potential of faster and less expensive testing of multiple genes simultaneously in the very next future so it is probably that platforms to sequence all the genes that predispose to PCC/PGL and HNPGLs will be developed very soon at low cost allowing extensive genetic screening for all the patient.

1.6. Hypoxia and tumorigenesis

The molecular mechanisms involved in the tumorigenesis of PGLs are poorly understood. The most accepted hypothesis suggest HIF-1 may play a central role activating the hypoxia signaling pathway at least in the case of *SDH* and *VHL* mutations (94, 95). HIF-1 is a heterodimer formed by the HIF-1 β constitutively expressed subunit and the HIF-1 α subunit which is regulated in an oxygen-dependent manner. In the presence of oxygen, prolyl hydroxylases, PHDs, hydroxylate two prolines of HIF-1 α and convert the tricarboxylic acid cycle intermediate 2-oxoglutarate to succinate (96). Hydroxylated HIF-1 α is targeted by VHL to ubiquitination and degradation in the proteasoma. Under hypoxic conditions, PHDs activity is diminished due to the oxygen-limiting conditions thereby allowing HIF-1 α stabilization and transcriptional activation of genes with adaptive functions.

It has been shown that PHDs may be regulated not only by oxygen, but also by succinate-fumarate reactive oxygen species (ROS), that are generated in the mitochondrial electron transport chain. These factors may lead to “pseudohypoxic” stabilization of HIF-1 α (97-99) (Fig 6). As *SDH* mutations have been shown to result in the accumulation of succinate and ROS, the most accepted hypothesis is that the “pseudohypoxic” HIF-1 α stabilization drives PGLs development. HIF-1 α induces expression of a broad range of target genes, including those that stimulate cell proliferation and angiogenesis that may contribute to tumorigenesis (Fig. 6). MicroRNAs play also an important role in regulating downstream signaling of the HIF-1 α pathway (100). MicroRNAs are short non-coding RNAs that post-transcriptionally control gene expression through translational repression and/or mRNA degradation by binding to the 3' UTRs of genes. There are recent evidences that HIF-1 α induces the expression of several biologically interesting microRNAs such as miR-23, miR-24, miR-26, miR-210, and miR-373 being miR-210 the most consistently and robustly induced microRNA under hypoxia (101). Interestingly, upregulation of miR-210 has been recently shown to modulate mitochondrial function and activate the generation of reactive ROS via downregulation of ISCU1/2 (iron-sulfur cluster scaffold homolog) (102) However the role of hypoxia-related miRNAs in the pathogenesis of PGLs is presently unknown.

Recent studies support the role of hypoxia in the pathogenesis of PGLs in presence of mutation in *SDH* or *VHL*, however these study are based on global expression profile that do not include healthy control (102, 103, 104); therefore, a possibility remains that

these data could reflect differences in the magnitude of a hypoxic response gene profile common to all PGLs and PCCs independently on the genetic defects.

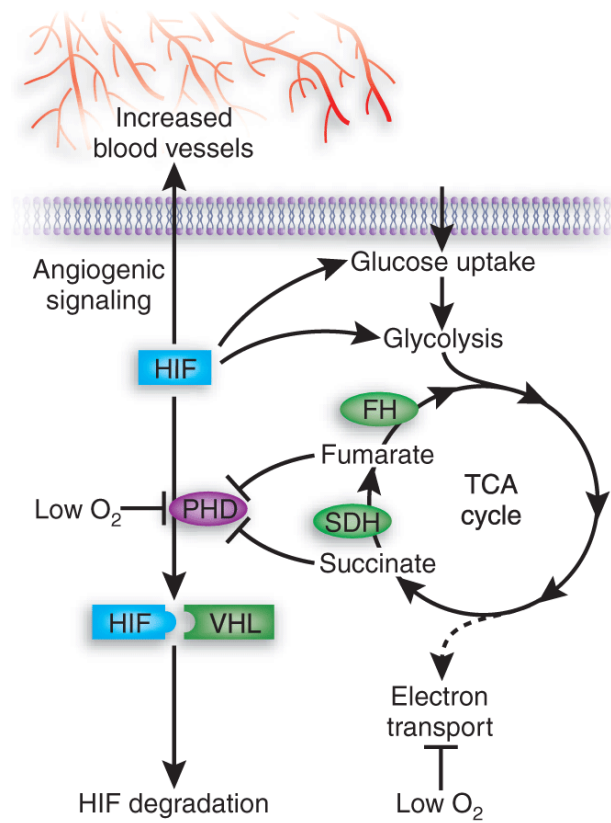


Figure 6. HIF stabilization. In hypoxic conditions, PHD is inhibited and HIF is stabilized. Dysfunction of fumarate hydratase (FH) and succinate dehydrogenase (SDH), enzymes of the tricarboxylic acid (TCA) cycle, led to HIF stabilization. (Image taken from reference 105).

2.OBJECTIVES

Objectives

The global purpose of this work was to understand the molecular mechanisms involved in the development of HNPGLS. The particular objective were:

1. Identificate the gene and miRNA profiles deregulated in HNPGLs incomparison with normal paraganglias.
2. Identificate de molecuar markers of sporadic and familial HNPGLs.
3. Unveil the role of the intracelular signaling pathway activated by hypoxia in the pathogenesis of sporadic and familial HNPGLs.
4. Identificate genic alteration involved in the development of sporadic HNPGLs.

5.

3. MATERIALS AND METHODS

3. Materials and Methods

3.1 Biological sample

The studies performed in this work were realized on human tissues, derived from head and neck paragangliomas (HNPGs) and normal paraganglia and cells lines described below.

- HeLa cells derived from cervix adenocarcinoma;
- SCC38 and SCC42B cells head and neck squamous cell carcinoma;
- RCC4⁻ and RCC4⁺ cells were kindly provided by Manuel O. de Landazuri, RCC4⁻ cells derived from clear cell renal cell carcinoma (ccRCC) carrying loss of *VHL* and RCC4⁺ cells derived from RCC4⁻ cells stably transfected with a plasmid encoding wild type *VHL*;
- 786_OpRV⁻ and 786_OpRV-*VHL* were kindly provided Manuel O. de Landazuri, 786_OpRV-*VHL* derived from renal carcinoma lacking hypoxia inducible factor (HIF)-1 α and *VHL*, 786_OpRV-*VHL* derived from OpRV⁻ stably transfected with plasmid encoding wild type *VHL*.

3.2 Tumors and normal paraganglia samples

Tumor samples were obtained from 52 patients with parasympathetic HNPGs, diagnosed and treated between 1996 and 2014 in the Hospital Central de Asturias, Oviedo, Hospital Gregorio Marañón, Madrid and Hospital de Sant Pau, Barcelona, Spain. Three normal carotid bodies were obtained from organ donors. Carotid artery bifurcations were excised from organ donors and placed in RNAlater (Ambion). Each carotid body was then carefully dissected from the artery and cleaned of surrounding connective tissue under a magnifying glass. The quality of the tissues for subsequent RNA-based studies was always assured by histological analysis. Informed consent was obtained from all patients and the legal representatives of organ donors. For RNA-DNA based studies, fragments were obtained from the core of the tumor. Both, normal carotid body and tumor specimens were snap-frozen at time of surgical resection and stored at -80 °C in RNAlater (Ambion) until processed. Clinical data are summarized in table 3.

Table 3. Patient's characteristics.

sample	gender	Age ¹	Localization ²	Gene ³ mutated	mutation	Somatic <i>VHL</i> CNV ⁴	Somatic <i>VHL</i> Mutation ⁵	<i>VHL</i> mRNA ⁶	<i>VHL</i> Protein ⁷
PGL5	F	50	T	<i>SDHD</i>	c.367G>A	del <i>VHL</i>	none	3.92	UN
PGL71	M	44	CB	<i>SDHD</i>	c.337_340delGACT	del <i>VHL</i>	none	6.06	UN
PGL58	M	39	CB	<i>SDHD</i>	c.191_del192delTC	del exon2	none	5.65	NEG
PGL81	F	39	J	<i>SDHB</i>	c.201-?_286+?del	del <i>VHL</i>	none	0.73	POS
PGL86	F	54	J	<i>SDHB</i>	c.79C>T	del exon2	none	UN	UN
PGL12	F	29	CB	<i>SDHD</i>	c.386dupT	none	none	0.73	NEG
PGL7	F	55	CB	<i>SDHB</i>	c.725G>A	none	none	6.84	UN
PGL14	F	25	CB	<i>SDHD</i>	c.33C>A	none	none	4.66	POS
PGL32	F	39	CB	<i>SDHD</i>	c.386dupT	none	none	0.61	NEG
PGL54	M	44	CB	<i>SDHD</i>	c.191_192delTC	del <i>VHL</i>	none	1.34	NEG
PGL60	F	40	V	<i>SDHD</i>	c.383InsT	none	none	UN	NEG
PGL63	M	36	CB	<i>SDHD</i>	c.190-192dupTC	none	none	19.49	NEG
PGL68	M	25	CB	<i>SDHD</i>	c.337-340delGACT	none	none	3.62	NEG
PGL61	M	45	CB	<i>SDHD</i>	c.374delA	none	none	1.56	POS
PGL55	F	45	J	<i>SDHB</i>	c.544_550delGGGCTCT	none	none	4.23	POS
PGL87	M	44	J	<i>SDHB</i>	c.166_170delCCTCA	none	none	0.82	POS
PGL38	F	27	T	<i>SDHC</i>	c.21-?_77+?del	none	none	3.29	NEG
PGL46	F	41	V	<i>SDHB</i>	c.761C>A	none	none	UN	NEG
PGL51	M	29	AR	<i>SDHB</i>	c.-151-?_72+?del	none	none	0.87	NEG
PGL75	F	35	CB	<i>SDHD</i>	UN	none	none	UN	NEG
PGL56	F	36	CB	<i>SDHD</i>	c.129G>A	none	none	UN	POS
PGL57	F	36	CB	<i>SDHD</i>	c.129G>A	none	none	UN	NEG
PGL74	F	36	CB	<i>SDHD</i>	c.129G>A	none	none	UN	NEG
PGL83	M	53	CB	UN	UN	none	none	UN	NEG
PGL95	M	43	CB	<i>SDHD</i>	c.50G>T pR17L	UN	none	UN	NEG
PGL96	M	43	J	<i>SDHD</i>	c.50G>T pR17L	UN	none	UN	UN
PGL100	F	42	J	none	-	UN	none	UN	UN
PGL2	F	79	T	none	-	UN	none	UN	UN
PGL3	F	53	J	none	-	del <i>VHL</i>	c.227_229delTCT p.F76del	0.32	UN
PGL23	M	43	CB	none	-	none	c.482G>GA p.R161Q	UN	POS
PGL47	M	41	V	none	-	none	c.551C>CT p.L184L	0.37	POS
PGL6	M	39	JT	none	-	del exon1	none	0.15	UN
PGL9	F	UN	V	none	-	del exon1	none	3.32	UN
PGL19	F	66	J	none	-	del exon 1	none	1.38	POS
PGL21	M	40	CB	none	-	del exon1+3	none	1.95	POS
PGL35	F	61	JT	none	-	del exon1	none	4.66	NV
PGL52	M	29	JT	none	-	del exon1+3	none	0.76	NEG
PGL84	F	33	J	none	-	del exon 2	none	UN	UN
PGL91	F	31	JT	none	-	del <i>VHL</i>	none	UN	UN
PGL49	F	62	CB	none	-	del exon 1	none	0.64	NEG

PGL88	F	57	J	none	-	none	none	UN	UN
PGL22	F	32	J	none	-	none	none	21.78	NEG
PGL44	F	56	JT	none	-	none	none	0.43	NEG
PGL66	F	34	J	none	-	none	none	8.59	UN
PGL17	M	30	J	none	-	none	none	25.19	UN
PGL18	F	UN	CB	none	-	none	none	5.23	UN
PGL24	F	UN	JT	none	-	none	none	UN	UN
PGL25	F	57	V	none	-	none	none	0.48	UN
PGL27	F	51	J	none	-	none	none	1.08	NEG
PGL29	M	41	J	none	-	none	none	1.89	NEG
PGL36	F	60	J	none	-	none	none	3.23	NEG
PGL62	F	45	J	none	-	none	none	27.47	UN
PGL76	F	UN	UN	none	-	none	none	UN	UN
PGL77	M	30	CB	none	-	none	none	1.05	POS
PGL79	M	37	JT	none	-	none	none	UN	NV
PGL80	M	42	J	none	-	none	none	UN	UN
PGL82	F	55	J	none	-	none	none	26.55	UN
PGL89	F	52	CB	none	-	none	none	2.28	NEG
PGL90	M	49	J	none	-	none	none	UN	UN
PGL93	F	75	CB	none	-	none	none	0.54	NEG
PGL94	F	63	J	none	-	none	none	UN	NV
PGL97	F	50	UN	none	-	none	none	UN	POS
PGL98	F	65	T	none	-	UN	none	UN	POS
PGL99	F	53	CB	none	-	UN	none	UN	UN

3.3 Cell culture

PGL38 and PGL33 cell lines were obtained from two HNPGLs carrying *SDHC* mutation (*SDHC* del EX2) or without *SDH* mutation respectively. Both tumors arised from tympanic glomus. Tumor tissues were enzymatically dissociated in PBS (OXIOD) containing 0.6 mg/ml Bovine Serum Albumin (Sigma), 50 µM CaCl₂, 0.05 µg/ml DNaseI (Applichem) 1 mg/ml Collagenase Type IV (Serva) and 0.3 mg/ml Trypsin (Invitrogen) for 30 min at 37°C, with shaking and mechanic disruption every 10 min. After the enzymatic treatment, dissociated cells were centrifuged for 5 min at 200 x *g*. Afterward, the pellet was resuspended in Quantum 263 medium (PAA Laboratories) supplemented with 10% Fetal Bovine Serum Gold (PAA Laboratories), 100 IU Penicillin (PAA Laboratories), 100 ug/ml Streptomycin (PAA Laboratories), and 2mM L-glutamine (PAA Laboratories). Cells were maintained at 1% oxygen in a hypoxic incubator (HERAcell 150) that maintained a constant environment (5% CO₂ and 1% O₂ balanced with N₂).

The established human head and neck squamous cell carcinoma-derived cell line SCC38 and SCC42B has been previously characterized (**106, 107**). SCC38, SCC42B and HeLa cells were grown in Dulbecco's modified Eagle's medium (DMEM) supplemented with 10% Fetal Bovine Serum Gold (PAA), 100 IU Penicillin (PAA Laboratories), 100 ug/ml Streptomycin (PAA Laboratories), 2mM L-Glutamine (PAA Laboratories), 20 mM Hepes Buffer (PAA Laboratories), 1X MEM NEAA (non-essential aminoacid) (PAA Laboratories).

786_0pRV-VHL/- and RCC4+/- cell lines were cultured in Roswell Park Memorial Institute medium (RPMI) (GIBCO®) supplemented with 10% Fetal Bovine Serum Gold (PAA Laboratories), 100 IU Penicillin (PAA Laboratories), 100ug/ml Streptomycin (PAA Laboratories) and 1 µg/mL Geneticin® (GIBCO®). Cells were routinely cultured in 95% air, 5% CO₂ (normoxic conditions) at 37°C. For hypoxic treatments, cells at 70–80% confluence were either exposed to normoxia or placed in a hypoxic incubator (HERAcell 150) at 1% O₂ for 24 or 48 hours.

3.4 Chemical treatments

3.4.1 DMOG treatment

To mimic hypoxic condition different chemical agents can be used. Dimethyloxaloyglycine (DMOG) is an inhibitor of prolyl hydroxylase (PHD) and asparaginyl hydroxylase FIH-1 (Factor inhibiting HIF, FIH) and it has been observed to upregulate HIF-1α. A stock solution of DMOG (kindly prepared by..., Sevilla) 500 mM was prepared by adding 90 mg of DMOG in 500 µL of Dimethyl sulfoxide (DMSO) (Sigma). Cells were cultured in a 6 well plate and incubated at 37°C in normoxic condition until they reach the 80% of confluency. Cells were then treated with DMOG at 1mM final concentration. Control cells were treated with DMSO to check the possible effect of this solvent on cell survival. Protein levels of HIF-1α and CaIX mRNA levels were analyzed to confirm DMOG induced activation of HIF-1α pathway.

3.4.2 TTFA treatment

Thenoyltrifluoroacetone, C₈H₅F₃O₂S, (TTFA) (Sigma) is an inhibitor of the Complex II (SDH) of the respiratory chain in the mitochondria. 786_OpRV-VHL /- and RCC4+/- cells at 80% confluence were treated with TTFA at final concentration of 500 µM for 24 hours. Control cells were treated with DMSO.

3.5 SiRNA treatment and transient transfection

Pools of three to five target-specific siRNAs, *VHL* siRNA (Santa Cruz Biotechnology), *HIF-1 α* siRNA (Santa Cruz Biotechnology) were used to knockdown *VHL* or *HIF-1 α* expression respectively. siCONTROL Nontargeting pool (Dharmacon Research, Lafayette, CO, USA) were used as transfection control. siRNAs were transfected using Lipofecamine 2000 (Invitrogen, Life Technologies™) following manufacture's instruction. Briefly, 250.000 cells were cultured in a 6 well plate and grown overnight at 37°C in normoxic condition in DMEM without antibiotic. Next day 100 pmol siRNA or 4 ug of plasmid DNA (Figure 1) was diluted in 250 μ L of Opti-MEM®I Reduced Serum medium (GIBCO®, Life Technologies™). In another tube, 10 μ L of Lipofectamine 2000 was diluted in 250 μ L of Opti-MEM I Reduced Serum medium and incubated for 5 min at room temperature. Then the diluted siRNA was combined with the diluted Lipofectamine 2000, mixed gently and incubated for 20 min at room temperature. 500 μ L of the mix were added to each well containing cells. After 5 hours of transfection, medium without antibiotic was replaced. Inhibition of the target genes were confirmed by real time q-PCR 48–72 h after transfection.

3.6 In situ mutagenesis

This protocol was realized with GENEART® Site-Direct Mutagenesis System (Invitrogen, Life Biotechnologies™) following manufacture's instruction to obtain two plasmids which carry the two *VHL* mutations found in PGL3 and PGL23 (one mutation each).

Briefly, first of all specific primers were designed as follows:

- Both primers (forward and reverse) contained the desired mutation ;
- The mutation site was located centrally on both primers;
- Both primers were of 35 to 45 nt length, not including the mutation site.
- Oligonucleotides were purified by HPLC to increase the mutagenesis efficiency.

The *VHL* mutation found in PGL3 was c227-229 delTCT, primers designed for this mutation were:

- PGL3mutFW 5'-CCTCCCAGGTCAGCAATCGCAGTCCGC-3'
- PGL3mutRV 5'-GCGGACTGCGATTGCATATGACCTGGGAGG-3'

The *VHL* mutation founded in PGL23 was c482 G>A, primers deigned for this mutation were:

- PGL23mutFW 5'-GTATACTCTGAAAGAGCTATGCCTCCAGGTTGTCCG-3'
- PGL23mutRV 5'-ACAACCTGGAGGCATTGCTCTTTCAGAGTATAC-3'

For each mutation the following reactions were performed using the HA-VHL-CDNA 3.1 (see Fig 1).

PCR Reaction

1X Accurime™ *Pfx* Reaction mix
1X Enhancer
0.3 µM Primer mix
20 ng Plasmid DNA
4U DNA Methylase
1X SAM
1U AccuPrime™ *Pfx*
PCR water to 50 µL

PCR Programm

Step 1. 37°C for 20 min
Step 2. 94°C for 2 min
Step 3. 94 °C for 20 s
Step 4. 57°C for 30 s
Step 5. 68°C for 2min and 30 s } 18 cycles
Step 6. 68 °C for 5 min
Step 7. 4°C forever

After reaction 5 µL of product were analyzed in a 0.8% agarose gel and then the Recombinaion Reaction was performed.

Recombination Reaction

1X Reaction Buffer
10 µL PCR water
4 µL PCR sample
1X Enzymer mix

Reaction was mixed well and incubated at room temperature for 10 min, then was stopped by adding 25mM EDTA and store on ice; trasformation was immediatly performed.

Trasformation into DH5 α TM-T1^R *E.coli*

50 μ L of DH5 α TM-T1^R *E.coli* was placed on ice for approximatey 5-7 min. 2 μ L of the Recombination Reaction was added to the bacterias and mixed by tapping gently. Vials was covered with ice and incubated for 12 min. The remaining Recombination Reaction was stored at -20°C. Then was incubated at 42°C for 30 s in a water bath then was immediatly placed on ice (covered completely) for 2 min. The vial was removed from ice and 250 μ L pre-warmed SOC (see 2.16) were added in sterile condition and incubed 1 h at 37°C at 225 rpm in a shaking incubator (Trasformation Reaction). During this time 5 plates with LA with Ampicillin (50 μ g/mL) (see 2.8) were warmed in an incubator at 37°C. The Trasformation Reaction was diluyed 1:10 in 100 μ L of SOC and transfered in the pre-warmed LA plate. The remaing reaction was stored at 4°C. Plates were inverted and incubated at 37°C for 16-20h. 10 colonies for mutation were selected; plasmid was isolated by Wizard[®] Plus SV Minipreps DNA Purification System (Promega) and analyzed by sequenciation.

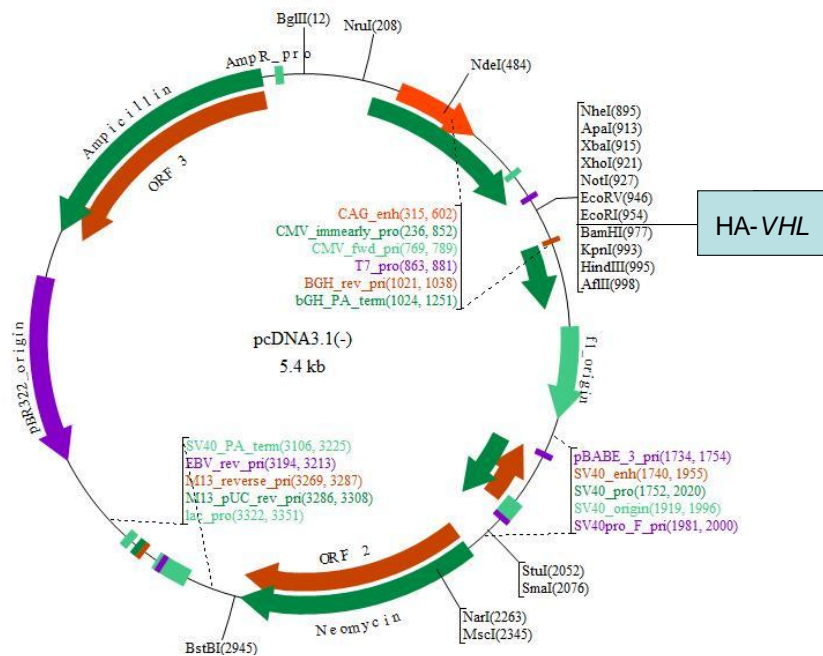


Figure 1. HA-VHL-CDNA 3.1 map. This plamid was used as mold for the in situ mutagenesis. It confers procariete Ampicillin resistance and eukariote Neomycin resistance.

3.7 Plasmid isolation

Plasmids were purified from bacteria using the kit Wizard[®] Plus SV Minipreps DNA Purification System (Promega) following manufacture's instruction. Briefly, a single colony of transformed bacteria was picked and grown in 5 mL LB with Amp (50 µg/mL) (see 2.8) in a shaker incubator at 37°C overnight. The day after grown bacteria were centrifuged 5 min at 10.000xg, the media was discarded and the pellet was resuspended in 250 µL of Cell Resuspension Solution by vortexing. 250 µL of Cell Lysis Solution were added, mixed by inverting the tube 4 times and incubated 5 min. Then 10 µL of Alkaline Protease were added and mixed by inverting the tube 4 times and incubated at room temperature for 5 min. 350 µL of Neutralization Solution were added and mixed immediately by inverting the tube 4 times. Tube was centrifuged at 14.000 rpm for 10 min at room temperature. The clear lysate was transferred into a Spin Column placed in a 2 mL microcentrifuge tube by decanting and centrifuged at 14.000 rpm for 1 min. The flowthrough was discarded and 750 µL of Column Wash Solution were added to the column. Centrifugation was performed at 14.000 rpm for 1 min, the wash was repeated with 250 µL of Column Wash Solution and centrifuged for 2 min at maximum speed. The column was placed in a new 2 mL microcentrifuge tube and centrifuged for 1 min at maximum speed. The column was transferred to a new sterile 1.5 mL microcentrifuge tube and plasmid DNA was eluted with 50 µL of Nuclease-free water. DNA was stored at -20°C

3.8 Bacterial culture medium

Luria Broth

10g Tryptone

10g NaCl

5g Yeast Extract

H₂O to 1L

LB was autoclaved.

Luria Broth agar (LA) with Ampicilli

10g Tryptone

10g NaCl

5g Yeast Extract

15 g Agar

H₂O to 1L

LA was autoclaved and Ampicillin was added to the final concentration of 50 µg/mL.

Super Optimal Broth with Catabolite Repression (SOC)

10 g Tryptone

2.5 g Yeast extract

0.5 g NaCl

1,25mM KCl

pH was adjusted to 7 with NaOH 5N. Mixture was autoclaved and then 5mM of MgCl₂ (2M) filtrated and 10 mM of glucose filtrated were added in steril condition.

3.9 DNA extraction

For tissue DNA extraction “QIAamp DNA Mini and Blood Mini KIT” (QIAGEN) was used following manufacture’s instruction. Briefly, about 30 mg of tumor tissues were cutted into small pieces and placed in a microcentrifuge tube with 180 µL ATL buffer and 20 µL of proteinase K (1mg/mL), mixed by vortexing and placed at 56°C until tissue was complitely dissolved (1-2 days). Then 200 µL of AL buffer were added, mixed by vortexing and incubated at 70°C for 10min. 200 µL of absolute ethanol were added to the sample and mixed by vortexing for 15 s. The sample was carefully applied to a QIAamp minicolumn located in a 2 mL collection tube and centrifuged at 6000xg for 1min. The column was placed into a new collection tube and washed with 500µL of AW1 buffer followed by wash with 500 µL of AW2 buffer. The column was placed into a new collection tube and centrifuged at full speed for 1 min. For the DNA elution, the QIAamp minicolumn was placed into a clean 1,5 mL microcentrifuge tube and 50 µL of AE buffer were added. The sample was incubated at room temperature for 1min and then centrifuged at 6000g for 1 min.

DNA quantity was routinely assessed on a NanoDrop 1000 spectrophotometer (Thermo Scientific) or on DeNOVIX DS-11 spectrophotometer. For the exoma secuencing analysis DNA was quantified with Qubit (Life Technologies) following the instruction of the manufacturer. DNA was stored at -20°C.

DNA was extracted from blood using DNAzol Reagent Invitrogen. 4 mL of whole blood were added into a 50 mL tube and mixed with 45 mL of Erythrocytes Lysis Buffer (150mM NH₄Cl, 10mM KHCO₃, 0,1mM N₄EDTA). The sample was mantained for 15 min at room temperature and carefully mixed every 2-3 min by inverting the tube. The liquid becomes more brillant and less dense. The sample was centrifuged at 700xg for

30 min at 4°C. Supernatant was discarded and the pellet was resuspended in 0,8 mL of Erythrocytes Lysis Buffer and transferred to a new 1,5 mL microcentrifuge tube. Sample was centrifuged at 300xg for 3 min at 4°C, the supernatant was discarded and the white pellet was resuspended in 500 µL of DNAzol Reagent (Invitrogen). Sample was mixed well with a micropipette and manual agitation for 3 min. 250 µL of absolute ethanol were added and strongly vortexed; sample was centrifuged at 400xg and the supernatant was removed carefully. Pellet was washed twice with 0.8 mL ethanol 70% and DNA was resuspended in 100 uL of NaOH 8 mM. DNA was stored at -20°C.

3.10 RNA extraction

“miRVANA miRNA Isolation KIT” (Life Technologies®) was used to obtain total RNA from cultured cells or tissues following the manufacture’s instruction.

Briefly, cells grown in a 75 cm² flask with at 80% confluency were washed with PBS before addition of 500 uL of Lysis Buffer, lysed cells were recollected with a scraper and placed into a 1,5 mL microcentrifuge tube. For tumor tissues 700 ul of Lysis Buffer were added to about 50 mg of tumor and homogenized in a 2 mL microcentrifuge tube with a T-10 Basic Ultraturrax (IKA). 1/10 volume of miRNA Homogenate Additive was added to the sample and immediatly mixed with vortex and incubated on ice for 10 min. 1 volume of acid Phenol:ChCl₃ 5:1 pH 4 solution was added to the sample and mixed by vortex for 30 s then centrifuged at maximum speed for 5 min. Sample was separated in two fases: the upper one, with RNA, was recollected and placed into a new 1.5 mL microcentrifuge tube. 1.25 volumes of absolute ethanol were added and well mixed. The sample was placed into a miRVANA column in a 2 mL tube and centrifuged at 10000 rpm for 6s. The column was washed by addition of 700 µL of miRNA Wash Buffer 1, centrifugation for 6 s at 10.000 rpm, followed by addition of 500 uL of miRNA Wash Buffer 2 and centrifugation at 10.000 rpm for 6 s. This last wash step was repited twice. The column was centrifuged 2 min at maximun speed and then placed into a new 1.5 mL microcentrifuge tube. RNA was eluted with 70 µL of 95°C pre-heated miRNA Elution Buffer. RNA was quantified with a NanoDrop 1000 spectrophotometer (Thermoscientific) and stored at -80°C.

3.11 cDNA synthesis with SuperScript First-Strand Synthesis System for RT-PCR” KIT (Invitrogen)

cDNA synthesis was performed by using the “SuperScript First-Strand Synthesis System for RT-PCR” KIT (Invitrogen), 1 µg of RNA in a volume of 7 µL in a 0,1 mL microcentrifuge tube. 3 uL of Pre-Reaction Mixture was prepared as follow:

- 3.3 mM of dNTPs mix (10mM)
- 0.16 µg/µL of Oligo (dT)₁₂₋₁₈ (0.5 µg/µL)
- 16.6 ng/µL of Random hexamers (50 ng/µL)

Pre-Reaction Mixture was added to each RNA mixture and incubate at 65°C for 5 min and at 4 °C for at least 1 min in a 2720 Thermal Cycler (Applied Biosystem). Then 1X Reaction Mixture was prepared as follow:

- 2X of RT Buffer (10X)
- 10 mM of MgCl₂ (25mM)
- 20 mM of DTT (0.1M)
- 1U RNase OUT Recombinant RNase Inhibitor (1U/µL)

9 µL of reaction mixture were added to each RNA mixture, mixed gently and incubated at 25°C for 2 min. 1 µL (50 units) of SuperScript II RT was added to each tube and incubated at 25 °C for 10 min, then at 42 °C for 50 min and at 70 °C for 15 min in a 2720 Thermal Cycler (Applied Biosystem). Sample was chilled on ice, 1 µL of RNase H (1U/µL) was added and incubated at 37°C for 20 min. cDNA was directly used for real time q-PCR or stored at -20°C until used. For RNA derived from PGL derived cells, PGL33 and PGL38, 1 ng of total RNA was used in 1 µl RT reaction using the AmpliGrid Single Cell One-Step RT-PCR System in an AmpliSpeed slide cycler (Advalytix, Olympus Life Science Research Europa GmbH) following the instruction recommended by the manufacturer.

3.12 Real Time q-PCR with Syber Green® Master Mix (Life Technologies)

For the Real Time q-PCR was realized with Syber Green® Master Mix (Life Technologies) following manufacture’s instruction. Briefly, reaction was performed using 3.75 µL of a dilution 1/10 of cDNA synthesized from 1 ug RNA. In a sterile 1.5 mL microcentrifuge tube were added the following reactive on ice:

7.5 μ L Water, nuclease free
0.3 μ M Primer FW
0.3 μ M Primer RV
18.75 μ L Syber Green®

The reaction mixture was mixed gently and centrifuged. 33.75 μ L of the reaction mixture were added to the cDNA mixture and 10 μ L of the sample was placed in triplicate in a MicroAmp Fast Optical 96-Well Reaction Plate with Barcode (0.1 mL). Plate was placed in Step One Plus Real Time PCR system (Applied Biosystem) device and the following program was started.

Step 1. 95°C for 15 min
Step 2. 95°C for 15 s
Step 3. 60°C for 1 min
Step 4. 95°C for 15 s → go to step 3 and repeat 40 times
Step 5. 60°C for 1 min
Step 6. 95°C for 15 min

Data analysis was performed using the $\Delta\Delta$ C_T method and the endogenous gene Cyclophilin was used for normalization.

3.13 cDNA synthesis “RT-PCR TaqMan MicroRNA Assay Kit” (Applied Biosystem)

This KIT was used to synthesize cDNA from single miRNAs following the manufacturer's instruction. Briefly, the reaction was prepared on ice as follows:

1 mM dNTPs (with dTTP)
1U Reverse Transcriptase
1X Reverse Buffer
2U RNAase Inhibitor
Nuclease free water to 15 μ L
1X miRNA primer
10 ng RNA

The reaction was carefully mixed and centrifuged and incubated at 16 °C for 30 min, 42°C for 30 min, 85°C for 5 min then chilled to 4°C. cDNA was used directly for real time q-PCR using TaqMan assay or stored at -20°C.

3.14 Real Time q-PCR with TaqMan 2X Universal PCR Master Mix, No AmpErase UNG (Applied Biosystems)

In a sterile 1.5 mL microcentrifuge tube reaction was prepared has follow.

1X TaqMan (2X) Universal PCR Master Mix, No AmpErase UNG

7.67 μ L Nuclease free water

1XTaq Man MicroRNA Assay (20X)

1.33 μ L cDNA

The reaction mixture was mixly gently and centrifuged. 20 μ L of the reaction was placed in quadruplicated in a MicroAmp Fast Optical 96-Well Reaction Plate with Barcode (0,1 mL). Plate was placed in Step One Plus Real Time PCR system (Applied Biosystem) device and the following programm was started.

Step1. 50°C for 2 min

Step2. 95°C for 10 min

Step3. 95°C for 15 s

Step4. 60°C for 1 min → go to step 3 and repite 40 times.

Relative miRNA expression was normalized against endogenous small nucleolar RNA, RNU44, control using the comparative delta-delta CT method.

3.15 Multiplex Ligation Probe-dependent Amplification (SALSA MLPA P016-C2 *VHL*, MRC Holland, The Netherlands)

To determine the copy number of *VHL* gene in PGLs tumors “Multiplex Ligation Probe-dependent Amplification” (SALSA MLPA P016-C2 *VHL*, MRC Holland, The Netherlands) was used following the manufacture’s instructions.

Briefly, DNA from healty blood donor was used as reference. This P016-C2 probemix contain 9 probes for the *VHL* gene (two or more probe for each exon), as well as 6 probes for genes located close to *VHL* (*FANCD2*, *C3orf10/HSPC300*, *IRAK2* and *GHRL*) and 2 probes on 3p wich are further telomeric or centromeric from *VHL*. In addition, 12 reference probes detecting sequences on other cromosomes are presents (Table 3).

Table 3. SALSA MLPA P016-C2 *VHL* Probemix

Length (nt)	SALSA MLPA probe	Chromosomal Position		
		Reference	Other	VHL
64-70-76-82	Q-fragments: DNA quantity			
88-92-96	D-fragments indicates incomplete denaturation			
100	X-fragment: Specific for the X chromosome			
105	Y-fragment: Specific for the Y chromosome			
166	Reference probe 09890-L10303	16p13		
175	VHL probe 13624-L16363			Exon 2
184	CNTN6 probe 06307-L05830		3p26.3	
193	C3ORF10 probe 14676-L16328		3p25.3	
201	VHL probe 02390-L16140			Exon 2
211	Reference probe 13450-L14905	5q31		
219	VHL probe 01626-L01211			Exon 1
229	IRAK2 probe 02264-L01750		3p25.3	
238	MLH1 probe 00892-L00480		3p22.1	
247	VHL probe 01162-L00718			Exon 3
256	Reference probe 01055-L00628	17q21		
265	Reference probe 02454-L01898	15q21		
274	VHL probe 01628-L01213			Exon 1
283	FANCD2 probe 02138-L01631		3p25.3	
301	GHRL probe 02266-L01752		3p25.3	
310	FANCD2 probe 02140-L01633		3p25.3	
319	Reference probe 05981-L05406	20p12		
328	VHL probe 13625-L15079			Exon 1
337	Reference probe 01082-L00660	22q11		
346	Reference probe 01335-L00879	7q11		
355	Reference probe 00547-L00116	11q22		
364	C3ORF10 probe 14675-L16327		3p25.3	
373	VHL probe 01158-L13266			Exon 1
382	Reference probe 00973-L00560	10q21		
391	VHL probe 13322-L14735			Exon 2
400	Reference probe 00801-L00639	13q14		
409	Reference probe 00669-L00373	11p13		
428	VHL probe 01161-L00717			Exon 3
427	Reference probe 00680-L00121	7q34		

DAY 1: DNA denaturation

5 µL of DNA sample (50 ng) were added to 0.2 mL labeled microcentrifuge tube. DNA was incubated for 5 min at 98°C and cooled to 25°C.

DAY 1: Hybridisation Reaction

Hybridisation Master Mix was prepared adding, for each reaction, 1.5 µL MLPA Buffer and 1.5 mL Probemix. After denaturation 3 µL of the Hybridisation Master Mix were

added to each sample tube. Sample was incubated for 1 min at 95°C and for 16-20 h at 60°C.

DAY 2: Ligation Reaction

Ligase-65 master mix was prepared as follow.

25 µL Nuclease free water

3 µL Ligase Buffer A

3 µL Ligase Buffer B

1 µL Ligase -65 enzyme

Ligase-65 Master Mix was well mixed and 32 µL were added to each reaction tube at 54°C mixing gently by pipetting up and down. Ligation reaction was continued at 54°C for 15 min followed by 5 min at 98°C for heat inactivation of the ligase and then paused at 20°C.

DAY 2: PCR Reaction

Polymerase Master Mix was prepared on ice by adding 7.5 µL dH₂O, 2 µL SALSA PCR Primer mix and 0.5 mL SALSA Polymerase. It was mixed well by pipetting up and down. At room temperature 10 µL of Polymerase Master Mix were added to each tube and the PCR Reaction was performed with the following thermocycler programm.

Step 1. 30 s at 95°C
Step 2. 30 s at 60°C
Step 3. 60 s at 72°C } 35 cycles
Step 4. 20 min at 72°C
Pause at 15°C

Tubes with PCR products were sent to the “Tecnical Scientific Service” of the University of Oviedo in where the Fragment Separation by Capillary Electrophoresis was performed.

Data Analysis and Results Interpretation

Prior to probe ratio calculation, MLPA peak patterns (electropherograms) were inspected to determine the quality of the MLPA experiment. For this purpose raw data

and size-called data were valued using the software Peak Scanner following the instruction of the manufacture.

When the data met all the criteria Dosage Quotient (copy number) was calculated. Data that has passed raw data and peak pattern evaluation was used for data normalization. Two step-model normalization was performed using a self-made analysis sheets. First the relative fluorescence intensity of each peak is determined (intra-normalization); in a second step, this relative peak was compared to that in the other samples (inter-normalization). The final ratio for a given probe in a test sample compared to that same probe in the reference samples is called the Dosage Quotient of that probe. The dosage quotient results should meet two criteria:

1. the standard deviation of all probe of the reference runs should be ≤ 0.1 ;
2. the dosage quotient of the reference probes of the sample runs should be between 0.8 and 1.2.

When this criteria were met, the interpretation of results was performed. Keeping in mind that MRC-Holland designed probes avoids known SNPs and that copy number changes detected with MPLA need to be confirmed with another methods, we used the following cut-off values for the dosage quotient (DQ) of the probes to identify abnormal *VHL* copy number (Table 4).

Table 4. Dosage quotient summary

Copy Number Status	Dosage Quotient
Normal	$0.85 < DQ < 1.15$
Heterozygous duplication	$1.35 < DQ < 1.55$
Homozygous duplication	$1.7 < DQ < 2.2$
Heterozygous deletion	$0.35 < DQ < 0.65$
Homozygous deletion	0

3.16 Real time q-PCR method to confirm results from MLPA

DNA copy numbers for *VHL* gene were confirmed by real time q-PCR optimizing a previously described sensitive and specific method (**108**). Real-time PCR was done in an ABI Prism 7500 Sequence Detection System using SYBR Green PCR Master mix (AppliedBiosystems) and the following thermocycler conditions: 10 min at 95°C, 40 cycles at 95°C for 15 s and 1 min at 60°C. *GPR15* gene was used as a reference locus

on chromosome with normal copy number. Primers for amplification of the three *VHL* exons were as described in (108). Primers concentrations were adjusted by using an optimization protocol with normal human blood DNA as template. For exons 1 and 3, each forward and reverse primer was used at 70 nM final concentration. For exon 2, primers were used at 333 nM. Each assay included a no-template control (in duplex), 30 ng of DNA from normal blood sample (in triplicate) and 30 ng of test DNA (in triplicate). Relative DNA quantity was determined using the delta-Ct formula as described in (108). For normalization of the relative quantities, the *VHL* copy numbers were divided by the geometric mean of the reference *GPR15* copy number. Using this method, a haploid copy number of 1 is expected for a normal sample and a value of 0,5 for a sample with a *VHL* deletion. Primers used are described in table 3.

3.17 Western blot

Protein extracts were obtained from HNSCC-derived cell lines at 80–90% confluence by scraping on ice in Lysis Buffer (50 mmol/L HEPES at pH 7.9 , 250 mmol/L NaCl, 5 mmol/L EDTA, 0.2% NP40, 10% glycerol, and protease inhibitors: 0.5 mmol/L phenylmethylsulfonyl fluoride, 1 Ag/mL aprotinin, 10 Ag/mL leupeptin, 1 mmol/L Na₃VO₄). The protein concentration was determined in the supernatant with Bradford protein assay reagent (Bio-Rad). Equal amount of protein were separated on SDS-PAGE (7.5% for HIF-1 α and 12% for SDHB and ISCU) and transferred to Immun-Blot polyvinylidene difluoride membrane (Bio-Rad). Membranes were immunoblotted with anti-HIF-1 α (BD Biosciences), anti-SDHB (Sigma-Aldich, St Louis, MO, USA, anti ISCU1/2 (ProteinTech) at 1:1000 dilution. For protein load control, mouse monoclonal anti- α -tubulin or anti- β -actina (Sigma-Aldrich, St. Louis, MO) was used at 1:10.000 dilution. Bound antibodies were detected using enhanced chemiluminescence reagent (Amersham Pharmacia Biotech) according to the protocol of the manufacturer.

3.18 Bisulfite Conversion and Pyrosequencing

This protocol was used for the methylation analysis of *VHL*. In the presence of sodium bisulfite no methylated cytosine are converted to uracil while methyleted cytocines are not modified. After the PCR amplification uracils are converted to thymine so and they can be distiguisced from cytocine that was metilated in the original sequence by sequencing.

3.18.1 Bisulfite Conversion

500 ng of DNA was used for the bisulfite conversion that was realized with EZ DNA Methylation-Gold™ Kit (Zymo Research) CT Conversion Reagent was prepared by adding 900 µl water, 300 µl of M-Dilution Buffer, and 50 µl M-Dissolving Buffer to a tube of CT Conversion Reagent. It was mixed by vortexing 10 min at room temperature. 130 µL of CT conversion Reagent were added to 20 µL of each DNA sample in a PCR tube and mixed by pipetting up and down. The tubes were placed in a thermal cycler and the following steps were performed:

Step 1. 98°C for 10 minutes

Step 2. 64°C for 2.5 hours

Step 3. 4°C storage up to 20 hours

3.18.2 Bisulfite Pyrosequencing

It is a quantitative method that allows determines the cytosine/thymine proportion in the CpG island of the gene in study. Primers in two regions of *VHL* promoters (V1 and V2) were designed by Pyrosequencing™ Assay Design Software v1.0, de Biotage AB in the Laboratory of Epigenetic of the University of Oviedo, avoiding CpG island or SNPs (Table 5). PCR was performed following the instruction of **(109)**. 5µL of the PCR product were separated on a 1% agarose gel in TAE 1% to check the intensity and the specificity. Product was purified in the PyroMark™ Q24 Vacuum Prep Workstation and desnaturalized at 80°C for 10 min. The primers were added and the pyrosequencing was performed in Pyromark™ Q24 (Qiagen) device. Results were analyzed with Pyromark Q24 v2.0.6 software (Quiagen) obteing a porcentaje of methylation for each CpG analyzed. DNA extracted from carotid body of organ donor was used as control.

Table 5. Primers used for amplification and pyrosequencing.

Primer for pyrosequencing	Sequence
Pyro-VHL-V2 seq	TTAAATAATAAATAAAAATAATTAG
Pyro-VHL-V1 seq	AAATTTTATAGTGGAATATAGTA
Pyro-VHL-V1F	GGTTAAGGTTGTAGTGAGTTAAGT
Bio-Pyro-VHL-V1R	CAAAAAAATCCTCCAACACC
Pyro-VHL-V2F	AGGAGGATTATTTGAATTTAGGGTT
Pyro-VHL-V2R	ATACAACCTTAACCTCCTAACT

3.19 Mutation analysis

Patients studied for germline *SDH* mutations were performed by direct sequencing and for *SDH* exon deletions by MLPA (*P226-B1-SDHB-SDHC-SDHD*, MRC-Holland) in the laboratory of Molecular Oncology of the Hospital Central de Asturias and by the laboratory of Gregorio Marañón. Somatic *SDHB*, *SDHC*, *SDHD*, *SDHA*, and *SDHAF2* gene mutations were explored by direct sequencing in the 3 tumor tissues of cluster C1 and in PGL47 at the level of both cDNA and genomic DNA. Mutation analysis for *VHL* and *HIF-2 α* gene was performed by direct sequencing of germline and tumor DNA for each patient of cluster C1. Mutation analyses for *VHL* gene in non-pHx-HNPGLs were limited to tumor DNA. Tumors of cluster C1 was also analyzed for the presence of somatic mutation *HIF2- α* and in Pro402 and Pro564 residues of *HIF1- α* . Primers used are described in Table 4.

3.20 Polymerase Chain reaction (PCR)

For the sequencation the exons were amplified by PCR using BIOTAQDNA PolymeraseTM (Bioline), following the manufacture's instruction. Briefly, the followinf mixture was prepared in a total volume of 20 μ L.

PCR MIX

1X NH₄ reaction Buffer

2mM MgCl₂

0.8mM dNTPs

0.4 μ L Primer Forward

0.4 μ L primer Revers

1U BIOTAQ DNA Polymerase

In a PCR tube were added 5,4 μ L of the PCR mix and 200 ng of DNA template in a in a final volume of 20 μ L. For each gene a negative control without DNA template was performed. In the case of region with high percentage of GC 10% DMSO was used. PCR tubes were placed in a Thermocycler and the following program was performed

PCR pogram

1.95°C 5 min

2.95°C 30 sec

3.55°C 30 sec (could vary depending on the primers used)

4.72°C 30 sec (go to step 2 and repite 25 times)

5.72°C 7 min

6.4°C hold

To check the PCR product size, 5 µL of PCR product were separated in an electroforesis gel of agarose 1%. DNA was visualized through the incorporation of Etidium Bromide (Sigma Aldrich) using UV transillumiator and molecular weight ladder used used was Gene Ruler 100 bp DNA Ladder (Thermo Scientific). Primers used for sequenciation and amplificacion are in Table 6

Table 6. Primers used for amplification and sequenciation

Primer	Sequence	Company
SDHAF1	CTTTGCCTGGCTGCTATCTC	invitrogen
SDHAF2	GGGGAGTTCCACTTCAACAA	invitrogen
SDHAF3	CCAACAGATTCCCAAAAGGA	invitrogen
SDHAF4	CTCGTTAATCAGGCGGTCAT	invitrogen
SDHAF5	CTTCCGGCTCAGCTCCTC	invitrogen
SDHAF6	TCCTTTTGGGAATCTGTTGG	invitrogen
SDHAF7	GAACCTCTATGACCGCCTGA	invitrogen
SDHAF8	CACGCAGTCTCTGCTCTTTG	invitrogen
SDHAF9	TGCCCCAGATCTTGAGTACC	invitrogen
SDHAF10	ATCACTTGAGGCAGGACCAG	invitrogen
SDHAF11	GGGTTCACTCTGTGGATGGT	invitrogen
SDHAF12	AGAGATAGCAGCCAGGCAAA	invitrogen
SDHAF13	CATGCGCAGGGACGCACCTT	invitrogen
SDHA1	TGGGAAAATCAGCAAGCTCT	invitrogen
SDHA2	CACAGTCAGCCTCGTTCAA	invitrogen
SDHA3	TCAAGGCGAAAGGTTTATGG	invitrogen
SDHA4	AGGACCTGCCCTTGTAAGT	invitrogen
SDHA5	TCGCACTGTGCATAGAGGAC	invitrogen
SDHA6	GCCTCTTCCTTCTCGGATCT	invitrogen
SDHA7	TTATAACATGGGCGGCATTC	invitrogen
SDHA8	TTTTCCCACAACCTTCTTGC	invitrogen
SDHA9	CCCTGTCTATGTGGACGTT	invitrogen
SDHA10	TCAAATGGATTTGGAAATAAAAGA	invitrogen
SDHA11	AGGAACCCGAGGTTTTCACT	invitrogen
SDHA12	GAAATGCCACCTCCAGTTGT	invitrogen
SDHA13=11	AGGAACCCGAGGTTTTCACT	invitrogen
SDHA14=12	GAAATGCCACCTCCAGTTGT	invitrogen
SDHA15	GACAACCTGGAGGTGGCATT	invitrogen
SDHA16	CCAAACTTGAGGCTCTGTCC	invitrogen
SDHA17	GGACAGAGCCTCAAGTTTGG	invitrogen
SDHA18	TTGCTCTTATGCGATGGATG	invitrogen
SDHA19	TACTGCACCGATCCTGTCTC	invitrogen
SDHA20	GGACCTCAGCGTTCCCTTA	invitrogen
SDHA21	AGTGAAAACCTCGGGTTCCT	invitrogen
SDHA22	AAAATGTTGGTGCCACCAC	invitrogen
SDHA23	GCAACAGCAGACATGTCTGGG	invitrogen
SDHA24	CGTAGCCTCCTGTGGCAACA	invitrogen
SDHA25	ATCGGACTGGCCACTCGCTA	invitrogen

SDHA26	TTGTAGTTGGTGGGAATGCC	invitrogen
SDHA27	CGCCTGCCTGGCATTTCAGA	invitrogen
SDHA28	CGTGCCTCTGCTCCGTAGAT	invitrogen
SDHA-HMG-1	ACTGCGCGGGCGGCAACAGCAG	invitrogen
SDHA-HMG-2	TCTAGCTCGACCACGGCGGC	invitrogen
SDHA-HMG-3	ATCCACTACATGACGGAGCA	invitrogen
SDHA-HMG-4	CATATATGCCTGTAGGGTGGGA	invitrogen
SDHA-HMG-5	TTGTTGCCACAGGAGGCTAC	invitrogen
SDHA-HMG-6	GACTTTATCTCCAGGCCTGCA	invitrogen
SDHA-HMG-7	TTGGACCTGGTTGTCTTTGG	invitrogen
SDHA-HMG-8	CATCAATCCGCACCTTGTAG	invitrogen
SDHA-HMG-9	TGCAGGCCTGGAGATAAAGTC	invitrogen
SDHA-HMG-10	GGCAAGCTCCCAGCCACTA	invitrogen
SDHAF14	AAAATGGCGGTGTCTACAGT	invitrogen
SDHAex14F	GCTCTGTTAGAGTAATAAGAAAC	invitrogen
SDHAex14R	GAAGCCC GACTGCTGTCTG	invitrogen
SDHAex6F	CTGCCTTGTCTGTACTGCTC	invitrogen
SDHAex6R	CAAGGCCTGTGTCTAAACCGT	invitrogen
SDHAex1F	CGCTCGACTCCGGCGTGGT	invitrogen
SDHAex1R	TCCC GATCCCGGGACAGA	invitrogen
SDHAex2F	GTTTGCAAGGGGAAATTA CTATC	invitrogen
SDHAex2R	TTTACTTGATCTAAATTTAAATCTAG	invitrogen
SDHAex3F	AGGTGCGAATGTGCCACC	invitrogen
SDHAex3R	GGCCATGTGGCTGGAGCAGG	invitrogen
SDHAex4F	GCCTGGAAGACAAAAGTTGGC	invitrogen
SDHAex4R	TTCTTTTGGCTGCCACATCC	invitrogen
SDHAex5F	TCTTTTTCCGTTATGAACTATGC	invitrogen
SDHAex5R	CGCTGCATGCGCCCCACGCT	invitrogen
SDHAex7F	TGTCCATTCTGTGATCTCACC	invitrogen
SDHAex7R	AGTTAGGACCTGAGAGCTGA	invitrogen
SDHAex8F	TCTAGCAATTGTTAGGTAATAAAT	invitrogen
SDHAex8R	AGACGCCTGCCAGCAGCTA	invitrogen
SDHAex9F	CACACTTCCAAGATGACGTAT	invitrogen
SDHAex9R	TGCGAGGTGGGCCCCGTC	invitrogen
SDHAex10F	GACACCCTGTTGGGGAAG	invitrogen
SDHAex10R	AAAAAGAAAAAAGACTTTCTAACG	invitrogen
SDHAex11F	GTTAGCTCAGGAGACTTACA	invitrogen
SDHAex11R	CACTTGGAAGTGGAAGCTGAAT	invitrogen
SDHAex12-13F	TCCTAATTTTTCTGTTTAATTTATG	invitrogen
SDHAex12-13R	CTGAGTCCCACCAGGTGGC	invitrogen
SDHAex15F	GAATCTTAAAGTTCACATGCCA	invitrogen
SDHAex15R	GAATCTTAAAGTTCACATGCCA	invitrogen
SDHA ex6 F new	TCTCTGCGATATGATACCAGC	invitrogen
SDHA ex6 F new	CCTGTGGCAACAACAGTGTT	invitrogen
VHL proF	GTTACAACAGCCTACGGTG	invitrogen
VHL pro R	CCGTCTTCTTCAGGGCCG	invitrogen
VHL 1aF	CGAAGACTACGGAGGTGCGAC	invitrogen
VHL 1bF	TCCGGCCCCGGGTGGTCTGGAT	invitrogen
VHL 1R	CCGAAGTCTGGCACGATAGCA	invitrogen
VHL EX1 R	GGCTTCAGACCGTGCTATCGT	invitrogen
VHL EX2 F	ATTACAGGTGTGGGCCACCG	invitrogen
VHL EX 2 R	ACGTGCCTGACATCAGGCAA	invitrogen
VHL EX3 F	GTTCTTGTACTGAGACCCTA	invitrogen
VHL EX3 R	GCTGAGATGAAACAGTGTA	invitrogen

VHL EX3 F new	TTGTTCGTTCCCTTGTACTGAG	invitrogen
VHL EX1F lab inv	CGCCGCATCCACAGCTA	invitrogen
VHL EX1R lab inv	GGCTTCAGACCGTGCTATCG	invitrogen
GPR15 F	TTGCTGGTAATGGGCACACA	invitrogen
GPR15 R	TTGCTGGTAATGGGCACACA	invitrogen
VHL EX2 F Lab Invest	CAATGTTGACGGACAGCCTATTT	invitrogen
VHL EX2 R Lab Invest	GTCTATCCTGTACTTACCACAACAACCT	invitrogen
VHL EX3 F Lab Invest	GACCTGGAGCGGCTGACA	invitrogen
VHL EX3 R Lab Invest	TACCATCAAAAGCTGAGATGAAACA	invitrogen
vhl pro new1	TAACGAGTTGGCCTAGCCT	invitrogen
vhl pro new2	AGGATCCTTCTGCGCACGC	invitrogen
SDHBF	CATATGCAGACTTATGAAGTT	invitrogen
SDHBR	ATTAAGCATCCAATACCATG	invitrogen
SDHC EX1F	CACATGACACCCCAACCC	invitrogen
SDHC EX1R	GACGGGTCCGTGTCCTATTTGT	invitrogen
SDHC EX2F	TATTTTATCTATCCCTTCAC	invitrogen
SDHC EX2R	AGAGGTCTGAATGTTTGAAT	invitrogen
SDHC EX3F	CATGCCTGCTTGGTATTGC	invitrogen
SDHC EX3R	AGTCTTGAAAGTGGGTGATGGAG	invitrogen
SDHC EX4F	CTATGGTGTGCATCTTTTCCTTT	invitrogen
SDHC EX4R	CTCGTGTGACGTTTGAGTATTA	invitrogen
SDHC EX5F	TCATATTAGTTGTAACCTTATGAGCAGC	invitrogen
SDHC EX5R	GAGGGGTGAGGGAATGAC	invitrogen
SDHC EX6F	TGTTAATGTCCTATTTACTGAA	invitrogen
SDHC EX6R	ATTTGTTTATTCCTCTTGAAAA	invitrogen
VHL cDNA F	CCCAGGTCATCTTCTGCAAT	invitrogen
VHL cDNA R	ACATTTGGGTGGTCTTCCAG	invitrogen
CF123	CATCTGCACTGCCAAGACTGA	invitrogen
CF124	TTGCCAAACACCACATGCTT	invitrogen
Ca9 FW	CGCTGAGGAAGGCTCAGAGA	invitrogen
Ca9 RV	GGCAGGAGTGCAGATATGTCC	invitrogen
VHLseq3	AGCCTAGTCAAGCCTGAG	teknochroma
HIF2 EX1f	CCCAGTCACCTTTCTCCAC	vwr-thermo
HIF2 EX1r	GAAGACCTCTCAGCACTCTTC	vwr-thermo
HIF2 EX2f	ATGTCCTGGCCAGAGGT	vwr-thermo
HIF2 EX2r	GGAACATGCTGGTAAGGC	vwr-thermo
HIF2 EX3f	AATGCCTATCTGTGCCAGT	vwr-thermo
HIF2 EX3r	GATTGTGGCTAGCACCTTC	vwr-thermo
HIF2 EX4f	GGAAGTGGCTCAGCTTA	vwr-thermo
HIF2 EX4r	CTCCCTTATACCCGTAGACAA	vwr-thermo
HIF2 EX5,6f	ATATAACAATAGGCTGCCAAG	vwr-thermo
HIF2 EX5,6r	TCCCCACACACACAGGTAAG	vwr-thermo
HIF2 EX7f	TCTGGGGTTAGCTCCTGC	vwr-thermo
HIF2 EX7r	CACTCAAGGCCACATACCAC	vwr-thermo
HIF2 EX8f	GATCTGCTGAGCCTGTGG	vwr-thermo
HIF2 EX8r	CTGAGTCTGGGAAGCTTGG	vwr-thermo
HIF2 EX9f	CGGAGAGCTTAGCTATGAGG	vwr-thermo
HIF2 EX9r	GGGGTAGCTCTGGTTAAGAA	vwr-thermo
HIF2 EX10f	GGCATGCCTTCCAGAC	vwr-thermo
HIF2 EX10r	CCCTTCAGCCATCTGG	vwr-thermo
HIF2 EX11f	TCTTCTCCATGCTGGACT	vwr-thermo
HIF2 EX11r	CAAGAATGGATGTGAGCCT	vwr-thermo
HIF2 EX12f	AGGAGCTGAGTTGGAATAGTG	vwr-thermo
HIF2 EX12r	CCAGCTATCTTACTAGTGGGTG	vwr-thermo

HIF2 EX13f	CCTAAGATGAGAAGGCACTGA	vwr-thermo
HIF2 EX13r	CTATGCTGGCTTGGAAGG	vwr-thermo
HIF2 EX14f	AAGCCAGCAAGTGCCAG	vwr-thermo
HIF2 EX14r	GAGCCCCAGTCCTTCCAC	vwr-thermo
HIF2 EX15f	AAGGGATGCTAGGGCTTC	vwr-thermo
HIF2 EX15r	GCCTGGCACTGTGCAGAC	vwr-thermo
HIF2 EX16f	GGAGCAGAGTGAAATTAG	vwr-thermo
HIF2 EX16r	CCACTGCTTGGTGACCTG	vwr-thermo
EX9HIF1a-f	CAATTTCTCTTGTTTTGACAG	vwr-thermo
EX 9HIF1a-r	ACACAATTTAGGGGATTAACA	vwr-thermo
EX 12HIF1a-f	AAGGTGTGGCCATTGTAAAAA	vwr-thermo
EX 12HIF1a-r	TTGCGTTAGGGCATATATATCAGA	vwr-thermo
VHLmutdelCTT-f	CCTCCCAGGTCATCTGCAATCGCAGTCCGC	vwr-thermo
VHLmutdelCTT-r	GCGGACTGCGATTGCATATGACCTGGGAGG	vwr-thermo
VHLmutG-A-f	GTATACTCTGAAAGAGCAATGCCTCCAGGTTGTCCG	vwr-thermo
VHLmutG-A-r	CGGACAACCTGGAGGCATTGCTCTTTCAGAGTATAC	vwr-thermo

3.21 Purification of PCR products

PCRs products were purified using ATPTM Gel/PCR Fragment DNA extraction KIT (ATP Biotech Inc.) following the manufacture's instruction. Briefly 20 µL of reaction products were transferred into a microcentrifuge tube and 5 volumes of DF Buffer were added. The sample mixture was added to a DF column in a microcentrifuge tube and centrifugated at 13.000 rpm for 30 sec; the flow-trough was discarded. 600 µL of Wash Buffer were added and centrifugated for 30 sec; the flow-trough was discarded and centrifugation was repited to dry the filter at full speed for 3 min. Column was transferred into a new microcentrifuge tube and DNA was eluted with 15 µL of Elution Buffer.

3.22 Immunocytochemistry

Cells grown in CultureSlides (BD Falcon) were washed twice with PBS, fixed with absolute ethanol for 1h and rendered permeable with successive treatment with ethanol at concentration of 95%, 80%, 70%, 50% and water for 5 minutes each. Cells were then covered with EnVisionTM FLEX WASH BUFFER 1X (Dako) for 5 minutes, treated with EnVisionTM FLEX PEROXIDASE_BLOCKING REAGENT (Dako) for 5 minutes and washed again with EnVisionTM FLEX WASH BUFFER 1X (Dako) for 5 min. Cells were incubated with specific antibody diluited as indicated in the table 3 and incubated over night at 4°C. After the incubation cells were washed with PBS for 5 min and incubated for 20 min with EnVisionTM FLEX HRP (Dako), washed with PBS for 5 min and incubated with DAB (Dako) prepared following the manufacture's instruction for 5 min. To stain the nuclei cells were incubated with EnVisionTM FLEX Hematoxylin

(Dako) for 8 min. Sample was dehydrated with successive wash with ethanol 50%, 70%, 96%, 100% and xylol and covered with a microscope cover glass. Images were taken with Olympus BX61 microscope.

3.23 Immunofluorimetry

Cells grown in μ -Plate 24 well ibiTreat (ibidi) were washed twice with PBS, fixed with methanol for 5 min and permeabilized with PBS for 5 min. Fixed cells were treated with EnVision™ FLEX PEROXIDASE_BLOCKING REAGENT (Dako) for 5 minutes and then washed with PBS twice. Cells were incubated with anti-VHL (1:100) for 1h at room temperature, after the incubation cells were washed with PBS twice and incubated with Labeled-Chiken Anti-Mouse Alexa Fluor 555 (Invitrogen) for 1 hour at room temperature in darkness. Sample was washed twice with PBS and incubated with VECTASHIELD Mounting Medium with DAPI (VECTOR® laboratories). Images were taken in a Zeiss Axio Observer Z Inverted Microscope.

3.24 Immunohistochemistry

Tumor samples were fixed with formol and included in paraffin then were cutted in 4 μ m cut and were attached on a slide trated with silicon (ChemMate, BioTEK Solution; Santa Barbara, CA, USA). Sample were desparafinized and unmasked with PTlink device (DAKO) using a specific pre-treatment (table 3) for 20 minute at 95°C. Then sample were located in the Autostainer (DAKO) device that automatically perform the immunohistochemistry using EnvisionFLEX (DAKO) reagents. Conditions used for each antibody are shown in table 7.

Table 7. Antibody condition for immunohistochemistry.

Antibody	Commercial House	Pre-treatment	Dilution	Time (min)
anti-HIF-1a	BD	EDTA	1:50	60
anti-CalX	abcam	EDTA	1:1000	30
anti-SDHB	SIGMA	EDTA	1:800	30
anti-SDHA	abcam	EDTA	1:1000	30
anti-VHL	BD	citrate	1:100	15
anti-MBP	SIGMA	EDTA	1:150	30
anti-TGFBR3	abcam	EDTA	1:15	50
anti-nestin	abcam	citrate	1:1000	20
anti-S100	DAKO	proteinase K	1:1000	20
anti-TH	abcam	EDTA	1:400	30
anti-CD31	abcam	EDTA	1:100	10

3.25 Microarrays and TaqMan Low-Density Array (TLDA)

RNA quality was determined using Bioanalyser 2100 (Agilent Technologies, Palo Alto, CA) following the manufacturer's instruction and only RNA samples with an RNA integrity number (RIN) between 8 and 10 were used. About 3-10 µg of total RNA (0.1 µg per mg of tissue) were obtained from the carotid bodies extracted from healthy donors. For microarray hybridization, RNA was processed for hybridization to Affymetrix GeneChip Human Genome U133 Plus 2.0 Arrays according to the manufacturer's instructions. TLDA (Applied Biosystems) was used to assay the expression of 369 human miRNAs present in miRBase release 16.0. For TLDA, 100 ng of total RNA obtained from tumor and healthy tissues was used in the megaplex reverse transcription (RT) reaction containing about 450 miRNA-specific RT primers provided by the manufacturer. No prior miRNA preamplification step was needed. The RT product was mixed with 2X TaqMan Universal PCR Master Mix, No AmpErase UNG (Applied Biosystems) and loaded onto the TLDA containing the 48-plex PCR reaction mix. TLDA were run on a 7900HT Thermocycler (Applied Biosystems) using Sequence Detection Systems (SDS) software version 2.3. A single TLDA was used per sample. Manual inspection of all amplification plots was performed and miRNAs were excluded from the analysis if: *Ct* values were too high (above 35, indicating a miRNA expression too low for accurate detection), or if amplification was not achieved in all samples. Data analysis was performed using SDS RQ manager v1.2 (Applied Biosystems) which utilizes the delta-delta CT method. The endogenous small nucleolar control RNA, RNU44, was used for normalization. miRNAs that were expressed differentially between normal and tumor samples were detected with one-way analysis of variance (ANOVA) using the Partek Genomics Suite. The recovered P-values of the comparisons were then corrected using a step-up false discovery rate value of 5%. The resulting list of significantly differentially expressed miRNAs was filtered to include only those that demonstrated 2-fold or greater up or down-regulation.

3.26 Vascular Density

To measure vascular density, the number of CD34 immunostained blood vessels was counted in 3 "hot spot" fields of 1 squared millimetre in tissue sections with the use of stereological grids overimposed to the microscopic field. We used the free image processing and analysis program UTHSCSA Image Tool. Vessels were counted according to the stereological rules **(110)**.

3.27 Statistical Analysis

Statistical analyses were performed using the SPSS statistical software version 8.0 (SPSS Inc., Chicago, IL.). Correlations between tumor size or tumor location were computed using the Chi-Square test.

3.28 Microarray data analysis

Raw signal intensities for each probe set in the .CEL files were analyzed using version 6.5 of the Partek® Genomics Suite™ (Partek Inc., MO, USA). The robust multiarray average (RMA) normalization method was used for RMA background correction, quantile normalization and medianpolish probe set summarization. Examination of the frequency of expression values after normalization of the data revealed consistent values between all samples. Expression values were transformed to log₂ before statistical analysis. To identify outliers in our sample sets and to investigate global similarities of samples, a principal component analysis (PCA) was performed. Genes that were expressed differentially between two groups of samples were detected with one-way analysis of variance (ANOVA). The recovered P-values of the comparisons were then corrected using a step-up false discovery rate (FDR) value of 5%. The resulting list of significantly differentially expressed genes was filtered to include only genes that demonstrated 2-fold or greater up or down-regulation. To search for enrichment of specific biological processes, the genes showing significantly differential expression between two groups were analyzed using the Gene Ontology Enrichment tool in the Partek Genomic Suite Software and DAVID (Database for Annotation, Visualization, and Integrated Discovery). Significant processes (GOTERM) with Benjamini P<0.05 were generated.

3.29 Bioinformatics Analysis of Oncomine Cancer Gene Microarray Database

We used Oncomine Cancer Microarray database (<http://www.oncomine.org/>) to compare the gene expression signature of pHx-HNPGLs to that of other cancer tissues. The analysis type <cancer vs. non-tumor> was applied to filter microarray datasets exploring cancer relative to its non-tumor tissue. Then, two types of analysis were performed: (1) we searched the Oncomine database using the literature defined concept: “Upregulated genes in response to hypoxia and in response to HIF-1 expression” which yielded 47 gene lists from 10 types of solid tumors (odds ratio=2; p value=1E-4; Oncomine analysis). These gene lists were then compared with the pHx-HNPGL gene lists for overlap. The percentage of overlapping genes was then

calculated for each microarray study. (2) Expression of genes not contained in the Oncomine <Upregulated genes in response to hypoxia and in response to HIF-1 expression> concept but found upregulated in pHx-HNPGLs were individually examined in the 47 datasets previously identified using a threshold p-value of 1E-4, threshold fold change of 2 and threshold gene rank of “top 10%”. Gene rank reflects the rank of that gene in the dataset, based on its p-value. The percentage of pHx-HNPGL-related genes found upregulated in each study was then calculated. Student's *t*-test was used for analyzing differences between published datasets in the database.

4. RESULTS

4. RESULTS

4.1 Expression profiles analysis of HNPGs vs normal samples.

The most accepted hypothesis of the pathogenesis of PCC/PGLs is the activation of the hypoxia pathway via HIF-1a stabilization, however studies of expression profiles, until the date, are centred on PGL/PCC and do not include many HNPGs, in addition they do not use normal paraganglia for the comparison. To get further insight the gene expression program of HNPGs we compared the global expression profile of 17 HNPGs (Table 1) and 3 normal paraganglia obtained from healthy donors (Figure 7).

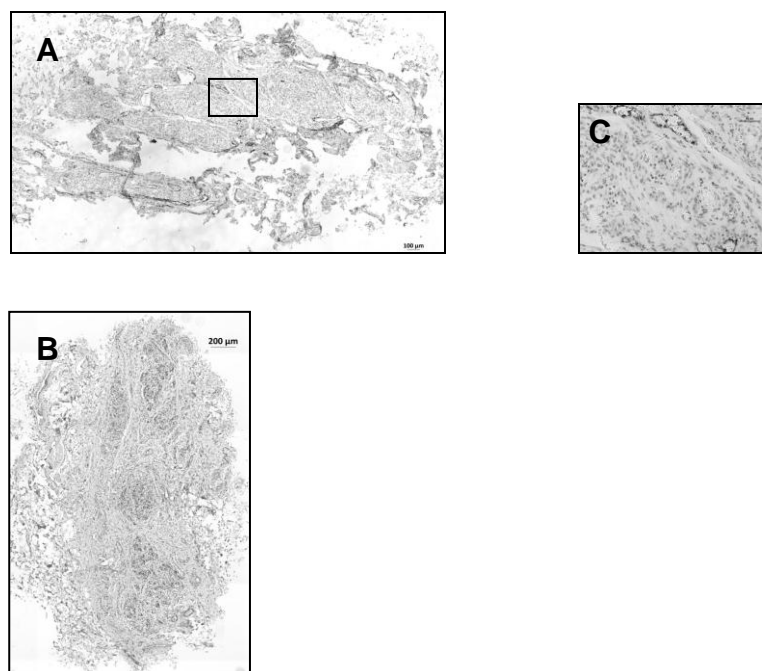


Figure 7. Histological examination of two normal carotid bodies obtained from healthy whole body donors. Hematoxylin eosin staining was performed in two normal carotid bodies used for molecular studies. (A, B) Images of two carotid bodies were taken in an AxioObserver.Z1 microscope (Zeiss) using an EC Plan-Neofluor 10x/0.30 Ph1 objective and a 4x4 tile. Stitching was performed with the Zen software. (C) Higher magnification (x200) of the area outlined in the panel A.

Table 8. Patient's characteristics.

Patient	Gender	Age at diagnosis	Family history (PCC/PGL)	Tumor Site ¹	Tumor Size ²	Gene Mutated ³	mutation nucleotide	mutation protein
PGL 2	F	79	No	JT	1	None		
PGL3	F	53	No	JT	1	None		
PGL6	M	27	No	JT	3	None		
PGL7	F	55	No	CB	1	SDHB	c.725G>A	p.Arg242His
PGL8	F	48	Yes	CB	1	SDHD	c.14G>A	p.Trp5x
PGL9	F	39	No	V	Un	None		
PGL11	F	49	No	V	3	None		
PGL14	F	25	No	CB	1	SDHD	c.33C>A	p.Cys11x
PGL15	M	32	No	JT	1	SDHB	c.269G>A	p.Arg90Gln
PGL18	F	Un	Un	CB	Un	None		
PGL19	F	66	No	JT	2	None		
PGL21	M	40	No	CB	1	None		
PGL22	F	29	No	JT	2	None		
PGL23	M	41	No	CB	2	None		
PGL28	M	63	No	T	1	None		
PGL32	F	29	No	CB	1	SDHD	c.386dupT	p.Leu129fs
PGL34	F	29	No	JT	Un	None		

(1) JT, jugulotympanic; CB, carotid body; V, vagal. (2) Tumor size (mm²) was calculated by the ellipsoid volume formula $\pi/6 \times a \times b \times c$ where a, b, and c are the three major diameters (a=width, b=length, and c=depth) of the tumors (mm). 1, small tumors (less than 50 mm³); 2, medium size-tumors (50-100 mm³); 3, large tumors (above 100 mm³). (3) Some tumors did not harbor any mutation and were sporadic (None).

Microarrays were performed using the GeneChip Human Genome U133 Plus 2.0 Arrays (Affymetrix). Examination of the frequency of expression values after normalization of the data revealed consistent values between all samples (Figure 8). Principal component analysis (PCA) revealed that HNPGLs grouped together and separated from normal carotid bodies; the same result was obtained with unsupervised hierarchical cluster analysis (Figure 9A and 9B).

Global expression comparison of the normal and tumor samples showed 1296 differentially expressed genes, 923 of which were down-regulated in HNPGLs and 373 genes were up-regulated (2x fold change, p-value based on the false discovery rate of < 0.05).

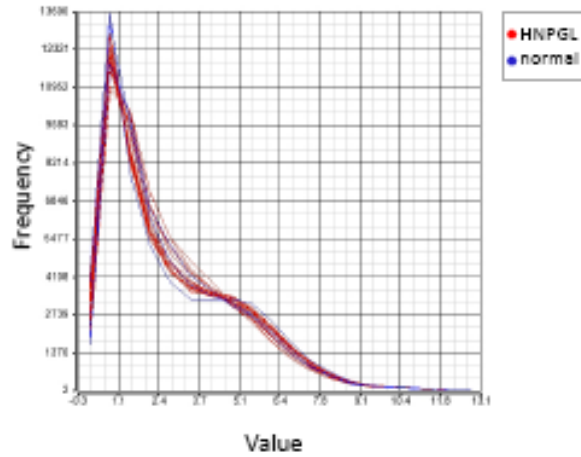
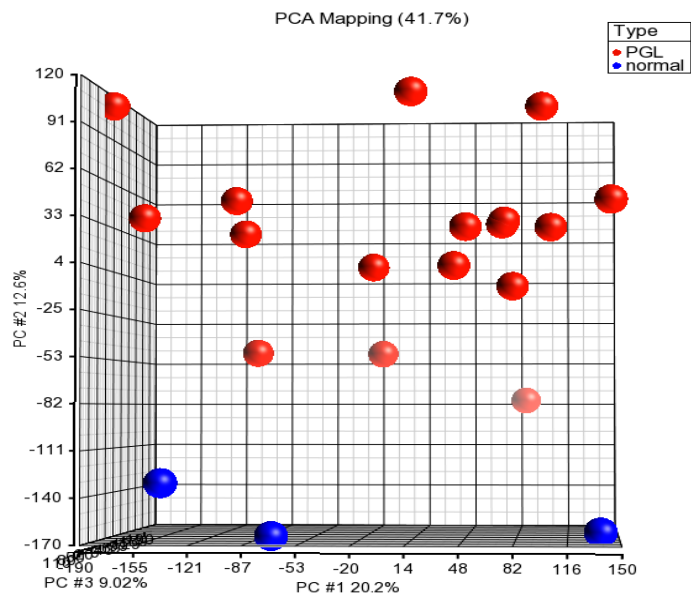


Figure 8. Evaluation of gene expression microarray data set. RNA from HNPGLs and normal carotid bodies were converted to cDNA, labeled and hybridized to Affymetrix GeneChip Human Genome U133. Scanned data were imported to Partek Genomics Suite software (Partek) and normalized using RMA algorithm. A plot of frequency versus signal value is shown for each dataset. The histogram shows that all samples follow the same distribution pattern indicating that there are no obvious outliers in the data.

A



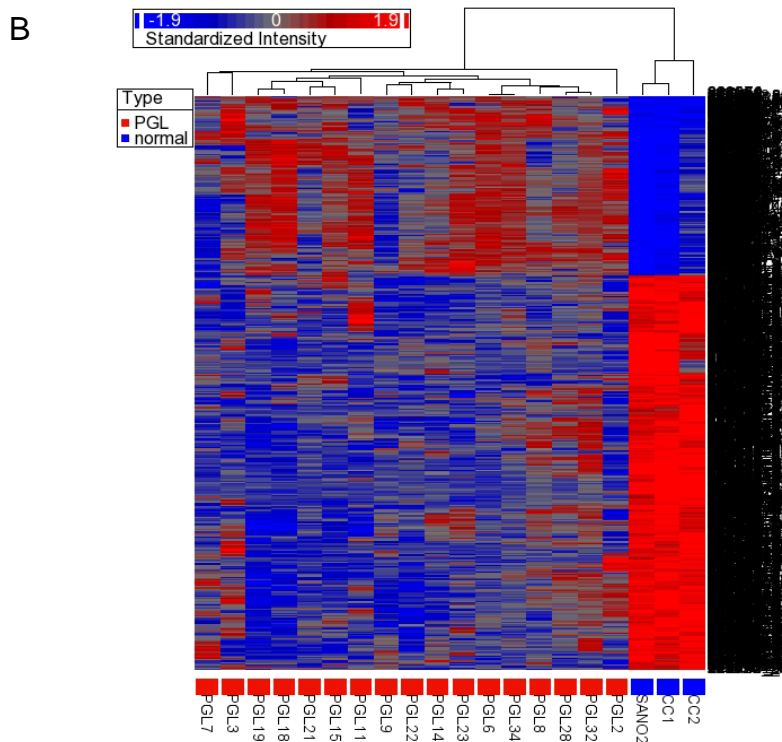


Figure 9. Global mRNA expression analysis. (A) PCA revealed a distinct global gene expression signature for HNPGLs (red) and normal paraganglia (blue). x, y, and z axes represent three major principal components (PC). (B) Hierarchical unsupervised cluster analysis of genes differentially expressed between HNPGLs and normal paraganglia (FDR<0.05, with fold change>2). Red and blue colors indicate high and low expression levels, respectively. Gray color indicates no change in expression levels.

The Gene Ontology Enrichment tool of the Partek Genomic Suite Software and DAVID software were used for the gene ontology analysis of the differentially expressed genes (Table 9 and Supplementary Table S1). This analysis revealed that there is a significant enrichment ($p < 0.05$) of genes involved in locomotion, immune and inflammatory response, morphogenesis, development and angiogenesis, among others (Fig 10).

Table 9. Gene Ontology (GO) biological process altered in HNPGLs.

Term	Count	%	P-Value	Benjamini and Hochberg FDR
cellular ion homeostasis	42	4,1	3,4E-5	9,6E-3
inflammatory response	34	3,3	7,7E-4	4,9E-2
negative regulation of cell projection organization	8	0,8	7,4E-4	4,8E-2
negative regulation of neurogenesis	10	1,0	7,8E-4	4,8E-2
appendage development	16	1,5	6,4E-4	4,3E-2
limb development	16	1,5	6,4E-4	4,3E-2
muscle tissue development	18	1,7	6,4E-4	4,3E-2

positive regulation of immune system process	28	2,7	4,2E-4	3,8E-2
regulation of cell projection organization	15	1,5	4,3E-4	3,8E-2
cell motion	46	4,5	4,4E-4	3,8E-2
axon ensheathment	10	1,0	4,6E-4	3,8E-2
ensheathment of neurons	10	1,0	4,6E-4	3,8E-2
protein maturation	18	1,7	4,8E-4	3,8E-2
regulation of neuron projection development	13	1,3	4,9E-4	3,8E-2
vesicle-mediated transport	53	5,1	5,1E-4	3,8E-2
actin filament-based process	28	2,7	5,1E-4	3,8E-2
small GTPase mediated signal transduction	33	3,2	5,3E-4	3,8E-2
regulation of protein kinase cascade	29	2,8	3,8E-4	3,6E-2
regulation of transferase activity	39	3,8	2,8E-4	2,9E-2
membrane invagination	27	2,6	2,8E-4	2,8E-2
endocytosis	27	2,6	2,8E-4	2,8E-2
angiogenesis	21	2,0	2,4E-4	2,7E-2
actin cytoskeleton organization	28	2,7	1,8E-4	2,4E-2
tissue morphogenesis	24	2,3	2,0E-4	2,4E-2
negative regulation of cell differentiation	27	2,6	2,1E-4	2,4E-2
negative regulation of cellular component organization	21	2,0	1,4E-4	2,1E-2
muscle organ development	27	2,6	1,4E-4	2,1E-2
regulation of phosphate metabolic process	49	4,7	1,0E-4	2,0E-2
response to wounding	52	5,0	1,3E-4	2,0E-2
positive regulation of cell communication	37	3,6	1,0E-4	1,9E-2
regulation of cell morphogenesis involved in differentiation	15	1,5	8,9E-5	1,8E-2
negative regulation of cell development	12	1,2	5,7E-5	1,4E-2
blood vessel morphogenesis	30	2,9	7,6E-6	1,2E-2

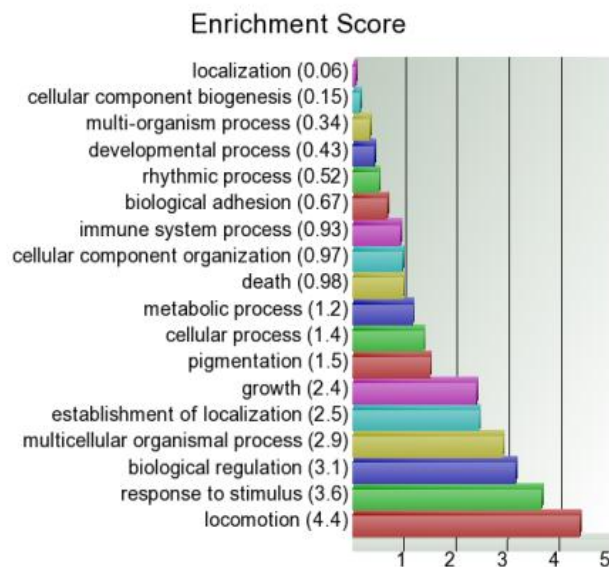
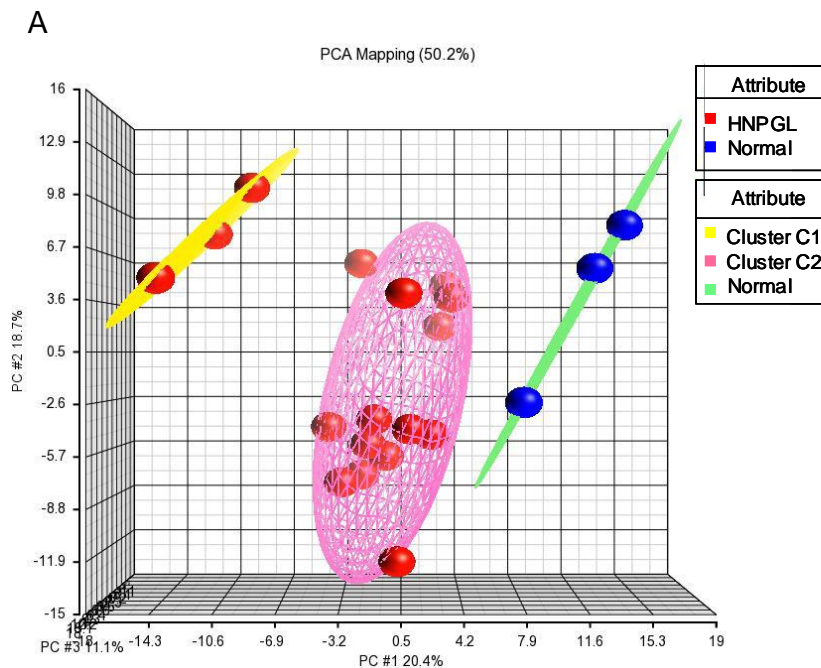


Figure 10. Biological process analysis of genes deregulated in HNPGLs. Enrichment scores are the negative $\log_{10} X^2$ *P*-value (higher score indicates greater enrichment).

Given that the most accepted hypothesis of tumorigenesis of PGLs is the activation of a pseudo-hypoxic pathway, it was surprising the observation of the absence of enrichment of hypoxia related genes in HNPGLs in this global comparison analysis.

To determine whether a putative hypoxic/pseudohypoxic gene expression profile is present only in a subset of HNPGLs, a list of published hypoxia-regulated genes taken from recent relevant reports was elaborated (Supplementary Table S2) (111-113) to perform PCA and unsupervised cluster analysis of the HNPGLs and normal paraganglia. The PCA showed that normal tissues, again, were grouped together and segregated from HNPGLs which, in turn, were clearly separated into two clusters, one containing three sporadic HNPGLs (cluster C1) and the other containing the rest of samples (cluster C2) (Figure 11A). Unsupervised hierarchical clustering also showed a clear distinction in C1- vs C2-tumors (Figure 11B).



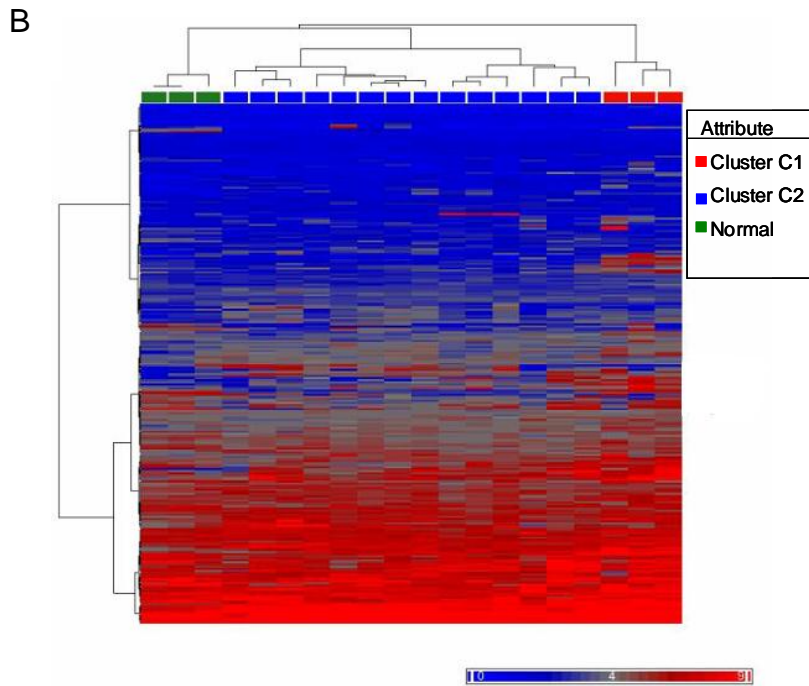
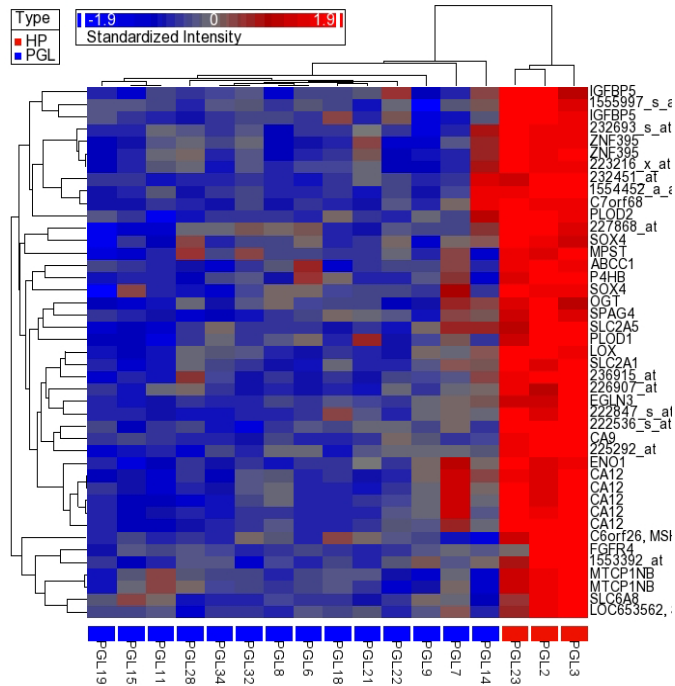


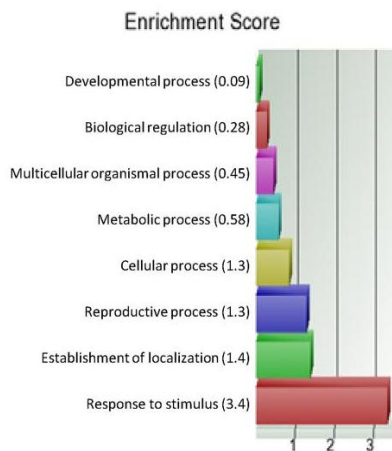
Figure 11. Analysis of hypoxia-related gene expression. (A) PCA showing a distinct hypoxia-like gene expression signature for normal paraganglia (blue spheres) and HNPGLs (red spheres). Two distinct clusters of tumor samples; one cluster consists of 3 sporadic tumors (yellow ellipsoid; cluster C1) and the other cluster consists of the remaining 14 tumors including 5 SDH-related and 9 sporadics (pink ellipsoid; cluster C2). (B) Unsupervised hierarchical cluster analysis of normal paraganglia and HNPGLs showing normal paraganglia grouping together and separated from tumors which segregated in two groups (clusters C1 and C2).

Gene expression analysis of the hypoxia-related genes identified 28 genes (29 probe sets) that were differentially expressed between these two groups of HNPGLs, 27 of which were up-regulated in C1-tumors by more than 2-fold and p-values based on false discovery rate of less than 0.05. The analysis of global differential gene expression patterns between C1- and C2-tumors considering the whole genome revealed 27 differentially expressed genes, of which 11 (>40%) were related to hypoxia gene expression response (Figure 12A-C). Collectively, these data supports the conclusion that C1-tumors actually differ from C2 in the pattern of expression of hypoxia related genes.

A



B



C

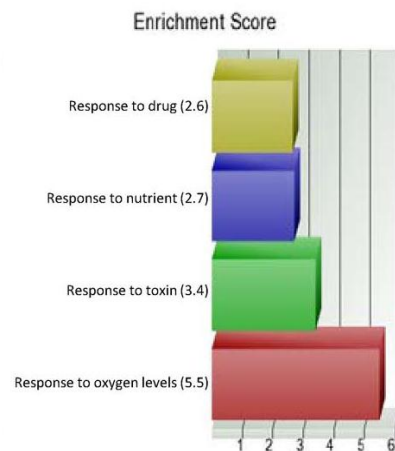


Figure 12. (A) Hierarchical supervised cluster analysis of genes differentially expressed between tumors of C1 and C2 (false discovery rate<0.05, with > 2-fold change) using the complete set of genes in the microarray. *Red* and *blue* indicate high and low expression levels, respectively. *Grey* indicates no change in expression levels. (B) Biological process analysis of genes deregulated in C1 vs. C2 HNPGLs. (C) Within the most-enriched pathway (response to stimulus, *red bar* in B), most of the genes were involved in response to oxygen levels.

We next compared the gene expression levels of hypoxia related genes in the clusters C1 and C2 versus normal paraganglia. The results are shown in the Venn diagram (Fig. 13). Only a few genes are commonly deregulated in the two clusters, these are

genes involved in angiogenesis (*COL4A1*, *GPI*, *PGF*, *COL4A2*), glycolysis (*GPI*, *PFKP*), and extracellular matrix remodeling (*COL4A1*, *COL4A2*, *LOXL2*). A more significant number of hypoxia regulated genes were unique to either C1- or C2-tumors. In C1-tumors the upregulated genes showed a significant enrichment ($p < 0.05$) in biological processes characteristics of the hypoxic response like glycolysis (*ENO1*, *GAPDH*), regulation of cell death (*BNIP3*, *BNIP3L*, *EGLN3*), and blood vessel development (*VEGFA*, *ANGPTL4*, *LOX*, *COL5A1*). By contrast, a significant number of hypoxia-related genes (19 of a total of 47 deregulated genes) were found downregulated in C2-tumors. Remarkably, among these downregulated genes there are known target of HIF-1 α , as *HIG2* and *EGLN3*, which were found upregulated in C1-tumors.

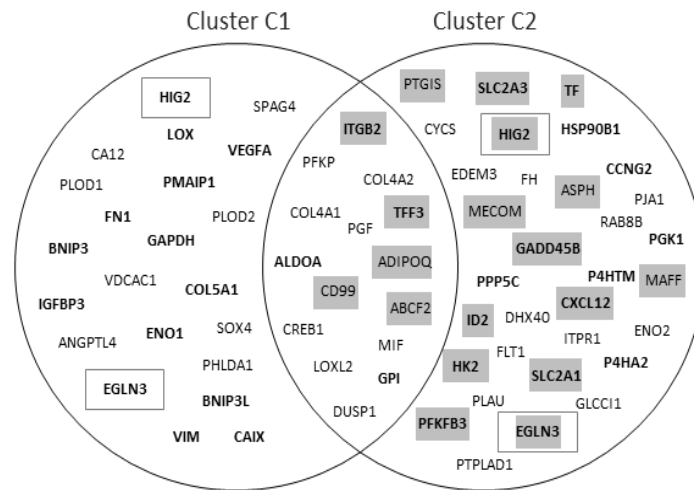


Figure 13. Venn diagram showing the pseudohypoxia gene signatures characterizing the two clusters of HNPGs compared with the normal tissue. Known HIF-1 α gene targets are in bold, down-regulated genes are shaded, and up-regulated genes are unshaded.

4.2 Validation of microarrays data

The microarray results were validated by real-time PCR for selected genes that have a hypoxic regulation and were found up-regulated in C1 cluster (*VEGFA*, *CAIX*, *BNIP3*, and *EGLN3*) (Fig. 14). This analysis corroborated the differential expression in both groups of HNPG samples in comparison with normal carotid body. Therefore, the mRNA levels were accurately reflected by the microarray data.

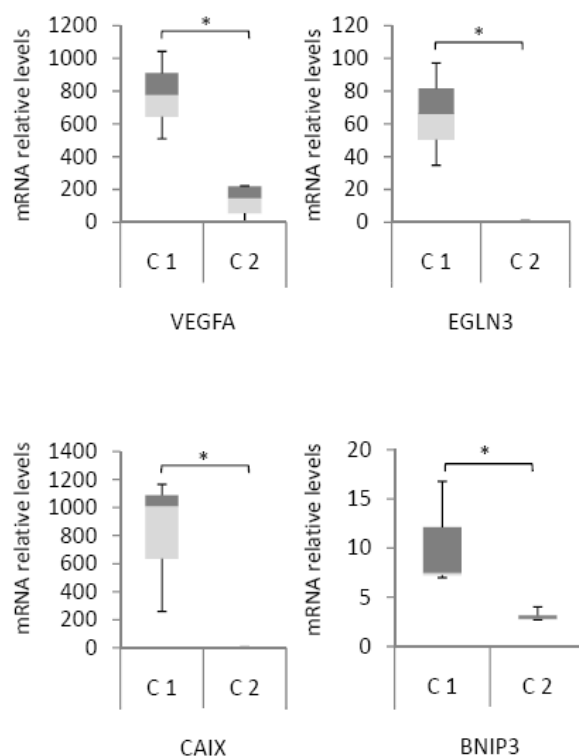


Figure 14. Validation of the microarray data by qRT-PCR analysis of four representative hypoxia-related genes. qRT-PCR was performed for 4 selected genes (*VEGFA*, *EGLN3*, *CAIX*, and *BNIP3*) on 3 C1, and 4 C2-tumors used for microarray analysis. Values for each gene were normalized to expression levels of *cyclophilin A*. Expression values were consistent with the microarray expression data. Values are expressed as mean ratios \pm Standard Deviation (SD) comparing expression in C1 versus C2 tumors. * $p < 0.05$ paired Student's *t* test.

4.3 Relationship between the pseudohypoxic gene signatures of HNPGLs and the *SDH* mutation status

To determine whether the gene expression signature could discriminate between HNPGLs that carry *SDH* mutation from sporadic HNPGLs, global gene expression analysis was performed considering the presence or the absence of germline mutation in *SDH*. As shown in Table 8, 12 HNPGLs of the microarrays study were sporadic and 5 had a germline *SDH* mutation (two *SDHB* and three *SDHD*). PCA analysis performed considering the whole genome showed that *SDH*-related HNPGLs did not segregate from sporadic tumors. PCA analysis was repeated considering only a reduced gene list that included either the most widely investigated hypoxia-related genes or the most differentially expressed genes, but *SDH*-related HNPGLs and sporadics still grouped together. Furthermore, no significantly deregulated genes were found by differential expression analysis of the two types of tumors.

4.4 C1-tumor analysis for somatic mutation in *SDH*

The finding of a pseudohypoxic gene expression signature in tumors lacking *SDH* germinal mutation was striking. To rule out the presence of a mutation in *SDH* at somatic level, that could drive the pseudohypoxic signature, we performed sequencing and MLPA analysis of *SDHC*, *SDHB*, *SDHD*, *SDHA* and *SDHAF2* of the C1 tumors. This analysis revealed neither mutations nor large deletions in tumoral DNA. Several *SDHA* polymorphisms (**79**, **114**) were found (Table 10); they are known and frequent SNPs that we didn't consider as pathogenic. The presence of germline *VHL* mutations were also ruled out in these patients.

Table 10. *SDHA* sequence variants in C1 HNPGLs

SNPs				Tumor Samples			
sequence	Location	Coding Effect	NCBI SNP	PGL2	PGL3	PGL23	PGL47
c.113A>T	Exon 2	p.D38V	rs34635677	No	Yes	No	No
c.309A>G	Exon 3	p.A103A	rs34930948	No	No	No	Yes
c.619A>C	Exon 5	p.R207R	rs6555055	Yes	No	Yes	Yes
c.684T>C	Exon 6	p.N228N	rs2115272	Yes	No	Yes	Yes
c.685G>A	Exon 6	p.G229R	rs41495051	No	No	Yes	No
c.705C>T	Exon 6	p.I235I	rs144513891	No	No	Yes	No
c.723C>T	Exon 6	p.D 241D	rs146653693	No	Yes	No	No
c.891T>C	Exon 7	p.P297P	rs1126417	Yes	Yes	Yes	No
c.1038C>G	Exon 8	p.S346S	rs1041949	No	No	Yes	Yes
c.1170C>T	Exon 9	p.F390F	rs35277230	No	No	Yes	No
c.1680G>A	Exon 13	p.T560T	rs1139449	Yes	No	Yes	Yes
c.1752A>G	Exon 13	p.A584A	rs13070	Yes	No	Yes	Yes
c.1886A>T	Exon 14	p.Y629F	rs6960	Yes	No	Yes	Yes
c.1932G>A	Exon 15	p.V644V	rs6961	Yes	No	Yes	Yes
c.1969G>A	Exon 15	p.V657I	rs6962	Yes	No	No	Yes
c.1974G>C	Exon 15	p.P658P	rs1042446	Yes	No	No	No

4.5 Vascular density of C1-C2-HNPGLs and normal paraganglia.

As we already ruled out the presence of a germline or somatic *SDH* mutation in C1-tumors, we hypothesized that the pseudohypoxic signature of C1-tumors could be driven by the presence of a hypoxic microenvironment. To check this hypothesis an immunohistochemistry of CD34 protein that localizes at blood vessels was performed.

Results revealed that there was no significant difference in vascular density between C1- and C2-tumors (C1: $78 \pm 2,35$; C2: $102,12 \pm 34$; $p=0,173$), sporadic and *SDH*-related tumors (sporadic: $88,9 \pm 22,6$; *SDH*-tumors: $111,6 \pm 41,28$; $p= 0,105$), and normal paraganglia and HNPGLs (NP: 88 ± 10 ; 221 C1+C2 HNPGLs: 95 ± 31 , $p=0,343$). Therefore, although tissue oxygen levels have not been directly determined, the data suggest that the pseudohypoxic signature of C1-tumors is not caused by true hypoxia. On the other hand, tumor angiogenesis does not seem to be different in C1 versus C2-tumors neither in sporadic versus *SDH*-mutants.

4.6 Analysis of HIF-1 α and HIF-2 α protein expression in HNPGL.

The above results indicate that C1-tumors present a pseudo-hypoxic signature that is independent from germline mutation in *SDH* or *VHL* genes, somatic mutation in *SDH* genes or the presence of a hypoxic micro-environment.

To get some insight the cause of the pseudo-hypoxic signature present in cluster C1, an immunohistochemistry for HIF-1 α HIF-2 α was performed. Eight of the 17 HNPGL tissue samples of the microarray study were available for this analysis. Seven samples were of C2-cluster and only 1 was of C1-cluster. HIF-1 α protein accumulation was detected in vascular endothelial cells in both tumor and non-tumor paraganglia and it was use as internal positive control. Neuroendocrine cells of normal carotid body were negative. In contrast, 5 of 8 tissues derived from HNPGLs accumulated nuclear HIF-1 α protein in more than 10% of tumor type I cells. Only one tumor sample, which belonged to C2 cluster, showed a predominant HIF-1 α expression in type II cells as identified by S100/HIF-1 α co-staining (Fig. 15). Although the functional significance of this distinct pattern of cellular staining is presently unknown, the fact that this tumor sample displays a pseudohypoxic gene signature similar to HNPGL tumors showing HIF-1 α staining in type I cells suggests that accumulation of HIF-1 α in sustentacular cells may induce a similar pattern of hypoxic gene expression as in type I cells. Similar to previous reports on other types of tumors (**115**), HIF-1 α -positively stained type I cells were distributed in clusters within the tumor and both, the percentage of cells and the intensity of staining were variable among the analyzed tumor samples. C1-tumor displayed the highest percentage of HIF-1 α positive type I cells (>90%; Figure 15B) whereas C2-tumors showed low levels of expression of HIF-1 α (range between 0% to 40% of positive cells; Figure 15C and D). We did not find accumulation of HIF-2 α in any sample. These data suggest that the pseudohypoxic profile in C1-tumors is mainly driven by HIF-1 α protein.

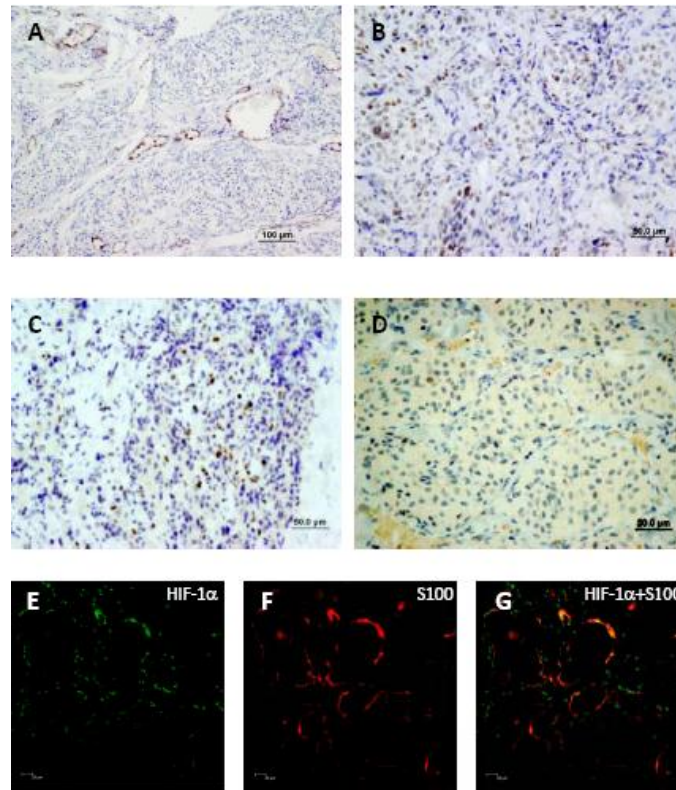


Figure 15. Immunohistochemical analysis of HIF-1 α . (A) Immunostaining of normal carotid body. (B-D) Immunostaining of HNPGL samples (B, tumor of cluster C1; C and D, two independent tumors of cluster C2). Immunostaining is not detected in normal type I and II cells but endothelial cells are HIF-1 α positive. Note that higher levels of nuclear immunostaining of tumor type I cells is detected in the C1-tumor than in the C2-tumors. Original magnifications, x100 (A), x200 (B-D). (E-G) Confocal microscopy images of a C2-HNPGL sample showing that HIF-1 α is predominantly expressed in type II cells in this particular sample (E) HIF-1 α , green fluorescence; (F) S100, red fluorescence; (G) merged image showing colocalization between HIF-1 α and S100 signals.

4.7 Hypoxia related miR-210 is overexpressed in C1-HNPGL.

To get further insight the pseudo-hypoxic signature of C1-tumors we analyzed the putative miRNA associated deregulations. miRNA expression profiling using TaqMan real-time PCR assays technology (TLDA) was conducted on the HNPGL and normal carotid body samples used for the microarray expression analysis described in Table 8. Genome-wide miRNA expression profiling of 369 human miRNAs present in miRBase release 16.0, revealed 15 miRNAs that were found downregulated in all HNPGL versus control samples (fold change >2 and FDR<0.05) (Table 11). MiR-101 have been reported to be downregulated by hypoxia (**116**) whereas there were 4 miRNAs (let-7c,

miR-26a, miR-26b, and miR-125b) that have been describe to be overexpressed in hypoxic condition (117), but were found down-regulated in HNPGLs.

Table 11. List of miRNAs significantly deregulated in HNPGLs in comparison with normal paraganglia

miRNA	p-value	Fold-Change (HNPGLs vs normal)
hsa-miR-26a	4.99E-09	-2.02
hsa-miR-338	2.13E-07	-2.19
hsa-miR-100	2.29E-06	-2.01
hsa-miR-130a	4.77E-06	-2.22
hsa-miR-99a	1.31E-05	-2.32
hsa-let-7c	2.86E-05	-2.2
hsa-miR-125b	5.01E-05	-2.02
hsa-miR-101	7.61E-05	-2.07
hsa-miR-29a	0.0005	-2.04
hsa-miR-26b	0.0007	-2.02
hsa-miR-203	0.001	-2.09
hsa-miR-190	0.0014	-2.45
hsa-miR-142-5p	0.0015	-2.31
hsa-miR-140	0.0018	-2.08
hsa-miR-139	0.0023	-2.99

Analysis of the differential miRNA expression between C1- and C2- tumors revealed that only one miRNA is significantly up-regulated (p value <0.0001) in C1-tumors in comparison with C2-tumors; this is miR210, a well known target of HIF-1 α .

This result was validated by qRT-PCR analysis, confirming the differential expression of miR-210 between C1 and C2 tumors. The correlation of miR-210 with CAIX, one of the hypoxia inducible genes found over-expressed in C1-tumors, was also checked and confirmed (Figure 16).

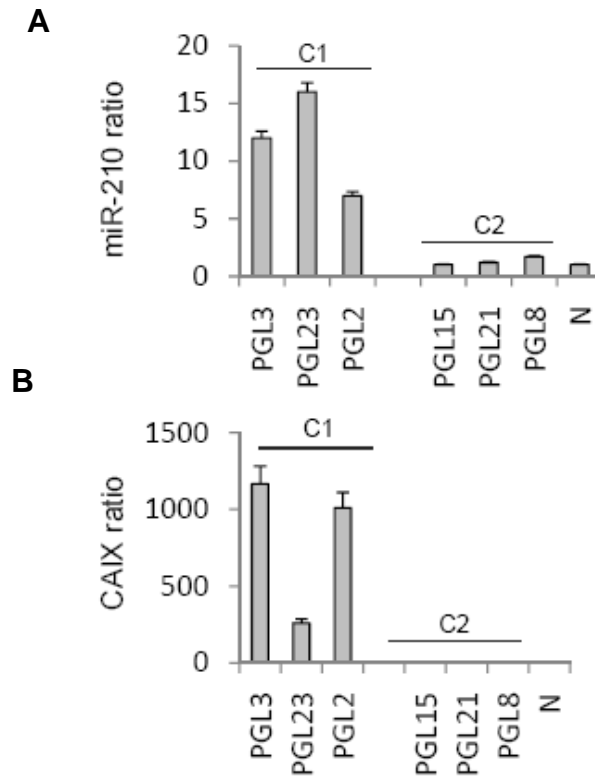


Figure 16. miR-210 over-expression and concomitant CAIX upregulation detected in C1-tumors with HIF-1 α pseudohypoxic gene signature. miR-210 (A) and CAIX (B) mRNA levels were determined by qRT-PCR in RNA isolated from HNPGL tumor samples of clusters C1, and C2, and normal carotid body (N). Values are mean of average \pm SD from triplicate measurement.

4.8 Link between hypoxia/HIF-1 α and *ISCU* and miR-210 expression.

To identify targets of miR-210 we searched for previously reported and validated studies. Among published miR-210 targets, *ISCU1/2* attracted our attention because of its role in mediates the folding of iron-sulfur center in metalloproteins as SDHB which harbor 3 iron-sulfur centers (118, 119). Thus, we postulated that miR-210 could induce the inhibition of *ISCU* and, consequently, an abnormal assembly of SDH complex. To test this hypothesis, we analyzed de mRNA levels of *ISCU1/2* in C1 and C2 tumors. The data revealed that the RNA levels of miR-210 and *ISCU* were inversely correlated in the two clusters of HNPGLs (Fig. 17).

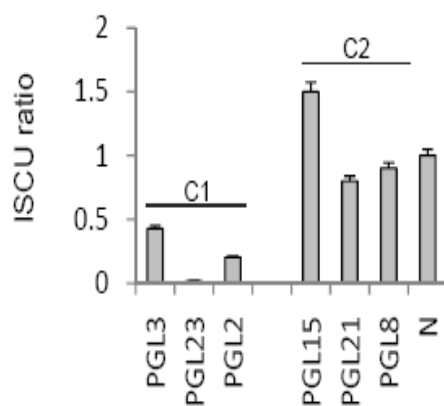


Figure 17. ISCU downregulation in HNPGLs of cluster 1. ISCU mRNA levels was determined by qRT-PCR in RNA isolated from HNPGL tumor samples of clusters C1, and C2, and normal carotid body (N). Values are mean of average \pm SD from triplicate measurement.

We then decided to determine whether the activation of *HIF-1 α* is a mechanism involved in the regulation of miR-210 and *ISCU* in the context of human HNPGL as previously suggested in breast cancer and head and neck squamous cell carcinomas (118, 119). After several attempts, we successfully cultured tumor cells from two independent excises surgically HNPGL tumors (PGL33 and PGL38). The cells lines were synaptophysin negative and S100 positive as the tumor of origin (Fig.18). To induce the accumulation of HIF-1 α protein, HNPGL-derived cells were exposed to hypoxia (1% of oxygen) for 24 hours and the miR-210 expression levels were analyzed in comparison to cell lines maintained in normoxic conditions. As shown in Figure 19, HNPGL-derived cells expressed higher levels of *VEGA* (a hypoxia-regulated gene) in hypoxia than in normoxia, which demonstrated that they maintained the hypoxic response intact. Increased miR-210 and concurrent decreased *ISCU* mRNA levels were also found in PGL33 and PGL38 cells exposed to hypoxia in comparison to the cells exposed to normoxic condition. These data suggest that the accumulation of HIF-1 α and the subsequent over-expression of miR-210 may regulate *ISCU* expression in C1-tumors.

PGL-derived cell lines had a remarkably slow growth-rate that hampered any genetic manipulations to specifically demonstrate the role of HIF-1 α in the miR-210-*ISCU* cellular levels. Therefore, to confirm previous published data showing that upregulation of miR-210 and subsequent downregulation of *ISCU* in hypoxia is HIF1 α -dependent (120), we used a previously characterized hypoxic-responsive cell line, SCC38, derived from head and neck squamous cell carcinomas (29).

SCC38 cells were exposed to normoxia or hypoxia (1% O₂ for 24 hours) in the presence of either HIF-1 α siRNA or control-siRNA. miR-210 expression was enhanced under hypoxic conditions and this effect was specifically reverted by HIF-1 α siRNA (Fig. 19). Inhibition of HIF-1 α expression also reduced miR-210 levels under normoxic conditions corroborating our previous observation of normoxic HIF-1 α accumulation in these cells (106).

As expected, SCC38 cells also overexpressed a well-characterized hypoxic responsive gene, *VEGFA*, in hypoxia conditions in a HIF-1 α -dependent manner. As shown in HNPGL-derived cells, we found that the RNA levels of miR-210 and *ISCU* were inversely correlated in cells exposed to either hypoxia or normoxia. Furthermore, increased *ISCU* and concurrent decreased miR-210 RNA levels were found in SCC38 cells treated with HIF-1 α siRNA under either normoxic or hypoxic conditions. Thus miR-210 and *ISCU* RNA levels are under the control of HIF-1 α .

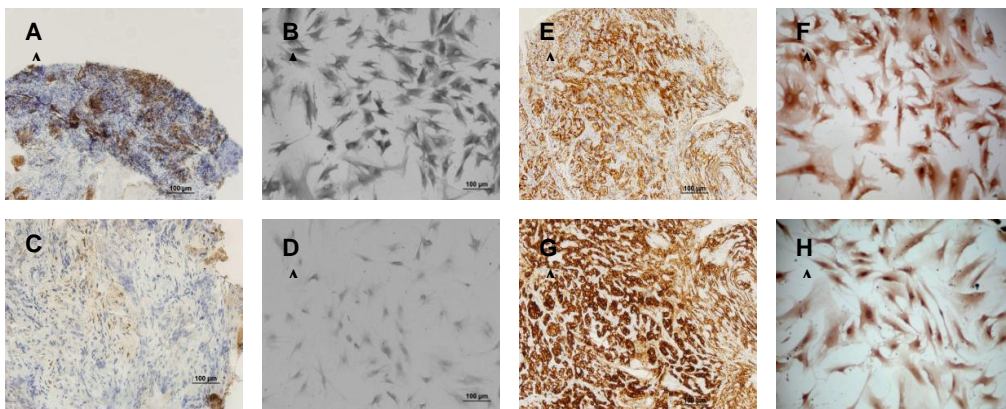


Figure 18. Immunohistochemical analysis of cells lines derived from HNPGLs. (A, E) PGL33 and (B, F) the cell line derived, (C, G) PGL38 and (D, H) the cell line derived were immunostained with synaptophysin (A,B,C,D) and S100 (E,F,G,H).

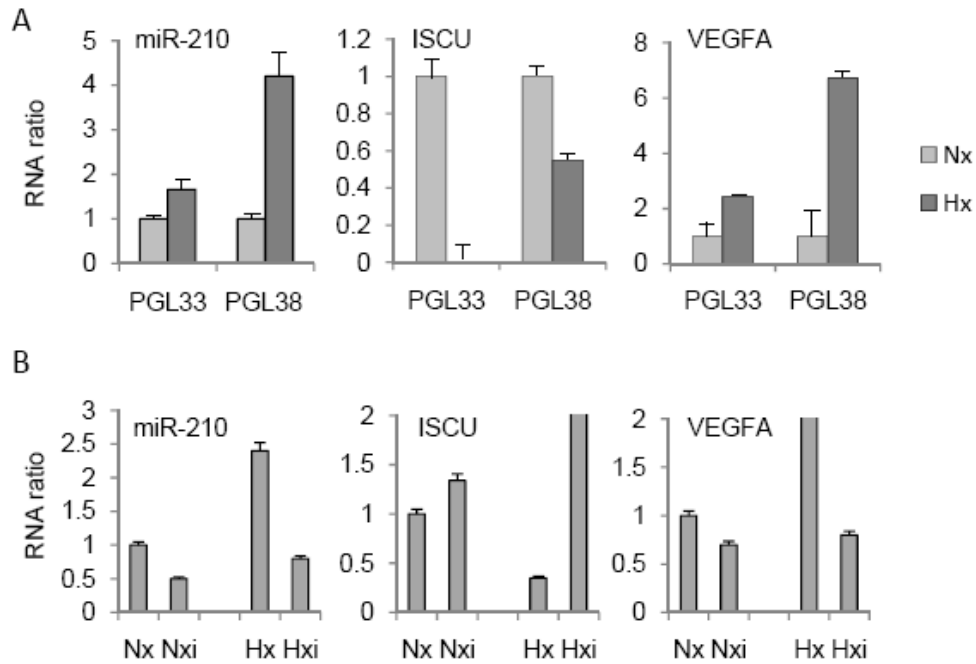


Figure 19. Hypoxia induces miR-210 up-regulation and ISCU downregulation by a HIF-1 α dependent mechanism. (A) Tumor cells isolated from two HNPGLs (PGL33 and PGL38) were exposed to normoxia (21% oxygen) or hypoxia (1% oxygen) for 24 h. The levels of miR-210, ISCU, and VEGFA were analyzed by qRT-PCR. Average fold change values \pm S.D. for 2 separate experiments are represented. (B) SCC38 cells were exposed to hypoxia (24 h at 1% oxygen) or continued in normoxia 72 h after treatment with either HIF-1 α - (Nxi, Hxi) or control-siRNA (Nx, Hx). Values are mean of average \pm S.D. from three independent experiments done in triplicate.

4.9 Identification of negative SDHB immunostaining in association with deregulation of HIF-1 α , miR-210, and ISCU.

ISCU is involved in the formation of iron-sulfur clusters of metalloprotein. These clusters are donors and acceptors of electrons in a variety of biological reactions including mitochondrial respiratory complex I-II electron transport mediated, among other, by SDHB which contains three iron-sulfur-clusters. Thus we hypothesized that ISCU dysfunction could impact on complex II activity.

Recent publications reveal that loss of SDHB protein expression, detected by immunohistochemistry, is a reliable marker of SDH dysfunction caused by *SDH* mutation. Accordingly, tumors from patients with *SDHA*, *SDHB*, *SDHC*, or *SDHD* mutations result in a negative tumoral SDHB immunohistochemistry, while sporadic cases are positively stained with anti-SDHB antibody (121). We therefore analyzed the intratumoral SDHB levels by immunohistochemical analysis in 8 (1 *SDHB*-, 2 *SDHD*-, 5

sporadic-tumors) of the 17 HNPGLs included in the genetic analysis (Table 12) plus three additional samples with *SDHD* germline mutations. One of the sporadic tumors was a C1-HNPGLs whereas the rest of sporadic- and *SDH*-HNPGLs belonged to C2 cluster. In the 6 *SDH*-mutated tumours, a strong cytoplasmic speckled pattern of staining was present in normal cells of the intratumoral inflammatory area and the vascular network whereas SDHB immunoreactivity was either clearly absent or weakly detected in $\leq 10\%$ of tumor cells (Figure 20 and Table 12). Conversely, a strong speckled cytoplasmic perinuclear and sub-membrane immunostaining was detected in 100% of tumor cells in four of the five sporadic samples. Interestingly, the sporadic tumor that has been identified as a C1-tumor, displayed a weaker SDHB immunostaining that was present in only 20-30% of cells, a pattern of staining clearly different from that observed in the other sporadic-HNPGLs. This suggests that HIF-1 α /miR-210/ISCU pathway could be involved in SDHB protein downregulation.

To test this hypothesis, we went back SCC38 hypoxic sensitive cell line to perform *in vitro* study. Scc38 cells were placed under hypoxic condition (1% O₂) for 24 h. Then HIF-1 α , ISCU and SDHB were analyzed at the protein level by western blotting in comparison with normoxic conditions. The data showed an increase of HIF-1 α protein with concomitant decrease of ISCU and SDHB proteins in hypoxia as compared with normoxia (Fig. 21).

Collectively, these data indicate that a canonical hypoxic/pseudohypoxic gene signature could be pathogenically involved in a subset of HNPGLs in the absence of germline and somatic *SDH* mutations. The pseudohypoxic/hypoxic fingerprint is featured by overexpression of HIF-1 α protein and its target genes, upregulation of miR-210, and downregulation of both *ISCU* mRNA and SDHB protein levels.

Table 12. Patient's characteristics and immunohistochemistry results.

Patient	Male/Female	Age at diagnosis (years)	Family history (HNPNGL/PCC)	Tumor site ¹	Tumor size ²	Gene mutated ³	Mutation nucleotide	Mutation protein	Tumor subset ⁴	HIF-1 α IHC ⁵	SDHB IHC ⁶	SDHA IHC ⁶
PGL 2	F	79	No	JT	1	None			C1	UN	UN	UN
PGL3	F	53	No	JT	1	None			C1	UN	UN	UN
PGL 6	M	27	No	JT	3	None			C2	UN	UN	UN
PGL 7	F	55	No	CB	1	SDHB	c.725G>A	p.Arg242His	C2	UN	UN	UN
PGL 8	F	48	Yes	CB	1	SDHD	c.14G>A	p.Trp5x	C2	40	0	UN
PGL 9	F	39	No	V	UN	None			C2	UN	UN	UN
PGL 11	F	49	No	V	3	None			C2	UN	1	1
PGL 14	F	25	No	CB	1	SDHD	c.33C>A	p.Cys11x	C2	10*	0	1
PGL 15	M	32	No	JT	1	SDHB	c.269G>A	p.Arg90Gln	C2	0	0	UN
PGL 18	F	UN	UN	CB	UN	UN			C2	UN	UN	UN
PGL 19	F	66	No	JT	2	None			C2	40	1	1
PGL 21	M	40	No	CB	1	None			C2	0	1	1
PGL 22	F	29	No	JT	2	None			C2	20	1	UN
PGL 23	M	41	No	CB	2	None			C1	90	0	1
PGL 28	M	63	No	T	1	UN			C2	UN	UN	UN
PGL 32	F	29	No	CB	1	SDHD	c.386dupT	p.Leu129fs	C2	0	0	1
PGL 34	F	29	No	JT	UN	None			C2	UN	UN	UN

1 JT, jugulotympanic; CB, carotid body; V, vagal.

2 Tumor size (mm³) was calculated by the ellipsoid volume formula $\pi/6 \times a \times b \times c$ where a,b, and c are the three major diameters (a=width, b=length, and c=depth) of the tumors; 1, small tumors (less than 50 mm³); 2, medium size-tumors (50-100 mm³); 3, large tumors (above 100 mm³).

3 Some tumors did not harbor any mutation and were sporadic (None). UN, no valuable.

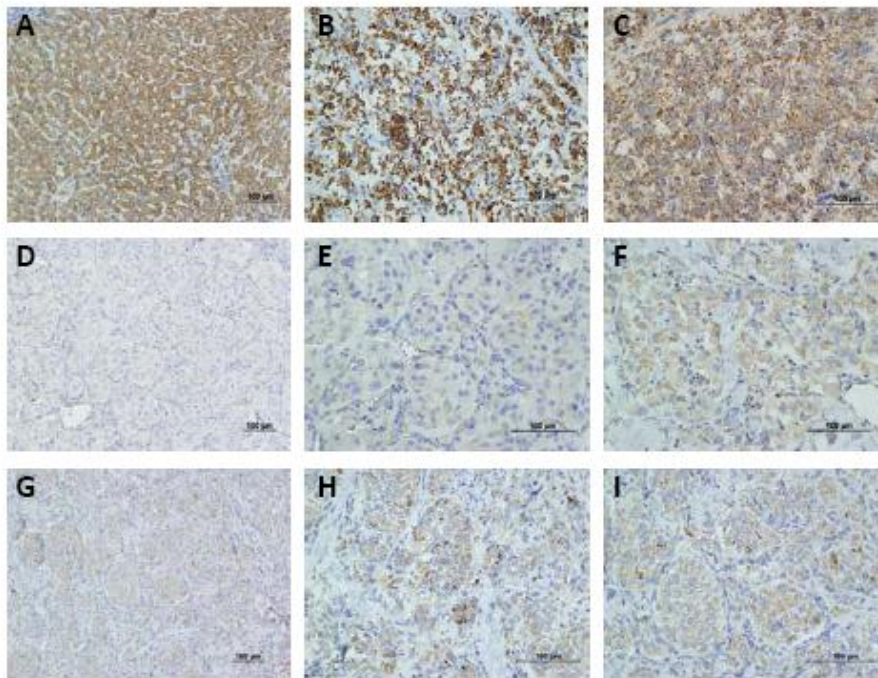


Figure 20. Immunohistochemical analysis of SDHB. (A) Hepatocarcinoma used as positive control. (B and C) Two sporadic C2-HNPNGL samples. (D-F) Two C2-HNPNGLs from patients with germline SDHD

mutation (D and E are different magnifications of the same tumor sample). Strong speckled SDHB immunostaining is observed in sporadic HNPGL whereas C2-HNPGLs from patients with germline SDHD mutations show very weak and diffuse staining. (G-I) Images from one sporadic C1-HNPGL sample. Note that the sporadic C1-HNPGL clearly shows lower levels of immunostaining than the sporadic C2-HNPGLs even in the hot-spot areas (H and I). Original magnifications, x200 (A, D, G), x400 (B, C, E, F, H, I).

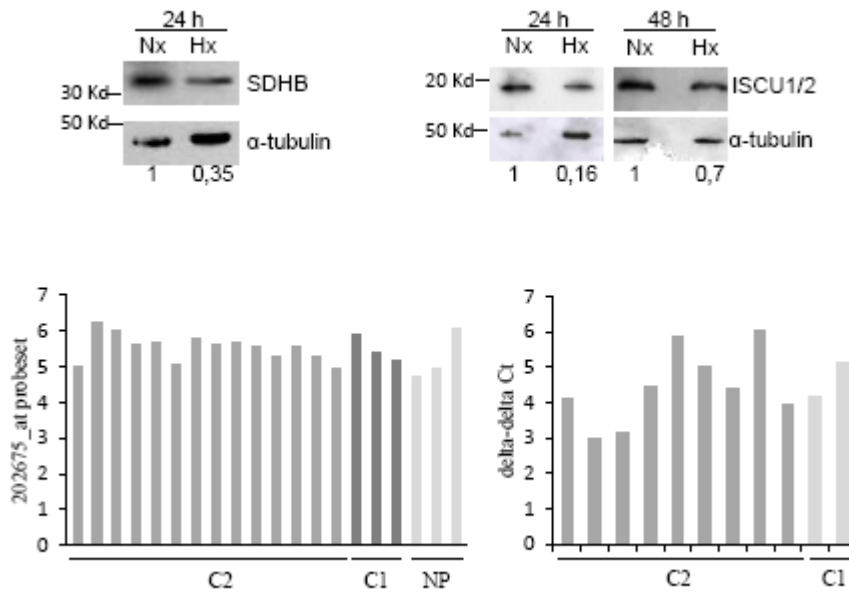


Figure 21. Western blot illustrating that hypoxia condition reduces SDHB and ISCU protein levels. (A, B) SCC38 cells were exposed to normoxia (Nx) or hypoxia (Hx, 1% oxygen) for the indicated times. The membranes were stripped and reprobed with anti- α -tubulin antibody to assure even loading of proteins in each lane. Relative quantities of SDHB or ISCU were determined by densitometry measurements normalized to α -tubulin loading controls. (C and D) SDHB expression values detected by microarray analysis with 202675_at probeset (C) and qRT-PCR (D) in NP, C1, and C2-tumors. As shown, SDHB mRNA levels in NP, C1, and C2-tumors are similar suggesting that SDHB downregulation in C1-tumors is post-transcriptional.

4.10 Validation of the data on HIF-1 α /miR-210/ISCU/SDHB pathway in HNPGLs.

To validate the above data, we used an independent cohort of 12 tumors (Table 13) in which the levels of SDHB, HIF-1 α miR-210 and ISCU mRNA were determined. Among these tumors, only one (PGL47) showed miR-210 up-regulation and concomitant ISCU downregulation, loss of SDHB protein staining and nuclear HIF-1 α protein accumulation (Fig. 22). This sample did not carry either germinal or somatic *SDH* mutations (Table 13). As expected, the rest of the non-*SDH* mutant tumors

showed strong SDHB staining. These data, indicate that PGL47 could be another pseudo-hypoxic tumor similar to those of cluster C1.

Thus far, the data reveal that:

1. A canonical HIF-1 α mediated pseudohypoxia gene signature is not a common feature of *SDH* mutant HNPGLs.
2. A classical HIF-1 α mediated gene/miRNA program may develop in HNPGLs in absence of *SDHx* alteration by a still unknown mechanism.

Table 13. Characteristics of patients included in the extended study.

Patient	Male/Female	Age at diagnosis (years)	Family history (HNPGL/PCC)	Tumor site ¹	Tumor size ²	Gene mutated ³	Mutation nucleotide	Mutation protein	miR-210 ⁴	HIF-1 α IHQ ⁵	SDHB IHQ ⁶	SDHA IHQ ⁶
PGL 44	F	57	No	JT	1	None			0	0	1	1
PGL 35	F	62	No	JT	2	None			0	0	1	1
PGL 52	M	29	No	JT	3	None			0	25	1	1
PGL 47	M	41	No	V	2	None			1	60	0	1
PGL 49	F	63	No	CB	1	None			0	5	1	1
PGL 46	F	41	No	V	1	SDHB	c.761C>A	p.Pro254Leu	0	0	0	1
PGL 55	F	45	No	JT	1	SDHB	c.544_550delGGGCTCT	p.Gly182_Thr183delfsX219)	0	5	0	1
PGL 73	F	67	No	JT	1	SDHB	c.166_170delCCTCA	p.Pro56fs (X5)	0	30	0	UN
PGL 61	M	45	No	CB	2	SDHD	c.374delA	p.Lys125fsX134	0	5	0	1
PGL 56	F	37	Yes	CB	1	SDHD	c.129G>A	p.Trp34X	0	0	0	1
PGL 54	M	44	No	CB	UN	SDHD	c.191_192delTC	p.Leu64ProfsX4	0	0	UN	UN
PGL 36	F	50	UN	JT	1	UN			0	0	1	1

1 JT, jugulotympanic; CB, carotid body; V, vagal.

2 Tumor size (mm³) was calculated by the ellipsoid volume formula $\pi/6 \times a \times b \times c$ where a,b, and c are the three major diameters (a=width, b=length, and c=depth) of the tumors; 1, small tumors (less than 50 mm³); 2, medium size-tumors (50-100 mm³); 3, large tumors (above 100 mm³).

3 Some tumors did not harbor any mutation and were sporadic (None). UN, no valuable.

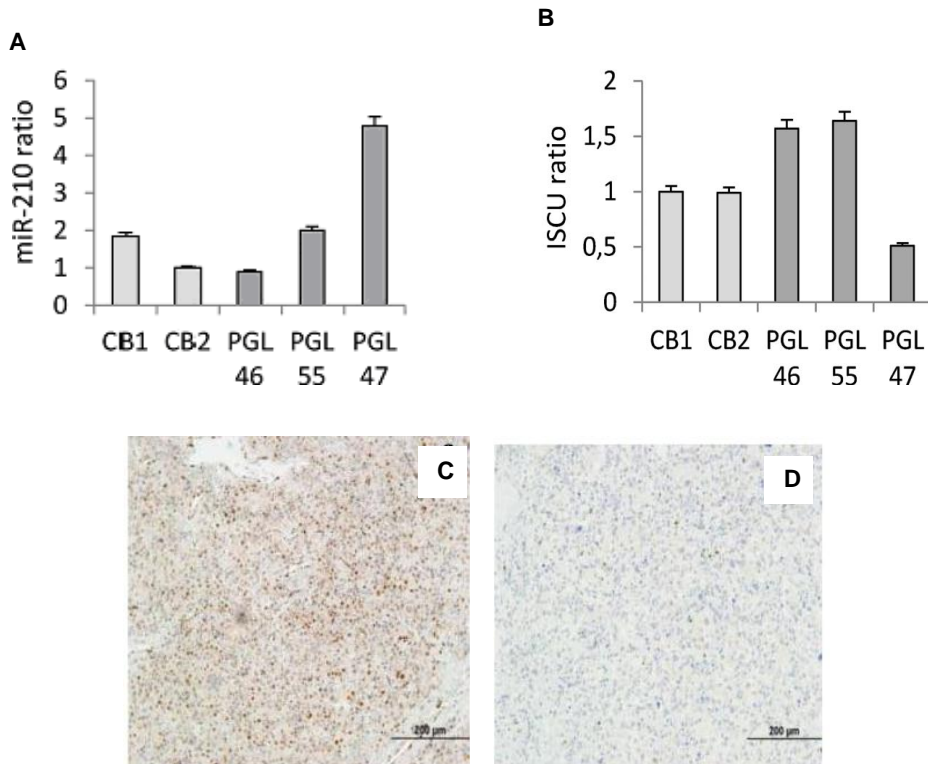


Figure 22. (A, B) q-RT-PCR realized in 2 normal paraganglia (CB1 and CB2) and in HNPGLs of an extended study, observe miR-210 overexpression and concomitant *ISCU* down-regulation in PGL47. (C) HIF-1 α immunohistochemistry realized in PGL47 shows nuclear protein accumulation. (D) SDHB immunohistochemistry realized in PGL47 shows loss of the protein.

4.11 Mecanismos of HIF-1 α upregulation in non-*SDH_x* HNPGLs.

To get some insights into the mechanism involved in the activation of the pseudohypoxic pathway found in the sporadic HNPGLs of cluster C1 (PGL2, PGL3, PGL23) and PGL47, we compared pseudo-hypoxic signature profile found in C1-tumors (Table 14) (18) with the genome-wide transcription patterns reported in genetically defined PCC/PGLs. For this analysis we used a total of 6 gene datasets taken from two recent reports (122, 123). Four of them were from Burnichon et al (122) and included lists of genes specifically over-expressed in tumors that carry mutation in *SDHx*- (list a), *SDHx+VHL*- (list b), *VHL*- (list c), or *RET/NFI/TMEM127*- (list d); and two datasets were from Lopez-Jimenez et al (123) and included lists of genes differentially expressed in tumors that carry either *SDHx+VHL*- versus *RET/NF1* (list e) mutation or *VHL*- versus *SDHB*-tumors (list f) (Suplemetal Table S3).

The comparison shows that there are no commonly deregulated genes between pHx-HNPGLs and either *SDHx*- (list a) or *RET/NFI/TMEM127*-tumors (list b). By contrast, the analysis revealed that the pHx-HNPGLs share some molecular features with *SDHx+VHL*- and *VHL*-tumors (Figure 23). An overlap of 5 and 11 genes was found between pHx-HNPGLs and *SDHx+VHL*-tumors when lists b and e, respectively, were used for comparison. In addition, 7 and 11 gene transcripts were common between *VHL*-tumors (gene lists c and f) and pHx-HNPGLs. Commonly up-regulated genes included targets of the HIF-1 α such as *EGLN3*, *SPAG4*, *SLC2A1*, *ENO1*, *PPFIA4*, *STC2*, and *TMEM45A* suggesting deregulation of pVHL/HIF-1 α signaling pathway in pHx-HNPGLs. Thus, the transcriptional profiles of pHx HNPGLs are more related to both, *SDH*- and *VHL*-PCC/TAPGLs than to *RET/NFI/TMEM127*-PCC/TAPGLs. As we already ruled out the presence of somatic and germline *SDHx* mutations in pHx-HNPGLs (124), it was tempting to speculate that pHx- HNPGLs carry somatic *VHL* gene alterations.

Table 14. List of genes differentially expressed in pHx-HNPGLs versus non-pHx-HNPGLs.

Gene Symbol	p-value	Fold-Change	Gene Symbol	p-value	Fold-Change
CA9	1.28E-08	860,779	EPO	5.51E-03	284,811
COL27A1	3.11E-05	250,103	NAMPT	5.60E-03	239,646
CA12	4.32E-05	221,219	MSH5	6.24E-03	202,335
ZNF395	4.42E-05	282,198	STC2	8.87E-03	3,185
LOX	7.97E-05	101,474	MTCP1NB	8.91E-03	370,347
C7orf68	1.21E-04	959,692	ABCC1	9.84E-03	207,359
BNIP3L	3.29E-04	213,169	EFCAB3	1.15E-02	244,237
SOX4	3.75E-04	263,545	PPP1R14C	1.19E-02	520,584
GBE1	4.29E-04	231,203	FGFR4	1.89E-02	299,698
PPFIA4	5.83E-04	276,147	P4HB	1.93E-02	256,031
EGLN1	6.25E-04	240,024	BNIP3	1.96E-02	366,676
VEGFA	8.18E-04	542,631	MPST	1.97E-02	24,655
EGLN3	8.58E-04	10,909	PLOD1	3.20E-02	25,702
IGFBP5	9.11E-04	648,206	HK2	4.61E-02	696,936
SLC2A1	1.24E-03	518,098	ENO1	5.38E-02	343,922
ALDH4A1	1.31E-03	24,459	PLOD2	1.16E-01	134,237
ABCB1	1.85E-03	-114,069	OGT	2.20E-01	268,189
LOXL2	1.91E-03	411,209	SLC2A5	2.37E-01	903,466
SPAG4	2.25E-03	492,096	SLC6A8	3.92E-01	520,306
TMEM45A	3.51E-03	379,799	ANGPTL4	4.27E-01	7,892
VIM	4.45E-03	544,062	WSB1	4.65E-01	289,705
COL5A1	4.46E-03	357,689	SEC61G	5.33E-01	210,132
DDIT4	4.88E-03	298,886	P4HA1	8.72E-01	321,053

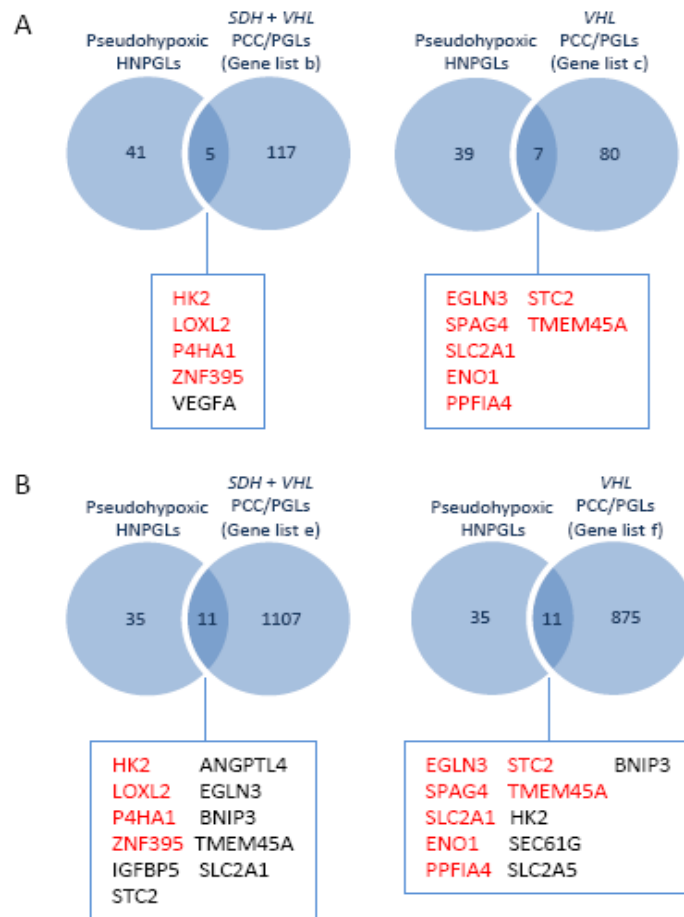


Figure 23. Comparisons of gene expression in pHx-HNPGLs and *SDHx+VHL*- or *VHL*-PCC/TAPGLs. The Venn diagram shows the number of genes differentially expressed in pHx-HNPGLs, and the number of genes identified in 2 previous PCC/TAPGLs studies (A, Burnichon's; B, Lopez-Jimenez's). The genes in common are indicated below the diagram and color-coded (red: genes in common overexpressed in pHx-HNPGLs and PCC/TAPGLs found in studies A and B; black, genes in common downregulated in pHx-HNPGLs and PCC/TAPGLs found in studies A or B).

4.12 Somatic *VHL* mutations in HNPGLs in association with HIF-1 α /miR-210 gene signature.

To assess the contribution of *VHL* in the activation of the HIF-1 α /miR-210 signaling pathway identified in pHx-HNPGLs, *VHL* was sequenced in genomic DNA from tumors and peripheral blood of C1-patients (PGL2, PGL3, PGL23) and PGL47.

A synonymous variant c.552C<T (p.L184L) was found in both, tumor and blood DNA, in one of the patients (PGL47). This likely non pathogenic variant was not a known polymorphism contained in the database of SNPs neither in the TCA Cycle Gene

Mutation Database (125) nor in the 1000 Genomes Project (<http://browser.1000genomes.org/>). We already ruled out the presence of germline sequence variations in the other 3 patients. However, *VHL* sequence analysis in the tumoral DNA of these patients revealed somatic mutations in 2 of them (Table 14). PGL23 carried a missense mutation c.482G>A (p.R161Q) which has been described previously in sporadic PCCs and families with type 2 VHL diseases, characterized by the developing of PCCs, hemangioblastomas and clear cell renal cell carcinomas (ccRCC) (126-128). PGL3 harbored an in-frame microdeletion c.227_229delTCT (p.F76del) known to be responsible for type 1 VHL disease characterized by retinal and central nervous system hemangioblastomas, and ccRCC but not PCCs (129, 130). Mutations were also confirmed by sequencing analysis in tumor cDNAs. We did not find *VHL* somatic variants in PGL2. In this patient and in PGL47, we also ruled out the presence of somatic gain-of-function mutations in *HIF-2 α* , which have been identified in sympathetic PGLs as inducer gene of the pseudohypoxic transcription program (85-89). We neither found somatic mutations in the oxygen-sensing domains of the *HIF-1 α* gene, which could be responsible for HIF-1 α protein accumulation.

We next investigated the copy number dosage of the *VHL* gene by MLPA analysis to determine whether the somatic *VHL* mutations were associated with LOH of the wild type allele. The data revealed that PGL3 with p.F76del mutation carried loss of the wild type *VHL* allele, as a second hit according to Knudson's two-hit model (131). However, no altered *VHL* gene copy numbers were found in the other three pHx-HNPGLs. The MLPA data were confirmed by quantitative PCR in genomic DNA using a sensitive and specific method modified from (108). The lack of LOH at the *VHL* locus in the PGL23 tumor suggests that the p.R161Q variant functions in haploinsufficiency or, alternatively, *VHL* could be methylated in this tumor. However, *VHL* transcription does not seem to be suppressed given that we did not find difference between the normalized values of U133A array *VHL* probe sets in the mutant PGL23 sample versus normal paraganglia.

In summary, we found that two of four pHx-HNPGLs carry a *VHL* gene mutation and in one of them the mutation is accompanied by *VHL* LOH; thus, *VHL* impaired function could be the trigger mechanism of HIF-1 α /miR-210 activation found in a subset of pHx-HNPGLs.

The above assumption implies that *VHL* gene mutations would not be present in non-pHx-HNPGLs. To check this, we extended the *VHL* gene mutation analysis to an

additional series of 49 HNPGLs (29 sporadic, 8 SDHB, 11 SDHD, 1SDHC) that were analyzed for CAIX mRNA level and miR-210 expression, the data revealed that no one over-expressed neither CAIX nor miR-210. In addition, accumulation of nuclear HIF-1 α protein was either not present or detected in less than 25% of type I cells in all tumors except for one sample that showed positive staining in about 40% of cells. However, this tumor did not show over-expression of miR-210 or CAIX (Fig. 24). Overall these data showed that the activation of HIF-1 α /CAIX/miR-210 signaling pathway is present only in a subset of sporadic HNPGLs that carry somatic *VHL* mutations.

Table 14. Clinical and genetic feature of patient included in VHL gene analysis.

Patient ID ¹	Gender (F/M)	Age at diagnosis	Tumor location ²	Benign/malignant (B/M)	Germline SDHx mutation (nucleotide) ³	Germline SDHx mutation (protein)	Germline VHL mutation (nucleotide)	Somatic VHL mutation (nucleotide)	Somatic VHL mutation (protein)
<i>non-SDHx mutant HNPGLs</i>									
2	F	79	JT	B	None	None	None	None	None
3	F	53	JT	B	None	None	None	c.227_229delTCT	p.F76del
23	M	42	CB	B	None	None	None	c.482G>A	p.R161Q
47	M	41	V	B	None	None	c.552C>T	c.551C>T	p.L184L
6	M	27	JT	M	None	None	ND	None	None
9	F	39	V	B	None	None	ND	None	None
19	F	66	JT	B	None	None	ND	None	None
21	M	40	CB	B	None	None	ND	None	None
35	F	62	JT	B	None	None	ND	None	None
52	M	29	JT	B	None	None	ND	None	None
84	F	33	J	B	None	None	ND	None	None
91	F	33	JT	B	None	None	ND	None	None
49	F	63	CB	B	None	None	ND	None	None
88	F	57	JT	B	None	None	ND	None	None
22	F	29	JT	B	None	None	ND	None	None
44	F	57	JT	B	None	None	ND	None	None
66	F	74	UN	B	None	None	ND	None	None
17	M	30	JT	B	None	None	ND	None	None
18	F	67	CB	B	None	None	ND	None	None
24	F	67	JT	B	None	None	ND	None	None
25	F	57	V	B	None	None	ND	None	None
27	F	51	J	B	None	None	ND	None	None
29	M	68	V	B	None	None	ND	None	None
36	F	60	JT	B	None	None	ND	None	None
62	F	45	J	B	None	None	ND	None	None
76	UN	UN	UN	B	None	None	ND	None	None
77	M	29	CB	B	None	None	ND	None	None
79	M	37	JT	B	None	None	ND	None	None
80	M	42	J	B	None	None	ND	None	None
83	M	53	CB	B	None	None	ND	None	None
82	F	51	JT	B	None	None	ND	None	None
89	F	52	CB	B	None	None	ND	None	None
90	M	49	J	B	None	None	ND	None	None
<i>SDHD mutant HNPGLs</i>									
5	F	50	JT	B	c.367G>A	p.Ala123Thr	ND	None	None
71	M	44	CB	B	C.337_340delGACT	p.Asp113Metfsx21	ND	None	None
58	M	39	V	B	c.191_del192delTTC	p.Leu64Profxs4	ND	None	None
12	F	28	J	B	c.386dupT	p.Leu129fs	ND	None	None
14	F	25	CB	B	c.33C>A	p.Cys11x	ND	None	None
32	F	29	CB	B	c.386dupT	p.Leu129fs	ND	None	None
54	M	44	CB	B	c.191_192delTTC	p.Leu64Profxs4	ND	None	None
63	M	36	CB	B	c.190-192dupTC	p.His65Serfsx22	ND	None	None
68	M	25	CB	B	c.337-340delGACT	p.Asp113fsx20	ND	None	None
61	M	45	CB	B	c.374delA	p.Lys125fsX134	ND	None	None
75	M	35	CB	B	UN		ND	None	None

SDHB mutant HNPGLs

81	F	39	JT	B	c.201-?_286+?del	p.?	ND	None	None
86	F	54	J	B	c.79C>T	p.Arg27X	ND	None	None
7	F	55	CB	B	c.725G>A	p.Arg242His	ND	None	None
60	F	40	V	B	c.383insT	p.Leu129fs	ND	None	None
55	F	45	JT	B	c.544_550delGGGCTCT	p.Gly182_Thr183delfsx219	ND	None	None
87	M	44	V	B	c.166_170delCCTCA	p.Pro56Tyrfsx5	ND	None	None
46	F	41	V	B	c.761C>A	p.Pro254Leu	ND	None	None
51	M	29	AB	B	c.-151-?_72+?del	p.?	ND	None	None

SDHC mutant HNPGLs

38	F	27	JT	B	c.21-?_77+?del	p.?	ND	None	None
----	---	----	----	---	----------------	-----	----	------	------

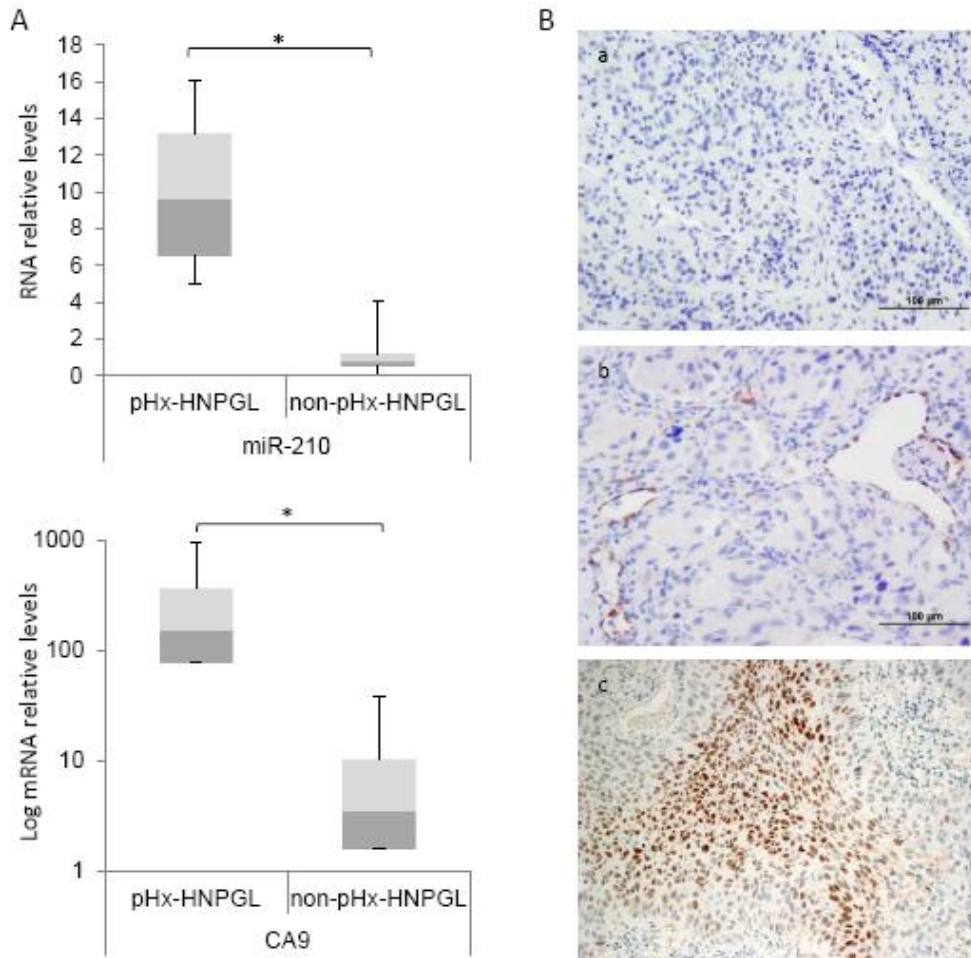


Figure 24. Absence of HIF-1 α , miR-210 and CA9 over-expression in HNPGLs lacking *VHL* gene mutations. (A) Quantitative PCR was performed for miR-210 and CA9 in 29 non-pHx HNPGLs (18 sporadics, 5 *SDHD*-mutants, 5 *SDHB*-mutants and 1 *SDHC*-mutant) and 4 pHx-HNPGLs. Values for CA9 gene were normalized to expression levels of *cyclophilin A*. Values are expressed as mean ratios \pm SD comparing expression in tumors versus a previously identified non-pHx-HNPGL (PGL19). * $p < 0.05$ paired Student's *t* test. (B) Representative images of immunohistochemical analysis of HIF-1 α in non-pHx-HNPGLs (a, b). Endothelial cells are HIF-1 α positive and serve as a positive control. Immunostaining of human head and neck squamous cell carcinoma was used as a positive control (c).

4.13 Oncomine meta-analysis reveals similarities of pHx-HNPGL with ccRCC.

Our data suggests that *VHL* mutations are casuistically involved in the activation of the pHx gene expression phenotype in a subgroup of sporadic HNPGLs which may be a relevant mechanism of tumorigenesis in HNPGLs. Accordingly, it has been described that pF76del and p.R161Q mutations abolish or reduce, respectively, pVHL ability to promote HIF-1 α and HIF-2 α ubiquitylation in vitro (47, 132). However it was surprising that pHx-HNPGLs and *VHL*-PCC/TAPGLS shared only few genes. Of note, only 1.24% and 8.04% of genes deregulated in *VHL*-PCC/TAPGL, as described by Lopez-Jimenez's and Burnichon's studies (122, 123), respectively, were found in the gene expression signature of pHx- HNPGLs. Moreover, *CA9*, one of the most sensitive markers of HIF-1 α activity, was found very highly overexpressed in pHx-HNPGLs but not in *VHL*-PCC/TAPGLs.

However a metanalysis revealed that C1-HNPGLs share feature with *VHL* related clear cell renal cell carcinoma (ccRCC). We compared the pHx profile of HNPGL of cluster C1 with the transcripcion profile reported on other types of cancer deposited in the Oncomine™ integrated cancer profiling database (Oncomine) (48) and we queried the datasets deposited in the Oncomine using a literature defined concept: "Upregulated genes in response to hypoxia and in response to HIF-1 α expression" which included a list of genes reported in literature to be upregulated by hypoxia and in response to HIF-1 α . We found 47 expression microarray datasets having both solid tumor tissues and normal counterparts from 1240 patients affected by 10 types of cancers that have an associated list of genes with the selected concept (odds ratio=2; p value=1E-4; Oncomine analysis). These gene lists were compared with the pHx-HNPGL gene expression profile for overlap. This analysis revealed that clear ccRCC is the cancer type that has the most extensive overlapping with PHx-HNPGLs (Figure 25). 57,9% to 73,7% (65,8% \pm 9,2) of hypoxia-related pHx-HNPGL genes were listed as upregulated in 6 datasets from ccRCC, whereas this percentage was significantly lower when *VHL*-PCC/TAPGL (overlapping: 23.7% \pm 3,7) or other types of cancer (overlapping: <39%) were used for comparison (Table 15). We next analyzed the expression profiles in cancer of each of the genes upregulated in pHx-HNPGLs that are not contained in the above selected Oncomine concept (26 genes including some known HIF targets such as *CA9*, *HK2* and *ENO1*) to unravel whether they are co-expressed with the hypoxia-related genes. A search of the overlap between this list of 26 genes and the lists of top 10% overexpressed genes (p=1E-4, fold change>2; Oncomine analysis) present in the above analyzed Oncomine datasets revealed that, on average, 34% \pm 11.25 of genes

upregulated in pHx-HNPGLs were also found up-regulated in all datasets from ccRCC. This overlapping was significantly higher than that found when comparison was performed with other types of cancers including *VHL*-PCC/PGL with which pHx-HNPGL showed an overlapping of 17,3% \pm 8,6. In summary, this meta-analysis revealed that 44.4% to 53.3% (47.77% \pm 7.9) of both hypoxia-related and -non related genes specifically overexpressed in pHx-HNPGLs are upregulated in ccRCC whereas the overlapping with sympathetic *VHL*-PCC/TAPGLs is significantly lower (19.99% \pm 6.28; $p=0.022$). In addition, comparison of all up-regulated genes in ccRCC across the 6 Oncomine microarray data showed that three of these genes (*C7orf68*, *CA9*, and *VEGFA*) are among the most highly expressed genes in ccRCC similarly to what we found in pHx-HNPGLs.

To further determine whether *VHL* PCC/TAPGLs and *VHL*-HNPGLs activate distinct *VHL*-dependent gene expression programs, the genes dysregulated in *VHL*-PCC/TAPGLs (Supplementary Table 2, lists c and f) and the lists of top 10% overexpressed genes ($p=1E-4$, fold change >2 ; Oncomine analysis) present in the Oncomine microarrays of ccRCC were also compared for overlap. This analysis revealed very little overlapping between *VHL*-PCC/TAPGLs and ccRCC gene expression signatures: at a cutoff of 1 study, 18,39% and 15% of *VHL*-PCC/TAPGL genes contained in lists c and f, respectively, were found in the ccRCC gene expression signature. Taken together, the Oncomine meta-analysis revealed that pHx-HNPGL and ccRCC are more closely related than *VHL*-PCC/TAPGL and ccRCC or pHx-HNPGLs, and thus, that alteration of the *VHL* gene have a significant role in tumorigenesis of some sporadic HNPGLs through the activation of a gene expression program similar to that of ccRCC.

Table 15. OncoPrint meta-analysis showing the overlapping of the gene expression signature found in pHx-HNPGL (hypoxia and non-hypoxia related genes) with that of cancers from other tissues.

Cancer tissue	Overlap median% (SD)	p-Value*
Kidney	47,4 (7,90)	
Brain	31,10 (11,65)	0,011
Breast	14,06 (4,62)	1,41E-04
Colorectal	20,44 (5,53)	6,23E-05
HNSCC	17,77 (9,16)	3,44E-05
Esophageal	19,99 (8,00)	8,93E-04
Gastric	11,10 (2,72)	2,26E-06
Pancreatic	18,33 (6,63)	1,55E-04

4.14 VHL mutation is involved in the activation of the hypoxia signaling via HIF-1 α .

To get further inside the role of *VHL* in the activation of the HIF-1 α /miR-210 signaling pathway we used two cell lines, RCC4 and 786_O, that lack functional pVHL (RCC4[-] and 786_O[-]) and their derivatives obtained by stable transfection with a vector expressing pVHL (RCC4[+] and 786[+]) to analyze the role of VHL in the miR-210 expression. Previous reports showed that RCC4 cells express HIF-1 α and HIF-2 α , while 786_O cells only express HIF-2 α (133).

We performed immunocytochemistry to confirm that 786_O(-) do not accumulate HIF-1 α in normoxia; surprisingly we found a faint nuclear accumulation of HIF-1 α in 786(-) cells exposed to hypoxia (1% O₂), suggesting that this cells express low amount of immunoreactive HIF-1 α . As expected RCC4(-) cells constitutively accumulate HIF-1 α in normoxia and no higher accumulation of this protein was observed in hypoxia. In contrast, HIF-1 α accumulation in RCC4(+) is observed only when cells are exposed to hypoxic condition (Fig. 26A).

We analyzed miR-210 and CAIX mRNA expression levels in these cell lines exposed to hypoxic or normoxic condition. Results show that RCC4(-) cells expressed 10-fold higher levels of miR-210 than RCC4(+) in normoxic conditions (Fig. 26B), while both over-expressed miR-210 in hypoxic conditions. By contrast, the levels of miR-210 were only slightly higher (1.4-fold higher) in 786_O(-) than 786_O(+) exposed to normoxia. In hypoxic conditions we observed the same subtle accumulation of miR-210 in 786_O(-) and in 786_O(+). CAIX mRNA levels were not detectable in 786_O(+)/(-) cell lines. As expected we found over-expression of CAIX in RCC4(-) respect to RCC4(+) exposed

to normoxia. No further accumulation was observed when cells were exposed to hypoxia (Fig 26).

These data indicate that the lack of functional pVHL induce over-expression of miR-210 and CAIX in presence of HIF-1 α , however HIF-2 α is not sufficient to activate this signaling pathway.

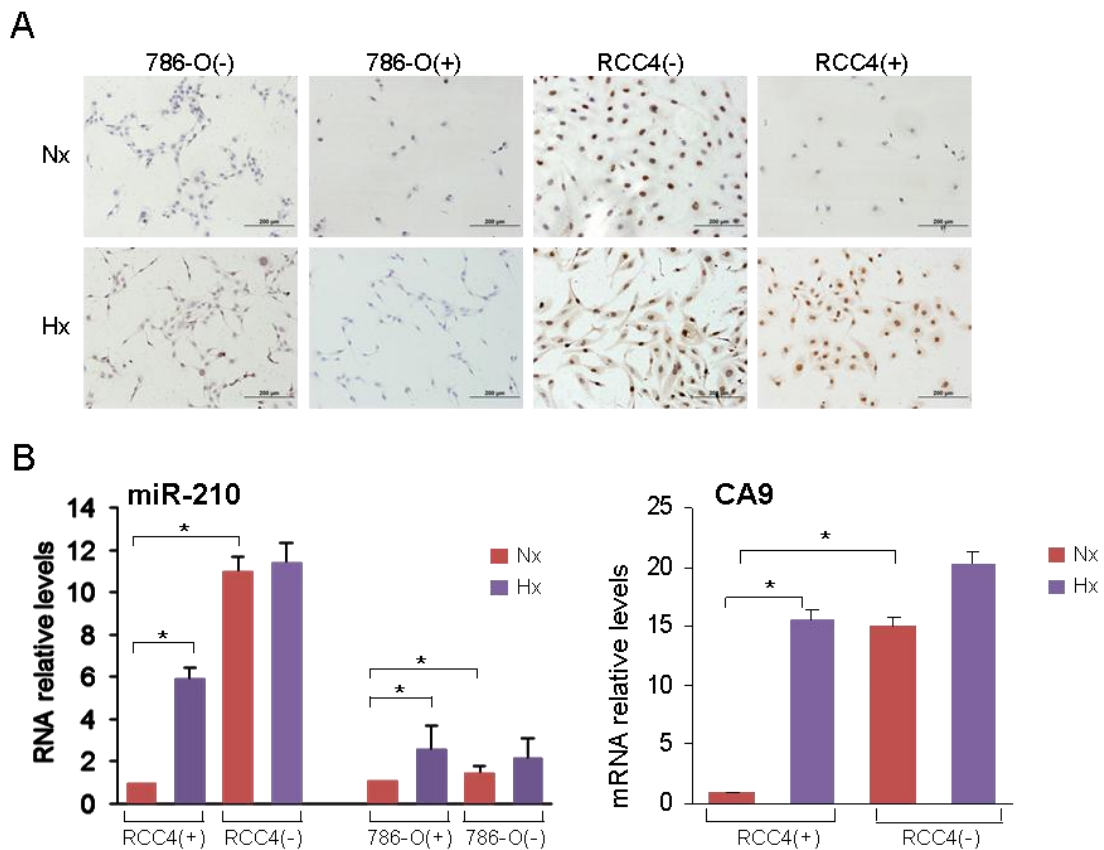


Figure 26. The miR-210 and CA9 RNA levels in *VHL*-deficient cells. A, HIF-1 α immunocytochemical analysis of RCC4 and 786-O cells lacking (-) or overexpressing (+) functional pVHL. Cells were incubated under normoxic (Nx) or hypoxic (Hx) conditions (1% O₂ for 12 hours) before immunostaining. B, The miR-210 and CA9 RNA were quantified by RT-qPCR in the indicated cell lines after incubation under normoxic or hypoxic (1% O₂, 12 hours) conditions. *, $P < .05$, unpaired t test.

4.15 pVHL loss of expression and *VHL* deletion do not activate HIF-1 α /CAIX pathway in HNPGL.

Decrease pVHL gene function results in loss of HIF-1 α degradation during normal oxygen conditions (pseudohypoxia). Surprisingly, as previously described, we found accumulation of HIF-1 α and over-expression of HIF-1 α target genes, miR210 and CAIX (mRNA levels), only in two tumors that carry *VHL* somatic mutation but not in any other

ones, including those carrying *VHL* gene deletions or decreased protein expression; we decided to re-evaluate HIF-1 α immunohistochemistry and analyze CAIX expression at the protein level in 31 HNPGLs to find potential, even subtle, differences between samples with or without *VHL* gene deletions or samples with different pVHL protein expression levels. Nuclear immunostaining of HIF-1 α was detected in 10 (32%) samples, cytoplasmic staining was not detected in any of the samples, we quantified the percentage of positive nuclei as well the intensity of staining and compared to pVHL expression. We found that HIF-1 α protein positive expression (measured as percentage of positive cells or as weak, medium or strong intensity) did not correlate with pVHL loss of expression ($P= 0.901$) or *VHL* gene deletions. On the other hand, CAIX immunostaining was not detected in any of the analyzed samples as expected by the previous analysis of CAIX transcript levels. As a positive control for CAIX expression, CAIX immunohistochemistry was performed in PGL23 carrying *VHL*-mutation (p.R161Q) and displaying a pseudohypoxic gene signature featured, among others, by high mRNA levels of CAIX. As expected, high membranous immunoreactivity was detected in this sample (Fig. 27). Collectively, the data indicate that a HIF-1 α /miR-210-CAIX gene signature is not activated by pVHL decreased expression in HNPGLs.

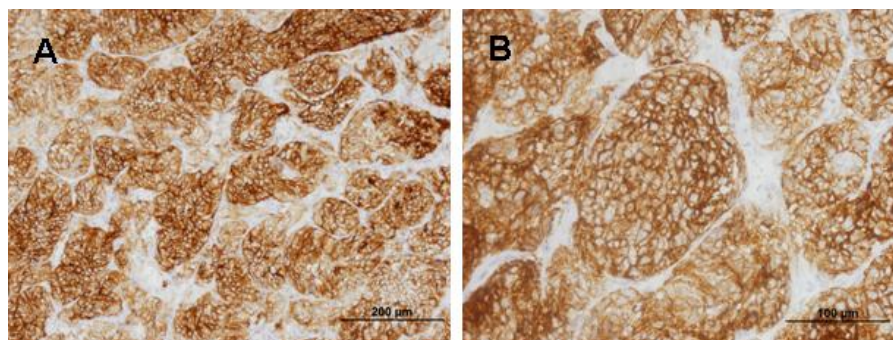


Figure 27. CAIX immunohistochemistry in PGL23 that present the higher mRNA level of CAIX and show activation of the pseudohypoxic pathway. (A) 10X magnification and (b) 20X magnification, observe high accumulation of CAIX in cytoplasm.

4.16 HIF-1 α is required for miR-210 over-expression.

We also explored the role of HIF-1 α in miRNA-210 expression *in vivo*. To this end, we obtained adrenal medulla and kidney from HIF-1 α flox Cre-ERTM mouse exposed to hypoxia (x% O₂ for 30 days). As a control, we also analyzed the mRNA levels of *EGLN3*, a HIF-1 α target gene. miR-210 and *EGLN3* mRNA levels were significantly lower in adrenal gland derived from HIF-1 α ^{-/-} than in HIF-1 α ^{+/+} mice. This is in agreement with our *in vitro* data. In contrast to this data, no differences in *EGLN3* or

miR-20 expression were detected in kidney indicating that adrenal gland and kidney respond differently to HIF-1 α deletion (Fig 28).

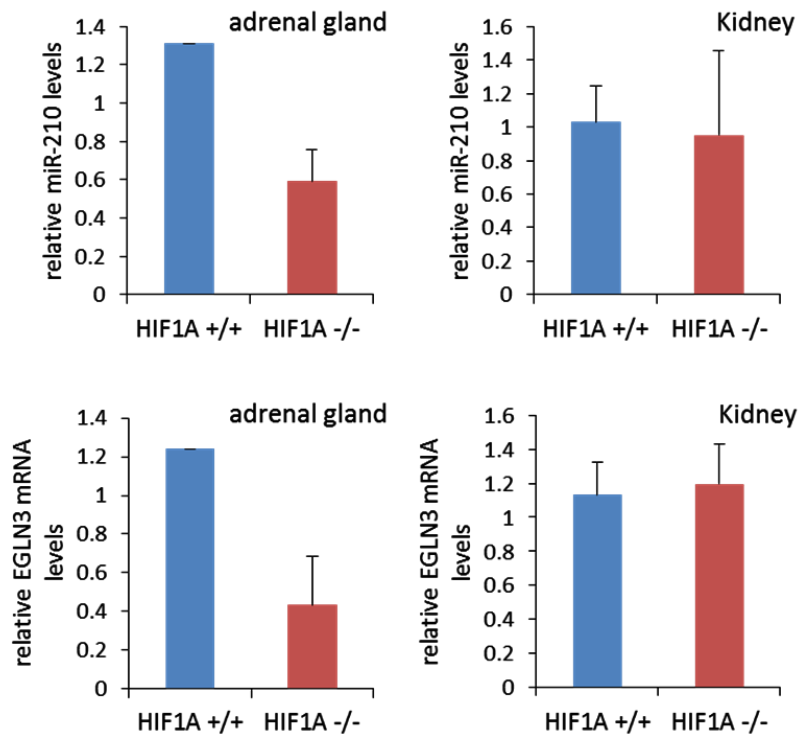


Figure 28. The miR-210 and *EGLN3* mRNA levels in HIF-/- mouse exposed to hypoxia. The miR-210 and *EGLN3* RNA were quantified by RT-qPCR in the indicated sample derived from mice exposed to hypoxic condition (Y %, X hours) conditions. *, $P < .05$, unpaired t test.

4.17 VHL mutation F76del activates HIF-1 α /CAIX/miR-210 pathway.

Thus far, our data indicate that HIF1- α is a key molecule for miR-210 over-expression. In addition, *VHL* mutation and the complete absence of pVHL seemingly activate the hypoxia pathway. However partial decrease of *VHL* seems to be not sufficient to activate the hypoxia pathway, as none of the HNPGLs carrying *VHL* gene partial deletions present over-expression of miR-210 or *CAIX*. To get further insight into the role of *VHL* in the activation of the hypoxia signaling pathway, we decided to inhibit *VHL* expression using specific siRNAs in SCC42B cells. A 80% less *VHL* mRNA was found in the cells transfected with *VHL* siRNA with respect to cells transfected with control siRNA (Fig 29 A). In contrast to our previous data in RCC4 cells, no over-expression of miR-210 was detected with decrease levels of *VHL* (Fig 29 B and C). By contrast *CAIX* mRNA levels increased about 6-fold in cells transfected with *VHL*-siRNA.

This level of over-expression was considerably lower than that observed by hypoxia (about 60-fold, data not shown). We confirmed that HIF-1 α accumulated in cells with decreased levels of pVHL. However, this does not seem to be sufficient to fully activate the pHx gene signature.

Then we used “Geneart site-direct mutagenesis system” (Invitrogen) to generate a plasmid carrying *VHL* p.F76del gene mutation and transfected it into SCC42B cells. We use LifeAct plasmid as a control of the transfection, as well as a plasmid encoding wild type pVHL as normal reference. miR-210 and CAIX were over-expressed in SCC42B cells transfected with plasmid carrying *VHL* mutation in comparison with cells transfected with plasmid carrying normal *VHL* (Figure 29 D and E). We perform a western blot to analyze if HIF-1 α was activated in the cells transfected with *VHL* mutated (p.F76del) and we incubated the transfected cells in normoxic and hypoxic condition (1% O₂ for 24 hours) to check the hypoxic response in presence of *VHL* mutation; we used cells transfected with *VHL* wild type and no transfected cells as control. Western blot analysis reveal that HIF-1 α accumulated by the expression of p.F76del *VHL* in normoxic as well hypoxic conditions. As expected, cells transfected with wild type pVHL accumulate HIF-1 α under hypoxic but not normoxic conditions. These data show that the p.F76del mutation is responsible for the activation of the pseudo-hypoxic pathway in PGL3.

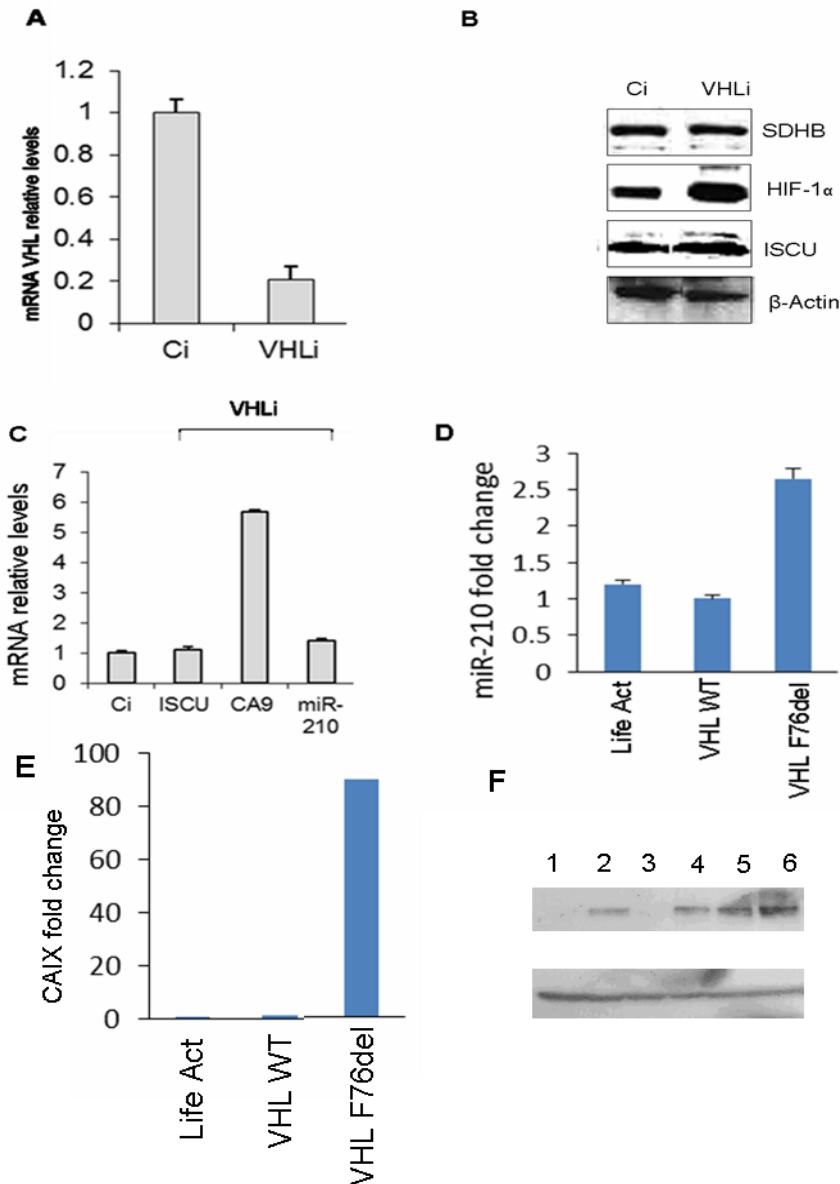


Figure 29. (A) SCC42 transfected with *VHL* siRNA (VHLi) and control SiRNA (Ci). VHLi transfected cells present 80% less *VHL* mRNA in comparison to cells transfected with Ci. (B) Western blot showing over-expression of HIF-1 α in SCC42 transfected with *VHL* siRNA (VHLi) in comparison to cells transfected with control siRNA (Ci), no diminution of SDHB or ISCU protein were observed. (C) miR-210 and CA9 RNA levels in SCC42B cells transfected with VHLi and Ci, observe no over-expression of miR-210 in presence of *VHL* inhibition, while there is a little over-expression of CAIX. (D) miR-210 and (E) CAIX RNA levels in SCC42B cells transfected with lifeAct (control of transfection), plasmid carrying normal *VHL* (VHL-WT) and plasmid carrying *VHL* with F76del mutation (VHL-F76del), observe the over-expression of miR-210 and CAIX, furthermore CAIX mRNA levels are higher in SCC42B transfected with plasmid carrying *VHL* mutated than in SCC42B cells transfected with *VHL* interference. (F) Western blot showing HIF-1 α protein accumulation in (1) control SCC42B cells no transfected in normoxic condition, (2) SCC42B cells transfected with plasmid carrying *VHL* mutated (VHL-F76del) in normoxic condition, (3) SCC42B cells transfected with plasmid carrying wild-type *VHL* (VHL-WT) in normoxic, (4) control SCC42B no transfected in hypoxic condition (1%O₂ for 24 h), (5) SCC42B cells transfected with plasmid carrying *VHL* mutated

(VHL-F76del) in hypoxic condition (1%O₂ for 24 h), (6) SCC42B cells transfected with plasmid carrying wild-type *VHL* (VHL-WT) in hypoxic condition(1%O₂ for 24 h).

To analyze the localization pVHL, we perform an immunofluorescence of pVHL in cells transfected with the plasmid that carry *VHL* mutation, using cell transfected with the plasmid carrying wild type *VHL* as control. Results show that pVHL localize in the cytoplasm and no difference between mutated vs wild-type *VHL*- transfected cells were observed (Fig. 30).

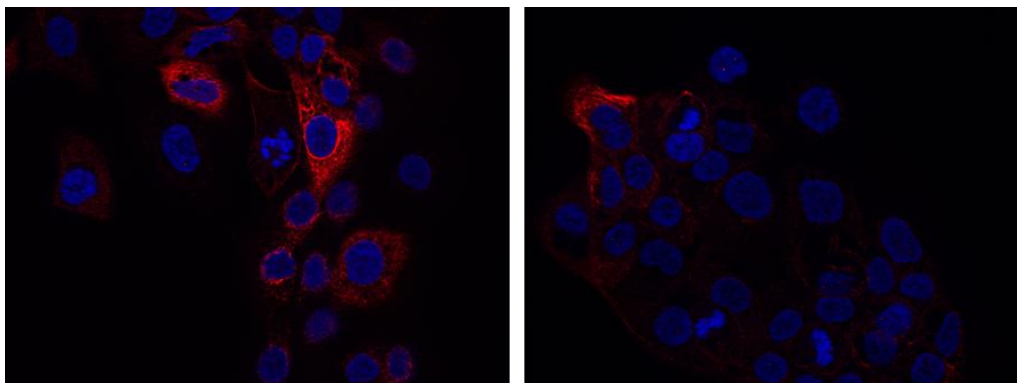


Figure 30. pVHL immunofluorescence in SCC42B transfected with (A) plasmid carrying wild type *VHL* and (B) plasmid carrying *VHL* with F76del mutation. pVHL localized in the cytoplasm of both transfected cells.

4.18 Loss of *SDH* does not activate the hypoxic pathway.

The microarray results show no activation of the hypoxic pathways in the presence of *SDH* mutation in HNPGLs. To analyze the role of *SDH* and *VHL* in the pathogenesis of HNPGLs, we decided to inhibit *SDH* using activity by using thenoyltrifluoroacetone (TTFA) in four cell lines: RCC4-, RCC4+, 786_OpRV- and 786_OpRV-*VHL*.

No difference in cell survival in cells treated with DMSO and TTFA was observed. We analyzed miR-210 and CAIX expression levels by RT-qPCR. As previously showed, cells lacking pVHL, but expressing normal levels of HIF-1 α (RCC4-), displayed over-expression of CAIX and miR-210 in comparison with cells expressing normal pVHL (RCC4+). This was not observed in 786-OpRV- cells that lack HIF-1 α in addition to pVHL, indicating that the complete loss of *VHL* activate the hypoxic pathway via HIF-1 α . However the inhibition of *SDH* induced by TTFA, did not activate the hypoxia pathway based on the absence of over-expression of miR-210 and CAIX (Fig. 31). Thus, our data suggest that inactivation of *SDH* complex is not involved in the induction of the hypoxia pathway in HNPGLs and in these cell lines.

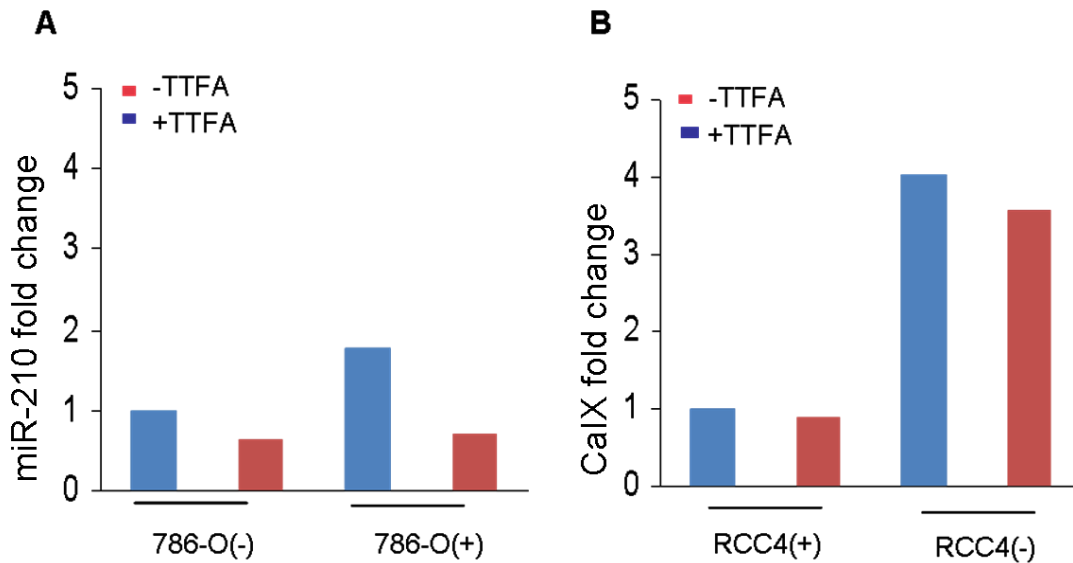


Fig. 31 The miR-210 and Ca9 mRNA levels in 786_O+/- and RCC4+/- exposed to TTFA. The miR-210 and CaIX RNA were quantified by RT-qPCR in the indicated sample. We do not observe over-expression of miR-210 or CaIX in presence of TTFA. *, $P < .05$, unpaired t test.

4.19 Analysis of VHL gene alteration in HNPGLs.

We described the presence of somatic VHL gene mutations in a small proportion of sporadic HNPGLs in association with activation of a HIF-1 α /miR-210 signaling axis which can potentially impact on the SDH function by the inhibition of ISCU1/2. This encouraged us to perform a comprehensive study of the alterations of the VHL gene in HNPGLs to explore its potential involvement in HNPGLs development. VHL DNA copy number, mRNA and protein expression data were generated from 58 HNPGLs tumor tissues. The clinical characteristics of this cohort have been previously reported and are presented in Table 14. As previously described, mutational analysis performed in this series of non-hypoxic HNPGLs cases did not reveal any point mutations or small insertions/deletions of the coding or splice-site regions of VHL gene at somatic level.

We firstly searched for VHL-intragenic deletions using the multiplex ligation-dependent probe amplification (MLPA) assay. The analysis identified 7 samples exhibiting VHL deletions of exon1 (Fig. 32). This was significantly observed in sporadic- (7/32, ~22%) but not in SDH-mutated HNPGLs (0/26), ($P = 0.011$).

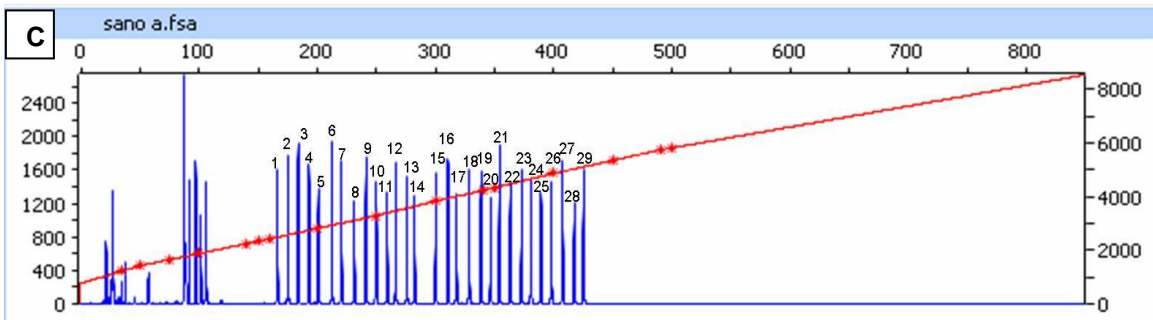
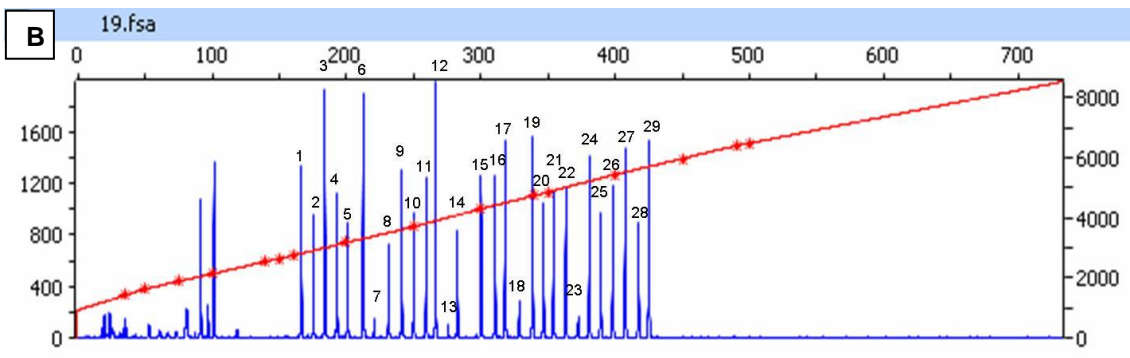
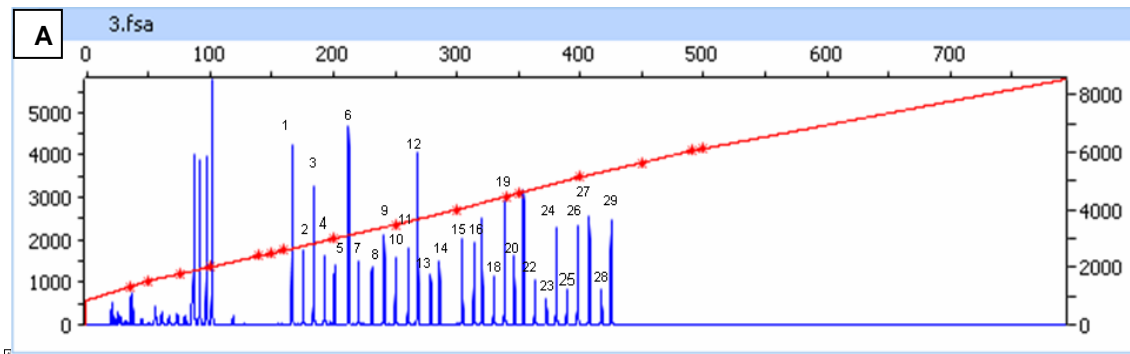


Figure 32. examples of MLPA graphics showing the expression levels of each probes in 3 samples, each peak corresponding to a probe as follow:

1. 166 Reference probe 09890-L10303 16p13
2. 175 **VHL probe** 13624-L16363 Exon 2
3. 184 *CNTN6* probe 06307-L05830 3p26.3
4. 193 *BRK1* probe 14676-L16328 3p25.3
5. 201 **VHL probe** 02390-L16140 Exon 2
6. 211 Reference probe 13450-L14905 5q31
7. 219 ± **VHL probe** 01626-L01211 Exon 1
8. 229 *IRAK2* probe 02264-L01750 3p25.3
9. 238 *MLH1* probe 00892-L00480 3p22.1
10. 247 **VHL probe** 01162-L00718 Exon 3
11. 256 Reference probe 01055-L00628 17q21
12. 265 Reference probe 02454-L01898 15q21
13. 274 **VHL probe** 01628-L01213 Exon 1

14. 283 *FANCD2* probe 02138-L01631 3p25.3
15. 301 *GHRL* probe 02266-L01752 3p25.3
16. 310 *FANCD2* probe 02140-L01633 3p25.3
17. 319 Reference probe 05981-L05406 20p12
18. 328 **VHL probe** 13625-L15079 **Exon 1**
19. 337 Reference probe 01082-L00660 22q11
20. 346 Reference probe 01335-L00879 7q11
21. 355 Reference probe 00547-L00116 11q22
22. 364 *BRK1* probe 14675-L16327 3p25.3
23. 373 **VHL probe** 01158-L13266 **Exon 1**
24. 382 Reference probe 00973-L00560 10q21
25. 391 **VHL probe** 13322-L14735 **Exon 2**
26. 400 Reference probe 00801-L00639 13q14
27. 409 Reference probe 00669-L00373 11p13
28. 418 ‡ **VHL probe** 01161-L00717 **Exon 3**
29. 427 Reference probe 00680-L00121 7q34

(A) MLPA of PGL3 showing that *VHL* gene is completely deleted; (B) MLPA of PGL19 showing the deletion of *VHL* exon1; (C) MLPA of normal sample.

VHL exon deletions were confirmed by quantitative PCR performed by an optimized protocol taken from (108) (Fig 33). We also realized CGH arrays (aCGH) enriched in probes on tumor suppressor genes which included *VHL*. This was done in two tumors (PGL6 and PGL62). As shown in Figure 34, the aCGH showed a more extensive deletion including the whole chromosome 3. On the contrary, no altered copy number variants were detected in PGL62 by aCGH thus confirming results from MLPA and qPCR data.

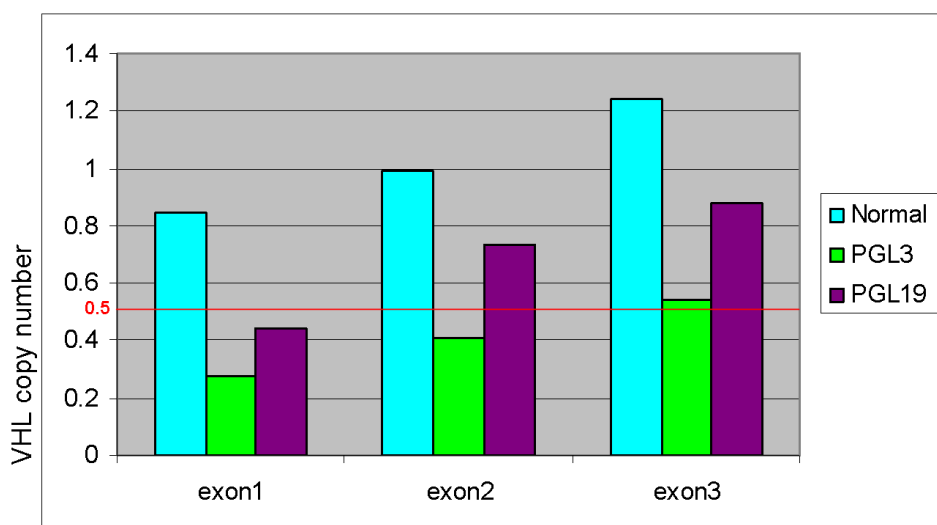


Figure 33. *VHL* copy number status determined by q-PCR optimized protocol from (37). For normalization of the relative quantities, the *VHL* copy numbers were divided by the geometric mean of the reference *GPR15* copy number. Using this method, a haploid copy number of 1 is expected for a normal sample and a value of 0,5 for a sample with a *VHL* deletion. Normal sample in blue show no variation of *VHL* copy number, PGL3, in green, show deletion of the exon1 and exon2, while exon3 is on the borderline of deletion, this is could be due to normal cell contamination in the tumor. PGL19, in purple, present deletion of exon1.

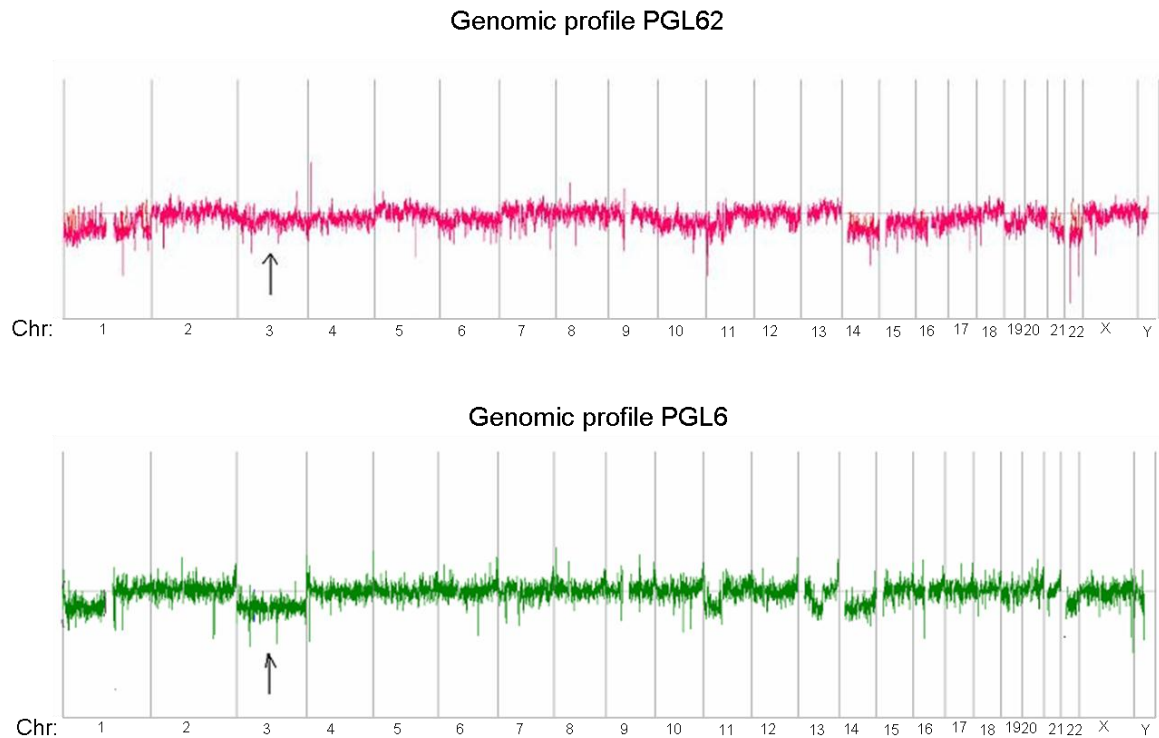


Figure 34. Overview of CGH analysis arrays. Genomic profile of PGL62 in red: chromosome 3, indicated by an arrow, is not deleted. Genomic profile of PGL6 in green: chromosome 3, indicated by an arrow is deleted.

We next analyzed the mRNA levels of *VHL* by RT-qPCR in 36 samples to compare the *VHL* expression between tumor samples with and without altered *VHL* copy number. As a control for evaluation of decreased *VHL* expression, we quantified *VHL* mRNA levels in PGL3, which carry *VHL* gene mutation (p.F76del) and loss of the wild type *VHL* allele. cDNA obtained from blood and a normal paraganglia were used for normalization of the data. As expected, a ~70% less transcript levels were detected in PGL3 in comparison with normal paraganglia. Decreased *VHL* transcript levels were also encountered in tumors with loss of *VHL* exon 1 in comparison with those tumors with normal copy number. However, only a trend towards statistical significance ($P=$

0.073) was observed likely because of variable presence of normal non-tumor cells in the tissues.

We therefore assessed whether pVHL protein expression was altered in HNPGLs carrying decreased *VHL* gene copy number. pVHL protein expression could be evaluated by immunohistochemistry in 35 tumors including 4 tumors carrying *VHL* gene deletions. Diffuse cytoplasmic staining either weak or strong was observed in 19 (~54%) samples. Among the group of tumors with *VHL* gene deletions, we found absence of immunostaining in one tumor and very weak immunoreactivity in another tumor whereas the remaining 2 tumors showed more intense cytoplasmic staining. However, in contrast with other positively stained samples, these two tumors showed positive strong nuclear immunoreactivity in addition to the cytoplasmic staining (Fig.35). Interestingly, nuclear staining was also observed in PGL3 which carry p.R161Q *VHL* somatic mutation. Interestingly, this immunohistochemical study also revealed that an unexpected high proportion of HNPGLs lacking *VHL* gene alterations had negative pVHL protein immunoreactivity (16/35, ~46%). Considering the total number of tumors with no alterations of the *VHL* gene (n=31), absence of pVHL immunoreactivity was found in both sporadic (5/11, 45.45%) and *SDH*-HNPGLs at similar frequency (11/20, 55%). Thus, *VHL* gene deletions and mutations could be responsible for the loss of pVHL protein expression or nuclear pVHL localization in some HNPGLs; while other still unknown cellular processes are involved in the silencing of pVHL in others.

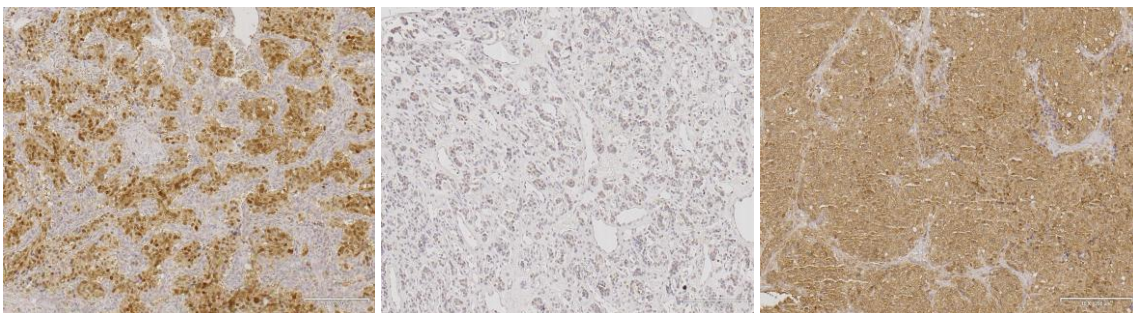


Figure 35. pVHL immunohistochemistry in 3 HNPGLs; a) nuclear and cytoplasmic stain (b) negative staining (c) cytoplasmic stain.

Given that, in addition to structural *VHL* alterations, gene hypermethylation may be involved in tumor suppressor gene inactivation, we analyzed CpG methylation status of 2 regions on the *VHL* promoter in 12 tumors, 7 of which lacking pVHL immunoreactivity and 4 showing weak immunostaining; DNA from 5 normal human carotid body was also analyzed as a control. The two regions analyzed were: region VHL-V1 with

contains 5 CpG island and region VHL-V2 which contains 7 CpG island; *VHL* promoter hypermethylation was not found in any HNPGLs and, therefore, gene methylation was ruled out as a mechanism for *VHL* loss of expression in HNPGLs (Table 10 and 11).

Table 16. Methylation status of 5 CpG island in region VHL-V1

		Pos. 1	Pos. 2	Pos. 3	Pos. 4	Pos. 5
Assay	Sample ID	Meth. (%)	Meth. (%)	Meth. (%)	Meth. (%)	Meth. (%)
VHL-v1	Control 1	1	2.07	1.15	0	1.41
VHL-v1	Control 2	1.59	1.37	0.91	0	1.31
VHL-v1	Control 3	0.68	1.39	0.72	0	0
VHL-v1	Control 4	0	0	0	0	0
VHL-v1	Control 5	1.53	5.1	3.44	1.22	-
VHL-v1	PGL17	1.77	2.48	2.59	1.02	2.04
VHL-v1	PGL18	1.41	2.76	2.44	1.19	2.53
VHL-v1	PGL22	1.92	1.8	2.08	0	0
VHL-v1	PGL24	2.15	3.53	2.04	0	0
VHL-v1	PGL36	1.77	2.64	2.81	1.74	0
VHL-v1	PGL56	1.13	2.93	2.88	0.97	2.48
VHL-v1	PGL62	1.39	2.07	2.02	0.82	0
VHL-v1	PGL64	2.54	3.28	3.68	2.02	6.76
VHL-v1	PGL77	9.12	0	0	0	4.8
VHL-v1	PGL79	1.59	2.85	2.58	1.33	3.41
VHL-v1	PGL95	1.38	3.67	2.65	1.24	2.63
VHL-v1	PGL96	0.9	2.27	2.25	0.72	1.42

Table 17. Methylation status of 7 CpG island in region VHL-V2

		Pos. 1	Pos. 2	Pos. 3	Pos. 4	Pos. 5	Pos. 6	Pos. 7
Assay	Sample ID	Meth. (%)	Meth. (%)	Meth. (%)	Meth. (%)	Meth. (%)	Meth. (%)	Meth. (%)
VHL-v2	Control 1	85.54	90.23	89.02	88.94	94.14	89.88	100
VHL-v2	Control 2	85.42	89.27	88.11	90.04	94.41	90.71	100
VHL-v2	Control 3	86.65	89.04	87.57	89.85	94.15	89.29	98.95
VHL-v2	Control 4	86.21	85.57	86.3	88.19	93.96	89.2	98.62
VHL-v2	Control 5	79.08	81.27	84.78	76.87	87.19	76.41	94.1
VHL-v2	PGL17	83.22	87.64	87.38	81.93	92.14	84.42	96.93
VHL-v2	PGL18	97.69	85.11	87.79	90.14	92.66	89.78	98.53
VHL-v2	PGL22	91.01	86.62	85.45	89.39	92.16	87.46	97.91
VHL-v2	PGL24	95	89.98	88.4	91.53	92.73	86.14	95.85
VHL-v2	PGL36	95.25	85.35	85.65	79.64	90.32	83.94	96.12
VHL-v2	PGL56	74.65	78.68	79.83	68.33	81.86	72.91	82.16
VHL-v2	PGL62	96.35	57.94	85.74	94.02	93.32	88.44	95.76
VHL-v2	PGL64	79.78	88.35	86.69	83.63	93.4	86.88	98.29
VHL-v2	PGL77	96.48	86.38	87.2	63.28	92.38	76.79	96.77
VHL-v2	PGL79	89.07	77	80.18	66.29	85.21	70.58	83.7
VHL-v2	PGL95	81.91	84.63	87.93	80.82	89.31	77.88	94.56
VHL-v2	PGL96	88.92	87.8	88.92	84.04	91.87	82.61	95.6

Overall, somatic *VHL* alterations by mutational inactivation, intragenic deletions or decreased protein expression was found in 47% (25/53) of HNPGLs. This is the most frequent somatic alteration in HNPGLs described to the date. *VHL* gene mutations and deletions were found only in non-SDH mutant HNPGLs, but other *VHL* alterations that lead to pVHL silencing are also present in *SDH*-HNPGLs.

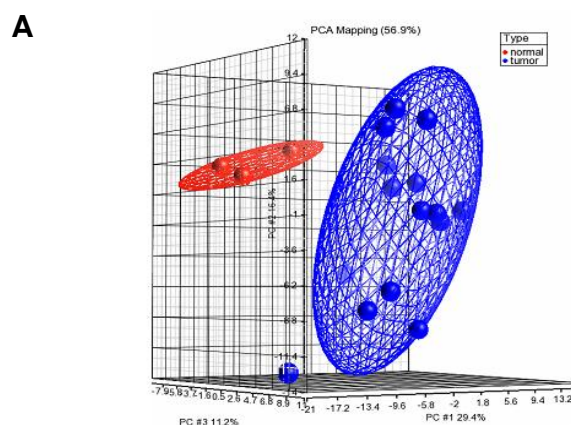
4.20 miRNA expression profiling of HNPGLs

The global profiling of miRNA expression on 17 HNPGLs (Table 8) and 3 normal carotid bodies revealed that HNPGLs grouped together and separated from normal carotid bodies (Fig 36). Differential miRNA expression analysis performed considering the presence or the absence of *SDH* mutation, tumor location or age of tumor onset revealed no significant difference between HNPGLs.

Differential miRNA expression between tumors and normal tissues showed that 5 miRNAs are downregulated in HNPGLs (fold change >2 and FDR<0.05) (Table 11). Interestingly we observed that some of these miRNAs are organized in a genomic cluster: the miR99a-let7c-miR-125b cluster.

miR-101 has been shown to be downregulated or up-regulated in various types of cancer, targets TGF- β signaling pathway by targeting the TGF β R1. (134). TGF β R1 was found up-regulated in the majority of HNPGLs as shown by analysis of the specific probe included in the microarray study.

PCA analysis revealed that three HNPGLs, PGL2, PGL7 and PGL3, cluster A separate from the rest of HNPGLs (cluster B) (Fig. 36B) This was also observed in the PCA analysis microarrays data described above (Fig. 36C).



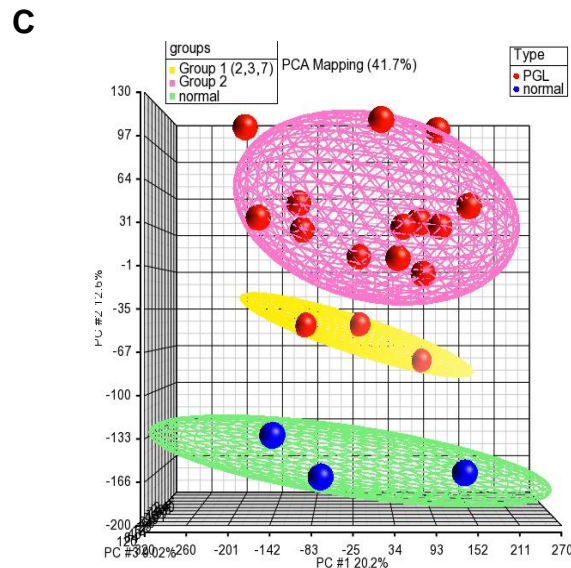
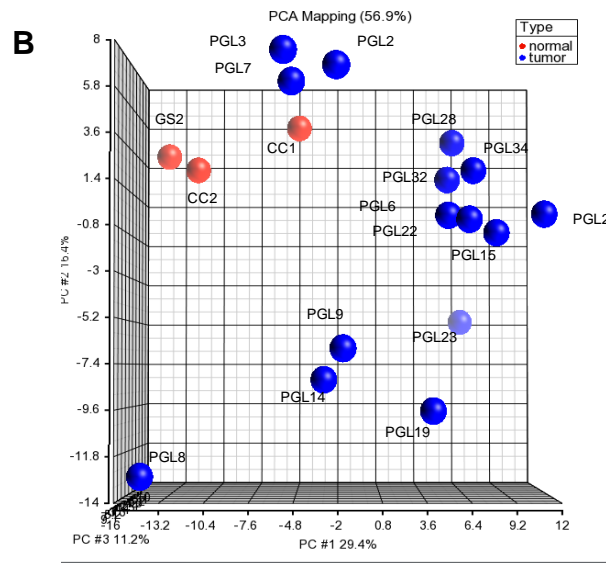


Figure 36. Global miRNA expression analysis. (A and B) two different point of view of PCA revealing a distinct global gene expression signature for HNPGLs (blue) and normal paraganglia (red). x, y, and z axes represent three major principal components (PC). (B) PCA from different point of view. Observe that PGL2, PGL3 and PGL7 separate from de rest of HNPGLs. (C) PCA from microarrays study; PGL2, PGL3 and PGL7 are in yellow and separate from the rest of HNPGLs.

This observation prompted us to analyze the miRNA expression profile of PGL2, PGL3 and PGL7 versus the rest of HNPGLs of the study and the normal paraganglia. The data showed that 51 miRNAs were dereguated in cluster A. We found 29 miRNAs to be downregulated and 22 miRNAs to be up-regulated in comparison to the HNPGLs.

Interestingly 21 of the downregulated are organized in mir-379/mir-656 cluster, located within the imprinted DLK1-DIO3 region on 14q32.31 (Table 18); 54 miRNAs are encoded by this imprinted region being one of the largest cluster described in mammals. DLK1-DIO3 cluster is known to be actively expressed in fully pluripotent stem cells but it is repressed in cells with partial pluripotency. So it seems that these two group differ, at least in part, by regulation of differentiation process. Highly specific targets of this cluster are genes involved in neurogenesis and embryonic development (135), other target genes are involved in regulation of transcription and RNA metabolism (136, 137, 138).

Tabla 18. miRNA of mir-379/mir-656 cluster down-regulated in cluster A.

Sample	PGL2	PGL3	PGL7
miR-337	0	0	0
miR-433	0.16	0.37	0.19
miR-127	0.23	0.40	0.18
miR-432	0.13	0.12	0.02
miR-376a	0.34	0.36	0.36
miR-654	0.25	0.01	0.01
miR-381	0.36	0.25	0.80
miR-487b	0.23	0.46	0.21
miR-544	0	1.72	0
miR-379	0.48	0.31	0.23
miR-411	0.25	0.32	0.20
miR-299-5p	1.07	0.49	0.58
miR-380-5p	0.01	0.28	0.38
miR-323	0.15	0.14	0.00
miR-329	10.85	0	0
miR-494	0.06	8.12	0.11
miR-485-3p	0.41	0.30	0.00
miR-485-5p	0.41	0.30	0.00
miR-453	0	24.80	0
miR-496	0	0	0
miR-409	0.01	0.54	0.01
miR-412	7.09	2.2	19.1
miR-369-5p	0.25	0.27	0.01
miR-410	0.13	0.13	0.05
miR-656	35.33	55.91	50.64
miR-382	0.45	0.32	0.06
miR-134	0.75	0.35	0.16
miR-485-3p	0.61	1.02	0.62
miR-485-5p	0.41	0.30	0.00

4.21 cluster A differ from the rest of HNPGLs in the expression of genes involved in differentiation and energetic metabolism.

The putative targets of miRNAs from the DLK1-DIO3 region include three genes in the polycomb repressive complex 2 (PRC2) gene silencing complex. It has been described that these genes are all expressed at lower levels in embryonic stem cells compared to pluripotent cells perhaps as a result of higher miRNA expression in the embryonic stem cells (139). Based on these observations we decided to re-analyze the global expression profile considering cluster A versus cluster B. The data showed 908 differentially expressed probes, 370 of which were down-regulated in cluster A and 538 genes were up-regulated (2X fold change, p-value based on the false discovery rate of < 0.05). (Supplementary Table S4). Interestingly the most suppressed gene in cluster A was *DLK1*, one of the paternally imprinted genes that map on 14q32.31 region. *MEG3*, a maternally imprinted gene mapping on the same region, was also found down-regulated. In addition, *EZH2*, a member PRC2 complex was over-expressed in cluster A compared cluster B and normal tissues.

Gene ontology (GO) analysis of the differentially expressed genes was performed using Partek Genomic Suite Software. Upregulated genes were found enriched in biological process correlated with energy metabolisms like hexose and glucose metabolic process, oxidation and reduction among others (Table 19) Downregulated genes were found enriched in several biological processes like secretion, neuron differentiation, neuron projection development among other (Table 20).

Table 19. Gene Ontology (GO) biological process upregulated in PGL2, PGL3 and PGL7.

Term	Count	%	P-Value	Benjamini and Hochberg FDR
protein complex assembly	24	0.7	2.10E-04	3.30E-01
protein complex biogenesis	24	0.7	2.10E-04	3.30E-01
hexose metabolic process	13	0.4	4.90E-04	3.70E-01
glucose metabolic process	11	0.3	1.00E-03	4.70E-01
oxidation reduction	26	0.7	1.10E-03	4.00E-01
monosaccharide metabolic process	13	0.4	1.70E-03	4.80E-01
macromolecular complex assembly	26	0.7	1.90E-03	4.40E-01
coenzyme metabolic process	10	0.3	3.70E-03	6.30E-01
response to drug	12	0.3	4.20E-03	6.30E-01
macromolecular complex subunit organization	26	0.7	4.40E-03	6.00E-01
skeletal system development	15	0.4	5.00E-03	6.10E-01
carboxylic acid catabolic process	8	0.2	6.90E-03	7.00E-01

organic acid catabolic process	8	0.2	6.90E-03	7.00E-01
glutamine family aminoacid catabolic process	4	0.1	7.00E-03	6.70E-01
anterior/posterior pattern formation	9	0.3	7.20E-03	6.50E-01
G2 phase of mitotic cells	3	0.1	7.90E-03	6.50E-01
G2 phase	3	0.1	7.90E-03	6.50E-01
pyruvate metabolic process	5	0.1	9.70E-03	7.10E-01
positive regulation of cellular biosynthetic process	24	0.7	1.10E-02	7.20E-01
cellular aminoacid catabolic process	6	0.2	1.20E-02	7.30E-01
positive regulation of biosynthetic process	24	0.7	1.30E-02	7.40E-01
gluconeogenesis	4	0.1	1.30E-02	7.30E-01
biological adhesion	24	0.7	1.40E-02	7.20E-01
cell adhesion	24	0.7	1.40E-02	7.20E-01
morphogenesis of an epithelium	7	0.2	1.60E-02	7.50E-01
cofactor metabolic process	10	0.3	1.70E-02	7.50E-01
embryonic skeletal system development	6	0.2	1.90E-02	7.80E-01
positive regulation of nitrogen compound metabolic process	22	0.6	2.00E-02	7.70E-01
amine catabolic process	6	0.2	2.00E-02	7.70E-01
glutamine family aminoacid metabolic process	5	0.1	2.00E-02	7.60E-01
thyroid gland development	3	0.1	2.30E-02	7.90E-01
hexose biosynthetic process	4	0.1	2.40E-02	7.90E-01
skeletal system morphogenesis	7	0.2	2.50E-02	8.00E-01
one-carbon metabolic process	7	0.2	2.50E-02	8.00E-01

Table 20. Gene Ontology (GO) biological process downregulated in PGL2, PGL3 and PGL7.

Term	Count	%	P-value	Benjamini and Hochberg FDR
secretion by cell	16	0.6	2.60E-07	3.74E-04
secretion	19	0.8	2.70E-07	2.00E-04
exocytosis	11	0.4	5.40E-06	2.60E-04
neuron differentiation	20	0.8	1.50E-05	5.50E-03
neuron projection development	15	0.6	1.70E-05	5.00E-03
neurotransmitter transport	9	0.4	2.30E-05	5.50E-03
vesicle-mediated transport	23	0.9	2.30E-05	4.80E-03
neuron projection morphogenesis	13	0.5	5.20E-05	9.50E-03
cell projection organization	17	0.7	7.20E-05	1.20E-02
cell projection morphogenesis	13	0.5	2.00E-04	2.80E-02
cell part morphogenesis	13	0.5	3.00E-04	3.90E-02
synaptic transmission	14	0.6	3.30E-04	4.00E-02
neuron development	15	0.6	3.50E-04	3.80E-02
axonogenesis	11	0.4	4.30E-04	4.40E-02
cell morphogenesis involved in differentiation	12	0.5	7.20E-04	6.80E-02
cell morphogenesis involved in neuron differentiation	11	0.4	8.10E-04	7.10E-02
regulation of exocytosis	5	0.2	1.30E-03	1.10E-01
transmembrane receptor protein tyrosine kinase signaling pathway	11	0.4	1.40E-03	1.00E-01
transmission of nerve impulse	14	0.6	1.50E-03	1.10E-01

cellular component morphogenesis	15	0.6	1.60E-03	1.10E-01
regulation of nervous system development	10	0.4	1.70E-03	1.10E-01
cell morphogenesis	14	0.6	1.70E-03	1.10E-01
regulation of cell development	10	0.4	2.60E-03	1.50E-01
homotypic cell-cell adhesion	3	0.1	4.00E-03	2.20E-01
cell adhesion	20	0.8	5.10E-03	2.60E-01
biological adhesion	20	0.8	5.10E-03	2.50E-01
heat generation	3	0.1	5.30E-03	2.50E-01
regulation of calcium ion-dependent exocytosis	3	0.1	6.80E-03	3.00E-01
renal system process	4	0.2	7.10E-03	3.00E-01
generation of a signal involved in cell-cell signaling	6	0.2	7.20E-03	3.00E-01

Cluster B, in addition to the up-regulated miRNA, present down-regulation of 28 miRNA. (Table 21).

Table 21. miRNAs down-regulated in cluster B.

miRNA
hsa-let-7a-4373169
hsa-let-7b-4373168
hsa-let-7d-4373166
hsa-let-7f-4373164
hsa-let-7g-4373163
hsa-miR-1-4373161
hsa-miR-142-3p-4373136
hsa-miR-148a-4373130
hsa-miR-17-5p-4373119
hsa-miR-19a-4373099
hsa-miR-19b-4373098
hsa-miR-195-4373105
hsa-miR-20a-4373286
hsa-miR-25-4373071
hsa-miR-30a-3p-4373062
hsa-miR-30a-5p-4373061
hsa-miR-30b-4373290
hsa-miR-30c-4373060
hsa-miR-30d-4373059
hsa-miR-30e-3p-4373057
hsa-miR-30e-5p-4373058
hsa-miR-345-4373039
hsa-miR-34a-4373278
hsa-miR-365-4373194
hsa-miR-497-4373222
hsa-miR-9-4373285
hsa-miR-9-4378074

hsa-miR-92-4373013

hsa-miR-93-4373012

Some of these miRNAs cluster together, among them, miR-17 family is involved in bone morphogenetic protein (BMP) signaling and is active in many tissues including proliferation, differentiation and maturation. It also regulates STAT3 that is a known to be a stem cell regulator. The clusters miR17-92 and miR106-363 are part of this family.

Another cluster we found downregulated in cluster B is the cluster MC-let-7a let-7-d, which is formed by three members: let-7a, let-7f-1 and et-7d and play a critical role in carcinogenesis. The others miRNAs are involved in diverse biological process like obesity and metabolic distress (miR-30e), migration and invasion (miR-30b) and oxidative phosphorylation of neural precursor cells (mir-34a) among others.

4.22 MAX mutation analysis

We sequenced *MAX* in 1,694 patients with PCC or PGL (without mutations in other major susceptibility genes). Sixteen *MAX* pathogenic mutations were identified in 23 index patients. All had adrenal tumors, including 13 bilateral or multiple PCCs within the same gland ($P < 0.001$), 15.8% developed additional tumors at thoracoabdominal sites, and 37% had familial antecedents. Age at diagnosis was lower ($P = 0.001$) in *MAX* mutation carriers compared with nonmutated cases. Two patients (10.5%) developed metastatic disease. So, germline mutations in *MAX* are responsible for 1.12% of PCC/PGL in patients without evidence of other known mutations and should be considered in the genetic work-up of these patients. No *MAX* mutation were found in HNPGLs (83).

5. DISCUSSION

5. Discussion

5.1 Sporadic and *SDH*- HNPGLs show a common gene expression signature.

This is the first work that compares the global gene expression profile in the HNPGLs versus normal paraganglia. Data show that HNPGLs share a common deregulate gene expression profile that differ from normal paraganglia and is independent of the presence of *SDH* mutation or the clinical characteristics of the patients (age, sex, family history).

As the most accepted hypothesis of paraganglioma pathogenesis propose an activation of the hypoxic signaling we expected to find enrichment in genes involved in the hypoxic response, but surprisingly we did not. HNPGLs were enriched in genes involved in locomotion, immune and inflammatory response and morphogenesis among others.

The role of inflammation in cancer is generally accepted, it is well known that is involved in different stages of tumor development, including initiation, promotion, malignant conversion, invasion, and metastasis. Morphogenesis is regulated during development and cancer by morphogenic fields; for instance, it is known that TGF- β 1 is a morphogen that regulate cells proliferation by modulation mitochondrial oxidative phosphorylation (140). Paragangliomas could be seen as a mitochondrial disease, as mitochondrial oxidative phosphorylation is impaired at least in presence of *SDH* or *VHL* mutation, so it is possible that the morphogenic response that we found deregulated in HNPGLs is a secondary effect of abnormal mitochondrial function.

5.2 Pseudohypoxic gene signature is driven by HIF-1 α activation in a subgroup of HNPGLs.

Previous reports describe a hypoxic gene signature common to *VHL* and *SDH* PGLs that distinguish them from NF1, RET and MEN 2 tumors (141 and 103). These results, in conjunction with biochemical studies, strongly support the role of hypoxia in the pathogenesis of PGLs with *VHL* or *SDH* mutations (104). More recent studies, however, found that both non-*VHL* and *SDHB* sympathetic PGLs actually differ from *VHL* tumors in their hypoxic gene signature and that the hypoxia related genes are not predominantly activated in *SDH* tumors. However all these studies only compare non-homogeneous sympathetic and parasympathetic PGLs and did not include normal sample, so this obviously hindered the identification of genes commonly deregulated in

different subtypes of PGLs, and did not allow assuring whether the parasympathetic HNPGLs actually develop a hypoxic gene signature as compared with the normal tissue.

The difficult to obtain normal paraganglia restricted us to use only 3 samples; however these normal samples show a common gene and miRNA expression profile that differ from those found in HNPGLs.

The approach used in the present study has lead, for the first time, to identify a subgroup of HNPGLs that present a pseudohypoxic signaling pathway in absence of *SDH_x* mutations. The differential expression analysis of hypoxic related genes reveals that HNPGLs are segregated in two clusters that share only few genes. Significantly, the pseudohypoxic gene signature was more highly enriched in known HIF-1 α -target genes in a subset (cluster C1) of HNPGLs. Conversely, the other subset of HNPGLs (cluster C2) over-expressed few known HIF-1 α -target genes and downregulated several HIF-1 α -inducible genes (*SLC2A1*, *HIG2*, *EGLN3*, *PFKFB3*, *TF* and *HK2* among others) two of which (*HIG2* and *EGLN3*) were actually found upregulated in the subset of tumors with enriched HIF-1 α related molecular signature.

We rule out the possibility that the activation of the pseudohypoxic signature could be driven by the presence of a hypoxic microenvironment in the C1-tumors as we found comparable number of vessels in C1-C2-tumors and normal paraganglia; we also discard presence of somatic *SDH* mutation or *VHL* germline mutation in C1-tumors that could activate the hypoxic signaling. We found several known SNPs in *SDHA*, which sequencing was particularly difficult due to the presence of two *SDHA* pseudogenes.

We corroborated that *HIF-1 α* is involved in pseudohypoxic gene signature by *HIF-1 α* immunohistochemistry. We found that less than 40% of tumor cells were HIF-1 α positive in all the analyzed C2 samples whereas the only C1-tumor for which a sample was available for both, microarray and histopathological studies, displayed more than 90% of *HIF-1 α* positive cells, a pattern of staining clearly different from that of C2-tumors. These data suggest that a canonical *HIF-1 α* -driven gene signature is present in C1-tumors whereas C2-tumors express either a less potent or a non-canonical *HIF-1 α* gene signature.

HIF-1 is a heterodimer protein, consisting HIF-1 α subunit that is negatively regulated by O₂ and a constitutively expressed HIF-1 β subunit (142, 143), that binds to the

consensus sequence 5'-RCGTG-3' that is present within or near HIF-1-regulated genes (144).

The battery of genes that is activated by HIF-1 α in response to hypoxia is unique within each cell, the number of HIF target genes, which currently exceeds 1,000, continues to increase (145, 146, 147). HIF-2 α , which is also O₂-regulated, dimerizes with HIF-1 β , and activates transcription of overlapping but different genes respect HIF-1 α ; we didn't find HIF-2 α nuclear accumulation in HNPGLs supporting that is HIF-1 α which is driving gene signature is present in C1-tumors.

5.3 A robust and distinct pseudohypoxic HIF-1 α -related miRNA profile defines a subset of sporadic HNPGLs.

We have identified a distinct subset of HNPGLs that exhibit a unique hypoxia-like gene signature that distinguish them from the rest of the tumors. We found the over-expression of miR-210 in C1-HNPGLs, a well known miRNA induced by HIF-1 α , furthermore we found the down-regulation of *ISCU1/2* in these tumors, that is a miR-210 recent discovery target (118, 119). We validate these results in an independent series of HNPGL and we found PGL47 as another pseudohypoxic-tumor (pHx-tumor) as present accumulation of HIF-1 α , over-expression of miR-210 and downregulation of *ISCU1/2* in absence of *SDH*-mutation.

The identification of miR-210 up-regulation in a subset of tumors raises the intriguing possibility of a novel mechanism of mitochondrial dysfunction in HNPGLs independent on *SDH* mutation. Several lines of evidences suggest that a *HIF-1 α /miR-210/ISCU* signaling pathway is operative in C1-HNPGLs. First, we found down-regulation of *ISCU1/2* only in HNPGLs of cluster 1 that over-express miR-210. Second, HNPGL-derived cells exposed to hypoxia increased miR-210 and decreased *ISCU* mRNA levels. Finally, the role of *HIF-1 α* in this regulatory pathway was confirmed *in vitro* by the use of siRNA against *HIF-1 α* .

ISCU1/2 is involved in the assembly of iron-sulfur (Fe-S) clusters that form the catalytic site of many metallo-proteins as complex I, II and III in the mitochondria, and aconitase (148). The over-expression of miR-210 led to a decrease in the Krebs cycle activity and mitochondrial function, by the down-regulation of *ISCU1/2*. This mechanism could led to an increase n the free radical generation in hypoxia, increases cell survival under hypoxia, induces a switch to glycolysis in normoxia and hypoxia (Warburg and Pasteur effects) and upregulation of the iron uptake required for cell growth (118, 119). This

provides a major new link between HIF and mitochondria dysfunction probably involved in the pathogenesis of HNPGLs. Given that the SDHB subunit of the mitochondria complex II contains three iron-sulfur clusters, we hypothesized that ISCU dysfunction could impact on complex II activity by impairing complex formation. Van Nederveen and colleagues recently showed that germline *SDHB*, *SDHC*, or *SDHD* and subsequent loss of complex II activity can be reliably identified by SDHB immunohistochemical analysis (121). In fact, in presence of an *SDH* mutation in any of the subunits, the SDHB immunohistochemistry is negative; while the sporadic cases present a SDHB positive staining. Negative SDHB staining has also been identified in *SDHD*-mutated renal-cell carcinoma (149) and in *SDH* deficient GIST (150). Therefore, when any component of the mitochondrial complex II is lost, evidence suggests that the complex II becomes unstable and immunohistochemical analysis to detect SDHB becomes negative. We confirmed these results in all HNPGL included in the present study, in agreement with that previous report, *SDH*-HNPGL were SDHB negative and we detected strong SDHB immunostaining in sporadic-HNPGLs. Interestingly however, a significantly weaker immunostaining was detected in the sporadic-HNPGL of cluster C1 and in PGL47, the pHx-tumor found in the validation analysis. In these samples molecular fingerprints of an active HIF-1 α -miR210-ISCU pathway had been identified, this support our hypothesis of that the downregulation of ISCU1/2 could lead to an impairment of SDHB Fe-S clusters formation.

Hypoxia is known to downregulate SDHB protein expression by a HIF-1 α -dependent posttranscriptional mechanism (141). Therefore, it is likely that a HIF-1 α /miR-210/ISCU pathway cause mitochondrial complex II instability and tumorigenesis that is associated with negative staining for SDHB. The finding of a molecular signature compatible with the activation of a HIF-1 α /miR-210/ISCU signaling pathway in HNPGL with decreased SDHB protein expression in the absence of *SDH* germline/somatic mutation provides a novel molecular mechanistic link between HIF and mitochondria dysfunction in human head and neck paragangliomas.

5.4 Comparison of the pseudohypoxia/hypoxia transcriptome common to all parasympathetic HNPGLs with that of sympathetic PGLs.

We observed that two subsets of HNPGLs found in the study (C1 and C2) share few genes commonly desregulate in the pseudohypoxic profile.

Between the commonly desregulated gene we found genes encoding for proteins involved in angiogenesis and extracellular matrix remodeling (*COL4A1*, *COL4A2*, *PGF*, *LOXL2*). Many reports describe the importance of ECM dynamics in many diseases and are a hallmark of cancer (151). Deregulation of ECM remodeling can lead to apoptotic evasion by mutant cells and can also regulate also stem cell proliferation and differentiation.

C1-tumors showed an enriched pseudohypoxic signature as they overexpress several hypoxic-induced genes:

-*VEGFA*, codifies a mitogen that act on endothelial cells and has various effect inducing angiogenesis, vasculogenesis, endothelial cell growth, promoting cell migration and inhibiting apoptosis. Tumours contain elevated VEGF levels at the rim of necrotic and hypoxic tissue;

-*ANGPTL4*, codifies a secreted protein that function as serum hormone that regulates glucose homeostasis, lipid metabolism and insulin sensitivity.

-*COL5A1* codifies an alpha chain for the low abundance fibrillar collagens;

-*LOX* codifies for an extracellular copper enzyme that initiate the crosslinking between collagens and elastin, may have a role as tumor suppressor;

-*PLOD1* and *PLOD2* codify for a lysyl hydroxylases of the endoplasmic reticulum, important for the stability of intermolecular crosslink;

-*FN1* codifies for fibronectin a glycoprotein involved in cell adhesion and migration process.

This suggests that C1-tumors may have a stronger angiogenic phenotype and increased collagen deposition than C2-tumors. Interestingly, some of these genes were also described upregulated in *VHL* compared with MEN 2 tumors and in *VHL* and *SDHB* tumors compared with *RET* and *NF1* tumors. This suggests that remodeling of extracellular matrix and activation of a pseudohypoxia/HIF-1 α -driven angiogenic pathway is common between a subgroup of parasympathetic HNPGLs and sympathetic *SDHB/VHL* PGLs. The observed concerted regulation of genes encoding for fibrillar collagens and key enzymes of collagen formation suggests an increase in the formation of collagen deposits in HNPGLs. This phenomenon is known to be favored by a hypoxic environment in a variety of tissues and have a clear patho-

physiological impact regulating tumor blood vessel formation and invasion (152). The role of extracellular matrix assembly has been previously studied in *VHL* tumors using *in vitro* cell systems (153). The authors showed that tightly assembled extracellular matrix is associated with low invasive potential in *VHL* tumors. Whether increased collagen deposition is related to the extremely low invasive potential in HNPGLs is an interesting hypothesis to be explored.

Glycolytic genes (*ALDOA*, *GPI*, and *PFKP*) were also identified in the hypoxic-like profile common to all HNPGLs. C1-tumors showed also enrichment in glycolytic genes presenting upregulation of *ENO1* and *GAPDH*, and expression levels of *SLC2A1* and *SLC2A3* (hypoxia-inducible glucose transporters) and *HK2* (glycolytic enzyme), comparable to that found in normal paraganglia; while C2-tumors showed reduced expression of *SLC2A1*, *SLC2A3* and *HK2*. Therefore, coordinated regulations of genes that promote a shift toward anaerobic glycolysis (the so-called Warburg effect) were not found in all HNPGLs but in C1-tumors. In agreement with our findings in C2-tumors, Favier et al. (103) reported that whereas increased angiogenesis is a common feature of *SDH* and *VHL* PGLs, stimulation of glycolytic genes including *HK2* and *SLC2A1*, was solely.

5.5 C1-HNPGLs share a common hypoxic profile with ccRCC.

We compare the pHx-profile of C1-tumor with the profile of PGL/PCC and we found that C1-HNPGLs only share few genes with PGL/PCC that harbored *VHL* mutation but not *SDHx*- or *RET/NFI/TMEM127*-mutation.

HIF responsive genes active in tumorigenesis specifically upregulated in pHx-HNPGLs include genes that encode proteins responsible for angiogenesis (*ANGPTL4*, *VEGFA*), glucose uptake and metabolism (*SLC2A1*, *HK2*, *ENO1*), apoptosis (*BNIP3*, *BNIP3L*, *DDIT4*), and gene products that are expected to have effects on the tumor microenvironment such as ECM formation and turnover (*LOX*, *LOXL2*, *COL5A1*, *P4HA1*, *PLOD1*, *PLOD2*). Sympathetic *VHL*-PCC/TAPGLs also upregulate HIF responsive genes related to glucose metabolism (*SLC2A1*, *HK2*, *ENO1*) and apoptosis (*BNIP3*). However, in contrast to HNPGLs, the level of expression of HIF-responsive genes involved in angiogenesis (*ANGPTL4*, *VEGFA*) and ECM remodeling (*LOXL2*, *P4HA1*) in *VHL*-PCC/TAPGLs is similar to that found in *SDHx*-PCC/TAPGLs (122, 94) suggesting that expression of these genes is not specifically related to pVHL dysfunction in sympathetic PGLs. Remarkably using a rich source of publically

available cancer microarray data as Oncomine database, we investigated the gene expression profiles of hypoxic and non-hypoxic pHx-HNPGLs-deregulated genes in different solid tumors. We found that ccRCC is the tumor type having the most extensive overlap with pHx-HNPGLs. It is known that ccRCC tumors often carry *VHL* mutation. Genes commonly upregulated in ccRCC and *VHL* mutant HNPGLs includes *CAIX*, one of the most highly over-expressed genes in pHx-HNPGLs which is also among the top ten more highly over-expressed genes in ccRCC. This gene was not found overexpressed in *VHL*PCC/TAPGLs or other types of cancers (at a cutoff of 3 studies). In addition, miR-210 expression has been shown to be significantly increased in ccRCC with *VHL* gene inactivation (154).

5.6 Identification of somatic *VHL* genes mutation in sporadic HNPGLs with psuedohypoxic gene expression profile.

These observations let us to hypothesize the presence of *VHL* somatic mutation in C1-tumors, so we analyzed C1-tumoral-DNA by Sanger sequenciation and we identified, for the first time, somatic *VHL* gene mutations in sporadic HNPGLs. These mutations are likely involved in their pathogenesis via activation of the HIF-1 α /miR-210 signaling pathway. It is known that missense germline *VHL* gene predispose to develop adrenal PCCs (type 2 *VHL* diseases) in the 10% to 20% of cases and that 10 to 14% of sporadic PCCs carry somatic mutations in *VHL* gene. However, only few cases of HNPGLs with germinal *VHL* mutation has been described (155, 156, 157). Because of these evidences it is probable that pVHL protein may have tissue-specific functions distinct in sympathetic and parasympathetic paraganglia, and that its role in the maintenance of tissue homeostasis is less critical in parasympathetic than in sympathetic paraganglia. Nevertheless, despite the well-established role of *VHL* in a subset of PCC/TAPGLs, this gene had not, until now, been examined for somatic mutations in sporadic HNPGLs.

This work identified two sporadic HNPGLs harboring activation of the HIF-1 α /miR-210 signaling pathway in which the *VHL* gene is inactivated via somatic mutation. In consistence with Knudson's two-hit model (131), we also show that mutation in one of the patients is coupled with a loss of the wild type allele. Remarkably, somatic *VHL* gene mutations were not found in HNPGLs lacking activation of the pHx signaling pathway. This genotype-phenotype correlation supports the notion that the *VHL* gene have a previously unrecognized role in the pathogenesis of a subset of sporadic

HNPGLs and that, as opposed to *SDHx*-mutant HNPGLs, activation of the HIF-1 α /miR-210 gene expression program plays a central role in *VHL*-related HNPGLs.

Nevertheless, other mechanisms are likely involved in the activation of pHx gene program in HNPGLs given that two tumors showing overexpression of HIF-1 α /miR-210 do not harbor *VHL* gene mutation or repressed transcription. This warrants further genetic studies to fully characterize this subset of sporadic HNPGLs, with special attention to other genes related to the pVHL-HIF signaling pathway (89). It is widely recognized that *VHL* mutations have different functional consequence depending on their location in the protein (130, 158, 159). In general, families with germline *VHL* deletions or mutations that predict a truncated pVHL protein have a lower penetrance for PCC and a higher penetrance for ccRCC (type 1 VHL disease); whereas most families with PCCs (type 2 VHL disease) have germline missense mutations that affect surface residues presumably allowing some retention of function to downregulate HIF. This genotype-phenotype associations along with data from *in vitro* studies (47, 48) suggests that the development of *VHL* associated PCCs is related to a HIF independent function of pVHL whereas HIF has a fundamental role in *VHL*-defective tumorigenesis in ccRCC. In the present work, we disclosed that two types of mutations (type 1 and 2) are present in HNPGL tumor tissues. The mutation identified in PGL23 (p.R161Q) has been previously described in sporadic PCCs and families with type 2 VHL disease (126-28). However, the p.F76del mutation, found in PGL3, has been previously identified in families with type 1 VHL disease affected by ccRCC and retinal hemangioblastomas but not PCCs (129, 130). Thus, this is the first description of a type 1 mutation (pF76del) in paragangliomas. Nonetheless, the fact that the two sporadic *VHL* mutant HNPGLs show an identical phenotype related to activation of the HIF gene expression program leads to the suggestion that this group of HNPGLs follows similar pathways of tumorigenesis governed by pVHL-mediated activation of HIF-mediated gene expression cell response. Accordingly, previously reported *in vitro* studies suggest that the two identified mutations may activate HIF complex. The p.R161Q mutation has been shown to lose about 50% functionality to degrade HIF-1 α and HIF-2 α (47). Similarly, the p.F76del mutation, found in PGL3, enlarges the HIF binding pocket in pVHL thus disrupting the dynamic coupling between HIF-1 α and pVHL (160). Therefore, as suggested in ccRCC, HIF seems to have a fundamental role in pVHL-defective tumorigenesis in pHx-HNPGLs. HIF responsive genes active in tumorigenesis specifically upregulated in pHx-HNPGLs include genes that encode proteins responsible for angiogenesis (*ANGPTL4*, *VEGFA*), glucose uptake and metabolism (*SLC2A1*, *HK2*, *ENO1*), apoptosis (*BNIP3*, *BNIP3L*, *DDIT4*), and gene

products that are expected to have effects on the tumor microenvironment such as ECM formation and turnover (*LOX*, *LOXL2*, *COL5A1*, *P4HA1*, *PLOD1*, *PLOD2*). Sympathetic *VHL*-PCC/TAPGLs also upregulate HIF responsive genes related to glucose metabolism (*SLC2A1*, *HK2*, *ENO1*) and apoptosis (*BNIP3*). However, in contrast to HNPGLs, the level of expression of HIF-responsive genes involved in angiogenesis (*ANGPTL4*, *VEGFA*) and ECM remodeling (*LOXL2*, *P4HA1*) in *VHL*-PCC/TAPGLs is similar to that found in *SDHx*-PCC/TAPGLs (**122**, **94**) suggesting that expression of these genes is not specifically related to pVHL dysfunction in sympathetic PGLs. This peculiarity along with the absence of overexpression in sympathetic *VHL*-PCC/TAPGLs of more than 50% of the pHx-HNPGLs-related genes suggests that the functional consequences of pVHL dysfunction in HNPGLs differ from that in *VHL*-PCC/TAPGLs. Furthermore the observation that the pHx gene signature of *VHL* mutated HNPGLs resembles that of ccRCC highly support the notion that pVHL have an important role in tumorigenesis in HNPGLs that differs from that found in *VHL*-PCC/TAPGLs, and that it is more strongly associated to HIF-dependent than HIF-independent tumor suppression functions of pVHL.

Our data revealed that although *VHL* somatic mutations are rare in HNPGLs, they presumably may occur in 6% of sporadic HNPGLs (2/33 sporadic tumors included in this study). To date, only a few cases of sporadic HNPGLs with somatic mutations in PGL susceptibility genes have been identified. In consonance with the predominant role of *SDHx* genes in the development of familial HNPGLs, these mutations were showed to affect the *SDHD* and *SDHB* genes (**161**, **162**). Although not specifically studied in HNPGLs, recent reports have shown that somatic gene mutations in *SDHx* genes are also rare in PCC/TAPGLs, occurring in approximately 1% of the cases (**163**, **4**, **164**, **122**). In contrast, 10 to 14% of sporadic PCCs carry somatic mutations in *RET* or *VHL* genes, and more than 20% of cases harbor somatic *NF1* mutations (**165**, **166**, **122**). No somatic mutations of these genes have been described in HNPGLs. Therefore, our data show that although *VHL* mutations in HNPGLs is not a frequent event, the *VHL* gene is the most frequent target of somatic mutations so far known in sporadic HNPGLs. Our results suggest that the *VHL* gene, involved in tumorigenesis in some hereditary and sporadic PCC/TAPGLs, may be an important player also in sporadic HNPGLs. This provides the foundation for the development and use of therapeutic approaches that target the pVHL/HIF pathway in a subset of sporadic HNPGLs.

5.7 Somatic *VHL* deletions are common in sporadic HNPGLs.

It has been described that the 20-30% of patients with Von Hippel Lindau disease carry *VHL* large (exon or entire gene) deletions (159). Type 2 VHL syndrome is usually associated with surface missense mutations. Type 1 VHL syndrome is most commonly caused by germline exon deletions and truncating mutations and is characterized by susceptibility to hemangioblastomas and RCC but not pheochromocytoma (48). *VHL* copy number alterations were observed also in sporadic pheocromocitoma and ccRCC, however this is the first study that analyze *VHL* deletion in HNPGLs.

We found that about the 12% of sporadic HNPGL carry *VHL* deletion of exon1, being the most frequent somatic alteration found in HNPGLs to the date; deletions were no related to activation of hypoxia signaling as we did not observe overexpression of HIF-1 α , CAIX or miR-210 in any of the sample with *VHL* deletion; deletions were not found in *SDH*-mutated HNPGLs. Results were confirmed by a specific RT-qPCR and by CGH.

Tumor sample that carry *VHL* mutation tend to express low *VHL* mRNA levels in comparison to tumor with normal copy number, however this result was not significant ($P= 0.073$) we suggest that this could be due to the contamination of the tumor with normal tissue. We perform pVHL immunostaining and we observed diffuse cytoplasmic staining either weak or strong was observed in (~54%) samples. Among the sporadic HNPGLs that carry somatic *VHL* mutation one was negative and another one present weak cytoplasmic staining, the other two samples present strong cytoplasmic staining, interestingly these two samples present also a strong nuclear staining that we also observed in PGL23 that carry *VHL* somatic mutation (p.R161Q). The significance of this is not clear as we observe also nuclear *VHL* staining in two sample without *VHL* deletion or mutation.

Despite the critical role played by *VHL* in destruction of hypoxia-inducible factor α (HIF α) via ubiquitin-mediated proteolysis, very little is known about the post-translational modification which regulates *VHL* activity. Previous reports shown that pVHL undergoes to SUMOylation (167) and ubiquitylation. Authors showed that ubiquitylated *VHL* is localized predominantly in the cytoplasm, while SUMOylated *VHL* results in increased *VHL* protein stability and nuclear redistribution (167). It has been described also that *VHL* is predominantly nuclear also at low cell density and cytoplasmic at high cell density (168) or upon transcriptional arrest or low pH (167). So the consequences of cytoplasmic or nuclear localization of pVHL are still unclear and

further studies are needed; however there are evidence supporting that nucleocytoplasmic shuttling of VHL may somehow be important for its anti-tumor effects, since the same (exon 2) that controlsshuttling is also a b-domain-binding surface for the VHL E3 ligase (169).

Loss of pVHL was observed in a high proportion of HNPGLs (46%) in both sporadic (5/11, 45.45%) and SDH-HNPGLs at similar frequency (11/20, 55%). Thus, other molecular mechanisms, in addition of VHL mutation or deletion are involved in the pVHL silencing in HNPGLs, we ruled out presence of *VHL* promtor sequence hypermetilation as possible mechanism by pyrosecuenciation. However a recent report shows that hypermethylation of *VHL* exon 1 may be an alternate mechanism of *VHL* gene silencing in RCC in addition to mutation and promoter methylation, so we can not discard that a similar process is occurring in HNPGLs with pVHL silenced (170).

Overall, data show that somatic *VHL* alterations by mutational inactivation, intragenic deletions or decreased protein expression was found in 47% (25/53) of HNPGLs being the most frequent altered target in HNPGLs found to the date. We did not find correlation between loss of pVHL and over-xpression of HIF-1 α or CAIX. In HNPGLs, it seems that only the somatic *VHL* mutations founded, are able to activate the hypoxia signaling pathway, while deletion or pVHL silencing by other still unknown mechanisms, may play different but not less important role in the pathogenesis of HNPGL.

It is largery know that pVHL is involucrate in many biological mechanisms; pVHL contains two functional domains, α that binds to elongin C and the β domain that acts as the substrate-recognition site for targeting proteins (171). Many studies have demonstrated that VHL is a multi-purpose adaptor protein that engages in regulation of the extracellular matrix (172,173), cellular differentiation (174), cell cycle (175) cell survival, apoptosis (176-178), and senescence (179), in addition to the main function as an adapter for targeting hypoxia-inducible factor (HIF) α subunit for proteolytic degradation (180,181).

Data suggest that, in HNPGLs, *SDH* is not involved in activation the hypoxia signaling pathway, first from the microarray we did not observe over-expression of hypoxia response gene, and second we found that, *in vitro*, the inhibition of SDH with tamoxifene do not led to over-expression of miR-210 or CAIX.

5.8 VHL mutation p.F76del led to the activation of HIF1- α /CAIX/miR-210 pathway.

The role of *VHL* in the pathogenesis of HNPGLs is quite complex as we only observe the activation of the hypoxia pathway in PGL3 and PGL23 that carry *VHL* mutation, but not in the HNPGL that carry *VHL* deletion. *In vitro* we observed that the total absence of *VHL*, in RCC4- cells, led to an increment of mir-210 and CAIX via HIF-1 α , but an inhibition of *VHL*, with a siRNA, seems to be not sufficient to activate the hypoxia pathway. Overall data suggest that is the mutation in *VHL*, but not the inhibition, is involved in the activation of the hypoxia pathway via HIF1- α . We corroborate this hypothesis by the construction of a plasmid carrying the *VHL* mutation found in PGL3 (p.F76del), cells transfected with this plasmid overexpressed HIF1- α /CAIX/miR-210 pathway. The localization of *VHL* in these transfected cells was cytoplasmatic, so the mutations seem to be not involved in the nuclear localization of pVHL. We also confirm that the pseudo-hypoxic pathway activation is HIF-1 α dependent by using adrenal medulla and kidney of mice knock out for HIF-1 α that were exposed to hypoxia environment. So we confirm that *VHL* mutation play a role in the pathogenesis of a subgroup of HNPGL by activating the hypoxia signaling pathway via HIF-1 α .

5.9 MAX mutation analysis in HNPGLs.

We collaborate in the study of *MAX* by sequencing to check the presence of pathogenic mutations that could be involved PGLs pathogenesis. In the study were analyzed 1,535 patient with PCC/PGLs and HNPGLs. We did not find any mutation in 17 apparently sporadic HNPGLs. In the study were found 23 patients with PCC that carry germinal mutation in *MAX* suggesting that this gene has a major role in the developing of PCC, but not HNPGLs (**81**).

5.10 miRNA expression profiling of HNPGLs.

This is the first study that compares miRNA expression profile of HNPGLs and normal paraganglia. MiRNAs are small, non-coding single stranded RNAs of 21-25 nucleotides in length that are generated from a primary miRNA transcript (pri-miRNA). Often several miRNAs organized in clusters mapping on the same region of a chromosome and are transcribed on one pri-miRNA transcript (**182**). Briefly, a nuclear ribonuclease termed Drosha excises 70-100 nucleotide hairpins, termed precursor miRNAs (pre-miRNAs) that is exported from the nucleus to the cytoplasm where, a second ribonuclease, Dicer, gave rise to a miRNA duplex. Then the RNA-Induced Silencing Complex (RISC) split and release one of the strands and the mature miRNA can bind

to complementary mRNAs, leading to either translational repression or mRNA degradation. Typically, one miRNA has multiple target mRNAs and, thus, can regulate several genes (**183**).

Data show that HNPGLs share a common deregulate miRNA expression profile that differ from normal paraganglia and is independent of the presence of *SDH* mutation or the clinical characteristic of the patients (age, sex, family history). We found 15 miRNA to be downregulated in HNPGLs, interestingly some of these were part of the cluster miR99a-let7c-miR-125b located on 21p11.1 miRNA 125b (miR-125b) gains particular interest because it has been found in a broad variety of tumors (**184**). However, while miR-125b upregulation in some tumor entities suggests oncogenic potential of miR-125b; downregulation in other tumor types suggests that miR-125b is rather tumor suppressive; for instance miR-125b has been shown to be downregulated in colorectal cancer, breast cancer, gastric cancer, non-small cell lung cancer (NSCLC) and glioblastomas (**185**).

Furthermore miR-99a, with miR-100 that was also found deregulated ourserie of HNPGLs, target mTOR and is involved in carcinogenesis. However we did not find up-regulation of the probes correspondig to mTOR in HNPGLs of the microarray study.

miR-101 is the TG β signaling pathway through the direct targeting of the receptor TBR1 and its transcriptional activator Kruppel-like factor 6 (KLF6). We found TBR1 up-regulated in the majority of HNPGLs of the study considering the specific probe for TBR1 in the microarrays study; so it would be interesting to realize further studies to corroborate these data and its possible implication in HNPGLs pathogenesis.

It has been shown that miR-101, and miR-130 target ATXN1 (**186**) a transcriptional repressor, component of Notch signaling pathway. ATXN1 is a possible target to confirm also in HNPGLs as we observed higher expression levels in the microarrays with the ATXN1 specific probe.

5.11 Part of the cluster mir-379/mir-656 is found downregulated in PGL2, PGL3 and PGL7.

HNPGLs show a common pattern of deregulation of the miRNA expression profile; however we observe a trend of three HNPGLs (PGL2, PGL7 and PGL3) to group together and separate from the other HNPGLs, if we observe the PCA of microarrays we can see the same tendency of these three samples to clustering together.

So we decide to perform the analysis of the miRNA differential expressed of these 3 samples versus the other HNPGLs of the study; results show that there are a 26 miRNA down-regulated in PGL2, PGL3 and PGL7. Interestingly, 21 of 26 of these miRNA are part of the cluster mir-379/mir-656.

Mir-379/mir-656 cluster is located in the DLK1-DIO3 genomic region, on human chromosome 14 (14q32) that contains the paternally expressed imprinted genes DLK1, RTL1, and DIO3 and the maternally expressed imprinted genes MEG3, MEG8 and antisense RTL1 (**187**). This region also hosts 53 miRNAs (forward strand) and one more (mir-1247) on the reverse strand. This cluster of 54 miRNAs is the largest one currently known in the human genome (**135**). This cluster is under positive control of Mef2 and was found deregulated in many type of cancers, furthermore a recent study revealed that the entire mir-379/mir-656 cluster functions as a potential tumor-suppressor locus in glioblastomamultiforme (GBM) and very likely, in multiple human cancers (**188**), one of the mechanisms involved in the downregulation of this cluster could be hypermethylation, loss of heterozigosity and down-regulation of *Mef* (**188-191**). The most likely candidate targets of this cluster are genes associated to the biological process as regulation of transcription, RNA metabolism, cell motility, neurogenesis, and embryonic development. While genes involved in regulation of transcription and RNA metabolism appear to be common targets for many miRNAs and have been reported in several studies (**136, 137, 138**), over-representation of target genes involved in neurogenesis, cell motility, and embryonic development is highly specific for the mir-379/mir-656 cluster. Protein coding genes within the Dlk1-Dio3 region are highly conserved across species, while the miRNA cluster is conserved only in mammals. This indicated that it might have evolved early during selection for mechanisms that regulate self-renewal processes, including those in human (**139**).

The putative targets of miRNAs from the *Dlk1-Dio3* region include three genes in the Polycomb repressive silencing complex 2 (PRC2). Polycomb group (PcG) proteins are epigenetic regulators of transcription that have key roles in stem-cell identity, differentiation and disease. Mechanistically, they function within multiprotein complexes, called Polycomb repressive complexes (PRCs), which modify histones (and other proteins) and silence target genes. PRC2 is involved in various biological processes, including differentiation, maintaining cell identity and proliferation, and stem-cell plasticity. The core of PRC2 complex comprises 4 components: EZH1/2, SUZ12, EED and RbAp46/48 (also known as RBBP7/4) responsible for the methylation (di- and tri-) of Lys 27 of histone H3 (H3K27me2/3)_{3,6} through its enzymatic subunits

EZH1 and EZH2 (**192**) It has been described that these genes are all expressed at lower levels in the embryonic stem cells compare to pluripotent cells, perhaps as a result of higher miRNA expression in embryonic stem cells, it seems that in embryonic stem cells repression of PRC2 complex formation contributes to the lack of methylation and silencing of the *Dlk1-Dio3* region, resulting in the activated expression of its encoded genes as observed in our results. The activated miRNAs may act in a feedback loop to further prevent the formation of PRC2 and maintain the active state of the *Dlk1-Dio3* region.

Then we perform global expression analysis of PGL2, PGL3, PGL7 versus the rest of HNPGLs of the study shows 370 probes down-regulated in PGL2, PGL3 and PGL7 and 538 probes up-regulated (2X fold change, p-value based on the false discovery rate of < 0.05) being the gene most downregulated *DLK1*, one of the paternal imprinted genes that map on 14q32.31 region.

DLK1 The delta-like 1 homolog gene encodes a transmembrane and secreted protein containing six epidermal growth factor (EGF) domains that is a member of the EGF-like family. This protein is highly homologous to the Notch ligand DLL1 but lacks the Delta/Serrate/Lag (DSL) motif that is critical for interacting with Notch receptors (**135, 193, 194**). DLK1 is involved in differentiation of many cell types, like adipogenesis (**195, 196, 197**), regulating osteoblast differentiation (**198, 199**) and inhibiting the differentiation and proliferation of hematopoietic cells (**200**). Recent study revealed that DLK1 may act as an oncogene in breast tumor through up-regulation of Notch (**201**). However its role in Notch activation is the centre of many controversies (**202, 194, 195**).

MEG3 was also found down-regulated in PGL2, PGL3 and PGL7; it is a long non coding RNA is the most studied transcript of DLK1-DIO3 region, however its function remains poorly understood. It has been described as tumor suppressor (**203**), and to exert anti-proliferative function through interactions with p53 and MDM2, and also by regulating directly or indirectly the phosphorylation of Rb (**204**). MEG3 also interacts with crucial signaling pathways involved in angiogenesis, cell proliferation and differentiation, survival regulation, and has been found deregulated in several types of tumors (**204**).

Interestingly we observed that EZH2, a component of PRC2 complex described above, was over-expressed in PGL2, PGL3 and PGL7 respect to the other HNPGLs and

normal samples, this could lead to a hypermethylation of *Dlk1-Dio3* region resulting in a repression of the genes and miRNAs in there codified.

Gene ontology (GO) analysis of the differentially expressed genes revealed that upregulated genes were found enriched in biological process correlated with energy metabolisms like hexose and glucose metabolic process, oxidation and reduction among others, while downregulated genes were found enriched in several biological processes like secretion, neuron differentiation, neuron projection development among other.

5.12 miRNAs founded down-regulated in all NPGLs but not in PGL2, PGL3 and PGL7.

In addition to those miRNAs that are part of mir-379/mir-656 cluster founded downregulated in PGL2, PGL3 and PGL7, we found 22 miRNA that seem to have an opposite regulation as they are downregulated in all HNPGLs, but not in PGL2, PGL3 and PGL7, in which they are found up-regulated or with no difference in the expression levels compared to the normal tissue.

Interestingly we found that some of these miRNA were part of the miR-17 family. This family consist of six members which are distributed in three paralog clusters: miR17-92 cluster, miR-106b-25 cluster and miR106a-363 cluster; miR-17 family is involved in bone morphogenetic protein (BMP) signaling that is active in many tissues including the central nervous system where regulate cell proliferation, differentiation and maturation. These clusters are highly conserved across species, are thought to have arisen from genetic duplications during evolution, and have been shown to be pro-oncogenic in a number of malignancies (**205-213**).

miR17-92 cluster is formed by miR-17, miR-20a and miR92 that are downregulated in all HNPGLs of our estudy with the exception of PGL2, PGL3 and PGL7. The miR-17-92 cluster is also known as oncomir-1 and is among the most potent of oncogenic miRNAs described to the date (**214, 215, 216**). Is over-expressed in a variety of human cancers, including lung carcinomas, B-cell lymphomas, and retinoblastomas (**217–206**).

miR-106b~25 cluster formed by miR106b, miR93 and miR25 is hosted in the intron 13 of MCM7 . In our study we found that miR-106b is down-regulated in all HNPGLs while miR93 and miR25 are not down-regulated in PGL2, PGL3 and PGL7. This cluster is involved in the regulation of adult neural stem/progenitor cell proliferation and neuronal differentiation. Further more is known that miR-25 has a number of potential target

mRNAs involved in insulin/insulin-like growth factor-1 (IGF) signaling. The regulatory site of this cluster is binding by FoxO3, a member of FoxO family involved in maintaining adult stem cells and extend lifespan downstream of insulin/IGF signaling (referencia)

miR-106a~363 cluster has also been described as oncogenic in a variety of tumors, for instance in the sarcoma de Ewin.

Another cluster we found downregulated in all HNPGLs with the exception of PGL2, PGL3 and PGL7 is the cluster MC-let-7a-1/let-7-d, which is formed by free member: let-7a-1, let-7f-1 and let-7d and is an important member of let-7 family. This cluster plays a critical role in development and carcinogenesis. It has been described that MYC can inhibit or promote MC-let7-a-1 let7-d promoter activity by binding the non canonical E-box 3 downstream the transcription start site or by binding the canonical E-box 2 upstream the transcription start site respectively (**218**). The other miRNAs founded down-regulated in HNPGLs but not in PGL2, PGL3 and PGL7 are no part of any cluster and are involved in many biological process, like obesity and metabolic distress (miR-30e), migration and invasion (miR-30b), oxidative phosphorylation of neural precursor among others (miR-34a).

6. CONCLUSIONES

6. Conclusiones

1. Los perfiles de expresión génica y de miRNA no discriminan entre HNPGLs esporádicos y HNPGLs con mutación en *SDH*.
2. Los perfiles de expresión génica y de miRNA diferencian dos grupos de HNPGLs: tumores esporádicos y con mutaciones en *SDH* que no presentan activación de la vía HIF-1 α /miR-210/ISCU (cluster C2) y tumores esporádicos en los que esta vía se encuentra activada (cluster C1).
3. La acumulación de HIF-1 α y la sobre-expresión de genes relacionados a hipoxia se asocia a la sobre-expresión de miR-210, inhibición de ISCU y disminución de los niveles de la proteína SDHB en ausencia de mutación en *SDH*.
4. Hemos identificado, por primera vez, HNPGLs con mutación somática de *VHL*. Estas mutaciones se encontraron en 2 de los 4 HNPGLs del cluster 1 que presentan activación de la vía de pseudohipoxia.
5. No se encontraron mutaciones somáticas de *VHL* en los tumores del cluster C2 que no presentan activación de la vía de pseudohipoxia.
6. El 12% de los HNPGLs esporádicos presentan disminución del número de copias génicas de *VHL*.
7. La proteína pVHL disminuye o se encuentra ausente en el 22% de los HNPGLs. Esto se observó en HNPGL esporádicos y con mutación de *SDH* con la misma frecuencia.
8. El silenciamiento de pVHL no es causado por hipermetilación del promotor de *VHL*.
9. *VHL* es el gen más frecuentemente alterado a nivel somático en los HNPGLs, conocido hasta la fecha.
10. La delección y el silenciamiento de pVHL no activan la vía HIF-1 α /CAIX/miR-210 en los HNPGLs.
11. La expresión en normoxia de CAIX/miR-210 está regulada por pVHL y HIF-1 α , pero no HIF-2 α . Los niveles de miR-210 se incrementan por la ausencia de *VHL* y por la expresión de la mutación pVHL-F76del. Sin embargo, la disminución parcial de los niveles de *VHL* no es suficiente para a sobre-expresión de miR-210.
12. Los HNPGLs con disminución de copias génicas de *VHL* mantienen niveles normales de expresión de genes involucrados en la fosforilación oxidativa, mientras que los HNPGLs con mutación de *VHL* tienen expresión disminuida.

- 13.** Los HNPGLs presentan disminución de la expresión de 15 miRNA en comparación con los PGs normales.
- 14.** El cluster DLK1-DIO3 que contiene el cluster miR-379/miR-656 se encuentra sobre-expresado en un subgrupo de HNPGLs. Este cluster de miRNAs está involucrado en el mantenimiento de las células madres, en la embriogénesis y en la diferenciación neural.

6. BIBLIOGRAPHY

7. Bibliography

1. Marcos Simões-Costa and Marianne E. Bronner. Insights into neural crest development and evolution from genomic analysis *Genome Res.* Jul 2013; 23(7): 1069–1080.
2. Gammill LS, Bronner-Fraser M. Neural crest specification: migrating into genomics. *Nat Rev Neurosci.* 2003 Oct;4(10):795-805.
3. Sauka-Spengler T, Bronner-Fraser M. A gene regulatory network orchestrates neural crest formation. *Nat Rev Mol Cell Biol.* 2008 Jul;9(7):557-68.
4. Pasini B, Stratakis CA. SDH mutations in tumorigenesis and inherited endocrine tumours: lesson from the pheochromocytoma-paraganglioma syndromes. *J Intern Med* 2009; 266: 19-42
5. B E Baysal. Clinical and molecular progress in hereditary paragangliomas *J. Med. Genet.* 2008;45;689-694.
6. Lee KY, Oh YW, Noh HJ, Lee YJ, Yong HS, Kang EY, Kim KA, Lee NJ. Extraadrenal paragangliomas of the body: imaging features. *AJR Am J Roentgenol.* 2006 Aug;187(2):492-504.
7. Marshall JM. Peripheral chemoreceptors and cardiovascular regulation. *Physiol Rev.* 1994 Jul;74(3):543-94.
8. Aida Platero-Luengo, Susana González-Granero, Rocío Durán, Blanca Díaz-Castro, José I. Piruat, José Manuel García-Verdugo, Ricardo Pardal José López-Barneo. An O₂-Sensitive Glomus Cell-Stem Cell Synapse Induces Carotid Body Growth in Chronic Hypoxia. *Cell.* 2014 Jan; 156 (1-2):291-303..
9. Hervonen A, Vaalasti A, Partanen M, Kanerva L, Vaalasti T. The paraganglia, a persisting endocrine system in man. *Am J Anat.* 1976 Jun;146(2):207-10.
10. N R. Prabhakar. Oxygen sensing by the carotid body chemoreceptors. *J. Appl Physiol.* 2000 Jun; (88): 2287-2295.
11. Verna A, Roumy M, Leitner LM. Loss of chemoreceptive properties of the rabbit carotid body after destruction of the glomus cells. *Brain Res.* 1975 Dec; 100(1):13-23.
12. Zhong H, Zhang M, Nurse CA. Synapse formation and hypoxic signalling in co-cultures of rat petrosal neurones and carotid body type 1 cells. *J Physiol.* 1997 Sep; 503 (3):599-612.
13. Ponte J, Sadler CL. Studies on the regenerated carotid sinus nerve of the rabbit. *J Physiol.* 1989 Mar; 410:411-24.

14. Prabhakar NR, Kumar GK, Nanduri J, Semenza GL. ROS signaling in systemic and cellular responses to chronic intermittent hypoxia. *Antioxid Redox Signal*. 2007 Sep;9(9):1397-403.
15. Fidone SJ, Gonzalez C, Dinger BG, Hanson GR. Mechanisms of chemotransmission in the mammalian carotid body. *Progr Brain Res*. 1988; (74):169-179.
16. Donnelly DF. Chemoreceptor nerve excitation may not be proportional to catecholamine secretion. *J Appl Physiol* (1985). 1996 Aug; 81(2):657-64.
17. Charles C Thomas *The Comparative Morphology of the Carotid Body and Carotid Sinus* *J Anat*. Oct 1959; 93Pt 4): 556.
18. Cavadas C, Silva AP, Mosimann F, Cotrim MD, Ribeiro CA, Brunner HR, Grouzmann E. NPY regulates catecholamine secretion from human adrenal chromaffin cells. *J Clin Endocrinol Metab*. 2001 Dec;86(12):5956-63.
19. Crivellato E, Nico B, Ribatti D. The chromaffin vesicle: advances in understanding the composition of a versatile, multifunctional secretory organelle. *Anat Rec (Hoboken)*. 2008 Dec;291(12):1587-602.
20. Doupe AJ, Landis SC, Patterson PH. Environmental influences in the development of neural crest derivatives: glucocorticoids, growth factors, and chromaffin cell plasticity. *J Neurosci*. 1985 Aug;5(8):2119-42.
21. A Verhofstad. Kinetics of adrenal medullary cells. *J Anat*. Oct 1993; 183(2): 315–326.
22. Nathalie C. Guérineau and Michel G. Desarménien. Developmental and stress-induced remodeling of cell-cell communication in the adrenal medullary tissue. *Cell Mol Neurobiol*. Nov 2010; 30(8): 1425–1431.
23. Fishbein L, Nathanson KL. Pheochromocytoma and paraganglioma: understanding the complexities of the genetic background. *Cancer Genet*. 2012 Jan-Feb;205(1-2):1-11.
24. Neumann HPH, Pawlu C, Peczkowska M, et al. Distinct clinical features of paraganglioma syndromes associated with SDHB and SDHD gene mutations. *JAMA* 2004;292:943-951.
25. Taïeb D, Timmers HJ, Hindi_e E, et al. EANM 2012 guidelines for radionuclide imaging of pheochromocytoma and paraganglioma. *Eur J Nucl Med. Mol Imaging* 2012;39:1977-1995.
26. Patetsios P, Gable DR, Garrett WV, et al. Management of carotid body paraganglioma and review of a 30-year experience. *Ann Vasc Surg* 2002;16:331-338.

27. Sykes JM, Ossoff RH. Paragangliomas of the head and neck. *Otolaryngol Clin North Am.* 1986;19(4):755-67.
28. Pellitteri PK, Rinaldo A, Myssiorek D, et al. Paragangliomas of the head and neck. *Oral Oncol* 2004;40:563-575.
29. Papaspyrou K, Mewes T, Rossmann H, et al. Head and neck paragangliomas: report of 175 patients (1989-2010). *Head Neck* 2012;34: 632_637.
30. Boedeker CC. Paragangliomas and paraganglioma syndromes. *GMS Curr Top Otorhinolaryngol Head Neck Surg* 2011;10:Doc03.
31. DeLellis RA, Lloyd RV, Heitz PU, et al. World Health Organization Classification of Tumours. In: DeLellis RVL, Ronald A, Heitz Philipp U, Eng Charis, editors. *Pathology and Genetics of Tumours of Endocrine Organs.* Lyon, France: IARC Press; 2004.
32. Lee JH, Barich F, Karnell LH, et al. National Cancer Data Base report on malignant paragangliomas of the head and neck. *Cancer* 2002;94:730_737.
33. Rinaldo A, Myssiorek D, Devaney KO, Ferlito A. Which paragangliomas of the head and neck have a higher rate of malignancy? *Oral Oncol* 2004; 40:458-460.
34. PH Neumann Head and neck paragangliomas: clinical and molecular genetic classification. *CLINICS* 2012;67(S1):19-28.
35. Mendenhall WM, Amdur RJ, Vaysberg M, Mendenhall CM, Werning JW. Head and neck paragangliomas. *Head Neck* 2011;33: 1530-1534.
36. Suarez C, Rodrigo JP, Bödeker CC, et al. Jugular and vagal paragangliomas: systematic study on management with surgery and radiotherapy. *Head Neck* 2013;35:1195-1204.
37. Cohen DL, Fraker D, Townsend RR. Lack of symptoms in patients with histological evidence of pheochromocytoma: a diagnostic challenge. *Ann N Y Acad Sci.* 2006; 1073:47–51.
38. Neumann HP, Bausch B, McWhinney SR, et al. Germ-line mutations in nonsyndromic pheochromocytoma. *N Engl J Med.* 2002; 346(19):1459–66.
39. Mannelli M, Castellano M, Schiavi F, et al. Clinically guided genetic screening in a large cohort of italian patients with pheochromocytomas and/or functional or nonfunctional paragangliomas. *J Clin Endocrinol Metab.* 2009; 94(5):1541–7.
40. Neumann HP, Erlic Z, Boedeker CC, et al. Clinical predictors for germline mutations in head and neck paraganglioma patients: cost reduction strategy in genetic diagnostic process as fall-out. *Cancer Res.* 2009; 69(8):3650–6.
41. Cascon A, Pita G, Burnichon N, et al. Genetics of pheochromocytoma and paraganglioma in Spanish patients. *J Clin Endocrinol Metab.* 2009; 94(5):1701–5.

42. Burnichon N, Rohmer V, Amar L, et al. The succinate dehydrogenase genetic testing in a large prospective series of patients with paragangliomas. *J Clin Endocrinol Metab.* 2009; 94(8):2817–27.
43. Carsten C. Boedeker, MD,¹ Erik F. Hensen, MD, PhD,² Hartmut P.H. Neumann, MD, Wolfgang Maier, MD,¹ Francien H. van Nederveen, MD, PhD, Carlos Suarez, MD, PhD, Henricus P. Kunst, MD, PhD,⁷ Juan P. Rodrigo, MD, PhD, Robert P. Takes, MD, PhD, Phillip K. Pellitteri, DO, Alessandra Rinaldo, MD. Genetics of hereditary head and neck paragangliomas. *Head Neck.* 2014 Jun;36(6):907-16.
44. Min JH, Yang H, Ivan M, et al. Structure of an HIF-1 α -pVHL complex: hydroxyproline recognition in signaling. *Science.* 2002; 296(5574):1886–9.
45. Kaelin WG Jr. Molecular basis of the VHL hereditary cancer syndrome. *Nat Rev Cancer.* 2002; 2(9):673–82.
46. Maher ER, Neumann HP, Richard S. von Hippel-Lindau disease: a clinical and scientific review. *Eur J Hum Genet.* 2011; 19(6):617–23.
47. Rechsteiner MP, von Teichman A, Nowicka A, et al. *VHL* Gene Mutations and Their Effects on Hypoxia Inducible Factor HIF(α): Identification of Potential Driver and Passenger Mutations. *Cancer Res.* 2011; 71(16):5500–11.
48. Forman JR, Worth CL, Bickerton GR, et al. Structural bioinformatics mutation analysis reveals genotype-phenotype correlations in von Hippel-Lindau disease and suggests molecular mechanisms of tumorigenesis. *Proteins.* 2009; 77(1):84–96.
49. Le LQ, Parada LF. Tumor microenvironment and neurofibromatosis type I: connecting the GAPs. *Oncogene.* 2007; 26(32):4609–16.
50. Johannessen CM, Reczek EE, James MF, et al. The NF1 tumor suppressor critically regulates TSC2 and mTOR. *Proc Natl Acad Sci U S A.* 2005; 102(24):8573–8.
51. Wohllk N, Schweizer H, Erlic Z, et al. Multiple endocrine neoplasia type 2. *Best Pract Res Clin Endocrinol Metab.* 2010; 24(3):371–87.
52. Yankovskaya V, Horsefield R, Törnroth S, Luna-Chavez C, Miyoshi H, Léger C, Byrne B, Cecchini G, Iwata S. Yankovskaya V, Horsefield R, Törnroth S, Luna-Chavez C, Miyoshi H, Léger C, Byrne B, Cecchini G, Iwata S. Architecture of succinate dehydrogenase and reactive oxygen species generation. *Science.* 2003 Jan 31;299(5607):700-4.
53. Eyal Gottlieb & Ian P. M. Tomlinson Mitochondrial tumour suppressors: a genetic and biochemical update. *Nat Rev Cancer.* 2005;(5):857-866.

54. Hirawake H, Taniwaki M, Tamura A, et al. Characterization of the human SDHD gene encoding the small subunit of cytochrome b (cybS) in mitochondrial succinate-ubiquinone oxidoreductase. *Biochim Biophys Acta*. 1999; 1412(3):295–300.
55. Hirawake H, Taniwaki M, Tamura A, et al. Cytochrome b in human complex II (succinateubiquinone oxidoreductase): cDNA cloning of the components in liver mitochondria and chromosome assignment of the genes for the large (SDHC) and small (SDHD) subunits to 1q21 and 11q23. *Cytogenet Cell Genet*. 1997; 79(1–2):132–8.
56. Hensen EF, Siemers MD, Jansen JC, et al. Mutations in SDHD are the major determinants of the clinical characteristics of Dutch head and neck paraganglioma patients. *Clin Endocrinol (Oxf)* 2011;75:650-655.
57. Ricketts CJ, Forman JR, Rattenberry E, et al. Tumor risks and genotype-phenotype-proteotype analysis in 358 patients with germline mutations in SDHB and SDHD. *Hum Mutat*. 2010; 31(1): 41–51.
58. Van Baars F, Cremers C, van den Broek P, Geerts S, Veldman J. Genetic aspects of nonchromaffin paraganglioma. *Hum Genet* 1982; 60:305-309.
59. Hao HX, Khalimonchuk O, Schraders M, et al. SDH5, a gene required for flavination of succinate dehydrogenase, is mutated in paraganglioma. *Science* 2009;325:1139_1142.
60. Bayley JP, Kunst HP, Cascon A, et al. SDHAF2 mutations in familial and sporadic paraganglioma and pheochromocytoma. *Lancet Oncol* 2010;11:366-372.
61. Kunst HP, Rutten MH, de M€onnink JP, et al. SDHAF2 (PGL2-SDH5) and hereditary head and neck paraganglioma. *Clin Cancer Res* 2011;17: 247-254.
62. Badenhop RF, Jansen JC, Fagan PA, et al. The prevalence of SDHB, SDHC, and SDHD mutations in patients with head and neck paraganglioma and association of mutations with clinical features. *J Med Genet*. 2004; 41(7):e99.
63. Baysal BE, Willett-Brozick JE, Lawrence EC, et al. Prevalence of SDHB, SDHC, and SDHD germline mutations in clinic patients with head and neck paragangliomas. *J Med Genet*. 2002; 39(3):178–83.
64. Muller U, Troidl C, Niemann S. SDHC mutations in hereditary paraganglioma/pheochromocytoma. *Fam Cancer*. 2005; 4(1):9–12.
65. Schiavi F, Boedeker CC, Bausch B, et al. Predictors and prevalence of paraganglioma syndrome associated with mutations of the SDHC gene. *JAMA*. 2005; 294(16):2057–63.

66. Niemann S, Muller U, Engelhardt D, Lohse P. Autosomal dominant malignant and catecholamine-producing paraganglioma caused by a splice donor site mutation in SDHC. *Hum Genet* 2003;113:92_94.
67. Baysal BE, Willett_Brozick JE, Filho PA, Lawrence EC, Myers EN, Ferrell RE. An Alu-mediated partial SDHC deletion causes familial and sporadic paraganglioma. *J Med Genet* 2004;41:703-709.
68. Astuti D, Latif F, Dallol A, et al. Gene mutations in the succinate dehydrogenase subunit SDHB cause susceptibility to familial pheochromocytoma and to familial paraganglioma. *Am J Hum Genet* 2001;69:49-54.
69. Erlic Z, Rybicki L, Peczkowska M, et al. Clinical predictors and algorithm for the genetic diagnosis of pheochromocytoma patients. *Clin Cancer Res* 2009;15:6378-6385.
70. Amar L, Baudin E, Burnichon N, et al. Succinate dehydrogenase B gene mutations predict survival in subjects with malignant pheochromocytomas or paragangliomas. *J Clin Endocrinol Metab* 2007;92:3822-3828.
71. van Hulsteijn LT, Dekkers OM, Hes FJ, Smit JW, Corssmit EP. Risk of malignant paraganglioma in SDHB-mutation and SDHD-mutation carriers: a systematic review and meta-analysis. *J Med Genet* 2012;49:768_776.
72. Kiss NB, Geli J, Lundberg F, Avci C, Velazquez-Fernandez D, Hashemi J, Weber G, Höög A, Ekström TJ, Bäckdahl M, Larsson C. Methylation of the p16INK4A promoter is associated with malignant behavior in abdominal extra-adrenal paragangliomas but not pheochromocytomas. *Endocr Relat Cancer*. 2008 Jun;15(2):609-21.
73. Ricketts C, Woodward ER, Killick P, et al. Germline SDHB mutations and familial renal cell carcinoma. *J Natl Cancer Inst*. 2008; 100(17):1260–2.
74. Gaal J, Stratakis CA, Carney JA, et al. SDHB immunohistochemistry: a useful tool in the diagnosis of Carney-Stratakis and Carney triad gastrointestinal stromal tumors. *Mod Pathol*. 2011; 24(1):147–51.
75. Gill AJ, Chou A, Vilain R, et al. Immunohistochemistry for SDHB divides gastrointestinal stromal tumors (GISTs) into 2 distinct types. *Am J Surg Pathol*. 2010; 34(5):636–44.
76. Vanharanta S, Buchta M, McWhinney SR, et al. Early-onset renal cell carcinoma as a novel extraparaganglial component of SDHB-associated heritable paraganglioma. *Am J Hum Genet*. 2004; 74(1):153–9.

77. Horvath R, Abicht A, Holinski-Feder E, et al. Leigh syndrome caused by mutations in the flavoprotein (Fp) subunit of succinate dehydrogenase (SDHA). *J Neurol Neurosurg Psychiatry*. 2006; 77(1):74–6.
78. Parfait B, Chretien D, Rotig A, et al. Compound heterozygous mutations in the flavoprotein gene of the respiratory chain complex II in a patient with Leigh syndrome. *Hum Genet*. 2000; 106(2): 236–43.
79. Burnichon N, Briere JJ, Libe R, et al. SDHA is a tumor suppressor gene causing paraganglioma. *Hum Mol Genet*. 2010; 19(15):3011–20.
80. Korpershoek E, Favier J, Gaal J, et al. SDHA Immunohistochemistry Detects Germline SDHA Gene Mutations in Apparently Sporadic Paragangliomas and Pheochromocytomas. *J Clin* 2011; 96:E1472_E1476.
81. Qin Y, Yao L, King EE, et al. Germline mutations in TMEM127 confer susceptibility to pheochromocytoma. *Nat Genet* 2010; 42:229-233.
82. Neumann HPH, Sullivan M, Winter A, et al. Germline mutations of the TMEM127 gene in patients with paraganglioma of head and neck and extraadrenal abdominal sites. *J Clin Endocrinol Metab* 2011;96: E1279-E1282.
83. Burnichon N, Cascón A, Schiavi F, Morales NP, Comino-Méndez I, Abermil N, Inglada-Pérez L, de Cubas AA, Amar L, Barontini M, de Quirós SB, Bertherat J, Bignon YJ, Blok MJ, Bobisse S, Borrego S, Castellano M, Chanson P, Chiara MD, Corssmit EP, Giacchè M, de Krijger RR, Ercolino T, Girerd X, Gómez-García EB, Gómez-Graña A, Guilhem I, Hes FJ, Honrado E, Korpershoek E, Lenders JW, Letón R, Mensenkamp AR, Merlo A, Mori L, Murat A, Pierre P, Plouin PF, Prodanov T, Quesada-Charneco M, Qin N, Rapizzi E, Raymond V, Reisch N, Roncador G, Ruiz-Ferrer M, Schillo F, Stegmann AP, Suarez C, Taschin E, Timmers HJ, Tops CM, Urioste M, Beuschlein F, Pacak K, Mannelli M, Dahia PL, Opocher G, Eisenhofer G, Gimenez-Roqueplo AP, Robledo M. MAX mutations cause hereditary and sporadic pheochromocytoma and paraganglioma. *Clin Cancer Res* 2012; 18:2828-2837.
84. Ladroue C, Carcenac R, Leporrier M, et al. PHD2 mutation and congenital erythrocytosis with paraganglioma. *N Engl J Med* 2008;359:2685-2692.
85. Lorenzo FR, Yang C, Ng Tang Fui M, Vankayalapati H, Zhuang Z, Huynh T, Grossmann M, Pacak K, Prchal JT. A novel EPAS1/HIF2A germline mutation in a congenital polycythemia with paraganglioma. *J Mol Med*. 2013 Apr;91(4):507-12.
86. Taïeb D, Yang C, Delenne B, Zhuang Z, Barlier A, Sebag F, Pacak K. First report of bilateral pheochromocytoma in the clinical spectrum of HIF2A-related polycythemia-paraganglioma syndrome. *J Clin Endocrinol Metab*. 2013 May;98(5):E908-13.

87. Comino-Mendez, I. *et al.* Tumoral EPAS1 (HIF2A) mutations explain sporadic pheochromocytoma and paraganglioma in the absence of erythrocytosis. *Hum. Mol. Genet.* **22**, 2169–2176 (2013).
88. Favier, J., Buffet, A. & Gimenez-Roqueplo, A. P. HIF2A mutations in paraganglioma with polycythemia. *N. Engl. J. Med.* **367**, 2161–2162 (2012).
89. Zhuang, Z. *et al.* Somatic HIF2A gain-of-function mutations in paraganglioma with polycythemia. *N. Engl. J. Med.* **367**, 922–930 (2012).
90. Pacak, K. *et al.* New syndrome of paraganglioma and somatostatinoma associated with polycythemia. *J. Clin. Oncol.* **31**, 1690–1698 (2013).
91. Castro-Vega LJ, Buffet A, De Cubas AA, Cascón A, Menara M, Khalifa E, Amar L, Azriel S, Bourdeau I, Chabre O, Currás-Freixes M, Franco-Vidal V, Guillaud-Bataille M, Simian C, Morin A, Letón R, Gómez-Graña A, Pollard PJ, Rustin P, Robledo M, Favier J, Gimenez-Roqueplo AP. Germline mutations in FH confer predisposition to malignant pheochromocytomas and paragangliomas. *Hum Mol Genet.* 2014 May 1;23(9):2440-6.
92. Schlisio S, Kenchappa RS, Vredeveld LC, *et al.* The kinesin KIF1Bbeta acts downstream from EglN3 to induce apoptosis and is a potential 1p36 tumor suppressor. *Genes Dev* 2008;22:884-893.
93. Pacak K, Eisenhofer G, Ahlman H, *et al.* Pheochromocytoma: recommendations for clinical practice from the First International Symposium. October 2005. *Nat Clin Pract Endocrinol Metab* 2007;3:92-102.
94. López-Jiménez E, Gómez-López G, Leandro-García LJ, Muñoz I, Schiavi F, Montero-Conde C, de Cubas AA, Ramires R, Landa I, Leskelä S, Maliszewska A, Inglada-Pérez L, de la Vega L, Rodríguez-Antona C, Letón R, Bernal C, de Campos JM, Díez-Tascón C, Fraga MF, Boullosa C, Pisano DG, Opocher G, Robledo M, Cascón A. Research resource: Transcriptional profiling reveals different pseudohypoxic signatures in SDHB and VHL-related pheochromocytomas. *Mol Endocrinol.* 2010 Dec;24(12):2382-91
95. Pollard, P.J., Briere, J.J., Alam, N.A., Barwell, J., Barclay, E., Wortham, N.C., Hunt, T., Mitchell, M., Olpin, S., Moat, S.J. *et al.* Accumulation of Krebs cycle intermediates and over- expression of HIF1alpha in tumours which result from germline FH and SDH mutations. *Hum. Mol. Genet.* 2005;(14)2231-2239.
96. Jaakkola, P., Mole, D.R., Tian, Y.M., Wilson, M.I., Gielbert, J., Gaskell, S.J., Kriegsheim, A., Hebestreit, H.F., Mukherji, M., Schofield, C.J. *et al.* Targeting of HIF- alpha to the von Hippel-Lindau ubiquitylation complex by O²-regulated prolyl hydroxylation. *Science* 2001;(292) 468-472.

97. Hewitson, K.S., Lienard, B.M., McDonough, M.A., Clifton, I.J., Butler, D., Soares, A.S., Oldham, N.J., McNeill, L.A. and Schofield, C.J. Structural and mechanistic studies on the inhibition of the hypoxia- inducible transcription factor hydroxylases by tricarboxylic acid cycle intermediates. *J. Biol. Chem.* 2007;(282):3293-3301.
98. Koivunen, P., Hirsila, M., Remes, A.M., Hassinen, I.E., Kivirikko, K.I. and Myllyharju, J. Inhibition of hypoxia- inducible factor (HIF) hydroxylases by citric acid cycle intermediates: possible links between cell metabolism and stabilization of HIF. *J. Biol. Chem.* 2007;(282):4524-4532.
99. Cash, T.P., Pan, Y. and Simon, M.C. Reactive oxygen species and cellular oxygen sensing. *Free Radic. Biol. Med.* 2007;(43):1219-1225.
100. Loscalzo, J. The cellular response to hypoxia: tuning the system with microRNAs. *J. Clin. Invest.* 2010(120):3815-3817.
101. Chan, S.Y. and Loscalzo, J. MicroRNA-210: A unique and pleiotropic hypoxamir. *Cell Cycle.* 2010;(9):1072-083.
102. Sanso G, Powers JF, Tischler AS, Hodin R, Heitritter S, Moore F, Dluhy R, Sosa JA, Ocal IT, Benn DE, Marsh DJ, Robinson BG, Schneider K, Garber J, Arum SM, Korbonits M, Grossman A, Pigny P, Toledo SP, Nosé V, Li C. A HIF1-alpha regulatory loop links hypoxia and mitochondrial signals in pheochromocytomas. *PLoS Genet.* 2005;(1)72-80.
103. Judith Favier, Jean-Jacques Brière, Nelly Burnichon, Julie Rivière, Laure Vescovo, Paule Benit, Isabelle Giscos-Douriez, Aurélien De Reyniès, Jérôme Bertherat, Cécile Badoual, Frédérique Tissier, Laurence Amar, Rosella Libé, Pierre-François Plouin, Xavier Jeunemaitre, Pierre Rustin, Anne-Paule Gimenez-Roqueplo. The Warburg effect is genetically determined in inherited pheochromocytomas. *PloS One.*2009;(4):e7094.
104. Bayley, J.P. and Devilee, P. Warburg tumours and the mechanisms of mitochondrial tumour suppressor genes. Barking up the right tree? *Curr. Opin. Genet. Dev.* 2010;(20):324-329.
105. Miguel A Esteban & Patrick H Maxwell. HIF, a missing link between metabolism and cancer *Nat Med.* 2005;(11):1047-48.
106. Secades P, Rodrigo JP, Hermsen M, Alvarez C, Suarez C, Chiara MD Increase in gene dosage is a mechanism of HIF-1alpha constitutive expression in head and neck squamous cell carcinomas. *Genes, chromosomes & cancer.* 2009(48):441-454.
107. Canel M, Secades P, Rodrigo JP, Cabanillas R, Herrero A, Suarez C, Chiara MD Overexpression of focal adhesion kinase in head and neck squamous cell

- carcinoma is 363 independent of fak gene copy number. *Clin Cancer Res.*2006; (12):3272-3279.
108. Hoebeeck, J., van der Luijt, R., Poppe, B., De Smet, E., Yigit, N., Claes, K., Zewald, R., de Jong, G.J., De Paepe, A., Speleman, F. *et al.* Rapid detection of VHL exon deletions using real-time quantitative PCR. *Lab Invest.* 2005;(85): 24-33.
 109. Tost J, Gut IG. DNA methylation analysis by pyrosequencing. *Nat Protoc.* (2007);2(9):2265-75.
 110. Gundersen HJ, Bendtsen TF, Korbo L, Marcussen N, Moller A, Nielsen K, Nyengaard JR, Pakkenberg B, Sorensen FB, Vesterby A, et al. Some new, simple and efficient stereological methods and their use in pathological research and diagnosis. *APMIS* 1988;(96):379-394.
 111. Benita, Y., Kikuchi, H., Smith, A.D., Zhang, M.Q., Chung, D.C. and Xavier, R.J. An integrative genomics approach identifies Hypoxia Inducible Factor-1 (HIF-1)-target genes that form the core response to hypoxia. *Nucleic Acids Res.*2009;(37):4587-4602.
 112. Chi, J.T., Wang, Z., Nuyten, D.S., Rodriguez, E.H., Schaner, M.E., Salim, A., Wang, Y.,Kristensen, G.B., Helland, A., Borresen- Dale, A.L. *et al.* (2006) Gene expression programs in response to hypoxia: cell type specificity and prognostic significance in human cancers. *PLoS Med.* 2006;(3):e47.
 113. Denko, N.C., Fontana, L.A., Hudson, K.M., Sutphin, P.D., Raychaudhuri, S., Altman, R. and Giaccia, A.J. Investigating hypoxic tumor physiology through gene expression patterns. *Oncogene.* 2003;(22):5907-5914.
 114. Baysal BE, Lawrence EC, Ferrell RE Sequence variation in human succinate dehydrogenase genes: evidence for long-term balancing selection on SDHA. *BMC biology.* 2007;(5):12.
 115. Cabanillas, R., Rodrigo, J.P., Secades, P., Astudillo, A., Nieto, C.S. and Chiara, M.D. The relation between hypoxia-inducible factor (HIF)-1alpha expression with p53 expression and outcome in surgically treated supraglottic laryngeal cancer. *J. Surg. Oncol.*2009;(99):373-378.
 116. Cao, P., Deng, Z., Wan, M., Huang, W., Cramer, S.D., Xu, J., Lei, M. and Sui, G. MicroRNA-101 negatively regulates Ezh2 and its expression is modulated by androgen receptor and HIF-1alpha/HIF-1beta. *Mol. Cancer.* 2010;(9):108.
 117. Kulshreshtha, R., Ferracin, M., Wojcik, S.E., Garzon, R., Alder, H., Agosto- Perez, F.J., Davuluri, R., Liu, C.G., Croce, C.M., Negrini, M. *et al.* A microRNA signature of hypoxia. *Mol. Cell. Biol.* 2007;(27):1859-1867.

118. Favaro, E., Ramachandran, A., McCormick, R., Gee, H., Blancher, C., Crosby, M., Devlin, C., Blick, C., Buffa, F., Li, J.L. *et al.* MicroRNA-210 regulates mitochondrial free radical response to hypoxia and krebs cycle in cancer cells by targeting iron sulfur cluster protein ISCU. *PloS One.* 2010;(5):e10345.
119. Chen, Z., Li, Y., Zhang, H., Huang, P. and Luthra, R. Hypoxia-regulated microRNA-210 modulates mitochondrial function and decreases ISCU and COX10 expression. *Oncogene.* 2010;(29):4362-4368.
120. Camps, C., Buffa, F.M., Colella, S., Moore, J., Sotiriou, C., Sheldon, H., Harris, A.L., Gleagle, J.M. and Ragoussis, J. hsa-miR- 210 Is induced by hypoxia and is an independent prognostic factor in breast cancer. *Clin Cancer Res.*2008;(14): 1340-1348.
121. van Nederveen, F.H., Gaal, J., Favier, J., Korpershoek, E., Oldenburg, R.A., de Bruyn, E.M., Sleddens, H.F., Derkx, P., Riviere, J., Dannenberg, H. *et al.* An immunohistochemical procedure to detect patients with paraganglioma and phaeochromocytoma with germline SDHB, SDHC, or SDHD gene mutations: a retrospective and prospective analysis. *Lancet Oncol.*2009;(10):764:771.
122. Burnichon, N., Vescovo, L., Amar, L., Libe, R., de Reynies, A., Venisse, A., Jouanno, E., Laurendeau, I., Parfait, B., Bertherat, J. *et al.* Integrative genomic analysis reveals somatic mutations in pheochromocytoma and paraganglioma. *Hum Mol Genet.* 2001;(20):3974-3985.
123. Lopez-Jimenez, E., Gomez-Lopez, G., Leandro-Garcia, L.J., Munoz, I., Schiavi, F., Montero-Conde, C., de Cubas, A.A., Ramires, R., Landa, I., Leskela, S. *et al.* (2010) Research resource: Transcriptional profiling reveals different pseudohypoxic signatures in SDHB and VHL-related pheochromocytomas. *Mol Endocrinol.* 2010;(24):2382-2391.
124. Merlo, A., de Quiros, S.B., Secades, P., Zambrano, I., Balbin, M., Astudillo, A., Scola, B., Aristegui, M., Suarez, C. and Chiara, M.D. (2012) Identification of a signaling axis HIF-1alpha/microRNA-210/ISCU independent of SDH mutation that defines a subgroup of head and neck paragangliomas. *J Clin Endocrinol Metab.* 2012;(97):2194-2200.
125. Bayley, J.P., Devilee, P. and Taschner, P.E. The SDH mutation database: an online resource for succinate dehydrogenase sequence variants involved in pheochromocytoma, paraganglioma and mitochondrial complex II deficiency. *BMC Med Genet.* 2005;(6):39.
126. Chen, F., Kishida, T., Yao, M., Hustad, T., Glavac, D., Dean, M., Gnarr, J.R., Orcutt, M.L., Duh, F.M., Glenn, G. *et al.* Germline mutations in the von Hippel-

- Lindau disease tumor suppressor gene: correlations with phenotype. *Hum Mutat.* 1995;(5):66-75.
- 127.** Zbar, B., Kishida, T., Chen, F., Schmidt, L., Maher, E.R., Richards, F.M., Crossey, P.A., Webster, A.R., Affara, N.A., Ferguson-Smith, M.A. *et al.* Germline mutations in the Von Hippel-Lindau disease (VHL) gene in families from North America, Europe, and Japan. *Hum Mutat.*1996;(8):348-357.
- 128.** Bar, M., Friedman, E., Jakobovitz, O., Leibowitz, G., Lerer, I., Abeliovich, D. and Gross, D.J. (1997) Sporadic pheochromocytomas are rarely associated with germline mutations in the von Hippel- Lindau and RET genes. *Clin Endocrinol (Oxf)*.1997(47):70.
- 129.** Crossey, P.A., Richards, F.M., Foster, K., Green, J.S., Prowse, A., Latif, F., Lerman, M.I., Zbar, B., Affara, N.A., Ferguson-Smith, M.A. *et al.* Identification of intragenic mutations in the von Hippel-Lindau disease tumour suppressor gene and correlation with disease phenotype. *Hum Mol Genet.* 1994;(3):1303-1308.
- 130.** Ong, K.R., Woodward, E.R., Killick, P., Lim, C., Macdonald, F. and Maher, E.R. Genotype-phenotype correlations in von Hippel-Lindau disease. *Hum Mutat.* 2007(28):143-149.
- 131.** Knudson, A.G., Jr. (1971) Mutation and cancer: statistical study of retinoblastoma. *Proc Natl Acad Sci U S A.* 1971;(68):820-823
- 132.** Clifford, S.C., Cockman, M.E., Smallwood, A.C., Mole, D.R., Woodward, E.R., Maxwell, P.H., Ratcliffe, P.J. and Maher, E.R. Contrasting effects on HIF-1 α regulation by disease-causing pVHL mutations correlate with patterns of tumourigenesis in von Hippel-Lindau disease. *Hum Mol Genet.* 2001;(10):1029-1038.
- 133.** Shinojima T, Oya M, Takayanagi A, Mizuno R, Shimizu N, Murai M. Renal cancer cells lacking hypoxia inducible factor (HIF)-1 α expression maintain vascular endothelial growth factor expression through HIF-2 α . *Carcinogenesis.* 2007;28:529–536.
- 134.** Tu X, Zhang H, Zhang J, Zhao S, Zheng X, Zhang Z, Zhu J, Chen J, Dong L, Zang Y, Zhang J. *J Pathol.* MicroRNA-101 suppresses liver fibrosis by targeting TGF β signaling pathway. 2014 May 9. Epub ahead of print.
- 135.** Glazov EA, McWilliam S, Barris WC, Dalrymple BP. Origin, evolution, and biological role of miRNA cluster in DLK-DIO3 genomic region in placental mammals..*Mol Biol Evol.* 2008;25(5):939-48.
- 136.** Lewis BP, Shih IH, Jones-Rhoades MW, Bartel DP, Burge CB. Prediction of mammalian microRNA targets. *Cell.* 2003;115:787–798

137. John B, Enright AJ, Aravin A, Tuschl T, Sander C, Marks DS. Human microRNA targets.. PLoS Biol. 2004; 2:e363.
138. Grun D, Wang YL, Langenberger D, Gunsalus KC, Rajewsky N. microRNA target predictions across seven Drosophila species and comparison to mammalian targets. PLoS Comput Biol. 2005;1:e13.
139. Liu L, Luo GZ, Yang W, Zhao X, Zheng Q, Lv Z, Li W, Wu HJ, Wang L, Wang XJ, Zhou Q. Activation of the imprinted Dlk1-Dio3 region correlates with pluripotency levels of mouse stem cells. J Biol Chem. 2010; 18;285(25):19483-90.
140. Fosslie E Ann Clin.. Cancer morphogenesis: role of mitochondrial failure. Lab Sci. 2008 38(4):307-29.
141. Dahia, P.L., Ross, K.N., Wright, M.E., Hayashida, C.Y., Santagata, S., Barontini, M., Kung, A.L., Sanso, G., Powers, J.F., Tischler, A.S. et al. (2005) A HIF1alpha regulatory loop links hypoxia and mitochondrial signals in pheochromocytomas. PLoS Genet., 1, 72-80.
142. Wang GL, Semenza GL. Purification and characterization of hypoxia-inducible factor 1. J Biol Chem. 1995;270(3):1230–1237..
143. Wang GL, Jiang BH, Rue EA, Semenza GL. Hypoxia-inducible factor 1 is a basic-helix-loop-helix-PAS heterodimer regulated by cellular O₂ tension. . Proc Natl Acad Sci U S A. 1995;92(12):5510–5514.
144. Semenza GL, et al. Hypoxia response elements in the aldolase A, enolase 1, and lactate dehydrogenase A gene promoters contain essential binding sites for hypoxia-inducible factor 1. J Biol Chem. 1996;271(51):32529–32537.
145. Mole DR, et al. Genome-wide association of hypoxia-inducible factor (HIF)-1α and HIF-2α DNA binding with expression profiling of hypoxia-inducible transcripts. J Biol Chem. 2009;284(25):16767–16775.
146. Xia X, et al. Integrative analysis of HIF binding and transactivation reveals its role in maintaining histone methylation homeostasis. Proc Natl Acad Sci U S A. 2009;106(11):4260–4265. doi: 10.1073.
147. Schödel J, Oikonomopoulos S, Ragoussis J, Pugh CW, Ratcliffe PJ, Mole DR. High-resolution genome-wide mapping of HIF-binding sites by ChIP-seq. Blood. 2011;117(23):e207–e217.
148. Rouault, T.A. and Tong, W.H. (2008) Iron- sulfur cluster biogenesis and human disease. Trends Genet., 24, 398-407.
149. Gill, A.J., Pachter, N.S., Clarkson, A., Tucker, K.M., Winship, I.M., Benn, D.E., Robinson, B.G. and Clifton- Bligh, R.J. Renal tumors and hereditary

- pheochromocytomaparanglioma syndrome type 4. *N. Engl. J. Med.*, (2011) 364, 885-886.
- 150.** Gill AJ. Succinate dehydrogenase (SDH) and mitochondrial driven neoplasia *Pathology*. 2012 44(4):285-92.
- 151.** Lu P¹, Weaver VM, Werb Z. The extracellular matrix: a dynamic niche in cancer progression. *J Cell Biol.* 2012 20;196(4):395-406.
- 152.** Bergers, G. and Benjamin, L.E. Tumorigenesis and the angiogenic switch. *Nat. Rev. Cancer*, (2003) 3, 401-410.
- 153.** Kurban, G., Hudon, V., Duplan, E., Ohh, M. and Pause, A. (2006) Characterization of a von Hippel Lindau pathway involved in extracellular matrix remodeling, cell invasion, and angiogenesis. *Cancer Res.*, 66, 1313-1319.
- 154.** Neal, C.S., Michael, M.Z., Rawlings, L.H., Van der Hoek, M.B. and Gleadle, J.M. The VHL-dependent regulation of microRNAs in renal cancer. *BMC Med*, 8, 64.
- 155.** Gaal, J., van Nederveen, F.H., Erlic, Z., Korpershoek, E., Oldenburg, R., Boedeker, C.C., Kontny, U., Neumann, H.P., Dinjens, W.N. and de Krijger, R.R. (2009) Parasympathetic paragangliomas are part of the Von Hippel-Lindau syndrome. *J Clin Endocrinol Metab*, 94, 4367-4371.
- 156.** Boedeker, C.C., Erlic, Z., Richard, S., Kontny, U., Gimenez-Roqueplo, A.P., Cascon, A., Robledo, M., de Campos, J.M., van Nederveen, F.H., de Krijger, R.R. et al. (2009) Head and neck paragangliomas in von Hippel-Lindau disease and multiple endocrine neoplasia type 2. *J Clin Endocrinol Metab*, 94, 1938-1944.
- 157.** Ercolino, T., Becherini, L., Valeri, A., Maiello, M., Gagliano, M.S., Parenti, G., Ramazzotti, M., Piscitelli, E., Simi, L., Pinzani, P. et al. (2008) Uncommon clinical presentations of pheochromocytoma and paraganglioma in two different patients affected by two distinct novel VHL germline mutations. *Clin Endocrinol (Oxf)*, 68, 762-768.
- 158.** Chen, F., Slife, L., Kishida, T., Mulvihill, J., Tisherman, S.E. and Zbar, B. (1996) Genotype-phenotype correlation in von Hippel-Lindau disease: identification of a mutation associated with VHL type 2A. *J Med Genet*, 33, 716-717.
- 159.** Maher, E.R., Webster, A.R., Richards, F.M., Green, J.S., Crossey, P.A., Payne, S.J. and Moore, A.T. (1996) Phenotypic expression in von Hippel-Lindau disease: correlations with germline VHL gene mutations. *J Med Genet*, 33, 328-332.
- 160.** Limaverde-Sousa G, d.A.B.E., Ferreira CG, Cláudio Casali-da-Rocha J. (2012) Simulation of the mutation F76del on the von Hippel-Lindau tumor suppressor protein: Mechanism of the disease and implications for drug development. *Proteins*, doi: 10.1002/prot.24191.

161. Riemann, K., Sotlar, K., Kupka, S., Braun, S., Zenner, H.P., Preyer, S., Pfister, M., Pusch, C.M. and Blin, N. (2004) Chromosome 11 monosomy in conjunction with a mutated SDHD initiation codon in nonfamilial paraganglioma cases. *Cancer Genet Cytogenet*, **150**, 128-135.
162. Braun, S., Riemann, K., Kupka, S., Leistenschneider, P., Sotlar, K., Schmid, H. and Blin, N. (2005) Active succinate dehydrogenase (SDH) and lack of SDHD mutations in sporadic paragangliomas. *Anticancer Res*, **25**, 2809-2814.
163. Gimm, O., Armanios, M., Dziema, H., Neumann, H.P. and Eng, C. (2000) Somatic and occult germline mutations in SDHD, a mitochondrial complex II gene, in nonfamilial pheochromocytoma. *Cancer Res*, **60**, 6822-6825.
164. van Nederveen, F.H., Korpershoek, E., Lenders, J.W., de Krijger, R.R. and Dinjens, W.N. (2007) Somatic SDHB mutation in an extraadrenal pheochromocytoma. *N Engl J Med*, **357**, 306-308.
165. Welander, J., Larsson, C., Backdahl, M., Hareni, N., Sivler, T., Brauckhoff, M., Soderkvist, P. and Gimm, O. Integrative genomics reveals frequent somatic NF1 mutations in sporadic pheochromocytomas. *Hum Mol Genet*, **21**, 5406-5416.
166. Burnichon, N., Buffet, A., Parfait, B., Letouze, E., Laurendeau, I., Lorient, C., Pasmant, E., Abermil, N., Valeyrie-Allanore, L., Bertherat, J. *et al.* (2012) Somatic NF1 inactivation is a frequent event in sporadic pheochromocytoma. *Hum Mol Genet*, **21**, 5397-5405.
167. Cai Q, Robertson ES. Ubiquitin/SUMO modification regulates VHL protein stability and nucleocytoplasmic localization. *PLoS One*. 2010 Sep 9;5(9).
168. Lee S, Chen DY, Humphrey JS, Gnarr JR, Linehan WM, et al. (1996) Nuclear/cytoplasmic localization of the von Hippel-Lindau tumor suppressor gene product is determined by cell density. *Proc Natl Acad Sci U S A* **93**: 1770–1775.
169. Lewis MD, Roberts BJ (2003) Role of nuclear and cytoplasmic localization in the tumour-suppressor activity of the von Hippel-Lindau protein. *Oncogene* **22**: 3992–3997.
170. Lian F, Sreedharan S, Arnold RS, Master VA, Ogan K, Pattaras JG, Roberts DL, Petros JA. Von Hippel-Lindau Exonic Methylation Analysis Using MALDI-TOF Mass Spectrometry *J Urol*. 2014;(14):03197-8.
171. Latif F, Tory K, Gnarr J, Yao M, Duh FM, et al. (1993) Identification of the von Hippel-Lindau disease tumor suppressor gene. *Science* **260**: 1317–1320.
172. Gnarr JR, Tory K, Weng Y, Schmidt L, Wei MH, et al. (1994) Mutations of the VHL tumour suppressor gene in renal carcinoma. *Nat Genet* **7**: 85–90.

- 173.** Iliopoulos O, Kibel A, Gray S, Kaelin WG, Jr. (1995) Tumour suppression by the human von Hippel-Lindau gene product. *Nat Med* 1: 822–826
- 174.** Frew IJ, Krek W (2008) pVHL: a multipurpose adaptor protein. *Sci Signal* 1:pe30.
- 175.** Stebbins CE, Kaelin WG, Jr., Pavletich NP (1999) Structure of the VHL/ElonginC- ElonginB complex: implications for VHL tumor suppressor function. *Science* 284: 455–461.
- 176.** Mikhaylova O, Ignacak ML, Barankiewicz TJ, Harbaugh SV, Yi Y, et al. (2008) The von Hippel-Lindau tumor suppressor protein and Egl-9-Type proline hydroxylases regulate the large subunit of RNA polymerase II in response to oxidative stress. *Mol Cell Biol* 28: 2701–2717.
- 177.** Yang H, Minamishima YA, Yan Q, Schlisio S, Ebert BL, et al. pVHL acts as an adaptor to promote the inhibitory phosphorylation of the NF-kappaB agonist Card9 by CK2. *Mol Cell* (2007) 28: 15–27.
- 178.** Chitalia VC, Foy RL, Bachschmid MM, Zeng L, Panchenko MV, et al. (2008) Jade-1 inhibits Wnt signalling by ubiquitylating beta-catenin and mediates Wnt pathway inhibition by pVHL. *Nat Cell Biol* 10: 1208–1216.
- 179.** Chung CD, Liao J, Liu B, Rao X, Jay P, et al. (1997) Specific inhibition of Stat3 signal transduction by PIAS3. *Science* 278: 1803–1805.
- 180.** Schmidt D, Muller S (2002) Members of the PIAS family act as SUMO ligases for c Jun and p53 and repress p53 activity. *Proc Natl Acad Sci U S A* 99: 2872–2877.
- 181.** Kotaja N, Karvonen U, Janne OA, Palvimo JJ (2002) PIAS proteins modulate transcription factors by functioning as SUMO-1 ligases. *Mol Cell Biol* 22:5222–5234.
- 182.** Altuvia Y, Landgraf P, Lithwick G, Elefant N, Pfeffer S, Aravin A, Brownstein MJ, Tuschl T, Margalit H. Clustering and conservation patterns of human microRNAs. *Nucleic Acids Res.* 2005;12:2697–2706. doi: 10.1093/nar/gki567.
- 183.** He L, Hannon GJ. MicroRNAs: small RNAs with a big role in gene regulation. *Nat Rev Genet.* 2004;12:522–531. doi: 10.1038/nrg1379.
- 184.** Xie B, Ding Q, Han H, Wu D. miRCancer: a microRNA–cancer association database constructed by text mining on literature. *Bioinformatics.* 2013;12:638–644. doi: 10.1093
- 185.** Julia Banzhaf-Strathmann and Dieter Edbauer. Good guy or bad guy: the opposing roles of microRNA 125b in cancer. *Cell Commun Signal.* 2014; 12: 30

- 186.** Yoontae Lee, Rodney C. Samaco, Jennifer R. Gatchel, Christina Thaller, Harry T. Orr, and Huda Y. Zoghbi miR-19, miR-101, and miR-130 co-regulate ATXN1 levels to potentially modulate SCA1 pathogenesis *Nat Neurosci.* 2008 Oct;11(10):1137-9.
- 187.** Benetatos L, Hatzimichael E, Londin E, Vartholomatos G, Loher P, Rigoutsos I, Briasoulis The microRNAs within the DLK1-DIO3 genomic region: involvement in disease pathogenesis. *E.Cell Mol Life Sci.* 2013 Mar; 70(5):795-814.
- 188.** Saurabh V Laddha1†, Subhashree Nayak2†, Deepanjan Paul3, Rajasekhara Reddy4, Charu Sharma5, Prerana Jha2, Manoj Hariharan1, Anurag Agrawal3, Shantanu Chowdhury1,6, Chitra Sarkar2 and Arijit Mukhopadhyay1,3* Genome-wide analysis reveals downregulation of miR-379/miR-656 cluster in human cancers.(2013) *Biology Direct* 8-10.
- 189.** Dichamp C, Taillibert S, guirre-Cruz L, Lejeune J, Marie Y, Kujas M, Delattre JY, Hoang-Xuan K, Sanson M: Loss of 14q chromosome in oligodendroglial and astrocytic tumors. *J Neurooncol* 2004, 67:281–285.
- 190.** Felsberg J, Yan PS, Huang TH, Milde U, Schramm J, Wiestler OD, Reifenberger G, Pietsch T, Waha A: DNA methylation and allelic losses on chromosome arm 14q in oligodendroglial tumours. *Neuropathol Appl Neurobiol* 2006, 32:517–524.
- 191.** Hu J, Pang JC, Tong CY, Lau B, Yin XL, Poon WS, Jiang CC, Zhou LF, Ng HK: High-resolution genome-wide allelotype analysis identifies loss of chromosome 14q as a recurrent genetic alteration in astrocytic tumours. *Br J Cancer* 2002, 87:218–224.
- 192.** Margueron R, Reinberg D. The Polycomb complex PRC2 and its mark in life *Nature.* 2011 Jan 20;469(7330):343-9.
- 193.** da Rocha ST, Edwards CA, Ito M, Ogata T, Ferguson-Smith AC (2008) Genomic imprinting at the mammalian Dlk1-Dio3 domain. *Trends Genet TIG* 24(6):306–316.
- 194.** Bray SJ, Takada S, Harrison E, Shen SC, Ferguson-Smith AC (2008) The atypical mammalian ligand Delta-like homologue 1 (Dlk1) can regulate Notch signalling in *Drosophila*. *BMC Dev Biol* 8: 11.
- 195.** Nueda ML, Baladron V, Sanchez-Solana B, Ballesteros MA, Laborda J (2007) The EGF-like protein dlk1 inhibits notch signaling and potentiates adipogenesis of mesenchymal cells. *J Mol Biol* 367: 1281–1293.

196. Nueda ML, Garcia-Ramirez JJ, Laborda J, Baladron V (2008) dlk1 specifically interacts with insulin-like growth factor binding protein 1 to modulate adipogenesis of 3T3-L1 cells. *J Mol Biol* 379: 428–442.
197. Wang Y, Sul HS (2009) Pref-1 regulates mesenchymal cell commitment and differentiation through Sox9. *Cell Metab* 9: 287–302.
198. Sul HS (2009) Minireview: Pref-1: role in adipogenesis and mesenchymal cell fate. *Mol Endocrinol* 23: 1717–1725.
199. bdallah BM, Boissy P, Tan Q, Dahlgaard J, Traustadottir GA, et al. (2007) dlk1/FA1 regulates the function of human bone marrow mesenchymal stem cells by modulating gene expression of pro-inflammatory cytokines and immune response-related factors. *J Biol Chem* 282: 7339–7351.
200. Li L, Forman SJ, Bhatia R (2005) Expression of DLK1 in hematopoietic cells results in inhibition of differentiation and proliferation. *Oncogene* 24: 4472–4476.
201. DLK1 Promotes Lung Cancer Cell Invasion through Upregulation of MMP9 Expression Depending on Notch Signaling Lin Li., Jinjing Tan., Ying Zhang, Naijun Han, Xuebing Di, Ting Xiao, Shujun Cheng, Yanning Gao*, Yu Liu* March 12, 2014 *Plos ONE*
202. Baladron V, Ruiz-Hidalgo MJ, Nueda ML, Diaz-Guerra MJ, Garcia-Ramirez JJ, et al. (2005) dlk acts as a negative regulator of Notch1 activation through interactions with specific EGF-like repeats. *Exp Cell Res* 303: 343–359.
203. Zhou Y, Zhang X, Klibanski A (2012) MEG3 noncoding RNA: a tumor suppressor. *J Mol Endocrinol* 48(3):R45–R53.
204. Benetatos L, Vartholomatos G, Hatzimichael E (2011) MEG3 imprinted gene contribution in tumorigenesis. *Int J Cancer J Int du cancer* 129(4):773–779.
205. Olive V, Jiang I, He L (2010) mir-17–92, a cluster of miRNAs in the midst of the cancer network. *Int J Biochem Cell Biol* 42: 1348–135471.
206. Matsubara H, Takeuchi T, Nishikawa E, Yanagisawa K, Hayashita Y, et al. (2007) Apoptosis induction by antisense oligonucleotides against miR-17-5p and miR-20a in lung cancers overexpressing miR-17–92. *Oncogene* 26: 6099–6105.
207. Landais S, Landry S, Legault P, Rassart E (2007) Oncogenic potential of the miR-106–363 cluster and its implication in human T-cell leukemia. *Cancer Res* 67: 5699–5707.
208. Wang Z, Liu M, Zhu H, Zhang W, He S, et al. . (2012) miR-106a Is frequently upregulated in gastric cancer and inhibits the extrinsic apoptotic pathway by targeting FAS. *Mol Carcinog*.

209. Thapa DR, Li X, Jamieson BD, Martinez-Maza O (2011) Overexpression of microRNAs from the miR-17–92 paralog clusters in AIDS-related non-Hodgkin's lymphomas. *PLoS One* 6: e20781.
210. Reichek JL, Duan F, Smith LM, Gustafson DM, O'Connor RS, et al. (2011) Genomic and clinical analysis of amplification of the 13q31 chromosomal region in alveolar rhabdomyosarcoma: a report from the Children's Oncology Group. *Clin Cancer Res* 17: 1463–1473.
211. Olive V, Bennett MJ, Walker JC, Ma C, Jiang I, et al. (2009) miR-19 is a key oncogenic component of mir-17–92. *Genes Dev* 23: 2839–2849.
212. Petrocca F, Vecchione A, Croce CM (2008) Emerging role of miR-106b-25/miR-17–92 clusters in the control of transforming growth factor beta signaling. *Cancer Res* 68: 8191–8194
213. Poliseno L, Salmena L, Riccardi L, Fornari A, Song MS, et al. (2010) Identification of the miR-106b~25 microRNA cluster as a proto-oncogenic PTEN-targeting intron that cooperates with its host gene MCM7 in transformation. *Sci Signal* 3: ra29.
214. Mendell JT. 2008. miRiad roles for the miR-17-92 cluster in development and disease. *Cell* 133:217–222.
215. Olive V, Jiang I, He L. 2010. miR-17-92, a cluster of miRNAs in the midst of the cancer network. *Int. J. Biochem. Cell Biol.* 42:1348 –1354.
216. Concepcion CP, Bonetti C, Ventura A. 2012. The microRNA-17-92 family of microRNA clusters in development and disease. *Cancer J.* 18: 262–267.
217. Conkrite K, Sundby M, Mukai S, Thomson JM, Mu D, Hammond SM, MacPherson D. miR-17-92 cooperates with RB pathway mutations to promote retinoblastoma. *Genes Dev.* 2011;(25):1734 –1745.
218. Wang Z. MYC Protein inhibits transcription of the MicroRNA Cluster MC-let7a-a let-7d via non canonical E-box. *JBC*, 2011;18(286):39703-14.

8. SUPPLEMENTAL MATERIAL

Supplemental Table S1

Probeset ID	Gene Symbol	Gene Title	p-value	Fold-change
212768_s_at	OLFM4	olfactomedin 4	7.50E-15	-6.05844
220595_at	PDZRN4	PDZ domain containing RING finger 4	1.12E-13	-19.0241
209614_at	ADH1A /// ADH1B /// ADH1C	alcohol dehydrogenase 1A (class I), alpha polypeptide /// alcohol dehydrogenase	1.52E-13	-19.6607
207175_at	ADIPOQ	adiponectin, C1Q and collagen domain containing	1.03E-12	-21.7721
231181_at	---	Transcribed locus	2.67E-12	-4.6265
231348_s_at	LMO3	LIM domain only 3 (rhombotin-like 2)	5.38E-12	-4.12762
220365_at	ALLC	allantoicase	1.63E-11	-3.72835
1570482_at	SLC22A3	Solute carrier family 22 (extraneuronal monoamine transporter), member 3	9.41E-11	-6.0808
206262_at	ADH1A /// ADH1B /// ADH1C	alcohol dehydrogenase 1A (class I), alpha polypeptide /// alcohol dehydrogenase	1.03E-10	-14.4897
214987_at	---	CDNA clone IMAGE:4801326	1.57E-10	-4.10304
205421_at	SLC22A3	solute carrier family 22 (extraneuronal monoamine transporter), member 3	3.88E-10	-28.4316
213955_at	MYOZ3	myozenin 3	6.33E-10	-3.55193
219820_at	SLC6A16	solute carrier family 6, member 16	7.89E-10	-3.44964
209072_at	MBP	myelin basic protein	8.06E-10	-26.8298
229916_at	ENPP6	ectonucleotide pyrophosphatase/phosphodiesterase 6	1.03E-09	-13.0988
210155_at	MYOC	myocilin, trabecular meshwork inducible glucocorticoid response	1.18E-09	-5.9926
229125_at	ANKRD38	ankyrin repeat domain 38	1.30E-09	-17.2041
205913_at	PLIN	perilipin	1.42E-09	-6.5614
233181_at	VIT	Vitrin	1.49E-09	-4.95073
236577_at	---	Transcribed locus	1.53E-09	-14.493
237465_at	USP53	Ubiquitin specific peptidase 53	1.56E-09	-22.0375
230534_at	MGC15634	hypothetical protein MGC15634	1.61E-09	-2.91335
236154_at	---	CDNA FLJ39382 fis, clone PERIC2000473	1.68E-09	-7.72182
209613_s_at	ADH1B	alcohol dehydrogenase IB (class I), beta polypeptide	1.72E-09	-167.554
210548_at	CCL23	chemokine (C-C motif) ligand 23	3.65E-09	-2.39037
240259_at	LOC646919 ///	hypothetical protein LOC646919 /// hypothetical protein	4.90E-09	-18.7868

	LOC650220	LOC650220		
227899_at	VIT	vitrin	5.02E-09	-27.6827
235377_at	C6orf142	chromosome 6 open reading frame 142	7.58E-09	-8.8617
226071_at	ADAMTSL4	ADAMTS-like 4	8.12E-09	-7.97861
239822_at	---	CDNA clone IMAGE:4816129	8.40E-09	-2.54269
230781_at	---	---	9.91E-09	-5.63208
244111_at	KA21	truncated type I keratin KA21	1.17E-08	-19.7812
239823_at	---	Transcribed locus	1.33E-08	-3.16166
232267_at	GPR133	G protein-coupled receptor 133	1.90E-08	-9.08235
207623_at	ABCF2	ATP-binding cassette, sub-family F (GCN20), member 2	1.93E-08	-5.59826
236989_at	---	Transcribed locus	1.97E-08	-2.66382
1558778_s_at	MKL2	MKL/myocardin-like 2	2.08E-08	-2.91685
238512_at	ST7L	Suppression of tumorigenicity 7 like	2.09E-08	-8.16982
209612_s_at	ADH1B	alcohol dehydrogenase IB (class I), beta polypeptide	2.24E-08	-92.9635
229177_at	MGC45438	hypothetical protein MGC45438	2.54E-08	-19.215
230569_at	KIAA1430	KIAA1430	2.70E-08	-2.44849
208470_s_at	HP /// HPR	haptoglobin /// haptoglobin- related protein	3.05E-08	-6.39914
236456_at	PTPN5	protein tyrosine phosphatase, non-receptor type 5 (striatum- enriched)	3.40E-08	-7.2145
240397_x_at	---	Transcribed locus	4.59E-08	-4.41063
241470_x_at	---	Transcribed locus, moderately similar to NP_05530-1.1 neuronal thread protein AD7	4.75E-08	-6.85492
236996_at	---	---	5.55E-08	-2.84459
241684_at	---	Transcribed locus, weakly similar to NP_060312.1 hypothetical protein FLJ20489 [6.41E-08	-2.91088
217504_at	ABCA6	ATP-binding cassette, sub-family A (ABC1), member 6	9.47E-08	-10.8786
235978_at	FABP4	Fatty acid binding protein 4, adipocyte	9.89E-08	-4.64949
1555520_at	PTCH	patched homolog (Drosophila)	1.20E-07	-2.07862
1559072_a_at	KIAA1904	KIAA1904 protein	1.24E-07	-2.84572
213493_at	SNED1	sushi, nidogen and EGF-like domains 1	1.25E-07	-4.01979
244704_at	NFYB	nuclear transcription factor Y, beta	1.27E-07	-2.7283
230311_s_at	PRDM6	PR domain containing 6	1.30E-07	-8.2821
213618_at	CENTD1	centaurin, delta 1	1.30E-07	-6.13185
236704_at	PDE4DIP	Phosphodiesterase 4D interacting protein (myomegalin)	1.33E-07	-3.73834
241215_at	MRAS	Muscle RAS oncogene homolog	1.47E-07	-2.9511
229975_at	---	Transcribed locus	1.48E-07	-15.4004
229839_at	SCARA5	Scavenger receptor class A,	1.51E-07	-57.2268

		member 5 (putative)		
231234_at	CTSC	cathepsin C	1.51E-07	-4.90547
229942_at	BNC2	Basonuclin 2	1.60E-07	-6.64232
214106_s_at	GMDS	GDP-mannose 4,6-dehydratase	1.71E-07	-2.89973
		Transcribed locus, moderately		
240272_at	---	similar to XP_511479.1	1.73E-07	-3.78402
		PREDICTED: similar to kerat		
244203_at	---	Transcribed locus	1.87E-07	-4.95073
229019_at	ZNF533	zinc finger protein 533	2.20E-07	-5.44212
201153_s_at	MBNL1	muscleblind-like (Drosophila)	2.21E-07	-2.48006
235382_at	FLJ90650	laeverin	2.30E-07	-3.37451
207255_at	LEPR	leptin receptor	2.69E-07	-3.1058
227265_at	KIAA1505	KIAA1505 protein	2.80E-07	-6.99502
229153_at	---	---	3.03E-07	-2.64257
220297_at	BTBD7	BTB (POZ) domain containing 7	3.59E-07	-2.64287
240413_at	PYHIN1	pyrin and HIN domain family, member 1	3.78E-07	-2.33523
		sushi, von Willebrand factor type		
219552_at	SVEP1	A, EGF and pentraxin domain containing 1	3.83E-07	-2.53956
235723_at	BNC2	basonuclin 2	4.03E-07	-4.87849
206737_at	WNT11	wingless-type MMTV integration site family, member 11	4.66E-07	-2.08959
235849_at	SCARA5	scavenger receptor class A, member 5 (putative)	4.86E-07	-26.4076
204982_at	GIT2	G protein-coupled receptor kinase interactor 2	4.88E-07	-2.86132
214661_s_at	C4orf9	chromosome 4 open reading frame 9	5.11E-07	-2.14365
1559057_at	CXorf45	Chromosome X open reading frame 45	5.29E-07	-2.25841
229974_at	EVC2	Ellis van Creveld syndrome 2 (limbin)	5.48E-07	-4.05799
224454_at	ETNK1	ethanolamine kinase 1 /// ethanolamine kinase 1	5.56E-07	-3.98448
206462_s_at	NTRK3	neurotrophic tyrosine kinase, receptor, type 3	5.67E-07	-2.4314
212927_at	SMC5L1	SMC5 structural maintenance of chromosomes 5-like 1 (yeast)	5.70E-07	-2.49296
205382_s_at	CFD	complement factor D (adipsin)	5.72E-07	-43.8204
	LOC642891	hypothetical protein LOC642891		
243432_at	///	/// hypothetical protein	5.93E-07	-3.20488
	LOC649158	LOC649158		
222043_at	CLU	clusterin	6.03E-07	-26.8918
213924_at	MPPE1	Metallophosphoesterase 1	7.64E-07	-11.989
208012_x_at	SP110	SP110 nuclear body protein	7.94E-07	-2.75023
1552457_a_at	ADAMTSL1	ADAMTS-like 1	8.42E-07	-2.6544
242605_at	DCN	Decorin	8.54E-07	-4.29532
1560739_a_at	UBE3C	Ubiquitin protein ligase E3C	9.47E-07	-2.16998
218901_at	PLSCR4	phospholipid scramblase 4	9.89E-07	-3.90713

224022_x_at	WNT16	wingless-type MMTV integration site family, member 16	1.03E-06	-2.28195
205752_s_at	GSTM5	glutathione S-transferase M5	1.05E-06	-5.51278
223468_s_at	RGMA	RGM domain family, member A	1.07E-06	-3.12873
218211_s_at	MLPH	melanophilin	1.07E-06	-4.29581
207820_at	ADH1A	alcohol dehydrogenase 1A (class I), alpha polypeptide	1.08E-06	-2.10807
234970_at	MTAC2D1	membrane targeting (tandem) C2 domain containing 1	1.09E-06	-4.98269
222376_at	---	Transcribed locus	1.10E-06	-2.50231
226342_at	SPTBN1	Spectrin, beta, non-erythrocytic 1	1.11E-06	-5.02894
226625_at	---	---	1.18E-06	-7.22839
207468_s_at	SFRP5	secreted frizzled-related protein 5	1.19E-06	-5.07077
204955_at	SRPX	sushi-repeat-containing protein, X-linked	1.23E-06	-10.2594
230595_at	LOC572558	hypothetical locus LOC572558	1.28E-06	-6.96205
232795_at	---	CDNA FLJ10145 fis, clone HEMBA1003322	1.34E-06	-2.75347
223843_at	SCARA3	scavenger receptor class A, member 3	1.36E-06	-12.2373
219398_at	CIDEC	cell death-inducing DFFA-like effector c	1.46E-06	-2.46709
230360_at	GLDN	gliomedin	1.47E-06	-14.9817
219938_s_at	PSTPIP2	proline-serine-threonine phosphatase interacting protein 2	1.55E-06	-2.40931
207545_s_at	NUMB	numb homolog (Drosophila)	1.56E-06	-2.0314
210335_at	PAMCI	peptidylglycine alpha-amidating monooxygenase COOH-terminal interactor	1.57E-06	-3.59563
235829_at	LOC643234	Hypothetical protein LOC643234	1.60E-06	-2.32195
206407_s_at	CCL13	chemokine (C-C motif) ligand 13	1.68E-06	-6.86535
222549_at	CLDN1	claudin 1	1.73E-06	-24.5476
219153_s_at	THSD4	thrombospondin, type I, domain containing 4	1.82E-06	-3.22354
236927_at	---	---	1.87E-06	-3.57556
205430_at	BMP5	bone morphogenetic protein 5	1.97E-06	-13.3781
209212_s_at	KLF5	Kruppel-like factor 5 (intestinal)	2.23E-06	-4.37345
204834_at	FGL2	fibrinogen-like 2	2.31E-06	-7.30057
219429_at	FA2H	fatty acid 2-hydroxylase	2.41E-06	-3.37328
220024_s_at	PRX	periaxin	2.65E-06	-3.09834
209211_at	KLF5	Kruppel-like factor 5 (intestinal)	2.76E-06	-16.3687
218631_at	AVPI1	arginine vasopressin-induced 1	2.76E-06	-2.6605
210852_s_at	AASS	aminoadipate-semialdehyde synthase	2.82E-06	-4.73559
228307_at	EMILIN3	elastin microfibril interfacier 3	2.93E-06	-4.27945
206181_at	SLAMF1	signaling lymphocytic activation molecule family member 1	2.97E-06	-2.40092
205083_at	AOX1	aldehyde oxidase 1	3.10E-06	-16.3439
1556627_at	DRP2	dystrophin related protein 2	3.11E-06	-2.84269
228411_at	ALS2CR19	amyotrophic lateral sclerosis 2	3.12E-06	-3.8447

		(juvenile) chromosome region, candidate 19		
232570_s_at	ADAM33	ADAM metallopeptidase domain 33	3.21E-06	-4.58088
230083_at	---	Full length insert cDNA clone YI48C03	3.66E-06	-11.6805
235414_at	ZNF383	zinc finger protein 383	3.70E-06	-2.18839
222453_at	CYBRD1	cytochrome b reductase 1	3.81E-06	-5.60464
214790_at	SENP6	SUMO1/sentrin specific peptidase 6	3.83E-06	-2.70898
202445_s_at	NOTCH2	Notch homolog 2 (Drosophila)	3.94E-06	-2.5729
204823_at	NAV3	neuron navigator 3	4.02E-06	-3.6223
209335_at	DCN	decorin	4.05E-06	-9.00225
230734_x_at	---	---	4.50E-06	-2.2582
213488_at	SNED1	sushi, nidogen and EGF-like domains 1	4.59E-06	-5.40474
209135_at	ASPH	aspartate beta-hydroxylase	4.62E-06	-2.54964
1559901_s_at	C21orf34	chromosome 21 open reading frame 34	4.69E-06	-3.47862
32099_at	SAFB2	scaffold attachment factor B2	4.78E-06	-2.00959
225745_at	LRP6	low density lipoprotein receptor- related protein 6	4.88E-06	-2.07414
238032_at	DHRS3	Dehydrogenase/reductase (SDR family) member 3	5.02E-06	-6.45013
243631_at	LOC642333	similar to M-phase phosphoprotein, mpp8	5.14E-06	-4.17094
227334_at	USP54	ubiquitin specific peptidase 54	5.27E-06	-2.38274
239132_at	NOS1	Nitric oxide synthase 1 (neuronal)	5.52E-06	-4.26276
209762_x_at	SP110	SP110 nuclear body protein	5.66E-06	-2.92652
218245_at	LRRC54	leucine rich repeat containing 54	5.78E-06	-2.89358
231180_at	---	---	6.16E-06	-2.41672
218744_s_at	PACSIN3	protein kinase C and casein kinase substrate in neurons 3	6.33E-06	-2.32872
205020_s_at	ARL4A	ADP-ribosylation factor-like 4A	7.09E-06	-3.78402
242436_at	PLEKHH2	Pleckstrin homology domain containing, family H (with MyTH4 domain) member 2	7.15E-06	-2.35878
201719_s_at	EPB41L2	erythrocyte membrane protein band 4.1-like 2	7.19E-06	-3.98781
202057_at	KPNA1	karyopherin alpha 1 (importin alpha 5)	7.38E-06	-2.14327
1555800_at	ZNF533	zinc finger protein 533	7.42E-06	-2.72305
228399_at	OSR1	odd-skipped related 1 (Drosophila)	7.48E-06	-5.4398
221675_s_at	CHPT1	choline phosphotransferase 1	7.53E-06	-2.72159
212738_at	ARHGAP19	Rho GTPase activating protein 19	7.54E-06	-2.7062
210168_at	C6	complement component 6	7.67E-06	-4.92249
228056_s_at	NAPSB	napsin B aspartic peptidase pseudogene	7.93E-06	-2.61906
230163_at	LOC143381	Hypothetical protein LOC143381	8.04E-06	-3.37262

230443_at	NHP2L1	NHP2 non-histone chromosome protein 2-like 1 (<i>S. cerevisiae</i>)	8.17E-06	-2.24058
226656_at	CRTAP	cartilage associated protein	8.23E-06	-2.75917
207067_s_at	HDC	histidine decarboxylase	8.34E-06	-2.04428
226435_at	PAPLN	papilin, proteoglycan-like sulfated glycoprotein	8.40E-06	-13.1594
235338_s_at	SETDB2	SET domain, bifurcated 2	8.87E-06	-2.87067
221081_s_at	DENND2D	DENN/MADD domain containing 2D	8.89E-06	-3.73518
239989_at	C9orf39	Chromosome 9 open reading frame 39	9.16E-06	-2.52408
212636_at	QKI	quaking homolog, KH domain RNA binding (mouse)	9.20E-06	-3.21212
230053_at	---	Transcribed locus	9.44E-06	-2.89757
239775_at	---	Transcribed locus, moderately similar to NP_05530-1.1 neuronal thread protein AD7	9.49E-06	-2.6765
205792_at	WISP2	WNT1 inducible signaling pathway protein 2	9.52E-06	-14.9368
238778_at	MPP7	membrane protein, palmitoylated 7 (MAGUK p55 subfamily member 7)	9.87E-06	-4.03148
59631_at	TXNRD3	thioredoxin reductase 3	9.94E-06	-2.14193
239984_at	SCN7A	Sodium channel, voltage-gated, type VII, alpha	1.01E-05	-10.3894
209894_at	LEPR	leptin receptor	1.04E-05	-13.0152
232424_at	PRDM16	PR domain containing 16	1.05E-05	-6.87233
219550_at	ROBO3	roundabout, axon guidance receptor, homolog 3 (<i>Drosophila</i>)	1.07E-05	-2.6063
229204_at	HP1BP3	Heterochromatin protein 1, binding protein 3	1.09E-05	-3.29533
208383_s_at	PCK1	phosphoenolpyruvate carboxykinase 1 (soluble)	1.09E-05	-14.4328
241359_at	---	CDNA FLJ20031 fis, clone ADSU02180	1.11E-05	-4.71312
205033_s_at	DEFA1 /// DEFA3 /// LOC653600	defensin, alpha 1 /// defensin, alpha 3, neutrophil-specific /// similar to Neut	1.14E-05	-6.79758
239786_at	---	Transcribed locus	1.17E-05	-2.07611
227731_at	---	CDNA FLJ11631 fis, clone HEMBA1004267	1.18E-05	-2.46091
230364_at	CHPT1	choline phosphotransferase 1 neurofibromin 1	1.20E-05	-3.6172
210631_at	NF1	(neurofibromatosis, von Recklinghausen disease, Watson disease)	1.21E-05	-2.28104
235209_at	RPESP	RPE-spondin	1.27E-05	-6.16591
223167_s_at	USP25	ubiquitin specific peptidase 25	1.27E-05	-3.23118
209568_s_at	RGL1	ral guanine nucleotide dissociation stimulator-like 1	1.28E-05	-3.53269

206307_s_at	FOXD1	forkhead box D1	1.28E-05	-9.63067
236422_at	FLJ22662	Hypothetical protein FLJ22662	1.28E-05	-2.13837
203071_at	SEMA3B	sema domain, immunoglobulin domain (Ig), short basic domain, secreted, (semaphor	1.29E-05	-5.67296
222279_at	RP3-377H14.5	hypothetical protein FLJ35429	1.30E-05	-2.73403
1553129_at	SVEP1	sushi, von Willebrand factor type A, EGF and pentraxin domain containing 1	1.38E-05	-2.08932
237038_at	CXCL14	chemokine (C-X-C motif) ligand 14	1.39E-05	-2.75474
227108_at	STARD9	START domain containing 9	1.41E-05	-2.93619
235610_at	ALKBH8	AlkB, alkylation repair homolog 8 (E. coli)	1.42E-05	-2.81363
237571_at	APP	Amyloid beta (A4) precursor protein (peptidase nexin-II, Alzheimer disease)	1.43E-05	-3.33945
239762_at	LOC286437	hypothetical protein LOC286437	1.46E-05	-2.50767
203851_at	IGFBP6	insulin-like growth factor binding protein 6	1.46E-05	-16.0662
231978_at	TPCN2	two pore segment channel 2	1.52E-05	-2.07565
220016_at	AHNAK	AHNAK nucleoprotein (desmoyokin)	1.52E-05	-3.94746
235964_x_at	C20orf118	Chromosome 20 open reading frame 118	1.54E-05	-3.26497
205379_at	CBR3	carbonyl reductase 3	1.59E-05	-4.5315
229114_at	---	CDNA clone IMAGE:4801326	1.61E-05	-7.23299
230661_at	LOC286191	Hypothetical protein LOC286191	1.63E-05	-6.68928
231182_at	WASPIP	Wiskott-Aldrich syndrome protein interacting protein	1.64E-05	-2.58746
1560425_s_at	PTPRD	Protein tyrosine phosphatase, receptor type, D	1.67E-05	-2.22101
205579_at	HRH1	histamine receptor H1	1.67E-05	-5.042
215436_at	HSDL2	Hydroxysteroid dehydrogenase like 2	1.70E-05	-2.02729
218845_at	DUSP22	dual specificity phosphatase 22	1.71E-05	-2.01806
232088_x_at	---	CDNA clone IMAGE:4829494	1.71E-05	-3.89431
228537_at	GLI2	GLI-Kruppel family member GLI2	1.72E-05	-2.35901
235155_at	BDH2	3-hydroxybutyrate dehydrogenase, type 2	1.74E-05	-3.71429
230161_at	CD99	CD99 molecule	1.88E-05	-3.0664
226765_at	---	CDNA clone IMAGE:3897439	1.93E-05	-3.18363
227492_at	OCLN	Occludin	1.96E-05	-3.60956
227379_at	OACT1	O-acyltransferase (membrane bound) domain containing 1	1.97E-05	-2.90612
232154_at	LOC199800	hypothetical protein LOC199800	2.05E-05	-3.51949
206423_at	ANGPTL7	angiopoietin-like 7	2.06E-05	-11.1872
235339_at	SETDB2	SET domain, bifurcated 2	2.08E-05	-2.46136
218823_s_at	KCTD9	potassium channel tetramerisation domain	2.08E-05	-2.39163

		containing 9		
228728_at	FLJ21986	hypothetical protein FLJ21986	2.10E-05	-6.97975
207082_at	CSF1	colony stimulating factor 1 (macrophage)	2.12E-05	-2.30185
239133_at	---	Transcribed locus	2.13E-05	-2.16271
231817_at	USP53	ubiquitin specific peptidase 53	2.19E-05	-6.21725
226304_at	HSPB6	heat shock protein, alpha- crystallin-related, B6	2.24E-05	-6.77453
226834_at	---	Transcribed locus, strongly similar to NP_079045.1 adipocyte- specific adhesion m	2.25E-05	-10.0326
228486_at	SLC44A1	solute carrier family 44, member 1	2.31E-05	-7.42751
230433_at	---	---	2.37E-05	-3.13254
210607_at	FLT3LG	fms-related tyrosine kinase 3 ligand	2.43E-05	-2.77982
210549_s_at	CCL23	chemokine (C-C motif) ligand 23	2.49E-05	-3.24915
241302_at	C7	Complement component 7	2.52E-05	-3.69556
227782_at	ZBTB7C	zinc finger and BTB domain containing 7C	2.57E-05	-3.17621
200785_s_at	LRP1	low density lipoprotein-related protein 1 (alpha-2-macroglobulin receptor)	2.59E-05	-3.64849
230692_at	LOC157503	hypothetical protein LOC157503	2.61E-05	-5.76235
231678_s_at	ADH4	alcohol dehydrogenase 4 (class II), pi polypeptide	2.63E-05	-2.2916
202481_at	DHRS3	dehydrogenase/reductase (SDR family) member 3	2.66E-05	-5.93731
228538_at	ZNF662	zinc finger protein 662	2.71E-05	-2.3367
230067_at	FLJ30707	Hypothetical protein FLJ30707	2.73E-05	-2.70183
244661_at	---	---	2.75E-05	-2.40196
228312_at	PI16	peptidase inhibitor 16	2.79E-05	-2.33916
1557053_s_at	UBE2G2 /// TAX1BP3	ubiquitin-conjugating enzyme E2G 2 (UBC7 homolog, yeast) /// Tax1 (human T-cell	2.79E-05	-2.07621
237444_at	---	Transcribed locus	2.80E-05	-3.98487
219081_at	ANKHD1	ankyrin repeat and KH domain containing 1	2.84E-05	-2.0447
237291_at	LOC344405	hypothetical LOC344405	2.84E-05	-2.68079
214744_s_at	RPL23	Ribosomal protein L23	2.88E-05	-2.16497
206529_x_at	SLC26A4	solute carrier family 26, member 4	2.93E-05	-2.38966
201525_at	APOD	apolipoprotein D	3.02E-05	-50.4937
244422_at	---	Transcribed locus	3.02E-05	-2.04319
224061_at	INMT	indolethylamine N- methyltransferase	3.02E-05	-9.13145
219812_at	MGC2463	hypothetical protein LOC79037	3.04E-05	-2.3453
1554237_at	SDCCAG8	serologically defined colon cancer antigen 8	3.05E-05	-3.18212
213942_at	MEGF6	multiple EGF-like-domains 6	3.14E-05	-2.42409
231776_at	EOMES	eomesodermin homolog (<i>Xenopus laevis</i>)	3.17E-05	-4.39839

219213_at	JAM2	junctional adhesion molecule 2	3.17E-05	-4.76428
223842_s_at	SCARA3	scavenger receptor class A, member 3	3.18E-05	-4.67603
240331_at	BMPR1B	Bone morphogenetic protein receptor, type IB	3.19E-05	-3.27683
206227_at	CILP	cartilage intermediate layer protein, nucleotide pyrophosphohydrolase	3.22E-05	-6.21794
225814_at	XRN1	5'-3' exoribonuclease 1	3.26E-05	-2.05631
226588_at	KIAA1604	KIAA1604 protein	3.39E-05	-2.11753
229604_at	CMAH	Cytidine monophosphate-N-acetylneuraminic acid hydroxylase (CMP-N-acetylneuramin	3.44E-05	-6.77419
238780_s_at	---	MRNA; cDNA DKFZp779F2345 (from clone DKFZp779F2345)	3.52E-05	-5.08338
1557123_a_at	RP4-756G23.1	hypothetical protein BC012882	3.61E-05	-2.54339
206552_s_at	TAC1	tachykinin, precursor 1 (substance K, substance P, neurokinin 1, neurokinin 2, n	3.65E-05	-35.9298
209795_at	CD69	CD69 molecule	3.66E-05	-9.63885
209960_at	HGF	hepatocyte growth factor (hepapoietin A; scatter factor)	3.66E-05	-6.93804
226571_s_at	---	Transcribed locus	3.67E-05	-3.09992
213960_at	---	CDNA FLJ37610 fis, clone BRCOC2011398	3.87E-05	-7.89387
205804_s_at	TRAF3IP3	TRAF3 interacting protein 3	3.89E-05	-2.09938
214180_at	MAN1C1	mannosidase, alpha, class 1C, member 1	3.90E-05	-6.39647
214073_at	CTTN	cortactin	3.91E-05	-4.67183
227984_at	LOC650392	Hypothetical protein LOC650392	3.95E-05	-3.32334
235335_at	ABCA9	ATP-binding cassette, sub-family A (ABC1), member 9	3.96E-05	-3.03375
210321_at	GZMH	granzyme H (cathepsin G-like 2, protein h-CCPX) /// granzyme H (cathepsin G-like	3.97E-05	-2.21625
242923_at	ZNF678	Zinc finger protein 678	3.97E-05	-2.22458
208131_s_at	PTGIS	prostaglandin I2 (prostacyclin) synthase /// prostaglandin I2 (prostacyclin) syn	3.99E-05	-16.302
232576_at	---	CDNA FLJ11519 fis, clone HEMBA1002348	4.00E-05	-2.32046
227503_at	PVRL3	Poliovirus receptor-related 3	4.04E-05	-3.78035
219416_at	SCARA3	scavenger receptor class A, member 3	4.09E-05	-3.54295
228029_at	ZNF721	zinc finger protein 721	4.11E-05	-2.34222
212929_s_at	FAM21B /// FAM21C /// RP11-56A2-1.1 /// LOC653450	family with sequence similarity 21, member B /// family with sequence similarity	4.12E-05	-2.3189

223596_at	SLC12A6	solute carrier family 12 (potassium/chloride transporters), member 6	4.12E-05	-2.29947
226326_at	PCGF5	polycomb group ring finger 5	4.23E-05	-2.17902
243256_at	MKNK1	MAP kinase interacting serine/threonine kinase 1	4.23E-05	-2.112
207072_at	IL18RAP	interleukin 18 receptor accessory protein	4.30E-05	-2.4488
215311_at	---	MRNA full length insert cDNA clone EUROIMAGE 21920	4.39E-05	-4.8323
202350_s_at	MATN2	matrilin 2	4.58E-05	-6.8773
236600_at	SPG20	spastic paraplegia 20, spartin (Troyer syndrome)	4.61E-05	-4.36297
220416_at	ATP8B4	ATPase, Class I, type 8B, member 4	4.63E-05	-3.10675
232027_at	SYNE1	Spectrin repeat containing, nuclear envelope 1	4.72E-05	-3.19351
222103_at	ATF1	Activating transcription factor 1	4.83E-05	-2.09293
228641_at	CARD8	caspase recruitment domain family, member 8	4.85E-05	-2.89274
205431_s_at	BMP5	bone morphogenetic protein 5	4.91E-05	-3.66454
236748_at	RASGEF1C	RasGEF domain family, member 1C	5.01E-05	-2.15621
203494_s_at	CEP57	centrosomal protein 57kDa	5.05E-05	-2.40663
43427_at	ACACB	acetyl-Coenzyme A carboxylase beta	5.13E-05	-4.11058
228549_at	---	---	5.15E-05	-2.8549
204963_at	SSPN	sarcospan (Kras oncogene- associated gene)	5.28E-05	-6.16719
225332_at	KRTAP4-7	Keratin associated protein 4-7	5.37E-05	-2.36428
227561_at	LOC651619	hypothetical protein LOC651619	5.40E-05	-3.68544
229027_at	PPM1A	Protein phosphatase 1A (formerly 2C), magnesium-dependent, alpha isoform	5.56E-05	-2.04778
203407_at	PPL	periplakin	5.74E-05	-13.2221
226522_at	PODN	podocan	5.74E-05	-7.75467
221928_at	ACACB	acetyl-Coenzyme A carboxylase beta	5.75E-05	-2.90563
209717_at	EVI5	ecotropic viral integration site 5	5.77E-05	-2.075
236027_at	C10orf78	chromosome 10 open reading frame 78	5.77E-05	-2.38792
241773_at	---	---	5.82E-05	-4.28658
222624_s_at	ZNF639	zinc finger protein 639	5.83E-05	-2.36187
213888_s_at	TRAF3IP3	TRAF3 interacting protein 3	5.87E-05	-3.54381
215918_s_at	SPTBN1	spectrin, beta, non-erythrocytic 1	5.88E-05	-6.58586
228778_at	MCPH1	Microcephaly, primary autosomal recessive 1	5.90E-05	-2.45826
222912_at	ARRB1	arrestin, beta 1	5.94E-05	-4.68532
227550_at	LOC143381	hypothetical protein LOC143381	6.03E-05	-4.86483
239272_at	MMP28	matrix metalloproteinase 28	6.07E-05	-3.49279

225442_at	---	Clone DPDP-3 dental pulp-derived protein 3, mRNA sequence	6.09E-05	-3.49025
226806_s_at	---	---	6.23E-05	-6.08796
243998_at	KA21	Truncated type I keratin KA21	6.29E-05	-3.99085
210944_s_at	CAPN3	calpain 3, (p94)	6.32E-05	-3.45232
1563498_s_at	LOC283130	hypothetical protein LOC283130	6.34E-05	-2.48535
231898_x_at	SOX2OT	SOX2 overlapping transcript (non-coding RNA)	6.34E-05	-4.46488
231174_s_at	---	Transcribed locus	6.37E-05	-3.6369
213247_at	SVEP1	sushi, von Willebrand factor type A, EGF and pentraxin domain containing 1	6.39E-05	-9.54956
236035_at	---	Transcribed locus	6.41E-05	-3.21685
240182_at	HLA-A	Major histocompatibility complex, class I, A	6.53E-05	-2.16114
219011_at	PLEKHA4	pleckstrin homology domain containing, family A	6.54E-05	-3.43207
209527_at	EXOSC2	(phosphoinositide binding specific) exosome component 2	6.56E-05	-2.12287
209589_s_at	EPHB2	EPH receptor B2	6.64E-05	-2.85227
235746_s_at	PLA2R1	phospholipase A2 receptor 1, 180kDa	6.70E-05	-5.46352
226021_at	RDH10	retinol dehydrogenase 10 (all-trans)	6.77E-05	-3.6135
219669_at	CD177	CD177 molecule	7.04E-05	-2.79321
35776_at	ITSN1	intersectin 1 (SH3 domain protein)	7.06E-05	-2.50589
203980_at	FABP4	fatty acid binding protein 4, adipocyte	7.07E-05	-31.2407
211663_x_at	PTGDS	prostaglandin D2 synthase 21kDa (brain) /// prostaglandin D2 synthase 21kDa (bra	7.10E-05	17.3196
238786_at	---	Transcribed locus	7.14E-05	-2.13034
206201_s_at	MEOX2	mesenchyme homeobox 2	7.17E-05	-22.163
242957_at	VWCE	von Willebrand factor C and EGF domains	7.22E-05	-2.61664
1568900_a_at	ZNF568	zinc finger protein 568	7.26E-05	-2.17953
1555762_s_at	RBM15	RNA binding motif protein 15	7.26E-05	-2.16591
205987_at	CD1C	CD1c molecule	7.27E-05	-2.3959
241933_at	---	---	7.33E-05	-2.06055
213225_at	PPM1B	protein phosphatase 1B (formerly 2C), magnesium-dependent, beta isoform	7.33E-05	-2.07766
229041_s_at	ITGB2	Integrin, beta 2 (complement component 3 receptor 3 and 4 subunit)	7.38E-05	-2.40335
225185_at	MRAS /// LOC653764	muscle RAS oncogene homolog /// similar to muscle RAS oncogene homolog	7.44E-05	-3.05556
237419_at	---	Transcribed locus	7.48E-05	-2.24707
226739_at	RNF169	ring finger protein 169	7.48E-05	-2.46053

1553132_a_at	MTAC2D1	membrane targeting (tandem) C2 domain containing 1	7.65E-05	-2.51667
225990_at	BOC	Boc homolog (mouse)	7.80E-05	-4.77755
209540_at	IGF1	insulin-like growth factor 1 (somatomedin C)	7.86E-05	-12.7731
204719_at	ABCA8	ATP-binding cassette, sub-family A (ABC1), member 8	7.86E-05	-13.2325
232068_s_at	TLR4	toll-like receptor 4	7.93E-05	-3.4744
213716_s_at	SECTM1	secreted and transmembrane 1	8.02E-05	-2.24617
218847_at	IGF2BP2	insulin-like growth factor 2 mRNA binding protein 2	8.11E-05	-3.49284
37577_at	ARHGAP19	Rho GTPase activating protein 19	8.12E-05	-3.49615
218983_at	C1RL	complement component 1, r subcomponent-like	8.22E-05	-7.09539
214434_at	HSPA12A	heat shock 70kDa protein 12A	8.34E-05	-3.08427
225524_at	ANTXR2	anthrax toxin receptor 2	8.37E-05	-3.04082
235210_s_at	RPESP	RPE-spondin	8.52E-05	-7.43021
32502_at	GDPD5	glycerophosphodiester phosphodiesterase domain containing 5	8.56E-05	-2.24874
235259_at	MGC29898	hypothetical protein MGC29898	8.78E-05	-2.61758
235639_at	---	Transcribed locus	8.80E-05	-7.06479
238151_at	TUBB6	Tubulin, beta 6	8.82E-05	-4.92082
209542_x_at	IGF1	insulin-like growth factor 1 (somatomedin C)	8.88E-05	-5.68386
238679_at	MESDC2	mesoderm development candidate 2	8.90E-05	-2.15388
204686_at	IRS1	insulin receptor substrate 1	8.97E-05	-4.00874
224339_s_at	ANGPTL1	angiopoietin-like 1 /// angiopoietin-like 1	9.05E-05	-2.60836
204010_s_at	KRAS	v-Ki-ras2 Kirsten rat sarcoma viral oncogene homolog	9.05E-05	-2.11603
219594_at	NINJ2	ninjurin 2	9.06E-05	-3.21002
205619_s_at	MEOX1	mesenchyme homeobox 1	9.06E-05	-13.5517
240556_at	DCN	Decorin	9.09E-05	-2.26341
212187_x_at	PTGDS	prostaglandin D2 synthase 21kDa (brain)	9.34E-05	-39.989
213800_at	CFH	complement factor H	9.45E-05	-8.09625
202965_s_at	CAPN6	calpain 6	9.53E-05	-8.34429
229880_at	LOC643517	hypothetical protein LOC643517	9.57E-05	-2.52172
230423_at	---	Transcribed locus, strongly similar to XP_373845.2 PREDICTED: hypothetical prote	9.58E-05	-2.12693
235182_at	C20orf82	chromosome 20 open reading frame 82	9.59E-05	-6.58568
238036_at	---	---	9.67E-05	-3.35182
205609_at	ANGPT1	angiopoietin 1	9.86E-05	-6.40239
220351_at	CCRL1	chemokine (C-C motif) receptor-like 1	9.93E-05	-8.12473
217833_at	SYNCRIP	synaptotagmin binding,	0.0001003	-2.12809

		cytoplasmic RNA interacting protein		
230722_at	BNC2	Basonuclin 2	0.0001008	-9.50103
210051_at	RAPGEF3	Rap guanine nucleotide exchange factor (GEF) 3	0.0001009	-5.27353
204606_at	CCL21	chemokine (C-C motif) ligand 21	0.0001017	-5.44632
209120_at	NR2F2	nuclear receptor subfamily 2, group F, member 2	0.000102	-2.67379
39248_at	AQP3	aquaporin 3 (Gill blood group)	0.0001027	-14.6771
206087_x_at	HFE	hemochromatosis	0.000103	-2.19198
211012_s_at	PML /// LOC161527 /// LOC652671	promyelocytic leukemia /// hypothetical protein LOC161527 /// /// similar to promyel	0.0001036	-2.44277
226773_at	---	MRNA (clone ICRFp50711077)	0.0001052	-2.54785
49452_at	ACACB	acetyl-Coenzyme A carboxylase beta	0.0001054	-4.28162
1558972_s_at	C6orf190	chromosome 6 open reading frame 190	0.0001059	-2.41465
206682_at	CLEC10A	C-type lectin domain family 10, member A	0.000106	-3.97195
210072_at	CCL19	chemokine (C-C motif) ligand 19	0.0001065	-14.7015
231001_at	LOC387758	similar to RIKEN cDNA 1110018M03	0.0001066	-6.55206
1555103_s_at	FGF7	fibroblast growth factor 7 (keratinocyte growth factor)	0.0001067	-8.4425
236396_at	---	Transcribed locus	0.0001077	-4.49896
213183_s_at	CDKN1C	Cyclin-dependent kinase inhibitor 1C (p57, Kip2)	0.0001078	-7.24831
231002_s_at	RABEP1	Rabaptin, RAB GTPase binding effector protein 1	0.0001078	-2.0435
228618_at	PEAR1	platelet endothelial aggregation receptor 1	0.0001098	-4.25282
226197_at	---	---	0.0001099	-4.9606
237056_at	INSC	inscuteable	0.000111	-3.15432
231382_at	FGF18	Fibroblast growth factor 18	0.0001115	-6.48889
225373_at	C10orf54	chromosome 10 open reading frame 54	0.0001118	-2.70175
33307_at	CTA-126B4.3	CGI-96 protein	0.0001122	-2.0573
229585_at	C9orf94	chromosome 9 open reading frame 94	0.0001168	-7.254
228853_at	LOC653890	similar to serine/threonine/tyrosine interacting protein	0.0001186	-2.13106
228573_at	---	Full-length cDNA clone CSODD001YA12 of Neuroblastoma	0.0001191	-3.64393
228568_at	Gcom1	Cot 50-normalized of Homo s GRINL1A combined protein	0.0001192	-2.50934
242181_at	---	CDNA FLJ33489 fis, clone BRAMY2003585	0.00012	-3.61056

209309_at	AZGP1	alpha-2-glycoprotein 1, zinc	0.0001204	-5.6232
238431_at	---	Transcribed locus	0.0001213	-2.16747
241393_at	IPP	Intracisternal A particle-promoted polypeptide	0.0001215	-2.01145
205226_at	PDGFRL	platelet-derived growth factor receptor-like	0.0001219	-15.6069
239796_x_at	TIRAP	toll-interleukin 1 receptor (TIR) domain containing adaptor protein	0.000123	-2.00362
225398_at	RPUSD4	RNA pseudouridylylase domain containing 4	0.0001233	-2.01085
231984_at	MTAP	methylthioadenosine phosphorylase	0.0001281	-2.44661
222209_s_at	TMEM135	transmembrane protein 135	0.0001285	-2.07592
210694_s_at	---	---	0.0001304	-2.48887
225646_at	CTSC	cathepsin C	0.0001334	-3.51039
228540_at	QKI	quaking homolog, KH domain RNA binding (mouse)	0.0001383	-2.28106
212915_at	PDZRN3	PDZ domain containing RING finger 3	0.0001388	-6.73192
204424_s_at	LMO3	LIM domain only 3 (rhombotin-like 2)	0.0001412	-11.2763
37462_i_at	SF3A2	splicing factor 3a, subunit 2, 66kDa	0.0001435	-4.93301
202994_s_at	FBLN1	fibulin 1	0.000146	-15.7869
221760_at	MAN1A1	Mannosidase, alpha, class 1A, member 1	0.0001461	-2.58064
220276_at	FLJ22655	hypothetical protein FLJ22655	0.0001468	-5.68375
232231_at	RUNX2	runt-related transcription factor 2	0.0001484	-3.90384
203886_s_at	FBLN2	fibulin 2	0.0001505	-7.06981
220327_at	VGLL3	vestigial like 3 (Drosophila)	0.0001526	-6.45008
225998_at	GAB1	GRB2-associated binding protein 1	0.0001537	-3.28665
228770_at	GPR146	G protein-coupled receptor 146	0.0001567	-3.77226
211748_x_at	PTGDS	prostaglandin D2 synthase 21kDa (brain) /// prostaglandin D2 synthase 21kDa (bra	0.0001573	-33.3631
229146_at	C7orf31	chromosome 7 open reading frame 31	0.0001617	-2.79417
237052_x_at	TNRC15	Trinucleotide repeat containing 15	0.0001633	-2.09679
225972_at	TMEM64	Transmembrane protein 64	0.0001639	-2.29714
242990_at	PPFIA1	Protein tyrosine phosphatase, receptor type, f polypeptide (PTPRF), interacting	0.000164	-2.291
212886_at	CCDC69	coiled-coil domain containing 69	0.0001647	-5.61423
229497_at	ANKDD1A	ankyrin repeat and death domain containing 1A	0.0001654	-3.94795
232305_at	HMGCLL1	3-hydroxymethyl-3-methylglutaryl-Coenzyme A lyase-like 1	0.0001664	-3.32159
226965_at	FAM116A	family with sequence similarity	0.000168	-2.08035

		116, member A		
208335_s_at	DARC	Duffy blood group, chemokine receptor	0.0001689	-24.7159
227620_at	---	---	0.0001705	-2.92575
213113_s_at	SLC43A3	solute carrier family 43, member 3	0.0001711	-3.40693
202863_at	SP100	SP100 nuclear antigen	0.0001742	-2.8408
219959_at	MOCOS	molybdenum cofactor sulfurase	0.0001745	-2.16494
217665_at	---	CDNA FLJ25947 fis, clone JTH14708	0.0001761	-2.42977
204201_s_at	PTPN13	protein tyrosine phosphatase, non-receptor type 13 (APO-1/CD95 (Fas)-associated	0.0001763	-3.20937
238041_at	TCF12	Transcription factor 12 (HTF4, helix-loop-helix transcription factors 4)	0.0001801	-2.23961
227178_at	CUGBP2	CUG triplet repeat, RNA binding protein 2	0.0001824	-2.26391
214725_at	RPESP	RPE-spondin	0.0001828	-2.29073
200986_at	SERPING1	serpin peptidase inhibitor, clade G (C1 inhibitor), member 1, (angioedema, hered	0.0001841	-3.90067
217807_s_at	GLTSCR2	glioma tumor suppressor candidate region gene 2	0.0001845	-2.66088
1552664_at	FLCN	folliculin	0.0001847	-2.13684
213572_s_at	SERPINB1	serpin peptidase inhibitor, clade B (ovalbumin), member 1	0.0001851	-2.05608
213675_at	---	CDNA FLJ25106 fis, clone CBR01467	0.0001866	-3.45424
230802_at	---	---	0.000188	-2.40427
227067_x_at	NOTCH2NL	Notch homolog 2 (Drosophila) N-terminal like	0.0001888	-4.29521
205236_x_at	SOD3	superoxide dismutase 3, extracellular	0.0001891	-4.59784
1554741_s_at	FGF7 /// KGFLP1 ///	fibroblast growth factor 7 (keratinocyte growth factor) /// keratinocyte growth	0.0001924	-6.49814
44790_s_at	C13orf18	chromosome 13 open reading frame 18	0.0001925	-3.26763
230986_at	KLF8	Kruppel-like factor 8	0.0001927	-4.70068
229092_at	NR2F2	Nuclear receptor subfamily 2, group F, member 2	0.0001935	-4.14761
1554067_at	FLJ32549	hypothetical protein FLJ32549	0.0001944	-2.37819
236123_at	ST7L	Suppression of tumorigenicity 7 like	0.0001959	-2.88943
202674_s_at	LMO7	LIM domain 7	0.0001998	-2.15078
239846_at	MTHFD1	Methylenetetrahydrofolate dehydrogenase (NADP+ dependent) 1, methenyltetrahydrof	0.0002043	-2.0601
214395_x_at	EEF1D	Eukaryotic translation elongation factor 1 delta (guanine nucleotide	0.0002043	-3.52325

		exchange pr		
241698_at	C2orf11	chromosome 2 open reading frame 11	0.0002058	-2.20084
209815_at	PTCH	patched homolog (Drosophila)	0.000206	-6.38407
227866_at	---	CDNA FLJ42493 fis, clone BRACE2034616	0.0002062	-2.85007
204960_at	PTPRCAP	protein tyrosine phosphatase, receptor type, C-associated protein	0.0002067	-2.05403
229194_at	PCGF5	polycomb group ring finger 5	0.0002099	-2.00496
1559942_at	MDFIC	MyoD family inhibitor domain containing	0.0002139	-2.16698
1556696_s_at	FLJ42709	Hypothetical gene supported by AK124699	0.0002145	-2.00378
237395_at	CYP4Z1	cytochrome P450, family 4, subfamily Z, polypeptide 1	0.000215	-2.1573
229741_at	VISA	Virus-induced signaling adapter	0.0002151	-2.10386
	LOC440667	///		
229872_s_at	LOC440669	hypothetical LOC440667 /// hypothetical LOC440669 /// hypothetical protein LOC64	0.0002179	-2.14116
	LOC642441	///		
230263_s_at	DOCK5	dedicator of cytokinesis 5	0.00022	-4.66545
213556_at	LOC390940	similar to R28379_1	0.0002206	-2.64387
224480_s_at	LPAAT- THETA	lysophosphatidic acid acyltransferase theta /// lysophosphatidic acid acyltransf	0.0002211	-3.52999
201827_at	SMARCD2	SWI/SNF related, matrix associated, actin dependent regulator of chromatin, subf	0.0002215	-2.65005
213397_x_at	RNASE4	ribonuclease, RNase A family, 4	0.0002257	-5.71958
235777_at	ANKRD44	ankyrin repeat domain 44	0.0002268	-3.72785
227041_at	---	CDNA FLJ31513 fis, clone NT2RI1000127	0.0002285	-2.83739
205758_at	CD8A	CD8a molecule /// CD8a molecule	0.0002298	-2.49049
238478_at	BNC2	Basonuclin 2	0.0002299	-8.45062
204131_s_at	FOXO3A	forkhead box O3A	0.0002301	-2.01593
227386_s_at	TTMB	TTMB protein	0.0002311	-3.53896
225108_at	AGPS	alkylglycerone phosphate synthase	0.0002318	-2.23266
235496_at	UNQ338	LGLL338	0.0002321	-2.73795
236606_at	SAV1	Salvador homolog 1 (Drosophila)	0.0002322	-2.39421
206068_s_at	ACADL	acyl-Coenzyme A dehydrogenase, long chain carboxylesterase 1	0.0002329	-7.67637
209616_s_at	CES1	(monocyte/macrophage serine esterase 1)	0.0002364	9.99523
230427_s_at	BAG5	BCL2-associated athanogene 5	0.0002371	-2.50092
235045_at	RBM7	RNA binding motif protein 7	0.000238	-2.28048
225165_at	PPP1R1B	protein phosphatase 1, regulatory	0.0002382	-2.11067

		(inhibitor) subunit 1B (dopamine and cAMP regu		
203127_s_at	SPTLC2	serine palmitoyltransferase, long chain base subunit 2	0.0002388	-2.02113
204731_at	TGFBR3	transforming growth factor, beta receptor III (betaglycan, 300kDa)	0.0002405	-4.16415
204655_at	CCL5	chemokine (C-C motif) ligand 5 /// chemokine (C-C motif) ligand 5	0.000242	-4.13185
1553683_s_at	FBXL14	F-box and leucine-rich repeat protein 14	0.0002427	-2.31185
223377_x_at	CISH	cytokine inducible SH2-containing protein	0.0002428	-3.0291
244313_at	CR1	complement component (3b/4b) receptor 1 (Knops blood group)	0.0002428	-4.02494
228504_at	---	Transcribed locus, strongly similar to NP_002967.1 sodium channel, voltage-gated	0.0002428	-23.399
228088_at	---	CDNA FLJ31513 fis, clone NT2RI1000127	0.0002443	-3.38801
213317_at	CLIC5 /// LOC653816	chloride intracellular channel 5 /// similar to chloride intracellular channel 5	0.0002474	-8.95381
226868_at	GLT8D3	glycosyltransferase 8 domain containing 3	0.0002495	-2.04291
224451_x_at	ARHGAP9	Rho GTPase activating protein 9 /// Rho GTPase activating protein 9	0.00025	-2.67489
201189_s_at	ITPR3	inositol 1,4,5-triphosphate receptor, type 3	0.0002563	-3.13089
212632_at	STX7	Syntaxin 7	0.0002566	-2.21013
1554014_at	CHD2	chromodomain helicase DNA binding protein 2	0.0002578	-2.89688
217525_at	OLFML1	olfactomedin-like 1	0.0002588	-5.17325
239370_at	---	---	0.0002596	-2.01147
214567_s_at	XCL1 /// XCL2	chemokine (C motif) ligand 1 /// chemokine (C motif) ligand 2	0.0002642	-2.87557
236698_at	---	Full-length cDNA clone CSODF025YA01 of Fetal brain of Homo sapiens (human)	0.0002643	-3.99008
207547_s_at	FAM107A	family with sequence similarity 107, member A	0.0002664	-3.49581
228916_at	CWF19L2	CWF19-like 2, cell cycle control (S. pombe)	0.0002676	-2.33336
206295_at	IL18	interleukin 18 (interferon-gamma-inducing factor)	0.0002691	-2.79388
222136_x_at	ZNF43	zinc finger protein 43	0.0002696	-2.13193
229590_at	RPL13	Ribosomal protein L13	0.0002712	-2.36665
204760_s_at	THRA /// NR1D1	thyroid hormone receptor, alpha (erythroblastic leukemia viral (v-erb-a) oncogen	0.0002719	-4.46405
223816_at	TSCOT	thymic stromal co-transporter	0.0002726	-2.71603

201250_s_at	SLC2A1	solute carrier family 2 (facilitated glucose transporter), member 1	0.000274	-7.73003
209541_at	IGF1	insulin-like growth factor 1 (somatomedin C)	0.0002747	-8.56244
227461_at	STON2	stonin 2	0.0002801	-5.79205
230790_x_at	---	---	0.000281	-3.77418
237040_at	CWF19L2	CWF19-like 2, cell cycle control (S. pombe)	0.0002814	-2.82722
244391_at	TSEN2	tRNA splicing endonuclease 2 homolog (S. cerevisiae)	0.0002816	-2.05433
1556427_s_at	LOC221091	similar to hypothetical protein	0.0002842	-16.5719
226127_at	ALKBH3	alkB, alkylation repair homolog 3 (E. coli)	0.0002842	-2.18356
229069_at	CIP29	cytokine induced protein 29 kDa	0.0002845	-2.22501
235061_at	PPM1K	protein phosphatase 1K (PP2C domain containing)	0.0002854	-2.78109
206987_x_at	FGF18	fibroblast growth factor 18	0.000286	-2.9012
206697_s_at	HP	haptoglobin	0.0002906	-3.9245
205560_at	PCSK5	proprotein convertase subtilisin/kexin type 5	0.0002918	-3.48211
225939_at	EIF4E3	eukaryotic translation initiation factor 4E member 3	0.0002936	-2.48581
216333_x_at	TNXB	tenascin XB	0.0002951	-6.96248
208392_x_at	SP110	SP110 nuclear body protein	0.000296	-2.00118
238026_at	RPL35A	Ribosomal protein L35a	0.0002963	-2.36259
226932_at	SSPN	Sarcospan (Kras oncogene-associated gene)	0.0002983	-5.83668
1555801_s_at	ZNF533	zinc finger protein 533	0.0003026	-2.00857
1557943_at	CNP	2',3'-cyclic nucleotide 3' phosphodiesterase	0.0003053	-2.64178
228450_at	PLEKHA7	pleckstrin homology domain containing, family A member 7	0.0003092	-4.12803
229844_at	---	Transcribed locus	0.0003112	-3.10535
213765_at	MFAP5	microfibrillar associated protein 5	0.000315	-29.4827
201871_s_at	LOC51035	unknown protein LOC51035	0.0003157	-2.13308
217863_at	PIAS1	protein inhibitor of activated STAT, 1	0.000317	-2.0294
213451_x_at	TNXB	tenascin XB	0.0003194	-7.22856
228082_at	ASAM	adipocyte-specific adhesion molecule	0.0003206	-2.45516
210613_s_at	SYNGR1	synaptogyrin 1	0.0003207	-3.12379
219230_at	TMEM100	transmembrane protein 100	0.0003225	10.6199
228333_at	---	Full length insert cDNA clone YT94E02	0.0003234	-2.76198
202724_s_at	FOXO1A	forkhead box O1A (rhabdomyosarcoma)	0.0003318	-3.03119
235173_at	LOC401093	hypothetical LOC401093	0.0003345	-2.52777
207735_at	RNF125	ring finger protein 125	0.0003378	-4.45554
239682_at	FLJ23861	Hypothetical protein FLJ23861	0.0003384	-2.58289
225447_at	GPD2	glycerol-3-phosphate	0.0003388	-2.43254

206666_at	GZMK	dehydrogenase 2 (mitochondrial) granzyme K (granzyme 3; tryptase II) /// granzyme K (granzyme 3; tryptase II)	0.000339	-4.018
205653_at	CTSG	cathepsin G	0.0003391	-3.9604
236657_at	---	Full length insert cDNA YI37C01	0.0003399	-2.12498
223278_at	GJB2	gap junction protein, beta 2, 26kDa (connexin 26)	0.0003421	-8.91346
214662_at	WDR43	WD repeat domain 43	0.000346	-2.07872
205908_s_at	OMD	osteomodulin	0.0003471	-17.1656
214083_at	PPP2R5C	Protein phosphatase 2, regulatory subunit B (B56), gamma isoform pleckstrin homology domain	0.0003475	-2.07198
227148_at	PLEKHH2	containing, family H (with MyTH4 domain) member 2	0.0003477	-4.85164
213094_at	GPR126	G protein-coupled receptor 126	0.000348	-4.36851
235199_at	---	Transcribed locus	0.0003495	-3.43478
228548_at	---	CDNA FLJ37418 fis, clone BRAWH2000488	0.00035	-2.67702
225008_at	MGC34646	Hypothetical protein MGC34646	0.0003575	-2.70068
1556346_at	COTL1	Coactosin-like 1 (Dictyostelium)	0.0003662	-2.25449
213567_at	---	Clone 23728 mRNA sequence	0.0003768	-2.17795
241739_at	OGFOD1	2-oxoglutarate and iron-dependent oxygenase domain containing 1	0.0003787	-3.06825
226317_at	PPP4R2	protein phosphatase 4, regulatory subunit 2	0.0003796	-2.12895
225950_at	SAMD8	Sterile alpha motif domain containing 8	0.0003809	-2.08535
241969_at	---	---	0.0003811	-4.3098
210139_s_at	PMP22	peripheral myelin protein 22	0.0003813	-2.51741
206093_x_at	TNXB	tenascin XB	0.0003816	-6.6219
243176_at	---	CDNA FLJ30090 fis, clone BNGH41000015	0.0003823	-2.36522
226846_at	PHYHD1	phytanoyl-CoA dioxygenase domain containing 1	0.0003855	-2.47089
1554779_s_at	PHLDB2	pleckstrin homology-like domain, family B, member 2	0.0003888	-4.68139
229404_at	TWIST2	twist homolog 2 (Drosophila)	0.0003916	-4.51281
223393_s_at	TSHZ3	teashirt family zinc finger 3	0.0003943	-2.8228
202437_s_at	CYP1B1	cytochrome P450, family 1, subfamily B, polypeptide 1	0.0003944	-3.99324
213560_at	GADD45B	Growth arrest and DNA-damage-inducible, beta	0.0003962	-2.57516
231929_at	---	Transcribed locus	0.0003968	-2.70584
225627_s_at	CACHD1	cache domain containing 1	0.0004045	-4.91717
1559005_s_at	C9orf39	chromosome 9 open reading frame 39	0.0004054	-2.24599
213103_at	STARD13	START domain containing 13	0.0004055	-2.06566
238018_at	LOC285016	hypothetical protein LOC285016	0.0004068	9.43976

214028_x_at	TDRD3	tudor domain containing 3 acetyl-Coenzyme A	0.000408	-2.01617
214274_s_at	ACAA1	acyltransferase 1 (peroxisomal 3- oxoacyl-Coenzyme A thiolase)	0.0004088	-2.01431
230623_x_at	USP28	ubiquitin specific peptidase 28	0.0004091	-2.13646
223980_s_at	SP110	SP110 nuclear body protein	0.0004147	-2.45425
223937_at	FOXP1	forkhead box P1	0.0004148	-2.17677
219947_at	CLEC4A	C-type lectin domain family 4, member A	0.0004181	-2.80993
221127_s_at	---	---	0.0004189	-3.22986
201034_at	ADD3	adducin 3 (gamma)	0.000423	-2.67503
218128_at	NFYB	nuclear transcription factor Y, beta	0.000426	-2.42069
214319_at	FRY	furry homolog (Drosophila)	0.0004276	-4.29755
227791_at	SLC9A9	solute carrier family 9 (sodium/hydrogen exchanger), member 9	0.0004375	-3.03154
202723_s_at	FOXO1A	forkhead box O1A (rhabdomyosarcoma)	0.0004402	-3.00599
206170_at	ADRB2	adrenergic, beta-2-, receptor, surface	0.0004416	-4.83785
214954_at	SUSD5	sushi domain containing 5	0.0004444	-5.64402
236383_at	---	Transcribed locus	0.0004446	-3.26509
223622_s_at	HYI	hydroxypyruvate isomerase homolog (E. coli)	0.000445	-2.52138
1558686_at	---	Full length insert cDNA YP99D02	0.000446	-2.23796
210031_at	CD247	CD247 molecule	0.0004475	-2.19073
228845_at	LOC196463	hypothetical protein LOC196463	0.0004498	-2.21233
203920_at	NR1H3	nuclear receptor subfamily 1, group H, member 3	0.0004509	-3.04078
226303_at	PGM5	phosphoglucomutase 5	0.0004524	-8.38609
222835_at	THSD4	Thrombospondin, type I, domain containing 4	0.0004548	-3.9436
221019_s_at	COLEC12	collectin sub-family member 12 /// collectin sub-family member 12	0.0004638	-9.73466
227478_at	LOC284262	hypothetical protein LOC284262	0.000467	-2.2568
211577_s_at	IGF1	insulin-like growth factor 1 (somatomedin C)	0.0004692	-4.80912
204623_at	TFF3	trefoil factor 3 (intestinal)	0.0004703	-2.33306
213764_s_at	MFAP5	microfibrillar associated protein 5	0.0004715	-49.0386
1562102_at	AKR1C2	Aldo-keto reductase family 1, member C2 (dihydrodiol dehydrogenase 2; bile acid	0.000475	-3.28768
238558_at	MBNL1	Muscleblind-like (Drosophila)	0.000483	-3.63377
231953_at	FALZ	fetal Alzheimer antigen	0.0004895	-2.11688
1569107_s_at	ZNF642	zinc finger protein 642	0.0005006	-2.00501
1555068_at	WNK1	WNK lysine deficient protein kinase 1	0.0005028	-2.62912
228751_at	CLK4	CDC-like kinase 4	0.000509	-2.89023

240188_at	TGFBR3	Transforming growth factor, beta receptor III (betaglycan, 300kDa)	0.0005092	-2.1361
235898_at	---	Transcribed locus	0.0005139	-2.08985
219132_at	PELI2	pellino homolog 2 (Drosophila)	0.0005218	-2.59833
226109_at	C21orf91	chromosome 21 open reading frame 91	0.0005244	-3.2013
213578_at	BMPRI1A	bone morphogenetic protein receptor, type IA	0.0005254	-2.7011
236115_at	HTR7P	5-hydroxytryptamine (serotonin) receptor 7 pseudogene	0.0005257	-2.01777
202664_at	WASPIP	Wiskott-Aldrich syndrome protein interacting protein	0.0005297	-2.34273
211029_x_at	FGF18	fibroblast growth factor 18 /// fibroblast growth factor 18	0.0005367	-2.59479
230003_at	---	Transcribed locus	0.0005398	-3.72613
204891_s_at	LCK	lymphocyte-specific protein tyrosine kinase	0.0005401	-2.83899
231145_at	PAX9	Paired box gene 9	0.0005477	-3.70381
224996_at	MGC34646	Hypothetical protein MGC34646	0.0005498	-2.09568
204777_s_at	MAL	mal, T-cell differentiation protein	0.0005547	-8.91506
204519_s_at	PLLP	plasma membrane proteolipid (plasmolipin)	0.0005581	-7.23145
227401_at	IL17D	interleukin 17D	0.0005601	-4.37078
239307_at	---	---	0.000561	-2.15051
228264_at	PHACS	1-aminocyclopropane-1-carboxylate synthase	0.0005653	-2.93885
221193_s_at	ZCCHC10	zinc finger, CCHC domain containing 10	0.0005733	-2.07354
231773_at	ANGPTL1	angiopoietin-like 1	0.0005736	-2.57661
201656_at	ITGA6	integrin, alpha 6	0.0005762	-2.42715
239632_at	---	Transcribed locus, weakly similar to XP_529033.1 PREDICTED: neuroligin 3 [Pan tr	0.0005787	-3.0687
227070_at	GLT8D2	glycosyltransferase 8 domain containing 2	0.0005833	-4.46995
222164_at	FGFR1	fibroblast growth factor receptor 1 (fms-related tyrosine kinase 2, Pfeiffer syn	0.0005864	-3.828
227467_at	RDH10	retinol dehydrogenase 10 (all-trans)	0.0005865	-2.5699
240214_at	---	---	0.0005879	-2.64707
229575_at	---	Transcribed locus	0.0005882	-2.18962
209513_s_at	HSDL2	hydroxysteroid dehydrogenase like 2	0.0005908	-2.18951
205498_at	GHR	growth hormone receptor	0.0005955	-7.44229
231098_at	---	Transcribed locus	0.0005957	-5.77384
232315_at	LOC400713	zinc finger-like	0.0005967	-5.33114
229344_x_at	FAM80B	family with sequence similarity 80, member B	0.0006012	-2.45002
207688_s_at	INHBC	inhibin, beta C	0.0006031	-3.11128

210640_s_at	GPR30	G protein-coupled receptor 30	0.0006086	-3.42951
202085_at	TJP2	tight junction protein 2 (zona occludens 2)	0.0006091	-4.01843
235635_at	ARHGAP5	Rho GTPase activating protein 5	0.0006118	-3.17798
225078_at	EMP2	epithelial membrane protein 2	0.0006123	-3.96448
218552_at	ECHDC2	enoyl Coenzyme A hydratase domain containing 2	0.0006144	-2.61735
204118_at	CD48	CD48 molecule /// CD48 molecule	0.0006153	-3.35361
205890_s_at	GABBR1 /// UBD	gamma-aminobutyric acid (GABA) B receptor, 1 /// ubiquitin D	0.0006154	-4.07443
204794_at	DUSP2	dual specificity phosphatase 2	0.0006249	-3.30985
213539_at	CD3D	CD3d molecule, delta (CD3-TCR complex)	0.0006257	-2.38647
219173_at	MYO15B	myosin XVb pseudogene	0.0006286	-2.72252
228850_s_at	---	---	0.0006294	-4.03672
239909_at	C9orf94	chromosome 9 open reading frame 94	0.0006346	-2.03653
205101_at	CIITA	class II, major histocompatibility complex, transactivator	0.0006358	-2.31342
230882_at	FLJ34048	hypothetical protein FLJ34048	0.0006394	-3.74092
235764_at	PRDM5	PR domain containing 5	0.000644	-2.23433
59644_at	BMP2K	BMP2 inducible kinase	0.0006475	-2.41501
228692_at	---	CDNA FLJ13569 fis, clone PLACE1008369	0.0006492	-3.69467
203879_at	PIK3CD	phosphoinositide-3-kinase, catalytic, delta polypeptide /// phosphoinositide-3-k	0.0006513	-2.70803
228593_at	LOC339483	hypothetical LOC339483	0.0006524	-2.45124
204442_x_at	LTBP4	latent transforming growth factor beta binding protein 4	0.0006552	-4.66487
214470_at	KLRB1	killer cell lectin-like receptor subfamily B, member 1 /// killer cell lectin-li	0.0006553	-3.83199
235466_s_at	LOC644053	hypothetical protein LOC644053	0.0006555	-2.03116
228032_s_at	---	CDNA FLJ36663 fis, clone UTERU2002826	0.000657	-2.748
201787_at	FBLN1	fibulin 1	0.0006618	-6.64054
211675_s_at	MDFIC	MyoD family inhibitor domain containing /// MyoD family inhibitor domain contain	0.0006853	-2.56525
220310_at	TUBAL3	tubulin, alpha-like 3	0.0006869	-4.12989
228186_s_at	RSPO3	R-spondin 3 homolog (Xenopus laevis)	0.0006884	-10.348
239578_at	TANC1	Tetratricopeptide repeat, ankyrin repeat and coiled-coil containing 1	0.0006885	-2.00331
239183_at	ANGPTL1	angiopoietin-like 1	0.0006924	-2.65435
238009_at	---	Transcribed locus, strongly similar to NP_00887-1.3 SRY (sex determining region Y	0.0006953	-2.7114
203343_at	UGDH	UDP-glucose dehydrogenase	0.0006981	-2.48458

228485_s_at	SLC44A1	solute carrier family 44, member 1	0.0007001	-2.93705
232017_at	TJP2	tight junction protein 2 (zona occludens 2)	0.0007095	-4.97483
212631_at	STX7	Syntaxin 7	0.0007113	-2.08733
219911_s_at	SLCO4A1	solute carrier organic anion transporter family, member 4A1	0.0007165	-2.69902
224979_s_at	USP36	ubiquitin specific peptidase 36	0.0007171	-2.0348
221599_at	C11orf67	chromosome 11 open reading frame 67	0.0007172	-2.04187
226192_at	---	---	0.0007181	-5.15386
1553587_a_at	POLE4	polymerase (DNA-directed), epsilon 4 (p12 subunit)	0.0007181	-2.89341
209821_at	C9orf26	chromosome 9 open reading frame 26 (NF-HEV)	0.0007221	-4.90201
202734_at	TRIP10	thyroid hormone receptor interactor 10	0.0007222	-2.70977
205878_at	POU6F1	POU domain, class 6, transcription factor 1	0.0007279	-2.4075
202748_at	GBP2	guanylate binding protein 2, interferon-inducible /// guanylate binding protein	0.0007306	-3.59341
233540_s_at	CDK5RAP2	CDK5 regulatory subunit associated protein 2	0.0007318	-3.05768
205755_at	ITIH3	inter-alpha (globulin) inhibitor H3	0.0007378	-2.06142
235534_at	---	Homo sapiens, clone IMAGE:5723825, mRNA	0.00074	-2.81979
218154_at	GSDMDC1	gasdermin domain containing 1	0.000744	-2.06358
213935_at	ABHD5	abhydrolase domain containing 5	0.0007444	-2.06651
223597_at	ITLN1	intelectin 1 (galactofuranose binding)	0.0007459	-3.01749
229589_x_at	BIVM	Basic, immunoglobulin-like variable motif containing procollagen C-endopeptidase enhancer 2	0.0007515	-3.02917
219295_s_at	PCOLCE2	procollagen C-endopeptidase enhancer 2	0.0007526	-7.78703
235432_at	NPHP3	nephronophthisis 3 (adolescent)	0.0007565	-2.28468
204735_at	PDE4A	phosphodiesterase 4A, cAMP-specific (phosphodiesterase E2 duncce homolog, Drosoph	0.0007649	-2.80452
213413_at	STON1	stonin 1	0.0007676	-3.58207
227850_x_at	CDC42EP5	CDC42 effector protein (Rho GTPase binding) 5	0.000769	-3.46698
235529_x_at	C20orf118	Chromosome 20 open reading frame 118	0.0007751	-2.90318
234339_s_at	GLTSCR2	glioma tumor suppressor candidate region gene 2	0.0007765	-2.62981
230379_x_at	PRO1853	hypothetical protein PRO1853	0.0007767	-2.4345
208614_s_at	FLNB	filamin B, beta (actin binding protein 278)	0.0007776	-2.89614
209869_at	ADRA2A	adrenergic, alpha-2A-, receptor /// adrenergic, alpha-2A-, receptor	0.0007784	-11.6832

210096_at	CYP4B1	cytochrome P450, family 4, subfamily B, polypeptide 1	0.0007785	-19.3224
214293_at	11-Sep	Septin 11	0.0007789	-2.45768
201368_at	ZFP36L2	zinc finger protein 36, C3H type-like 2	0.0007875	-3.10839
202657_s_at	SERTAD2	SERTA domain containing 2	0.0007887	-2.29882
204037_at	EDG2 /// LOC644923	endothelial differentiation, lysophosphatidic acid G-protein-coupled receptor, 2	0.0008001	-5.13342
219729_at	PRRX2	paired related homeobox 2	0.0008011	-2.01901
200696_s_at	GSN	gelsolin (amyloidosis, Finnish type)	0.0008018	-3.99174
228647_at	NINJ2	Full-length cDNA clone CS0DL011YB19 of B cells (Ramos cell line) Cot 25-normaliz	0.000803	-2.35581
205620_at	F10	coagulation factor X	0.0008066	-2.68836
231031_at	LOC441417	Hypothetical LOC441417	0.0008074	-4.3672
201369_s_at	ZFP36L2	zinc finger protein 36, C3H type-like 2	0.0008157	-3.98472
206978_at	CCR2	chemokine (C-C motif) receptor 2 /// chemokine (C-C motif) receptor 2	0.0008214	-4.4169
215001_s_at	GLUL	glutamate-ammonia ligase (glutamine synthetase)	0.0008259	-2.4807
1561658_at	PPP2R2B	Protein phosphatase 2 (formerly 2A), regulatory subunit B (PR 52), beta isoform	0.0008263	-2.82643
201811_x_at	SH3BP5	SH3-domain binding protein 5 (BTK-associated)	0.0008266	-2.72547
202864_s_at	SP100	SP100 nuclear antigen	0.0008289	-2.42714
225844_at	POLE4	polymerase (DNA-directed), epsilon 4 (p12 subunit)	0.0008315	-2.51975
229531_at	MCART6	Mitochondrial carrier triple repeat 6	0.0008334	-2.2586
205672_at	XPA	xeroderma pigmentosum, complementation group A	0.0008406	-2.09223
231969_at	STOX2	storkhead box 2	0.0008505	-3.78985
213260_at	---	CDNA FLJ11796 fis, clone HEMBA1006158, highly similar to Homo sapiens transcript	0.000852	-2.69882
211057_at	ROR1	receptor tyrosine kinase-like orphan receptor 1 /// receptor tyrosine kinase-lik	0.0008522	-2.39143
226521_s_at	CCDC98	coiled-coil domain containing 98	0.0008589	-2.42081
232060_at	ROR1	Receptor tyrosine kinase-like orphan receptor 1	0.000874	-6.62209
223640_at	HCST	hematopoietic cell signal transducer	0.0008773	-2.36684
221223_x_at	CISH	cytokine inducible SH2-containing protein	0.0008809	-2.05535
219291_at	DTWD1	DTW domain containing 1	0.000882	-2.23327

209381_x_at	SF3A2	splicing factor 3a, subunit 2, 66kDa	0.0008864	-2.97915
209285_s_at	C3orf63	chromosome 3 open reading frame 63	0.0008883	-2.25701
228726_at	---	---	0.0008911	-2.34504
235459_at	---	Transcribed locus	0.000892	-2.46101
203973_s_at	CEBPD	CCAAT/enhancer binding protein (C/EBP), delta	0.0008951	-4.02051
202769_at	CCNG2	cyclin G2	0.0008971	-2.47664
223502_s_at	TNFSF13B	tumor necrosis factor (ligand) superfamily, member 13b	0.0009087	-3.34507
227369_at	SERBP1	SERPINE1 mRNA binding protein 1	0.0009151	-2.30449
236184_at	ABCA9	ATP-binding cassette, sub-family A (ABC1), member 9	0.0009216	-2.15858
241981_at	FAM20A	family with sequence similarity 20, member A	0.0009254	-3.84989
225574_at	RWDD4A	RWD domain containing 4A	0.0009269	-2.01045
200834_s_at	RPS21	ribosomal protein S21	0.0009313	-2.12169
227063_at	C17orf61	chromosome 17 open reading frame 61	0.0009373	-2.42174
202966_at	CAPN6	calpain 6	0.0009419	-2.93445
201829_at	NET1	neuroepithelial cell transforming gene 1	0.0009431	-5.00892
205527_s_at	GEMIN4	gem (nuclear organelle) associated protein 4	0.0009506	-2.17782
217546_at	MT1M	metallothionein 1M	0.0009615	20.4299
244348_at	---	Transcribed locus	0.0009647	-2.07056
204237_at	GULP1	GULP, engulfment adaptor PTB domain containing 1	0.0009783	-3.28133
239277_at	---	---	0.0009812	-2.45507
228869_at	SLIC1	Selectin ligand interactor cytoplasmic-1	0.0009831	-2.83362
212637_s_at	WWP1	WW domain containing E3 ubiquitin protein ligase 1	0.0009913	-2.64691
202808_at	C10orf26	chromosome 10 open reading frame 26	0.0009985	-2.12071
220206_at	ZMYM1	zinc finger, MYM-type 1	0.0010004	-2.28994
209386_at	TM4SF1	transmembrane 4 L six family member 1	0.0010189	-2.43662
228949_at	GPR177	G protein-coupled receptor 177	0.0010242	-2.64355
209369_at	ANXA3	annexin A3	0.0010258	-5.0751
204359_at	FLRT2	fibronectin leucine rich transmembrane protein 2	0.0010289	-11.8365
31637_s_at	THRA /// NR1D1	thyroid hormone receptor, alpha (erythroblastic leukemia viral (v- erb-a) oncogen	0.0010335	-2.41355
222756_s_at	ARRB1	arrestin, beta 1	0.0010364	-2.68577
213644_at	CCDC46	coiled-coil domain containing 46	0.0010375	-2.31038
210280_at	MPZ	myelin protein zero (Charcot- Marie-Tooth neuropathy 1B)	0.0010385	-5.32963

219511_s_at	SNCAIP	synuclein, alpha interacting protein (synphilin)	0.0010486	-2.28036
227399_at	VGLL3	vestigial like 3 (Drosophila)	0.0010592	-6.24643
201843_s_at	EFEMP1	EGF-containing fibulin-like extracellular matrix protein 1	0.0010629	-12.6176
209263_x_at	TSPAN4	tetraspanin 4	0.0010666	-2.45449
224970_at	NFIA	nuclear factor I/A	0.0010742	-3.21496
201305_x_at	ANP32B	acidic (leucine-rich) nuclear phosphoprotein 32 family, member B	0.0010902	-2.28861
219573_at	LRRC16	leucine rich repeat containing 16	0.0010971	-2.19279
229266_at	LOC284033	hypothetical protein LOC284033	0.0011019	-3.23497
218943_s_at	DDX58	DEAD (Asp-Glu-Ala-Asp) box polypeptide 58	0.0011067	-3.00725
226878_at	HLA-DOA	major histocompatibility complex, class II, DO alpha	0.0011106	-2.54477
226769_at	LOC387758	similar to RIKEN cDNA 1110018M03	0.0011115	-8.39432
205907_s_at	OMD	osteomodulin	0.0011156	-17.721
219471_at	C13orf18	chromosome 13 open reading frame 18	0.0011186	-2.27264
205488_at	GZMA	granzyme A (granzyme 1, cytotoxic T-lymphocyte-associated serine esterase 3) ///	0.0011227	-5.26062
242532_at	---	---	0.001126	-2.60337
213340_s_at	KIAA0495	KIAA0495	0.0011503	-2.80645
212653_s_at	EHBP1	EH domain binding protein 1	0.0011668	-2.29889
208747_s_at	C1S	complement component 1, s subcomponent	0.0011683	-6.46047
242524_at	CBLN4	cerebellin 4 precursor	0.0011898	-2.79566
	FAM91A2			
	///			
	FLJ39739			
	///			
	LOC440685			
	///	family with sequence similarity 91,		
1568609_s_at	LOC644642	member A2 ///	0.0012081	-2.46934
	///	/// FLJ39739 protein		
	LOC644677	/// hypotheti		
	///			
	LOC645052			
	///			
	LOC653496			
224184_s_at	BOC	Boc homolog (mouse)	0.0012082	-2.71498
228718_at	ZNF44	zinc finger protein 44	0.0012092	-2.70253
226148_at	BTBD15	BTB (POZ) domain containing 15	0.0012233	-2.35811
235585_at	---	Transcribed locus	0.0012268	-2.06826
230168_at	---	Transcribed locus, moderately similar to XP_531878.2	0.0012307	-2.00718
		PREDICTED: similar to zinc		

1553613_s_at	FOXC1	forkhead box C1	0.0012316	-5.86067
207016_s_at	ALDH1A2	aldehyde dehydrogenase 1 family, member A2	0.0012482	-5.00308
209758_s_at	MFAP5	microfibrillar associated protein 5	0.0012679	-18.2378
213915_at	NKG7	natural killer cell group 7 sequence	0.0012696	-2.23966
1565639_a_at	PMP22	Peripheral myelin protein 22	0.0012697	-3.78672
203799_at	CD302	CD302 molecule	0.0012706	-3.10699
203649_s_at	PLA2G2A	phospholipase A2, group IIA (platelets, synovial fluid)	0.001275	-37.3762
217767_at	C3 /// LOC653879	complement component 3 /// similar to Complement C3 precursor	0.0012836	-11.6253
226634_at	LOC399818	similar to CG9643-PA	0.001284	-2.53006
239092_at	ITGA8	integrin, alpha 8	0.0012876	-2.68896
222290_at	OR2A20P /// OR2A9P	olfactory receptor, family 2, subfamily A, member 20 pseudogene /// olfactory re	0.0012961	-2.54517
211339_s_at	ITK	IL2-inducible T-cell kinase	0.0012968	-2.25389
204068_at	STK3	serine/threonine kinase 3 (STE20 homolog, yeast)	0.0013011	-2.2582
209842_at	SOX10	SRY (sex determining region Y)- box 10	0.0013021	-6.81189
205440_s_at	NPY1R	neuropeptide Y receptor Y1	0.0013149	-7.11511
226506_at	THSD4	thrombospondin, type I, domain containing 4	0.0013188	-2.52507
237248_at	PDE11A	Phosphodiesterase 11A	0.0013347	-4.46611
235749_at	UGCGL2	UDP-glucose ceramide glucosyltransferase-like 2	0.0013363	-2.50929
205992_s_at	IL15	interleukin 15	0.0013383	-3.29603
225946_at	RASSF8	Ras association (RalGDS/AF-6) domain family 8	0.0013464	-3.01578
235778_s_at	ANKRD44	ankyrin repeat domain 44 tissue factor pathway inhibitor	0.0013504	-2.02148
210665_at	TFPI	(lipoprotein-associated coagulation inhibitor)	0.0013556	-4.73954
236468_at	---	CDNA FLJ37467 fis, clone BRAWH2011920	0.0013598	-2.18132
229511_at	SMARCE1	SWI/SNF related, matrix associated, actin dependent regulator of chromatin, subf	0.0013688	-2.13392
205267_at	POU2AF1	POU domain, class 2, associating factor 1	0.0013709	-4.13838
207191_s_at	ISLR	immunoglobulin superfamily containing leucine-rich repeat	0.0013787	-3.64755
221564_at	PRMT2	protein arginine methyltransferase 2	0.0013805	-2.0775
234976_x_at	SLC4A5	Solute carrier family 4, sodium bicarbonate cotransporter, member 5	0.0014007	-3.49045

235347_at	IQCG	IQ motif containing G	0.0014145	-2.59461
235666_at	---	---	0.0014155	-7.49204
1552388_at	FLJ30901	hypothetical protein FLJ30901	0.0014254	-3.16015
224780_at	RBM17	RNA binding motif protein 17	0.001428	-2.1011
209699_x_at	AKR1C2	aldo-keto reductase family 1, member C2 (dihydrodiol dehydrogenase 2; bile acid	0.0014371	-5.18962
219093_at	FLJ20701	hypothetical protein FLJ20701 /// hypothetical protein FLJ20701	0.0014593	-6.35275
201893_x_at	DCN	decorin	0.0014681	-3.1164
202995_s_at	FBLN1	fibulin 1	0.0014721	-10.1517
1405_i_at	CCL5	chemokine (C-C motif) ligand 5	0.0014753	-4.27293
219970_at	GIPC2	GIPC PDZ domain containing family, member 2	0.001476	-3.31516
209904_at	TNNC1	troponin C type 1 (slow)	0.0014832	19.2048
227273_at	---	Transcribed locus	0.001487	-2.21515
206420_at	IGSF6	immunoglobulin superfamily, member 6	0.001489	-2.1559
227188_at	C21orf63	chromosome 21 open reading frame 63	0.0014925	-3.62802
235616_at	---	---	0.0015186	-2.76104
221922_at	GPSM2	G-protein signalling modulator 2 (AGS3-like, C. elegans)	0.001522	-2.70846
200965_s_at	ABLIM1	actin binding LIM protein 1	0.0015274	-2.70931
220941_s_at	C21orf91	chromosome 21 open reading frame 91	0.0015275	-2.22386
212419_at	C10orf56	chromosome 10 open reading frame 56	0.0015332	-3.09613
214791_at	LOC93349	hypothetical protein BC004921	0.0015394	-2.80842
242245_at	SYDE2	Synapse defective 1, Rho GTPase, homolog 2 (C. elegans)	0.0015444	-2.91091
201181_at	GNAI3	guanine nucleotide binding protein (G protein), alpha inhibiting activity polype	0.0015499	-2.22426
211986_at	AHNAK	AHNAK nucleoprotein (desmoyokin)	0.0015502	-3.42821
205981_s_at	ING2	inhibitor of growth family, member 2	0.0015508	-2.54334
1553338_at	C1orf55	chromosome 1 open reading frame 55	0.0015574	-2.58677
209169_at	GPM6B	glycoprotein M6B	0.0015701	-6.15389
212764_at	---	---	0.0015793	-2.04028
231867_at	ODZ2	odz, odd Oz/ten-m homolog 2 (Drosophila)	0.00158	-7.67784
206646_at	GLI1	glioma-associated oncogene homolog 1 (zinc finger protein)	0.0015817	-2.01899
222685_at	FAM29A	family with sequence similarity 29, member A	0.0016003	-2.01834
224325_at	FZD8	frizzled homolog 8 (Drosophila) /// frizzled homolog 8	0.0016078	-4.58615

(Drosophila)				
228006_at	---	---	0.0016205	-2.24753
222309_at	C6orf62	Chromosome 6 open reading frame 62	0.0016215	-2.12783
226822_at	STOX2	storkhead box 2	0.001629	-2.0795
213381_at	C10orf72	Chromosome 10 open reading frame 72	0.0016458	-2.45008
209763_at	CHRD1	chordin-like 1	0.0016473	-38.1872
206910_x_at	CFHR2	complement factor H-related 2	0.0016711	-2.03887
218002_s_at	CXCL14	chemokine (C-X-C motif) ligand 14	0.0016746	-88.9855
223631_s_at	C19orf33	chromosome 19 open reading frame 33	0.0016794	-10.1485
228195_at	MGC13057	Hypothetical protein MGC13057	0.0016827	-4.97771
218816_at	LRRC1	leucine rich repeat containing 1	0.0016963	-4.19989
227197_at	SGEF	Src homology 3 domain- containing guanine nucleotide exchange factor	0.0016965	-5.43337
243880_at	GOSR2	Golgi SNAP receptor complex member 2	0.001697	-2.19054
209827_s_at	IL16	interleukin 16 (lymphocyte chemoattractant factor)	0.0016992	-2.12848
239262_at	PRSS23	Protease, serine, 23	0.0017024	-6.20611
217408_at	MRPS18B	mitochondrial ribosomal protein S18B	0.0017246	-2.0501
232298_at	LOC401093	hypothetical LOC401093	0.0017257	-3.5423
231384_at	---	MRNA; cDNA DKFZp686F1745 (from clone DKFZp686F1745)	0.0017306	-3.2173
214369_s_at	RASGRP2	RAS guanyl releasing protein 2 (calcium and DAG-regulated)	0.0017337	-2.4117
205141_at	ANG /// RNASE4	angiogenin, ribonuclease, RNase A family, 5 /// ribonuclease, RNase A family, 4	0.0017342	-3.163
205214_at	STK17B	serine/threonine kinase 17b (apoptosis-inducing)	0.0017419	-3.17276
224162_s_at	FBXO31	F-box protein 31	0.0017612	-2.08257
218236_s_at	PRKD3	protein kinase D3	0.0017629	-2.29919
206049_at	SELP	selectin P (granule membrane protein 140kDa, antigen CD62)	0.0017632	-5.83608
232568_at	MGC24103	hypothetical protein MGC24103	0.0017762	-7.7394
230670_at	IGSF10	immunoglobulin superfamily, member 10	0.0017777	-3.55778
202054_s_at	ALDH3A2	aldehyde dehydrogenase 3 family, member A2	0.001789	-2.36204
238750_at	---	---	0.0018083	-2.11082
235127_at	PMP2	peripheral myelin protein 2	0.00181	-7.64906
214835_s_at	SUCLG2	succinate-CoA ligase, GDP- forming, beta subunit	0.0018157	-2.02558
221609_s_at	WNT6	wingless-type MMTV integration site family, member 6	0.0018159	-2.68666
205559_s_at	PCSK5	proprotein convertase	0.0018161	-4.75332

		subtilisin/kexin type 5		
214783_s_at	ANXA11	annexin A11	0.0018322	-2.7269
242273_at	---	Transcribed locus	0.0018357	-2.92246
238482_at	KLF7	Kruppel-like factor 7 (ubiquitous)	0.0018367	-2.20375
228700_at	---	CDNA FLJ11567 fis, clone HEMBA1003276	0.0018446	-2.52378
225407_at	MBP	myelin basic protein	0.0018482	-2.49545
219432_at	EVC	Ellis van Creveld syndrome	0.0018523	-3.06306
1561394_s_at	RP5- 1054A22.3	KIAA1755 protein	0.0018616	-5.26751
242940_x_at	DLX6	distal-less homeobox 6	0.0018618	-7.57649
203586_s_at	ARL4D	ADP-ribosylation factor-like 4D	0.0018697	-2.02628
232618_at	CYorf15A	chromosome Y open reading frame 15A	0.0018709	-4.01428
205858_at	NGFR	nerve growth factor receptor (TNFR superfamily, member 16)	0.001875	-6.10931
209816_at	PTCH	patched homolog (Drosophila)	0.0018754	-2.07166
203845_at	PCAF	p300/CBP-associated factor	0.0018778	-2.38464
237252_at	THBD	thrombomodulin	0.0018818	-2.61235
213931_at	ID2 /// ID2B	inhibitor of DNA binding 2, dominant negative helix-loop- helix protein /// inhib	0.0018823	-6.24304
204948_s_at	FST	follistatin	0.0018907	-2.38578
206464_at	BMX	BMX non-receptor tyrosine kinase	0.0018954	-2.41355
230800_at	ADCY4	adenylate cyclase 4	0.0018984	-2.61362
230866_at	CYSLTR1	cysteinyl leukotriene receptor 1	0.0019012	-4.02357
209879_at	SELPLG	selectin P ligand	0.0019212	-2.36882
228238_at	GAS5	growth arrest-specific 5	0.0019377	-2.46528
205904_at	MICA	MHC class I polypeptide-related sequence A	0.0019495	-3.07404
235305_s_at	ECHDC2	enoyl Coenzyme A hydratase domain containing 2	0.0019519	-2.66604
228372_at	C10orf128	chromosome 10 open reading frame 128	0.0019537	-3.74183
202638_s_at	ICAM1	intercellular adhesion molecule 1 (CD54), human rhinovirus receptor	0.0019668	-3.16764
205225_at	ESR1	estrogen receptor 1	0.0019878	-4.57138
209340_at	UAP1	UDP-N-acteylglucosamine pyrophosphorylase 1	0.0020052	-2.29902
223754_at	MGC13057	hypothetical protein MGC13057	0.0020291	-2.28391
223395_at	ABI3BP	ABI gene family, member 3 (NESH) binding protein	0.0020305	-7.56507
218087_s_at	SORBS1	sorbin and SH3 domain containing 1	0.0020308	-5.0405
211673_s_at	MOCS1	molybdenum cofactor synthesis 1 /// molybdenum cofactor synthesis 1	0.0020366	-2.45746
1557116_at	APOL6	apolipoprotein L, 6	0.002041	-2.0237
235846_at	RAD54B	RAD54 homolog B (S. cerevisiae)	0.0020583	-2.00106

228143_at	---	---	0.0020667	-22.7232
227646_at	---	CDNA FLJ39389 fis, clone PLACE6003621	0.002074	-2.84623
211466_at	NFIB	nuclear factor I/B	0.0020811	-3.00593
211981_at	COL4A1	collagen, type IV, alpha 1 phosphoribosylglycinamide formyltransferase, phosphoribosylglycinamide synthetas	1.80E-06	7.58511
212379_at	GART	collagen, type IV, alpha 2	3.47E-06	2.0723
211966_at	COL4A2	Zinc finger, DHHC-type containing 21	3.88E-06	15.4269
243835_at	ZDHHC21	integrin, beta 1 (fibronectin receptor, beta polypeptide, antigen CD29 includes	3.96E-06	2.42228
1553530_a_at	ITGB1	collagen, type IV, alpha 1 microtubule-actin crosslinking factor 1	6.10E-06	10.9979
211980_at	COL4A1	integrin, beta 1 (fibronectin receptor, beta polypeptide, antigen CD29 includes	9.64E-06	3.94661
215222_x_at	MACF1	actinin, alpha 1	1.10E-05	3.00339
1553678_a_at	ITGB1	myosin IB	1.70E-05	5.414
211160_x_at	ACTN1	glyceraldehyde-3-phosphate dehydrogenase	1.87E-05	2.52598
212365_at	MYO1B	ATPase, Class VI, type 11A CKLF-like MARVEL	2.01E-05	3.93718
AFFX- HUMGAPDH/ M33197_5_at	GAPDH	transmembrane domain containing 4	2.06E-05	1-1.0726
216488_s_at	ATP11A	biglycan	2.12E-05	2.04942
225009_at	CMTM4	ubiquitin specific peptidase 31 chromosome 9 open reading frame 10	2.14E-05	7.14164
201262_s_at	BGN	cytochrome c, somatic	2.30E-05	8.63673
226035_at	USP31	KIAA0494	2.32E-05	4.27723
200767_s_at	C9orf10	endothelin converting enzyme 1 microtubule-actin crosslinking factor 1	2.39E-05	2.06449
208905_at	CYCS	dynein, cytoplasmic 1, light intermediate chain 2	2.45E-05	2.7992
201775_s_at	KIAA0494	heat shock 70kDa protein 8	2.81E-05	2.47047
201750_s_at	ECE1	unc-5 homolog B (C. elegans)	3.05E-05	2.45156
208633_s_at	MACF1	membrane-bound transcription factor peptidase, site 1	3.33E-05	3.27399
203590_at	DYNC1LI2	H2A histone family, member Y	3.43E-05	2.09105
210338_s_at	HSPA8	septin 2	3.67E-05	7.21417
226899_at	UNC5B	eukaryotic translation initiation factor 4 gamma, 3	3.73E-05	4.9772
217543_s_at	MBTPS1	glyceraldehyde-3-phosphate	3.92E-05	3.87295
214501_s_at	H2AFY		3.93E-05	2.41098
1554747_a_at	O2-Sep		4.38E-05	6.31503
201935_s_at	EIF4G3		4.55E-05	2.89852
217398_x_at	GAPDH		4.82E-05	2.48843

		dehydrogenase		
214894_x_at	MACF1	microtubule-actin crosslinking factor 1	5.05E-05	2.06152
221503_s_at	KPNA3	karyopherin alpha 3 (importin alpha 4)	5.79E-05	3.43548
214880_x_at	CALD1	caldesmon 1	5.92E-05	2.36418
238406_x_at	SEZ6L2	Seizure related 6 homolog (mouse)-like 2	5.95E-05	2.29313
209627_s_at	OSBPL3	oxysterol binding protein-like 3 splicing factor, arginine/serine-rich 1 (splicing factor 2, alternate splicing f	6.25E-05	4.52783
201742_x_at	SFRS1		7.03E-05	7.44376
AFFX-HUMGAPDH/M33197_M_at	GAPDH	glyceraldehyde-3-phosphate dehydrogenase	7.18E-05	3.05921
223309_x_at	IPLA2(GAMMA)	intracellular membrane-associated calcium-independent phospholipase A2 gamma	7.19E-05	3.08419
233559_s_at	WDFY1	WD repeat and FYVE domain containing 1	7.54E-05	2.87671
226655_at	---	Full-length cDNA clone CS0DB009YL20 of Neuroblastoma Cot 10-normalized of Homo s	8.32E-05	2.22277
201242_s_at	ATP1B1	ATPase, Na ⁺ /K ⁺ transporting, beta 1 polypeptide	9.22E-05	12.521
206562_s_at	CSNK1A1	casein kinase 1, alpha 1	9.62E-05	4.10283
211968_s_at	HSP90AA1	heat shock protein 90kDa alpha (cytosolic), class A member 1	9.79E-05	7.55918
234331_s_at	---	---	9.80E-05	4.60447
200778_s_at	02-Sep	septin 2	9.82E-05	3.3532
200745_s_at	GNB1	guanine nucleotide binding protein (G protein), beta polypeptide 1	0.0001001	3.30664
205567_at	CHST1	carbohydrate (keratan sulfate Gal-6) sulfotransferase 1	0.0001106	3.55874
214875_x_at	APLP2	amyloid beta (A4) precursor-like protein 2	0.0001116	2.34729
200806_s_at	HSPD1	heat shock 60kDa protein 1 (chaperonin)	0.0001127	6.72247
226905_at	FAM101B	family with sequence similarity 101, member B	0.0001153	3.69839
213100_at	---	Full-length cDNA clone CLOBB018ZE07 of Neuroblastoma of Homo sapiens (human)	0.0001155	3.7893
208850_s_at	THY1	Thy-1 cell surface antigen	0.0001161	7.05621
206075_s_at	CSNK2A1	casein kinase 2, alpha 1 polypeptide	0.0001245	2.52702
208689_s_at	RPN2	ribophorin II	0.0001253	2.55818
210840_s_at	IQGAP1	IQ motif containing GTPase activating protein 1	0.0001271	2.36919

213887_s_at	POLR2E	polymerase (RNA) II (DNA directed) polypeptide E, 25kDa	0.0001317	4.46817
226450_at	---	MRNA full length insert cDNA clone EUROIMAGE 926491	0.0001328	3.91402
211536_x_at	MAP3K7	mitogen-activated protein kinase kinase kinase 7	0.0001387	3.06338
212951_at	GPR116	G protein-coupled receptor 116	0.000139	4.32137
208637_x_at	ACTN1	actinin, alpha 1	0.0001396	3.19806
211555_s_at	GUCY1B3	guanylate cyclase 1, soluble, beta 3	0.0001483	4.60969
200598_s_at	HSP90B1	heat shock protein 90kDa beta (Grp94), member 1	0.0001546	1-1.0704
1555778_a_at	POSTN	periostin, osteoblast specific factor	0.0001551	15.9949
200604_s_at	PRKAR1A	protein kinase, cAMP-dependent, regulatory, type I, alpha (tissue specific extin	0.0001593	4.60491
202205_at	VASP	vasodilator-stimulated phosphoprotein	0.0001613	3.13762
201104_x_at	NBPF14 /// KIAA1245 /// NBPF11 /// NBPF15 /// NBPF9 /// NBPF16	neuroblastoma breakpoint family, member 14 /// KIAA1245 /// neuroblastoma breakp	0.0001627	2.54977
201523_x_at	UBE2N	ubiquitin-conjugating enzyme E2N (UBC13 homolog, yeast)	0.0001639	3.14432
224335_s_at	BACE1	beta-site APP-cleaving enzyme 1 /// beta-site APP-cleaving enzyme 1	0.0001644	2.23151
200641_s_at	YWHAZ	tyrosine 3-monooxygenase/tryptophan 5-monooxygenase activation protein, zeta pol	0.0001668	8.63171
230191_at	TTBK1	tau tubulin kinase 1	0.0001703	2.07231
221551_x_at	ST6GALNAC4	ST6 (alpha-N-acetyl-neuraminy-2,3-beta-galactosyl-1,3)-N-acetylgalactosaminide	0.0001705	2.69364
AFFX-HSAC07/X00351_5_at	ACTB	actin, beta	0.0001716	10.5999
227432_s_at	ZNF557	zinc finger protein 557	0.0001737	4.15082
201070_x_at	SF3B1	splicing factor 3b, subunit 1, 155kDa	0.0001739	3.36481
201815_s_at	TBC1D5	TBC1 domain family, member 5	0.0001748	2.14124
208744_x_at	HSPH1	heat shock 105kDa/110kDa protein 1	0.0001798	6.47781
225042_s_at	C12orf22	chromosome 12 open reading frame 22	0.0001822	2.29579
208750_s_at	ARF1	ADP-ribosylation factor 1	0.0001847	9.15465
212720_at	PAPOLA	poly(A) polymerase alpha	0.0001881	6.42831

227256_at	USP31	ubiquitin specific peptidase 31	0.0001909	2.61424
203989_x_at	F2R	coagulation factor II (thrombin) receptor	0.0001912	4.72007
217140_s_at	VDAC1	voltage-dependent anion channel 1	0.0001919	4.70181
224829_at	CPEB4	cytoplasmic polyadenylation element binding protein 4	0.0001922	6.74652
212581_x_at	GAPDH	glyceraldehyde-3-phosphate dehydrogenase	0.0001977	2.20585
222979_s_at	SURF4	surfeit 4	0.0001999	2.7708
211964_at	COL4A2	collagen, type IV, alpha 2	0.0002035	2.89101
206574_s_at	PTP4A3	protein tyrosine phosphatase type IVA, member 3	0.0002055	5.95556
1555948_s_at	C9orf10	chromosome 9 open reading frame 10	0.0002061	4.86085
212746_s_at	CEP170	centrosomal protein 170kDa	0.0002118	2.40287
208661_s_at	TTC3	tetratricopeptide repeat domain 3	0.000213	5.23826
233874_at	KIAA1458	KIAA1458 protein	0.0002307	2.49331
209301_at	CA2	carbonic anhydrase II	0.0002315	13.0763
208899_x_at	ATP6V1D	ATPase, H+ transporting, lysosomal 34kDa, V1 subunit D	0.0002346	3.26931
1554482_a_at	SAR1B	SAR1 gene homolog B (S. cerevisiae)	0.0002346	3.90991
211769_x_at	SERINC3	serine incorporator 3 /// serine incorporator 3	0.0002441	4.14696
208734_x_at	RAB2	RAB2, member RAS oncogene family	0.0002507	2.77401
200617_at	KIAA0152	KIAA0152	0.0002569	2.59341
213872_at	C6orf62	Chromosome 6 open reading frame 62	0.0002597	16.1528
201096_s_at	ARF4	ADP-ribosylation factor 4	0.0002635	2.77049
224878_at	UBPH	ubiquitin-binding protein homolog	0.000265	2.11939
205572_at	ANGPT2	angiopoietin 2	0.0002663	9.14865
1552610_a_at	JAK1	Janus kinase 1 (a protein tyrosine kinase)	0.0002685	5.48717
1555326_a_at	ADAM9	ADAM metallopeptidase domain 9 (meltrin gamma)	0.0002691	3.7013
219719_at	HIGD1B	HIG1 domain family, member 1B	0.0002819	4.49136
221473_x_at	SERINC3	serine incorporator 3	0.0002844	3.38519
222977_at	SURF4	surfeit 4	0.0002916	2.74524
211148_s_at	ANGPT2	angiopoietin 2	0.0002938	10.9758
1557910_at	HSP90AB1	heat shock protein 90kDa alpha (cytosolic), class B member 1	0.0002967	28.3975
227032_at	PLXNA2	plexin A2	0.0003077	3.10371
220386_s_at	EML4	echinoderm microtubule associated protein like 4	0.0003127	2.51562
212340_at	YIPF6	Yip1 domain family, member 6	0.0003149	2.03195
204845_s_at	ENPEP	glutamyl aminopeptidase (aminopeptidase A)	0.0003155	8.58982
210337_s_at	ACLY	ATP citrate lyase	0.0003288	3.3898

202593_s_at	MIR16	membrane interacting protein of RGS16	0.0003308	4.2864
209006_s_at	C1orf63	chromosome 1 open reading frame 63	0.0003324	3.8485
200996_at	ACTR3	ARP3 actin-related protein 3 homolog (yeast) tyrosine 3-	0.0003348	2.14627
200640_at	YWHAZ	monooxygenase/tryptophan 5-monooxygenase activation protein, zeta pol	0.0003351	2.6028
204247_s_at	CDK5	cyclin-dependent kinase 5	0.0003356	3.70315
1564494_s_at	P4HB	procollagen-proline, 2-oxoglutarate 4-dioxygenase (proline 4-hydroxylase), beta	0.0003362	10.2789
AFFX- HSAC07/X003 51_M_at	ACTB	actin, beta	0.0003386	4.00569
200695_at	PPP2R1A	protein phosphatase 2 (formerly 2A), regulatory subunit A (PR 65), alpha isoform	0.0003386	2.83395
214726_x_at	ADD1	adducin 1 (alpha)	0.0003391	2.91267
1555725_a_at	RGS5	regulator of G-protein signalling 5	0.0003426	24.2887
218368_s_at	TNFRSF12A	tumor necrosis factor receptor superfamily, member 12A	0.0003427	2.61572
208629_s_at	HADHA	hydroxyacyl-Coenzyme A dehydrogenase/3-ketoacyl-Coenzyme A thiolase/enoyl-Coenzy	0.0003468	3.4081
41856_at	---	Full-length cDNA clone CLOBB018ZE07 of Neuroblastoma of Homo sapiens (human)	0.0003469	2.16875
212016_s_at	PTBP1	polypyrimidine tract binding protein 1	0.0003475	2.75924
201050_at	PLD3	phospholipase D family, member 3	0.0003499	7.85503
221423_s_at	YIPF5	Yip1 domain family, member 5 /// Yip1 domain family, member 5	0.0003533	5.08598
212178_s_at	POM121 /// LOC340318	POM121 membrane glycoprotein (rat) /// nuclear envelope pore membrane LOC340318	0.0003545	3.47912
212073_at	CSNK2A1 /// CSNK2A1P	casein kinase 2, alpha 1 polypeptide /// casein kinase 2, alpha 1 polypeptide ps	0.0003639	2.98145
223947_s_at	CRSP3	cofactor required for Sp1 transcriptional activation, subunit 3, 130kDa	0.0003724	2.05636
1557067_s_at	LUC7L	LUC7-like (<i>S. cerevisiae</i>)	0.0003807	2.68502
217294_s_at	ENO1	enolase 1, (alpha)	0.0003856	13.4984
230333_at	SAT	Spermidine/spermine N1-acetyltransferase	0.000391	1-1.4996
213453_x_at	GAPDH	glyceraldehyde-3-phosphate	0.0004146	2.24132

		dehydrogenase		
203007_x_at	LYPLA1	lysophospholipase I	0.0004212	3.44711
201444_s_at	ATP6AP2	ATPase, H+ transporting, lysosomal accessory protein 2	0.0004222	4.17677
204339_s_at	RGS4	regulator of G-protein signalling 4	0.000426	19.5557
213901_x_at	RBM9	RNA binding motif protein 9	0.00044	4.31143
208687_x_at	HSPA8	heat shock 70kDa protein 8	0.0004437	2.44268
209086_x_at	MCAM	melanoma cell adhesion molecule	0.0004469	2.94183
1552612_at	CDC42SE2	CDC42 small effector 2	0.0004514	2.06976
224730_at	WDR68	WD repeat domain 68	0.0004578	3.28628
201946_s_at	CCT2	chaperonin containing TCP1, subunit 2 (beta)	0.0004685	5.83571
200753_x_at	SFRS2	splicing factor, arginine/serine- rich 2	0.0004729	2.47772
211504_x_at	ROCK2	Rho-associated, coiled-coil containing protein kinase 2	0.0004763	2.78067
208867_s_at	CSNK1A1	casein kinase 1, alpha 1	0.0004763	3.72763
1566968_at	SPRY4	Sprouty homolog 4 (Drosophila)	0.0004772	4.1109
225551_at	C1orf71	chromosome 1 open reading frame 71	0.0004803	3.24052
235668_at	PRDM1	PR domain containing 1, with ZNF domain	0.0004824	2.35987
211936_at	HSPA5	heat shock 70kDa protein 5 (glucose-regulated protein, 78kDa)	0.0004846	2.18501
200787_s_at	PEA15	phosphoprotein enriched in astrocytes 15	0.0004903	5.35518
223921_s_at	GBA2	glucosidase, beta (bile acid) 2	0.0004978	2.15062
223202_s_at	RP13- 360B22.2 /// LOC653522	hypothetical protein FLJ22679 /// similar to hypothetical protein FLJ22679	0.0005003	2.63901
227338_at	LOC440983	hypothetical gene supported by BC066916	0.0005251	2.31401
213875_x_at	C6orf62	chromosome 6 open reading frame 62	0.0005302	3.2757
1555730_a_at	CFL1	cofilin 1 (non-muscle)	0.0005382	4.65044
202206_at	ARL4C	ADP-ribosylation factor-like 4C	0.0005437	8.26974
222395_s_at	UBE2Z	ubiquitin-conjugating enzyme E2Z (putative)	0.0005498	2.20623
209070_s_at	RGS5	regulator of G-protein signalling 5	0.0005533	1-1.1401
204338_s_at	RGS4	regulator of G-protein signalling 4	0.000561	33.795
229733_s_at	---	Transcribed locus, strongly similar to NP_055107.3 chromobox homolog 6 [Homo sap	0.0005686	6.96826
217799_x_at	UBE2H	ubiquitin-conjugating enzyme E2H (UBC8 homolog, yeast)	0.000569	2.20441
225906_at	---	CDNA FLJ38264 fis, clone FCBBF3001657	0.0005719	2.07811
202955_s_at	ARFGEF1	ADP-ribosylation factor guanine	0.0005845	2.62306

200665_s_at	SPARC	nucleotide-exchange factor 1(brefeldin A-inhibited secreted protein, acidic, cysteine-rich (osteonectin) /// secreted protein, acid	0.0005849	2.19663
217356_s_at	PGK1	phosphoglycerate kinase 1	0.0005973	4.41858
210869_s_at	MCAM	melanoma cell adhesion molecule	0.0005991	3.58489
209251_x_at	TUBA6	tubulin, alpha 6	0.0006048	2.06274
211750_x_at	TUBA6	tubulin, alpha 6 /// tubulin, alpha 6	0.0006066	2.07734
209231_s_at	DCTN5	dynactin 5 (p25)	0.0006276	2.48656
207431_s_at	DEGS1	degenerative spermatocyte homolog 1, lipid desaturase (Drosophila)	0.0006334	3.48693
1555618_s_at	SAE1	SUMO-1 activating enzyme subunit 1	0.0006341	3.22436
223585_x_at	KBTBD2	kelch repeat and BTB (POZ) domain containing 2	0.000635	4.3777
212979_s_at	KIAA0738	KIAA0738 gene product	0.0006362	4.74185
220342_x_at	EDEM3 /// LOC653815	ER degradation enhancer, mannosidase alpha-like 3 /// similar to chromosome 1 op	0.0006387	2.84876
226400_at	CDC42	Cell division cycle 42 (GTP binding protein, 25kDa)	0.0006601	2.51893
224396_s_at	ASPN	asporin (LRR class 1) /// asporin (LRR class 1)	0.0006638	7.24602
220202_s_at	MNAB	membrane associated DNA binding protein	0.0006676	3.08897
208721_s_at	ANAPC5	anaphase promoting complex subunit 5	0.0006717	3.69616
201475_x_at	MARS	methionine-tRNA synthetase	0.0006737	2.18332
203248_at	ZNF24	zinc finger protein 24	0.0006861	2.22304
214305_s_at	SF3B1	splicing factor 3b, subunit 1, 155kDa	0.0006866	2.91606
220477_s_at	C20orf30	chromosome 20 open reading frame 30	0.0006912	4.54177
224828_at	CPEB4	cytoplasmic polyadenylation element binding protein 4	0.0006919	4.53682
200769_s_at	MAT2A	methionine adenosyltransferase II, alpha	0.0006935	3.70802
217301_x_at	RBBP4	retinoblastoma binding protein 4	0.0006961	2.15393
201392_s_at	IGF2R	insulin-like growth factor 2 receptor	0.0006986	3.75923
209652_s_at	PGF	placental growth factor, vascular endothelial growth factor-related protein	0.0007058	3.0292
208453_s_at	XPNPEP1	X-prolyl aminopeptidase (aminopeptidase P) 1, soluble	0.0007085	2.84172
218178_s_at	CHMP1B	chromatin modifying protein 1B	0.000711	2.09058
208051_s_at	PAIP1	poly(A) binding protein interacting protein 1	0.0007212	3.30622

207791_s_at	RAB1A	RAB1A, member RAS oncogene family	0.0007257	3.64797
209064_x_at	PAIP1	poly(A) binding protein interacting protein 1	0.0007267	3.19553
202877_s_at	CD93	CD93 molecule /// CD93 molecule	0.0007308	3.72188
225240_s_at	MSI2	musashi homolog 2 (Drosophila)	0.0007373	2.57268
202998_s_at	LOXL2	lysyl oxidase-like 2	0.0007411	4.85957
222831_at	SAP30L	SAP30-like	0.0007474	2.0565
222810_s_at	RASAL2	RAS protein activator like 2	0.0007636	2.74103
1555419_a_at	ASAH1	N-acylsphingosine amidohydrolase (acid ceramidase) 1	0.0007638	3.06253
218888_s_at	NETO2	neuropilin (NRP) and tolloid (TLL)-like 2	0.000775	3.89666
211858_x_at	GNAS	GNAS complex locus	0.0007874	3.44935
202143_s_at	COPS8	COP9 constitutive photomorphogenic homolog subunit 8 (Arabidopsis)	0.0008282	4.47639
201979_s_at	PPP5C	protein phosphatase 5, catalytic subunit	0.000831	2.26207
230884_s_at	SPG7	spastic paraplegia 7, paraplegin (pure and complicated autosomal recessive)	0.0008407	3.75125
201127_s_at	ACLY	ATP citrate lyase	0.0008441	2.06594
214359_s_at	HSP90AB1	heat shock protein 90kDa alpha (cytosolic), class B member 1	0.0008574	4.34822
216883_x_at	PDE6D	phosphodiesterase 6D, cGMP-specific, rod, delta	0.0008735	2.20674
1554574_a_at	CYB5R3	cytochrome b5 reductase 3	0.0008869	5.27572
200656_s_at	P4HB	procollagen-proline, 2-oxoglutarate 4-dioxygenase (proline 4-hydroxylase), beta	0.0008976	3.88938
1555226_s_at	C1orf43	chromosome 1 open reading frame 43	0.0009027	5.09049
200607_s_at	RAD21	RAD21 homolog (S. pombe)	0.0009034	4.8113
200966_x_at	ALDOA	aldolase A, fructose-bisphosphate	0.0009044	2.60326
221039_s_at	DDEF1	development and differentiation enhancing factor 1	0.0009067	3.05927
211016_x_at	HSPA4	heat shock 70kDa protein 4	0.0009203	2.68684
233487_s_at	LRRC8A	leucine rich repeat containing 8 family, member A	0.0009234	2.37013
1566303_s_at	PPP1R11	protein phosphatase 1, regulatory (inhibitor) subunit 11	0.0009283	3.16014
224982_at	AKT1S1	AKT1 substrate 1 (proline-rich)	0.0009285	3.31242
201243_s_at	ATP1B1	ATPase, Na ⁺ /K ⁺ transporting, beta 1 polypeptide	0.0009312	4.3268
214548_x_at	GNAS	GNAS complex locus	0.0009326	3.68635
225127_at	GPR178	G protein-coupled receptor 178	0.0009402	2.59268
221507_at	TNPO2	transportin 2 (importin 3, karyopherin beta 2b)	0.0009484	3.00608

214228_x_at	TNFRSF4	tumor necrosis factor receptor superfamily, member 4	0.0009549	2.98778
221267_s_at	FAM108A1	family with sequence similarity 108, member A1 /// family with sequence similari	0.0009587	2.15818
201364_s_at	OAZ2	ornithine decarboxylase antizyme 2	0.0009602	2.76547
208684_at	COPA	coatomer protein complex, subunit alpha	0.0009606	2.2011
201869_s_at	TBL1X	transducin (beta)-like 1X-linked	0.0009717	3.22866
202374_s_at	RAB3GAP2	RAB3 GTPase activating protein subunit 2 (non-catalytic)	0.0009833	2.50742
207821_s_at	PTK2	PTK2 protein tyrosine kinase 2	0.0009841	2.539
1555945_s_at	C9orf10	chromosome 9 open reading frame 10	0.0009859	2.36915
222399_s_at	TM9SF3	transmembrane 9 superfamily member 3	0.0009921	2.37402
213011_s_at	TPI1	triosephosphate isomerase 1	0.0009937	2.12129
218748_s_at	EXOC5	exocyst complex component 5	0.0009976	4.99435
218876_at	CGI-38	brain specific protein /// brain specific protein	0.0009982	3.16721
208813_at	GOT1	glutamic-oxaloacetic transaminase 1, soluble (aspartate aminotransferase 1)	0.0010045	2.97521
1555388_s_at	SNX25	sorting nexin 25	0.0010064	2.29133
211668_s_at	PLAU	plasminogen activator, urokinase /// plasminogen activator, urokinase	0.0010121	4.33147
225070_at	C6orf68	Chromosome 6 open reading frame 68	0.001013	2.64455
201446_s_at	TIA1	TIA1 cytotoxic granule-associated RNA binding protein	0.0010188	2.55723
226216_at	---	CDNA: FLJ21874 fis, clone HEP02488	0.0010249	3.3957
210978_s_at	TAGLN2	transgelin 2	0.0010312	3.50596
213423_x_at	TUSC3	tumor suppressor candidate 3	0.0010323	4.5595
224612_s_at	DNAJC5	DnaJ (Hsp40) homolog, subfamily C, member 5	0.0010403	2.47486
212075_s_at	CSNK2A1	casein kinase 2, alpha 1 polypeptide	0.0010556	2.45277
221810_at	RAB15	RAB15, member RAS oncogene family	0.0010618	2.23836
200842_s_at	EPRS	glutamyl-prolyl-tRNA synthetase	0.0010626	3.03177
211574_s_at	CD46	CD46 molecule, complement regulatory protein	0.0010673	5.54549
223189_x_at	MLL5	myeloid/lymphoid or mixed-lineage leukemia 5 (trithorax homolog, Drosophila)	0.0010758	3.682
212950_at	GPR116	G protein-coupled receptor 116	0.0010866	3.22492
207549_x_at	CD46	CD46 molecule, complement regulatory protein	0.0010867	6.10355

218260_at	DDA1	DDA1	0.001097	3.24781
208737_at	ATP6V1G1	ATPase, H+ transporting, lysosomal 13kDa, V1 subunit G1 similar to DNA segment, Chr 11,	0.0011029	3.2127
224573_at	MGC71993	Brigham & Womens Genetics 0434 expressed	0.0011117	2.2845
1554462_a_at	DNAJB9	DnaJ (Hsp40) homolog, subfamily B, member 9	0.0011126	3.89239
200731_s_at	PTP4A1	protein tyrosine phosphatase type IVA, member 1	0.0011225	2.91614
201322_at	ATP5B	ATP synthase, H+ transporting, mitochondrial F1 complex, beta polypeptide	0.0011314	2.01939
204426_at	TMED2	transmembrane emp24 domain trafficking protein 2	0.0011316	6.17
210638_s_at	FBXO9	F-box protein 9	0.0011326	2.10918
201452_at	RHEB	Ras homolog enriched in brain guanine nucleotide binding	0.0011436	2.13505
200852_x_at	GNB2	protein (G protein), beta polypeptide 2	0.0011465	2.42684
212216_at	PREPL	prolyl endopeptidase-like	0.0011581	4.55695
214119_s_at	FKBP1A	FK506 binding protein 1A, 12kDa	0.0011663	2.49447
206448_at	ZNF365	zinc finger protein 365	0.0011696	8.0473
202874_s_at	ATP6V1C1	ATPase, H+ transporting, lysosomal 42kDa, V1 subunit C1	0.0011711	3.22782
201411_s_at	PLEKHB2	pleckstrin homology domain containing, family B (eectins) member 2	0.001186	3.87391
213594_x_at	FUSIP1 /// LOC642558	FUS interacting protein (serine/arginine-rich) 1 /// similar to FUS interacting	0.0011938	2.31479
209626_s_at	OSBPL3	oxysterol binding protein-like 3 ADP-ribosylation factor guanine	0.001204	2.53807
222518_at	ARFGEF2	nucleotide-exchange factor 2 (brefeldin A-inhibi	0.0012122	2.5171
205056_s_at	GPR162	G protein-coupled receptor 162	0.0012171	2.6217
203048_s_at	KIAA0372	KIAA0372	0.0012187	2.25368
1554577_a_at	PSMD10	proteasome (prosome, macropain) 26S subunit, non- ATPase, 10	0.0012337	3.63036
227364_at	---	---	0.0012372	3.86482
202154_x_at	TUBB3	tubulin, beta 3 tyrosine 3-	0.0012404	2.0844
217717_s_at	YWHAB	monooxygenase/tryptophan 5- monooxygenase activation protein, beta pol	0.001252	2.38885
215952_s_at	OAZ1	ornithine decarboxylase antizyme 1	0.0012593	2.60162
204427_s_at	TMED2	transmembrane emp24 domain trafficking protein 2	0.001271	6.1382

215714_s_at	SMARCA4	SWI/SNF related, matrix associated, actin dependent regulator of chromatin, subfamily 4	0.0012718	2.12326
208662_s_at	TTC3	tetratricopeptide repeat domain 3	0.0012904	2.83208
209228_x_at	TUSC3	tumor suppressor candidate 3	0.0012986	4.66022
232079_s_at	PVRL2 /// LOC643722	poliovirus receptor-related 2 (herpesvirus entry mediator B) /// similar to Poli	0.0013161	2.39125
201399_s_at	TRAM1	translocation associated membrane protein 1	0.0013236	3.3991
212065_s_at	USP34	ubiquitin specific peptidase 34	0.0013248	3.84788
216483_s_at	C19orf10	chromosome 19 open reading frame 10	0.001329	2.93726
213476_x_at	TUBB3	tubulin, beta 3	0.0013305	2.28862
208654_s_at	CD164	CD164 molecule, sialomucin	0.0013332	2.50733
223057_s_at	XPO5	exportin 5	0.0013403	2.071
1553535_a_at	RANGAP1	Ran GTPase activating protein 1	0.0013518	2.7276
200751_s_at	HNRPC	heterogeneous nuclear ribonucleoprotein C (C1/C2)	0.0013539	3.60369
202024_at	ASNA1	arsA arsenite transporter, ATP-binding, homolog 1 (bacterial)	0.0013571	2.52099
201856_s_at	ZFR	zinc finger RNA binding protein	0.0013604	3.19562
222386_s_at	COPZ1	coatamer protein complex, subunit zeta 1	0.0013839	2.34248
218309_at	CAMK2N1	calcium/calmodulin-dependent protein kinase II inhibitor 1	0.0013861	3.06383
201309_x_at	C5orf13	chromosome 5 open reading frame 13	0.0013892	6.09148
201708_s_at	NIPSNAP1	nipsnap homolog 1 (C. elegans)	0.0013969	2.23642
200822_x_at	TPI1	triosephosphate isomerase 1	0.0014355	2.01854
230656_s_at	CIRH1A	cirrhosis, autosomal recessive 1A (cirhin)	0.0014472	2.61503
212273_x_at	GNAS	GNAS complex locus	0.0014579	3.20735
208664_s_at	TTC3	tetratricopeptide repeat domain 3	0.0014682	4.79977
209730_at	SEMA3F	sema domain, immunoglobulin domain (Ig), short basic domain, secreted, (semaphorin 3F)	0.0014834	2.07692
208926_at	NEU1	sialidase 1 (lysosomal sialidase)	0.0014995	2.13937
229192_s_at	TBCD	tubulin-specific chaperone domain 4	0.0015114	2.33804
202027_at	C22orf5	chromosome 22 open reading frame 5	0.0015162	2.01596
225667_s_at	---	---	0.0015194	4.21611
202008_s_at	NID1	nidogen 1	0.0015197	3.76103
1553694_a_at	PIK3C2A	phosphoinositide-3-kinase, class 2, alpha polypeptide	0.0015237	4.32404
202079_s_at	TRAK1	trafficking protein, kinesin binding domain 1	0.0015279	2.31786
201037_at	PFKP	phosphofructokinase, platelet	0.0015306	2.6478
226310_at	RICTOR	rapamycin-insensitive companion of mTOR	0.0015459	2.37113

217831_s_at	NSFL1C	NSFL1 (p97) cofactor (p47)	0.0015507	2.26076
222155_s_at	GPR172A	G protein-coupled receptor 172A	0.0015534	2.82663
207379_at	EDIL3	EGF-like repeats and discoidin I-like domains 3	0.0015552	2.46671
200954_at	ATP6V0C	ATPase, H ⁺ transporting, lysosomal 16kDa, V0 subunit c	0.0015576	2.35231
220203_at	BMP8A	bone morphogenetic protein 8a	0.0015591	2.11927
205801_s_at	RASGRP3	RAS guanyl releasing protein 3 (calcium and DAG-regulated)	0.0015615	2.64912
204395_s_at	GRK5	G protein-coupled receptor kinase 5	0.0015625	2.17302
	NPIP ///			
	LOC23117			
	///			
	LOC339047			
214870_x_at	///	nuclear pore complex interacting protein /// KIAA0220-like protein	0.0015635	2.00404
	LOC440341	/// hypotheti		
	///			
	LOC642778			
	///			
	LOC642799			
224693_at	C20orf108	chromosome 20 open reading frame 108	0.0015738	2.02231
202768_at	FOSB	FBJ murine osteosarcoma viral oncogene homolog B	0.0015927	15.8256
202301_s_at	FLJ11021	similar to splicing factor, arginine/serine-rich 4	0.0015993	2.24488
229033_s_at	MUM1	melanoma associated antigen (mutated) 1	0.0016005	2.4918
201015_s_at	JUP	junction plakoglobin	0.0016053	2.13648
238543_x_at	MDGA1	MAM domain containing glycosylphosphatidylinositol anchor 1	0.0016089	2.08219
200008_s_at	GDI2	GDP dissociation inhibitor 2 /// GDP dissociation inhibitor 2	0.0016119	3.96852
200605_s_at	PRKAR1A	protein kinase, cAMP-dependent, regulatory, type I, alpha (tissue specific extin	0.0016167	2.77309
1555780_a_at	RHEB	Ras homolog enriched in brain	0.0016315	2.24494
226876_at	FAM101B	family with sequence similarity 101, member B	0.0016498	2.91055
208852_s_at	CANX	calnexin	0.0016832	2.50994
200780_x_at	GNAS	GNAS complex locus	0.0016846	3.08187
228116_at	---	Clone IMAGE:120162 mRNA sequence	0.0016906	3.60904
		CKLF-like MARVEL		
224998_at	CMTM4	transmembrane domain containing 4	0.0016943	2.54739
200756_x_at	CALU	calumenin	0.0016972	2.63041
211913_s_at	MERTK	c-mer proto-oncogene tyrosine kinase /// c-mer proto-oncogene	0.001702	2.28284

		tyrosine kinase		
212041_at	ATP6V0D1	ATPase, H+ transporting, lysosomal 38kDa, V0 subunit d1	0.0017028	2.67106
224787_s_at	RAB18	RAB18, member RAS oncogene family	0.0017065	2.62716
217885_at	IPO9	importin 9	0.001716	2.1855
226825_s_at	TPARL	TPA regulated locus	0.0017166	4.116
206491_s_at	NAPA	N-ethylmaleimide-sensitive factor attachment protein, alpha	0.0017194	2.67057
201435_s_at	EIF4E	eukaryotic translation initiation factor 4E	0.0017198	2.46427
217716_s_at	SEC61A1	Sec61 alpha 1 subunit (S. cerevisiae)	0.0017593	2.00898
211985_s_at	CALM1	calmodulin 1 (phosphorylase kinase, delta)	0.001764	3.23467
214687_x_at	ALDOA	aldolase A, fructose-bisphosphate	0.0017726	2.30197
201251_at	PKM2	pyruvate kinase, muscle	0.0017878	2.21983
202654_x_at	07-Mar	membrane-associated ring finger (C3HC4) 7	0.0017944	3.02922
241682_at	KLHL23	kelch-like 23 (Drosophila)	0.00183	2.6171
200813_s_at	PAFAH1B1	platelet-activating factor acetylhydrolase, isoform Ib, alpha subunit 45kDa	0.0018408	2.83597
200729_s_at	ACTR2	ARP2 actin-related protein 2 homolog (yeast)	0.0018674	2.95505
201167_x_at	ARHGDI	Rho GDP dissociation inhibitor (GDI) alpha	0.0018854	2.86438
228030_at	---	Transcribed locus	0.0018901	6.12459
208693_s_at	GARS	glycyl-tRNA synthetase	0.0018931	2.26707
200900_s_at	M6PR	mannose-6-phosphate receptor (cation dependent)	0.0019125	3.46704
200738_s_at	PGK1	phosphoglycerate kinase 1	0.0019157	2.10659
204463_s_at	EDNRA	endothelin receptor type A tyrosine 3-	0.0019307	4.39973
201020_at	YWHAH	monooxygenase/tryptophan 5-monooxygenase activation protein, eta poly	0.0019355	2.68769
202058_s_at	KPNA1	karyopherin alpha 1 (importin alpha 5)	0.0019457	2.67286
201663_s_at	SMC4L1	SMC4 structural maintenance of chromosomes 4-like 1 (yeast)	0.0019479	2.4404
214846_s_at	ALPK3	alpha-kinase 3	0.0019487	2.90276
234941_s_at	GPHN	gephyrin	0.0019555	2.94424
209186_at	ATP2A2	ATPase, Ca++ transporting, cardiac muscle, slow twitch 2	0.0019636	2.31056
222693_at	FNDC3B	fibronectin type III domain containing 3B	0.0019723	2.74403
225832_s_at	LOC221955	KCCR13L	0.0019779	2.04543
202773_s_at	SFRS8	splicing factor, arginine/serine-rich 8 (suppressor-of-white-	0.0019903	2.08623

208316_s_at	OCRL	apricot homolog, Dr oculocerebrorenal syndrome of Lowe	0.002	2.60805
222531_s_at	C14orf108	chromosome 14 open reading frame 108	0.002	2.40337
1554167_a_at	GOLGA7	golgi autoantigen, golgin subfamily a, 7	0.0020075	3.40833
213646_x_at	K-ALPHA-1	alpha tubulin	0.0020078	2.05214
217748_at	ADIPOR1	adiponectin receptor 1 /// adiponectin receptor 1	0.0020087	2.29093
209162_s_at	PRPF4	PRP4 pre-mRNA processing factor 4 homolog (yeast)	0.0020152	3.34936
210178_x_at	FUSIP1 /// LOC642558	FUS interacting protein (serine/arginine-rich) 1 /// similar to FUS interacting	0.002041	2.67528
230913_at	---	Full length insert cDNA clone ZE12B03	0.0020447	4.97248
217826_s_at	UBE2J1	ubiquitin-conjugating enzyme E2, J1 (UBC6 homolog, yeast)	0.002053	3.5576
212639_x_at	K-ALPHA-1	alpha tubulin	0.0020544	2.01119
203293_s_at	LMAN1	lectin, mannose-binding, 1	0.0020593	2.79184
228528_at	---	CDNA FLJ41270 fis, clone BRAMY2036387	0.0020786	5.56913
212162_at	KIDINS220	kinase D-interacting substance of 220 kDa	0.0020824	2.27507

Supplemental Table S2

Probe ID	Gene symbol	David Gene Name
214091_s_at	gpX3	glutathione peroxidase 3 (plasma)
217871_s_at	LOC284889	hypothetical protein LOC284889
202718_at	igfbp2	insulin-like growth factor binding protein 2, 36kDa
209993_at	ABCB1	ATP-binding cassette, sub-family B (MDR/TAP), member 1
203971_at	SLC31A1	solute carrier family 31 (copper transporters), member 1
224151_s_at	ak3	adenylate kinase 3
204623_at	Tff3	trefoil factor 3 (intestinal)
218488_at	EIF2B3	eukaryotic translation initiation factor 2B, subunit 3 gamma, 58kDa
200989_at	HIF1A	hypoxia inducible factor 1, alpha subunit (basic helix-loop-helix transcription factor)

211003_x_at	tgm2	transglutaminase 2 (C polypeptide, protein-glutamine-gamma-glutamyltransferase)
221523_s_at	Rragd	Ras-related GTP binding D
205251_at	PER2	period homolog 2 (Drosophila)
210881_s_at	INS-IGF2	insulin-like growth factor 2 (somatomedin A); insulin; INS-IGF2 readthrough transcript
210881_s_at	INS	insulin-like growth factor 2 (somatomedin A); insulin; INS-IGF2 readthrough transcript
210881_s_at	IGF2	insulin-like growth factor 2 (somatomedin A); insulin; INS-IGF2 readthrough transcript
211258_s_at	TGFA	transforming growth factor, alpha
209201_x_at	CXCR4	chemokine (C-X-C motif) receptor 4
202696_at	OXS1	oxidative-stress responsive 1
204298_s_at	lox	lysyl oxidase
205193_at	Maff	v-maf musculoaponeurotic fibrosarcoma oncogene homolog F (avian)
201248_s_at	srebf2	sterol regulatory element binding transcription factor 2
207851_s_at	INSR	insulin receptor
221884_at	MECOM	ecotropic viral integration site 1
210050_at	TPI1	TPI1 pseudogene; triosephosphate isomerase 1
210050_at	TPI1P1	TPI1 pseudogene; triosephosphate isomerase 1
201231_s_at	eno1	enolase 1, (alpha)
1553995_a_at	NT5E	5'-nucleotidase, ecto (CD73)
210009_s_at	GOSR2	golgi SNAP receptor complex member 2
206245_s_at	IVNS1ABP	influenza virus NS1A binding protein
201650_at	JUP	junction plakoglobin
202998_s_at	lox12	lysyl oxidase-like 2
213700_s_at	LOC652797	similar to Pyruvate kinase, isozymes M1/M2 (Pyruvate kinase muscle isozyme) (Cytosolic thyroid hormone-binding protein) (CTHBP) (THBP1); pyruvate kinase, muscle
213700_s_at	PKM2	similar to Pyruvate kinase, isozymes M1/M2 (Pyruvate kinase muscle isozyme) (Cytosolic thyroid hormone-binding protein) (CTHBP) (THBP1); pyruvate kinase, muscle
236227_at	TMEM161B	transmembrane protein 161B
225022_at	GOPC	golgi associated PDZ and coiled-coil motif containing
211981_at	Col4a1	collagen, type IV, alpha 1
200825_s_at	hyou1	hypoxia up-regulated 1
207092_at	LEP	leptin
222846_at	RAB8B	RAB8B, member RAS oncogene family
211668_s_at	PLAU	plasminogen activator, urokinase
200843_s_at	eprs	glutamyl-prolyl-tRNA synthetase
1555353_at	lrp1	low density lipoprotein-related protein 1 (alpha-2-macroglobulin receptor)
1555271_a_at	TERT	telomerase reverse transcriptase

214017_s_at	DHX34	DEAH (Asp-Glu-Ala-His) box polypeptide 34
219526_at	C14orf169	chromosome 14 open reading frame 169
208711_s_at	CCND1	cyclin D1
218625_at	NRN1	neuritin 1
203484_at	sec61g	Sec61 gamma subunit
213694_at	RSBN1	round spermatid basic protein 1
230161_at	CD99	CD99 molecule
219232_s_at	egl3	egl nine homolog 3 (C. elegans)
201037_at	pfkp	phosphofructokinase, platelet
202284_s_at	CDKN1A	cyclin-dependent kinase inhibitor 1A (p21, Cip1)
209652_s_at	PGF	placental growth factor
203282_at	GBE1	glucan (1,4-alpha-), branching enzyme 1
206662_at	GLRX	glutaredoxin (thioltransferase)
217047_s_at	Fam13a	family with sequence similarity 13, member A
203578_s_at	SLC7A6	solute carrier family 7 (cationic amino acid transporter, y+ system), member 6
205572_at	ANGPT2	angiopoietin 2
207623_at	ABCF2	ATP-binding cassette, sub-family F (GCN20), member 2
1555938_x_at	VIM	vimentin
201044_x_at	DUSP1	dual specificity phosphatase 1
217738_at	NAMPT	nicotinamide phosphoribosyltransferase
1563466_at	MYLK	myosin light chain kinase
208131_s_at	Ptgis	prostaglandin I2 (prostacyclin) synthase
211964_at	col4a2	collagen, type IV, alpha 2
218525_s_at	Hif1an	hypoxia inducible factor 1, alpha subunit inhibitor
1554627_a_at	ASCC1	activating signal cointegrator 1 complex subunit 1
213649_at	sfrs7	splicing factor, arginine/serine-rich 7, 35kDa
209193_at	Pim1	pim-1 oncogene
212488_at	Col5a1	collagen, type V, alpha 1
223738_s_at	pgm2	phosphoglucomutase 2
212180_at	CRKL	v-crk sarcoma virus CT10 oncogene homolog (avian)-like
202021_x_at	LOC730144	similar to eukaryotic translation initiation factor 1; eukaryotic translation initiation factor 1
202021_x_at	Eif1	similar to eukaryotic translation initiation factor 1; eukaryotic translation initiation factor 1
201809_s_at	ENG	endoglin
218222_x_at	ARNT	aryl hydrocarbon receptor nuclear translocator
202499_s_at	SLC2A3	solute carrier family 2 (facilitated glucose transporter), member 3
1555758_a_at	CDKN3	cyclin-dependent kinase inhibitor 3
200697_at	HK1	hexokinase 1

211167_s_at	gck	glucokinase (hexokinase 4)
221479_s_at	BNIP3L	BCL2/adenovirus E1B 19kDa interacting protein 3-like
214513_s_at	CREB1	cAMP responsive element binding protein 1
202690_s_at	SNRPD1	small nuclear ribonucleoprotein D1 polypeptide 16kDa; hypothetical protein LOC100129492
202690_s_at	LOC100129492	small nuclear ribonucleoprotein D1 polypeptide 16kDa; hypothetical protein LOC100129492
209101_at	CTGF	connective tissue growth factor similar to DEAH (Asp-Glu-Ala-His) box
222574_s_at	LOC100134387	polypeptide 40; DEAH (Asp-Glu-Ala-His) box polypeptide 40
222574_s_at	DHX40	similar to DEAH (Asp-Glu-Ala-His) box polypeptide 40; DEAH (Asp-Glu-Ala-His) box polypeptide 40
207785_s_at	Rbpj	recombination signal binding protein for immunoglobulin kappa J region
214978_s_at	Ppfia4	protein tyrosine phosphatase, receptor type, f polypeptide (PTPRF), interacting protein (liprin), alpha 4
202022_at	aldoc	aldolase C, fructose-bisphosphate
223385_at	Cyp2s1	cytochrome P450, family 2, subfamily S, polypeptide 1
204179_at	MB	myoglobin
227501_at	WSB1	WD repeat and SOCS box-containing 1
201979_s_at	ppp5c	protein phosphatase 5, catalytic subunit
205581_s_at	NOS3	nitric oxide synthase 3 (endothelial cell)
206877_at	MXD1	MAX dimerization protein 1
203692_s_at	E2F3	E2F transcription factor 3
220342_x_at	edem3	ER degradation enhancer, mannosidase alpha-like 3
200650_s_at	LdhA	lactate dehydrogenase A
204331_s_at	mRpS12	mitochondrial ribosomal protein S12
213240_s_at	Krt4	keratin 4
202610_s_at	Med14	mediator complex subunit 14
AFFX- HUMGAPDH/M33197_3 _at	LOC100133042	glyceraldehyde-3-phosphate dehydrogenase-like 6; hypothetical protein LOC100133042; glyceraldehyde-3-phosphate dehydrogenase
AFFX- HUMGAPDH/M33197_3 _at	GAPDH	glyceraldehyde-3-phosphate dehydrogenase-like 6; hypothetical protein LOC100133042; glyceraldehyde-3-phosphate dehydrogenase
AFFX- HUMGAPDH/M33197_3 _at	GAPDHL6	glyceraldehyde-3-phosphate dehydrogenase-like 6; hypothetical protein LOC100133042; glyceraldehyde-3-phosphate dehydrogenase
210735_s_at	ca12	carbonic anhydrase XII
205271_s_at	CDK20	cell cycle related kinase
203359_s_at	MYCBP	c-myc binding protein
209080_x_at	glrx3	glutaredoxin 3

200827_at	PLOD1	procollagen-lysine 1, 2-oxoglutarate 5-dioxygenase 1
229879_at	KRT8P9	keratin 8 pseudogene 9; similar to keratin 8; keratin 8
229879_at	LOC149501	keratin 8 pseudogene 9; similar to keratin 8; keratin 8
229879_at	krt8	keratin 8 pseudogene 9; similar to keratin 8; keratin 8
207257_at	EPO	erythropoietin
210037_s_at	NOS2	nitric oxide synthase 2, inducible
217678_at	SLC7A11	solute carrier family 7, (cationic amino acid transporter, y+ system) member 11
201968_s_at	pgm1	phosphoglucomutase 1
201625_s_at	INSIG1	insulin induced gene 1
202627_s_at	SERPINE1	serpin peptidase inhibitor, clade E (nexin, plasminogen activator inhibitor type 1), member 1
203665_at	hmox1	heme oxygenase (decycling) 1
203438_at	STC2	stanniocalcin 2
227863_at	CTSD	cathepsin D
212171_x_at	VEGFA	vascular endothelial growth factor A
202643_s_at	TNFAIP3	tumor necrosis factor, alpha-induced protein 3
223333_s_at	ANGPTL4	angiopoietin-like 4
214063_s_at	TF	transferrin
209430_at	Btaf1	BTAf1 RNA polymerase II, B-TFIID transcription factor-associated, 170kDa (Mot1 homolog, <i>S. cerevisiae</i>)
222033_s_at	FLT1	fms-related tyrosine kinase 1 (vascular endothelial growth factor/vascular permeability factor receptor)
1559227_s_at	vhl	von Hippel-Lindau tumor suppressor
1554420_at	atf3	activating transcription factor 3
203953_s_at	CLDN3	claudin 3
209709_s_at	HMMR	hyaluronan-mediated motility receptor (RHAMM)
237691_x_at	ENO3	enolase 3 (beta, muscle)
211559_s_at	CCNG2	cyclin G2
202140_s_at	clk3	CDC-like kinase 3
1564084_at	cad	carbamoyl-phosphate synthetase 2, aspartate transcarbamylase, and dihydroorotase
224314_s_at	egl1	egl nine homolog 1 (<i>C. elegans</i>)
217356_s_at	PGK1	phosphoglycerate kinase 1
202340_x_at	NR4A1	nuclear receptor subfamily 4, group A, member 1
219239_s_at	ZNF654	zinc finger protein 654
230126_s_at	KDM4B	lysine (K)-specific demethylase 4B
202733_at	P4HA2	prolyl 4-hydroxylase, alpha polypeptide II
213931_at	ID2	inhibitor of DNA binding 2, dominant

208308_s_at	GPI	negative helix-loop-helix protein
203722_at	ALDH4A1	glucose phosphate isomerase aldehyde dehydrogenase 4 family, member A1
210334_x_at	BIRC5	baculoviral IAP repeat-containing 5
211323_s_at	ITPR1	inositol 1,4,5-triphosphate receptor, type 1
224793_s_at	tgfbr1	transforming growth factor, beta receptor 1
202848_s_at	grk6	G protein-coupled receptor kinase 6
237215_s_at	TFRC	transferrin receptor (p90, CD71)
229124_at	PROK1	prokineticin 1
1564630_at	EDN1	endothelin 1
200720_s_at	ACTR1A	ARP1 actin-related protein 1 homolog A, centractin alpha (yeast)
227792_at	Itpripl2	inositol 1,4,5-triphosphate receptor interacting protein-like 2
216867_s_at	PDGFA	platelet-derived growth factor alpha polypeptide
1554452_a_at	C7orf68	chromosome 7 open reading frame 68
227253_at	CP	ceruloplasmin (ferroxidase)
204991_s_at	Nf2	neurofibromin 2 (merlin)
201202_at	pcnA	proliferating cell nuclear antigen
202887_s_at	ddit4	DNA-damage-inducible transcript 4
208922_s_at	NXF1	nuclear RNA export factor 1
236495_at	NAMPT	nicotinamide phosphoribosyltransferase
224959_at	Slc26a2	solute carrier family 26 (sulfate transporter), member 2
201313_at	eno2	enolase 2 (gamma, neuronal)
203749_s_at	rarA	retinoic acid receptor, alpha
1568611_at	P4HA2	prolyl 4-hydroxylase, alpha polypeptide II
201848_s_at	BNIP3	BCL2/adenovirus E1B 19kDa interacting protein 3
209735_at	Abcg2	ATP-binding cassette, sub-family G (WHITE), member 2
220942_x_at	Fam162a	family with sequence similarity 162, member A
201473_at	junb	jun B proto-oncogene
203055_s_at	Arhgef1	Rho guanine nucleotide exchange factor (GEF) 1
204200_s_at	Pdgfb	platelet-derived growth factor beta polypeptide (simian sarcoma viral (v-sis) oncogene homolog)
1557186_s_at	Tpcn1	two pore segment channel 1
219410_at	TMEM45A	transmembrane protein 45A
201549_x_at	LOC100133760	similar to Jumonji, AT rich interactive domain 1B (RBP2-like); lysine (K)-specific demethylase 5B
201549_x_at	KDM5B	similar to Jumonji, AT rich interactive domain 1B (RBP2-like); lysine (K)-specific demethylase 5B
202364_at	MXI1	MAX interactor 1

222125_s_at	P4HTM	prolyl 4-hydroxylase, transmembrane (endoplasmic reticulum)
213943_at	twist1	twist homolog 1 (Drosophila)
205199_at	CA9	carbonic anhydrase IX
205746_s_at	Adam17	ADAM metallopeptidase domain 17
209304_x_at	Gadd45b	growth arrest and DNA-damage-inducible, beta
207557_s_at	RYR2	ryanodine receptor 2 (cardiac)
203115_at	FECH	ferrochelatase (protoporphyrin)
200886_s_at	pgam1	phosphoglycerate mutase 1 (brain)
218105_s_at	mRpl4	mitochondrial ribosomal protein L4
201596_x_at	KRT18P19	keratin 18; keratin 18 pseudogene 26; keratin 18 pseudogene 19
201596_x_at	KRT18	keratin 18; keratin 18 pseudogene 26; keratin 18 pseudogene 19
201596_x_at	KRT18P26	keratin 18; keratin 18 pseudogene 26; keratin 18 pseudogene 19
227287_at	Cited2	Cbp/p300-interacting transactivator, with Glu/Asp-rich carboxy-terminal domain, 2
214861_at	KDM4C	lysine (K)-specific demethylase 4C
201102_s_at	PFKL	phosphofructokinase, liver
201865_x_at	NR3C1	nuclear receptor subfamily 3, group C, member 1 (glucocorticoid receptor)
224833_at	ETS1	v-ets erythroblastosis virus E26 oncogene homolog 1 (avian)
201170_s_at	bhlhe40	basic helix-loop-helix family, member e40
204285_s_at	PMAIP1	phorbol-12-myristate-13-acetate-induced protein 1
202023_at	EFNA1	ephrin-A1
218498_s_at	ERO1L	ERO1-like (<i>S. cerevisiae</i>)
235629_at	fn1	fibronectin 1
216197_at	ATF7IP	activating transcription factor 7 interacting protein
217777_s_at	ptplad1	protein tyrosine phosphatase-like A domain containing 1
200798_x_at	mcl1	myeloid cell leukemia sequence 1 (BCL2- related)
207543_s_at	P4HA1	prolyl 4-hydroxylase, alpha polypeptide I
203579_s_at	SLC7A6	solute carrier family 7 (cationic amino acid transporter, y+ system), member 6
214710_s_at	CCNB1	cyclin B1
207589_at	adra1b	adrenergic, alpha-1B-, receptor
205302_at	IGFBP1	insulin-like growth factor binding protein 1
212143_s_at	igfbp3	insulin-like growth factor binding protein 3
226534_at	KITLG	KIT ligand
219862_s_at	NARF	nuclear prelamin A recognition factor
230143_at	Rnf165	ring finger protein 165
244447_at	KLF10	Kruppel-like factor 10
203510_at	MET	met proto-oncogene (hepatocyte growth factor receptor)

225700_at	glcci1	glucocorticoid induced transcript 1
230746_s_at	stc1	stanniocalcin 1
212038_s_at	VDAC1P1	voltage-dependent anion channel 1; similar to voltage-dependent anion channel 1
212038_s_at	VDAC1	voltage-dependent anion channel 1; similar to voltage-dependent anion channel 1
224178_s_at	Sox6	SRY (sex determining region Y)-box 6
216449_x_at	Hsp90b1	heat shock protein 90kDa beta (Grp94), member 1
200632_s_at	ndrg1	N-myc downstream regulated 1
214687_x_at	ALDOA	aldolase A, fructose-bisphosphate
203393_at	hes1	hairy and enhancer of split 1, (Drosophila)
160020_at	MMP14	matrix metalloproteinase 14 (membrane-inserted)
206686_at	PDK1	pyruvate dehydrogenase kinase, isozyme 1
221691_x_at	LOC399804	nucleophosmin 1 (nucleolar phosphoprotein B23, numatrin) pseudogene 21; hypothetical LOC100131044; similar to nucleophosmin 1; nucleophosmin (nucleolar phosphoprotein B23, numatrin)
221691_x_at	LOC100131044	nucleophosmin 1 (nucleolar phosphoprotein B23, numatrin) pseudogene 21; hypothetical LOC100131044; similar to nucleophosmin 1; nucleophosmin (nucleolar phosphoprotein B23, numatrin)
221691_x_at	LOC729686	nucleophosmin 1 (nucleolar phosphoprotein B23, numatrin) pseudogene 21; hypothetical LOC100131044; similar to nucleophosmin 1; nucleophosmin (nucleolar phosphoprotein B23, numatrin)
221691_x_at	Npm1	nucleophosmin 1 (nucleolar phosphoprotein B23, numatrin) pseudogene 21; hypothetical LOC100131044; similar to nucleophosmin 1; nucleophosmin (nucleolar phosphoprotein B23, numatrin)
221691_x_at	LOC729342	nucleophosmin 1 (nucleolar phosphoprotein B23, numatrin) pseudogene 21; hypothetical LOC100131044; similar to nucleophosmin 1; nucleophosmin (nucleolar phosphoprotein B23, numatrin)
221691_x_at	NPM1P21	nucleophosmin 1 (nucleolar phosphoprotein B23, numatrin) pseudogene 21; hypothetical LOC100131044; similar to nucleophosmin 1; nucleophosmin (nucleolar phosphoprotein B23, numatrin)
221691_x_at	LOC440577	nucleophosmin 1 (nucleolar phosphoprotein B23, numatrin) pseudogene 21; hypothetical LOC100131044; similar to nucleophosmin 1; nucleophosmin (nucleolar phosphoprotein B23, numatrin)
208291_s_at	TH	tyrosine hydroxylase

201416_at	Sox4	SRY (sex determining region Y)-box 4
202464_s_at	pfkfb3	6-phosphofructo-2-kinase/fructose-2,6-biphosphatase 3
202934_at	HK2P1	hexokinase 2 pseudogene; hexokinase 2
202934_at	Hk2	hexokinase 2 pseudogene; hexokinase 2
212689_s_at	KDM3A	lysine (K)-specific demethylase 3A
209747_at	TGFB3	transforming growth factor, beta 3
217996_at	phl1a1	pleckstrin homology-like domain, family A, member 1
205044_at	GABRP	gamma-aminobutyric acid (GABA) A receptor, pi
242520_s_at	c1orf228	chromosome 1 open reading frame 228
201673_s_at	GYS1	glycogen synthase 1 (muscle)
208905_at	CYCS	cytochrome c, somatic
201945_at	Furin	furin (paired basic amino acid cleaving enzyme)
209687_at	CXCL12	chemokine (C-X-C motif) ligand 12 (stromal cell-derived factor 1)
214532_x_at	POU5F1B	POU class 5 homeobox 1B
219888_at	SPAG4	sperm associated antigen 4
206025_s_at	TNFAIP6	tumor necrosis factor, alpha-induced protein 6
203032_s_at	FH	fumarate hydratase
238091_at	rph3al	rabphilin 3A-like (without C2 domains)
49077_at	PPME1	protein phosphatase methylesterase 1
221530_s_at	BHLHE41	basic helix-loop-helix family, member e41
200956_s_at	ssrp1	structure specific recognition protein 1
207175_at	ADIPOQ	adiponectin, C1Q and collagen domain containing
209566_at	Insig2	insulin induced gene 2
215775_at	Thbs1	thrombospondin 1
222847_s_at	egl3	egl nine homolog 3 (C. elegans)
201133_s_at	pja2	praja ring finger 2
205122_at	TMEFF1	transmembrane protein with EGF-like and two follistatin-like domains 1; chromosome 9 open reading frame 30; hypothetical LOC729538
205122_at	C9orf30	transmembrane protein with EGF-like and two follistatin-like domains 1; chromosome 9 open reading frame 30; hypothetical LOC729538
205122_at	LOC729538	transmembrane protein with EGF-like and two follistatin-like domains 1; chromosome 9 open reading frame 30; hypothetical LOC729538
210845_s_at	PLAUR	plasminogen activator, urokinase receptor
202619_s_at	PLOD2	procollagen-lysine, 2-oxoglutarate 5-dioxygenase 2
202754_at	R3hdm1	R3H domain containing 1
208930_s_at	ilf3	interleukin enhancer binding factor 3, 90kDa

227337_at	Ankrd37	ankyrin repeat domain 37
201250_s_at	slc2a1	solute carrier family 2 (facilitated glucose transporter), member 1
205464_at	SCNN1B	sodium channel, nonvoltage-gated 1, beta
202234_s_at	SLC16A1	solute carrier family 16, member 1 (monocarboxylic acid transporter 1)
220781_at	Dec1	deleted in esophageal cancer 1
1566677_at	Mmp2	matrix metalloproteinase 2 (gelatinase A, 72kDa gelatinase, 72kDa type IV collagenase)
203957_at	e2f6	E2F transcription factor 6
202912_at	ADM	adrenomedullin

Supplemental Table S3. List a, b, c, d e and f

Burnichon et al. Hum Mol Genet. 2011, 20(20):3974-85

List a: overexpressed genes in *SDHx* tumors

APLP2
C12orf53
CNTN4
DDIT3 /// NR1H3
DSP
ELOVL7
ESRRA
FOXRED2
GOSR2
HCN3
LAPTM4B
LGR5
LOC727751
MEIS3
MMP24
NOXA1
PAWR
SIX1
SIX4
SLC16A10
SLC35F2
TRIB3

List b: overexpressed genes in *SDHx + VHL* tumors

ADORA2A	ESAM	P4HA1
AFAP1L1	ETS1	PABPC4L
AK3L1	FAM101B	PAWR
ANO1	FAM69B	PCSK6
AQP1	FAT1	PECAM1
ARG2	FGF12	PFKL
ARHGAP29	FIGN	PITPNC1
ARHGEF10	FLT1	PKIB
ARHGEF7	FNBP1L	PLS3
BLMH	FOLH1	PLVAP
C10orf10	GJC1	PLXND1
C13orf15	GNA14	PRRG1
C1orf126	GNAI3	RASGRP3
C1QTNF5	GPR4	RBMS2
C20orf46	GPR56	RBPMS
C21orf2	HK2	RGS4
C8orf58	INSR	SEC14L1
C9orf135	JAG1	SEMA3F
CA2	KBTBD11	SERBP1
CALCRL	KDM3A	SH3GLB1
CD93	KDR	SH3RF3
CDH13	LAYN	SHMT2
CDH5	LDHA	SLC16A1
CGNL1	LHFP	SLC22A23
CLEC14A	LOC100288985	SLC2A3
COL4A1	LOC643733	SMPDL3A
COX4I2	LOXL2	SOBP
CSRP2	MFAP3	SPARC

CXCR7	MOBKL1B	ST8SIA4
CXorf36	MPZL2	STC1
DARS	MST150	SUZ12
DENND2C	MTF2	TBC1D30
DGCR5	MTHFD2	TBL1X
DGCR9	MYCT1	TM4SF18
ECSCR	NDRG1	TMEM204
EDNRB	NDUFA4L2	TMTC4
EFHD2	NOX4	TSC22D1
EFNA1	NPNT	VEGFA
EFNB2	NRAS	ZAK
ENPEP	NTNG2	ZNF395
EPAS1	NTRK2	

Burnichon et al. Hum Mol Genet. 2011, 20(20):3974-85

List c: overexpressed genes in *VHL* tumors

ABP1	HSPB7	UBXN10
ADSSL1	HTATIP2	VPS13D
ALG14	KCNA6	WDR73
AP4B1	KCNC4	WDR78
ATG9B	KCND3	WNT3
BCAT1	KISS1R	YTHDF2
C12orf26	KLF9	ZSWIM5
C12orf76	KY	
C1orf151	LOC390205	
C1orf59	LOC643837	
C1QTNF2	LRRC40	
C20orf74	MARCH8	
CALY	MCHR1	
CAPZB	MRPL20	
CASZ1	MTP18	
CDH22	MYCBP	
CLCC1	PANK4	
CLCNKB	PCDH8	
CPSF3L	PIK3C3	
CRTAC1	PPFIA4	
CTSZ	PRKAA2	
CYB561D1	PTHLH	
CYB5A	RARRES2	
DDIT4L	RD3	
DDO	RER1	
DDOST	RSPH1	
EEF2K	RSPH9	
EFHC1	SH3RF3	
EGFL7	SLC16A3	
EGLN3	SLC2A1	
EML1	SLC36A1	

List d overexpressed genes in *RET/NF1/TMEM127* tumors

ACCN4	PPP1R1B
ADCYAP1	PRKCE
AKR1C1	PROK2
AKR1C2	ProSAPIP1
ANO4	RPH3A
ARHGAP26	SALL4
ARIH2	SEC22C
C16orf45	SHC3
C1QL1	SNPH
CADPS	STRA6
CALM1	SYN2
CCDC51	THUMPD3
CCDC72	TMEM20
CEND1	
EIF1B	
EIF4E3	
FAM30A	
FAM5B	
FHOD3	
FXC1	
GNG8	
HAPLN4	
IGF1R	
JAKMIP1	
KCNK7	
KCTD1	
KIAA0125	
LGI1	
LOC100126784	
LOC283392	
MAPKAPK3	

ENO1	SLC8A1	MDGA1
FAM125B	SOX7	MGC14436
FAM40A	SPAG4	NCAM2
FAM49A	STC2	NGB
FAM73A	TFAP2C	OPRM1
FGF11	TMEM176A	OSBPL6
GABRD	TMEM45A	PGP
GTDC1	TPRG1L	PLXNB1
HPCAL4	UBE2J2	PNMT

López-Jimenez et al. Mol Endocrinol. 2010 Dec;24(12):2382-91

List e: overexpressed genes in SDHx + VHL tumors vs RET/INF1

A2M	AMOTL2	BM668321	CCL18	COL5A2	DIO2
AA837799	AMZ1	BM680083	CCRL1	COL6A3	DKFZp586C0721
ABP1	ANGPT2	BM999343	CD109	COLEC12	DKFZp781M2440
ACP5	ANGPTL4	BNIP3	CD248	COP1	DMP1
ACTG2	ANK3	BTNL2	CD300A	COTL1	DOK6
ACTL8	ANKRD15	BU618641	CD34	COX4I2	DSCR1L1
ADAMDEC1	ANTXR1	BX427588	CD36	CPA3	ECM2
ADAMTS4	ANXA1	C10orf10	CD678339	CPM	ECSM2
ADAMTS5	AOC3	C10orf107	CD86	CPXM2	EDIL3
ADM	APCDD1	C10orf63	CD93	CR593388	EDNRA
ADORA2A	APOBEC2	C15orf5	CDH12	CR603437	EDNRB
ADRA1B	APOLD1	C16orf30	CDH13	CR626252	EFNA1
AF075027	AQP1	C18orf4	CDH7	CR749547	EFNB3
AGC1	AREG	C1orf24	CFH	CRB1	EGFL7
AHR	ARG2	C1QTNF2	CFHR1	CRTAC1	EGLN3
AI190733	ARHGAP15	C1QTNF5	CFHR3	CRYAB	ELTD1
AI344752	ARHGEF10	C1R	CFI	CSPG2	EMCN
AI793066	ARID5B	C20orf100	CGNL1	CSRP2	EMILIN2
AK001808	ARMC4	C20orf74	CHSY1	CTGF	EMP1
AK001903	ASPA	C20orf82	CLCNKA	CTHRC1	EMP1
AK022044	ASPHD2	C21orf7	CLDN5	CTNNB1	ENST00000176186
AK022110	ASPN	C22orf35	CLEC14A	CTSG	ENST00000309878
AK022150	ATP10A	C5orf23	CLEC2B	CTSK	ENST00000314238
AK023660	ATP1A2	C8orf13	CLEC3B	CUGBP2	ENST00000327299
AK026647	AV707343	C8orf4	CMKOR1	CX3CL1	ENST00000332814
AK026984	AW138903	C9orf135	CNGA3	CXCL12	ENST00000334994
AK057652	AW268902	C9orf28	CNN1	CXCR4	ENST00000341700
AK074614	AW467174	C9orf58	CNTNAP4	CXorf36	ENST00000354417
AK094995	AX721193	C9orf61	COL10A1	CYBRD1	ENST00000360669
AK123610	AY358804	CA2	COL12A1	CYP1B1	ENST00000366930

AK124698	BATF	CABP1	COL13A1	CYR61	ENST00000369397
AK125361	BC030100	CALCRL	COL14A1	CYR61	ENST00000370548
AK3L1	BC033829	CARD6	COL16A1	DACH2	ENST00000372263
AK3L2	BC034319	CASP1	COL18A1	DACT1	ENST00000373093
AKAP12	BC062780	CASP4	COL1A1	DB379047	ENST00000375280
AL036373	BC104421	CASP9	COL1A2	DB381305	ENST00000375377
AL133118	BCAT1	CAV1	COL20A1 0	DDIT4L	ENST00000377918
AL355687	BCL11A	CB123670	COL21A1	DEPDC6	ENST00000380438
AL359062	BDKRB2	CB305813	COL3A1	DGCR5	ENST00000382216
AL832717	BF213738	CCDC102B	COL4A1	DGKB	EPAS1
AL833655	BM129308	CCDC3	COL4A2	DHRS2	EPHA3

López-Jimenez et al. Mol Endocrinol. 2010 Dec;24(12):2382-91

List f: overexpressed genes in *VHL* versus *SDHB* tumors

AA292106	ASAM	C1orf151	CDH22	DNALI1	ENST00000383097	GABRG2
ABCC9	ATP10A	C1orf162	CDH23	DOCK8	EPB41L4B	GADD45G
ABP1	ATPIF1	C1orf59	CFH	DPF3	EPHX2	GALC
ACOT11	AU158345	C1QC	CGI-38	DPT	ETS2	GALNT8
ACTA1	AW467174	C1QTNF2	CGNL1	DPYS	EV12A	GFRA3
ACTC	AW901755	C20orf195	CHRM3	DRD1IP	EYA1	GLI3
ACTL8	B3GALT4	C20orf26	CKB	DUSP23	F12	GLIPR1
ADRA1B	B3GALT4	C20orf45	CLCNKA	DYNLRB2	F13A1	GLIPR1L2
ADSSL1	BAIAP3	C21orf34	CLDND2	ECEL1	FABP3	GPC3
AGRP	BAMBI	C3	CNGA3	EDARADD	FABP6	GPR103
AI190733	BC014971	C3AR1	CNTN3	EFHC2	FAM43B	GPR30
AI793066	BC030813	C4B	CNTN6	EFHD2	FAM50B	GPR65
AIF1	BC038245	C7orf29	COLEC11	EFS	FAM77C	GPR68
AIM2	BC047230	C8orf13	CPLX3	EGFL7	FAM79A	GPX3
AK022110	BC070363	C9orf135	CPVL	EGLN3	FAM80A	GRID2
AK026078	BC089451	C9orf24	CR595668	ELAVL4	FANK1	GRIN2C
AK026984	BCAT1	C9orf28	CR595983	ELAVL4	FCGBP	GSTM3
AK054939	BCL3	C9orf9	CR597270	EML1	FCGR3B	GTDC1
AK056401	BDKRB1	CABP1	CR607634	ENO1	FHL2	HAVCR2
AK074776	BDKRB2	CAMK1D	CR624517	ENST00000259219	FLJ13391	HCA112
AK091335	BE004814	CAMK1G	CRTAC1	ENST00000295549	FLJ20273	HCLS1
AK092535	BE798911	CAMK2B	CRYBA2	ENST00000307662	FLJ20701	HEPH
AK093202	BE926212	CAMK2N1	CRYBB1	ENST00000311208	FLJ22662	HIST1H2BK
AK096498	BG675674	CARD6	CTSG	ENST00000314088	FLJ30428	HK2
AK124281	BI828537	CASP1	CTSS	ENST00000318291	FLJ31485	HLA-DMA
AK125302	BNIP3	CASP4	CTSZ	ENST00000322032	FLJ33790	HLA-DMB
AK128814	BSPRY	CASP5	CX3CR1	ENST00000327299	FLJ39822	HLA-DOA
AK3L1	BX090709	CASP9	CYB5A	ENST00000328043	FLJ43390	HLA-DPA1
AK3L2	BX100717	CB305813	CYBB	ENST00000330861	FLJ46266	HLA-DPB1

AL834342	BX111592	CBLN4	CYGB	ENST00000332814	FMN1	HLA-DPB2
ALOX5AP	BX377179	CCDC8	DA237404	ENST00000354417	FMO2	HLA-DQB1
AMID	BX647543	CCNJL	DB097529	ENST00000355710	FMO3	HLA-DQB2
ANKRD37	C10orf10	CCR1	DB379047	ENST00000366569	FOLR2	HLA-DRB3
APLN	C10orf11	CD14	DCN	ENST00000368577	FPR1	HNMT
APOBEC2	C10orf59	CD242823	DDIT4L	ENST00000369697	FRAS1	HOP
APOL6	C10orf63	CD28	DDO	ENST00000371497	FSTL5	HPCAL4
AQP5	C10orf78	CD300A	DENND2D	ENST00000380064	FUCA1	HRASLS
ARHGAP22	C10orf79	CD53	DERL3	ENST00000381827	FYB	HSD11B1
ARHGAP4	C11orf75	CD678339	DMD	ENST00000382416	FZD10	HSPB7
ARMC4	C18orf4	CD9	DNAJA4	ENST00000382591	GABRD	HTATIP2

López-Jimenez et al. Mol Endocrinol. 2010 Dec;24(12):2382-91

List f: overexpressed genes in *VHL* versus *SDHB* tumors (cont)

HTR4	LOC124976	MAN1C1	NMB	PNMA5	RP1-93H18	SNTG1	THC2337832	TRAF3IP3
HTR5A	LOC146439	MAP2K3	NOS2A	POF1B	RPRM	SORCS3	THC2341118	TRIB2
IGFBP2	LOC198437	MAPK13	NOTCH2	PPFIA4	RUNX1	SOX7	THC2341505	TSGA2
IGHG1	LOC283143	MCHR1	NPAL2	PPIC	S100A13	SOX9	THC2344886	TSPAN2
IGKC	LOC388002	MEF2B	NR2F1	PQLC3	S100A6	SP5	THC2364841	TUBA1
IGSF10	LOC388335	MEIS3P1	NTRK1	PRKCZ	SAMSN1	SPAG4	THC2371963	TUBB2B
IL10RA	LOC389033	MET	NY-REN-7	PSCD4	SCAP1	SPOCK2	THC2375493	UBXD3
IL13RA2	LOC390595	MGC33846	OPCML	PSD3	SCIN	SPON1	THC2404004	VAMP8
IQCA	LOC400890	MGC4655	P4HA2	PTGIS	SDHB	SREBF1	THC2408277	VCAM1
ITGB2	LOC401152	MIF	PARVA	PTGS1	SEC61G	SSPN	THC2412859	VDR
JAKMIP1	LOC401778	MRC1L1	PCDH11Y	PTHLH	SECTM1	SSX2IP	THC2437069	VNN2
KA21	LOC402689	MS4A4A	PCDH9	PTK6	SEMA3C	ST6GAL1	THC2437757	WDFY4
KBTBD11	LOC440607	MS4A6A	PDE6H	PTN	SERPINA5	ST6GALNAC5	THC2437822	WDR66
KCNIP2	LOC497190	MT1E	PDGFC	PTPLAD2	SERPINB9	STC2	THC2439128	WFDC1
KCNJ5	LOC643355	MT1F	PDLIM2	PTPN20B	SFTPC	STK32C	THC2440787	WNT10A
KCNK12	LOC645904	MT1G	PDZK1	QDPR	SH2D2A	STMN1	TLR2	WNT3
KCNMB2	LOC653316	MT1H	PEBP4	RARRES2	SHC3	SULT4A1	TLR4	WNT4
KCNQ1	LOC653857	MT1X	PGF	RASEF	SLC16A12	SVEP1	TLR7	ZBTB1
KIAA0644	LOC664727	MT3	PHYHIP	RBP1	SLC16A3	SYT13	TMEM107	ZNF185
KIAA1324	LOXL1	MTP18	PIGT	REPS2	SLC24A3	TCERG1L	TMEM2	ZNF480
KL	LR8	MUC15	PLA2G4A	RERG	SLC2A1	TCF1	TMEM45A	ZSWIM5
KRT19	LRRC25	MYCBP	PLB1	RET	SLC2A5	TDO2	TMEM45B	
LAMB3	LRRC61	MYH6	PLCH2	RGN	SLC44A3	TEKT2	TMEM45B	
LAPTM5	LRRK2	MYLK	PLCXD3	RGS16	SLC6A2	TFAP2C	TNFRSF11B	
LAT2	LY86	NAG6	PLEK2	RGS22	SLC8A1	TFPI	TNFSF10	
LAYN	M31157	NDRG1	PLTP	RHOBTB3	SLCO2B1	THC2249196	TNT	
LEPREL1	MAF	NEFH	PLXNA4A	RNASE6	SMOC2	THC2249938	TOX	

Genes in lists a-f that overlap with upregulated genes found in both ccRCC-Oncomine multi-arrays (at a cutoff of 1 study) and pHx-HNPGLs are shadowed. Genes in lists c and f that overlap with upregulated genes found in ccRCC-Oncomine multi-arrays (at a cutoff of 1 study) but not pHx-HNPGLs are in bold.

Supplementary Table S4. List of genes differentially expressed in pHx-HNPGLs versus non-pHx-HNPGL.

Gene Symbol	p-value	Fold-Change	Gene Symbol	p-value	Fold-Change
DLK1	5.51E-13	-1537.21	HOMER3	1.18E-03	2.20
INSM1	4.49E-08	-203.92	SEPX1	9.34E-05	2.21
SLC35D3	1.87E-05	-167.77	TRPT1	1.67E-06	2.21
SLC18A2	1.57E-06	-132.92	ZMIZ2	2.00E-06	2.22
NBLA00301	1.76E-09	-125.06	B4GALT5	1.41E-04	2.22
STMN2	1.69E-10	-111.43		6.67E-04	2.22
NBLA00301	1.69E-09	-111.23	SIPAIL1	3.44E-04	2.23
CHRNA3	6.80E-07	-105.36	COQ9	6.03E-06	2.23
GNAS	1.70E-06	-98.88	WDR60	2.59E-06	2.23
STMN2	2.06E-09	-89.77	EHD1	5.64E-04	2.23
SYT1	3.01E-07	-77.46	PDCD6 /// RGS8	3.73E-04	2.24
SYT4	4.96E-08	-73.92	MED14	5.70E-04	2.25
CHGB	1.10E-04	-70.39	BTBD2	6.96E-04	2.25
DNER	3.73E-06	-68.77		2.68E-05	2.25
C22orf35	8.15E-08	-59.68	GTSE1	7.49E-04	2.25
MAB21L2	1.04E-07	-59.34		5.12E-04	2.25
C7orf16	5.46E-04	-53.33	HINT1	1.05E-04	2.25
LOC200169	6.27E-09	-53.06	GTF2H2	1.31E-04	2.26
CNTN1	4.89E-05	-49.07	SRGAP2P1	1.04E-04	2.27
MAB21L1	3.08E-05	-45.20		7.73E-05	2.27
CLGN	1.74E-05	-43.69	SFXN2	3.32E-04	2.28
---	8.11E-06	-42.60	srp54	1.52E-04	2.28
CNTN1	3.34E-05	-41.62	ATF7IP	5.78E-05	2.28
GPR158	2.85E-05	-41.42	FAM111A	7.81E-04	2.28
DLX1	8.32E-06	-39.88	LMF1	5.78E-04	2.28
BEX1	1.10E-05	-39.21	SRGAP2	2.82E-05	2.28
SCG5	8.67E-06	-39.05	SDK1	1.94E-05	2.29
GPR83	1.77E-04	-38.81		2.03E-05	2.29
SNAP25	5.28E-07	-35.31	FOXN3	2.77E-04	2.29
SLC18A2	1.35E-04	-34.73	TNFSF4	3.14E-04	2.29
INA	5.56E-08	-33.42		1.53E-04	2.30
RIMS3	3.61E-07	-31.57	MKI67	1.00E-04	2.30
DDC	8.93E-04	-29.99		8.41E-04	2.30
PHOX2A	4.08E-05	-29.79	PAPD4	1.18E-03	2.30
SCG3	9.94E-06	-28.96	ATF7IP	9.47E-06	2.31
PHOX2B	3.87E-05	-28.86	fam195a	3.14E-05	2.31
CHRNA3	1.06E-05	-28.21	GPD1	1.95E-06	2.31
L1CAM	1.67E-04	-27.79	ANKHD1	4.16E-04	2.32

MEG3	6.92E-06	-27.31	GSTK1	6.65E-06	2.32
RUFY3	7.96E-06	-26.56	HN1L	8.88E-04	2.32
RALYL	6.53E-06	-25.70		7.30E-04	2.33
KCNQ2	1.62E-04	-24.97	C5orf15	5.81E-07	2.33
PRPH	2.32E-06	-24.52		2.67E-10	2.33
ISL1	1.29E-04	-23.66	SSH2	5.57E-05	2.33
MEG3	3.41E-05	-23.60	OGT	1.01E-03	2.34
NDRG4	3.20E-06	-23.39	MGAT4B	3.25E-04	2.34
NBLA00301	1.99E-05	-22.77	LAMB1	1.18E-03	2.35
ELAVL3	6.68E-06	-21.58		6.66E-04	2.36
LOC202451	1.51E-06	-21.11		5.18E-04	2.36
CPLX2	9.67E-07	-19.95	DECR2	1.80E-04	2.37
SYT1	3.34E-04	-19.65	HELLS	4.77E-05	2.37
NCAM1	1.82E-04	-19.40	MGAT4B	9.16E-06	2.37
GRIA2	1.41E-04	-19.35	SLC44A1	1.53E-05	2.38
ELAVL2	1.51E-04	-19.35		8.89E-04	2.38
RIMBP2	2.82E-05	-19.19	GRINA	9.72E-08	2.38
KIF5C	1.15E-05	-19.17	GALNT10	2.41E-04	2.38
DNAJC6	2.79E-05	-18.66	SOX12	4.79E-06	2.39
PTPRN	4.43E-06	-18.52	NPM1	1.37E-05	2.41
DYNC1I1	7.92E-08	-17.81	TK1	3.59E-06	2.41
CDH19	6.17E-04	-17.58	IMMP2L	2.87E-04	2.41
CHRNA3	8.55E-06	-17.11	SIL1	1.55E-05	2.42
	1.12E-04	-16.79		2.66E-04	2.43
KIAA1576	2.90E-04	-16.55	NFIC	2.40E-05	2.43
SCG2	8.78E-06	-16.50	ROR1	4.07E-04	2.43
SNAP91	1.32E-05	-16.21	FLJ10357	1.13E-03	2.44
SEZ6L	1.98E-04	-15.98		6.92E-04	2.44
	1.17E-04	-15.68	DNAJC4	7.70E-05	2.44
LOC728392 /// NLRP1	5.07E-06	-15.52		4.84E-04	2.44
PTPRN2	4.35E-06	-15.51	MYL4	1.01E-03	2.44
SV2B	4.69E-04	-14.61	SF3A2	1.02E-03	2.45
UCHL1	2.98E-05	-14.52	OR7E37P	6.78E-04	2.45
DDC	7.83E-04	-14.33		3.68E-06	2.45
NRXN1	5.57E-04	-14.28		2.75E-04	2.46
KIAA1244	1.04E-05	-14.16		4.47E-05	2.47
PPP2R2C	8.17E-05	-14.15	AP1S2	2.36E-04	2.48
TCEAL7	1.46E-04	-14.06	PHTF2	2.02E-04	2.48
ZNF483	8.19E-05	-13.94		7.42E-04	2.48
PEG10	1.14E-03	-13.59	STATH	7.62E-05	2.48
LONRF2	1.85E-04	-13.19	BTBD7	2.39E-04	2.50
FLJ25967	2.16E-05	-12.94	RAB17	6.25E-04	2.50
NEGR1	8.59E-04	-12.91	CEP55	1.94E-05	2.50
SEZ6L2	1.94E-04	-12.88	ALDH7A1	1.10E-03	2.50
MEG3	5.75E-05	-12.75		4.66E-04	2.51
	4.78E-06	-12.71	MAN2A1	1.48E-04	2.51
SGIP1	1.08E-05	-12.70	BCKDK	6.03E-06	2.52
DLX2	4.24E-04	-12.56		6.12E-04	2.52
	5.12E-04	-12.27	FUCA2	2.13E-04	2.53
---	5.40E-05	-12.23	GLS	1.64E-04	2.54
GPRASP1	1.72E-05	-12.22	C11orf9	5.52E-05	2.54
	3.22E-04	-12.20	CILP	1.74E-04	2.55

	3.52E-04	-11.91	POSTN	1.17E-03	2.55
DPP6	9.12E-04	-11.89	GRTP1	2.56E-05	2.56
CDH18	4.82E-04	-11.87	Adrm1	1.70E-04	2.56
STMN4	4.21E-04	-11.76	KIAA1217	1.04E-04	2.56
QPCT	1.06E-04	-11.71	SLC37A3	6.36E-06	2.57
IL20RA	3.06E-04	-11.64		7.88E-04	2.57
C19orf30	4.06E-05	-11.40	LOC100216546	1.50E-04	2.57
NCAM1	6.07E-04	-11.36	MITF	6.49E-06	2.57
KIF1A	2.23E-05	-11.32	DLG1	4.12E-07	2.57
ADCYAP1R1	1.08E-04	-11.26		6.87E-04	2.58
SNRPN /// SNURF	5.41E-06	-11.19	SLC37A3	2.25E-05	2.59
HMP19	4.14E-04	-10.86	PPP1R14B	6.20E-04	2.59
JPH4	4.54E-05	-10.73	ACTN4	1.02E-03	2.60
SCN3B	5.52E-04	-10.69	LOC153684	3.30E-04	2.60
	4.56E-04	-10.51	NSUN5	6.96E-05	2.61
C20orf74	4.40E-05	-10.41	SRGAP1	4.72E-05	2.61
FLJ42562	1.04E-04	-10.41		8.42E-04	2.62
	3.58E-04	-10.41	USP2	4.91E-05	2.62
FLJ37228	9.64E-04	-10.14	PTH2R	2.89E-04	2.62
EFNB3	3.20E-05	-10.08	PDIA5	2.27E-04	2.62
RAMP1	4.26E-04	-10.07	SNTB2	6.36E-04	2.62
GCH1	2.01E-06	-9.97	CYP3A5	3.01E-05	2.63
ADRB1	8.85E-04	-9.95	ACY1	8.63E-04	2.63
PKIA	4.25E-04	-9.92	C11orf93	4.98E-05	2.63
ABCB1 /// ABCB4	1.13E-03	-9.89	fam195a	3.62E-05	2.63
	1.59E-04	-9.86	SHMT1	2.72E-06	2.64
C14orf132	2.84E-04	-9.77	HIPK2	6.09E-04	2.64
SCN2A2	4.28E-04	-9.74	CACNA1A	1.38E-04	2.64
EPHA3	4.89E-05	-9.72	ABI3BP	1.93E-05	2.65
EEF1A2	6.92E-04	-9.59		4.67E-04	2.65
LOC728215 /// LOC731895	3.52E-05	-9.54	IDH2	7.00E-05	2.66
	3.34E-04	-9.46		8.13E-04	2.66
MYT1L	1.98E-04	-9.44	SAPS3	8.67E-05	2.66
ST18	4.67E-04	-9.25	DSG2	2.89E-06	2.66
NELL2	1.10E-03	-9.21	JPH2	3.29E-04	2.66
PTGER3	6.77E-04	-8.80		7.36E-04	2.67
C6orf189	7.47E-04	-8.57	TPK1	6.91E-04	2.68
SEZ6L2	5.89E-04	-8.51	GLS	1.06E-05	2.68
KIF5C	6.23E-04	-8.49	AGXT2L2	2.32E-05	2.68
PNMA2	6.27E-04	-8.45	FAM20A	2.69E-04	2.69
CAMK4	8.38E-04	-8.40	CTNND1	2.97E-04	2.69
TMOD1	6.91E-04	-8.33	RRBP1	3.93E-04	2.70
	9.70E-04	-8.19	ENTPD5	7.70E-07	2.70
COL22A1	9.12E-04	-8.17	papd4	2.05E-04	2.71
DNAJC12	6.72E-07	-8.04	AIFM1	3.00E-06	2.71
KIF5A	2.99E-04	-8.03		8.87E-04	2.71
NMNAT2	1.57E-05	-7.96	MKI67	2.17E-05	2.71
APLP1	8.65E-04	-7.90	ST6GAL2	1.67E-05	2.72
BRUNOL6	2.61E-04	-7.85	SEMA5B	3.32E-04	2.73
NEBL	3.05E-05	-7.81	C1QTNF3	6.18E-06	2.73
DPP6	9.12E-04	-7.77		8.48E-05	2.73

---	6.06E-06	-7.69	LOC441242	3.39E-05	2.73
SORCS1	4.95E-04	-7.64	EGFR	1.12E-04	2.73
OLFM1	9.26E-04	-7.63		5.61E-04	2.74
SNAP25	3.28E-04	-7.50	CDC20	4.77E-05	2.74
	1.77E-06	-7.29	MGC35361	6.71E-06	2.77
HDAC9	5.49E-05	-7.26		5.79E-04	2.77
SNRPN /// SNURF	4.74E-05	-7.25	ZNF117	2.84E-04	2.77
CAB39L	1.14E-03	-7.23		4.93E-04	2.78
MEG3	4.62E-04	-7.20	LOC644242	1.11E-03	2.79
RAP1GAP2	6.34E-05	-7.10	Cttnbp2	3.26E-05	2.79
RUNDC3A	1.16E-03	-7.06	TSPAN33	2.01E-04	2.80
NEBL	3.12E-05	-6.99	NSUN5P2	3.33E-04	2.80
VGCNL1	5.63E-04	-6.98	SHCBP1	5.53E-06	2.82
PRR6	1.09E-04	-6.95	LAMA1	1.17E-03	2.82
PKIA	1.02E-03	-6.94	CENPT	7.73E-05	2.83
C9orf125	4.09E-05	-6.87	FLJ10357	6.89E-04	2.83
SYP	2.75E-04	-6.81	MAF	6.32E-04	2.83
LRCH2	8.26E-07	-6.72	NSUN5P2	1.04E-04	2.85
KIAA0888	6.02E-04	-6.67	BMP1	8.36E-04	2.85
LOC284214	8.18E-04	-6.56	SLC22A5	1.13E-03	2.85
CAMTA1	7.71E-05	-6.46	DNAJC4	2.87E-05	2.86
FAM155A	2.01E-06	-6.44	FGFR4	8.11E-05	2.86
JAKMIP1	1.01E-03	-6.41	SLC7A8	1.13E-03	2.86
CPEB1	4.98E-04	-6.39	C6orf108	1.09E-06	2.87
ASPHD2	1.26E-04	-6.37	FAM83H	1.57E-06	2.87
B3GNT7	4.94E-04	-6.34	MITF	1.87E-05	2.88
DNM3	8.34E-04	-6.33	NSUN5P1	2.01E-04	2.88
RUFY3	9.79E-04	-6.32	A2BP1	3.04E-04	2.88
LOC387856	1.05E-03	-6.32		2.34E-04	2.88
	1.67E-05	-6.30	HOXA10	4.68E-05	2.91
SEZ6L2	5.29E-04	-6.29		9.00E-04	2.91
STXBP1	1.04E-05	-6.29	PDE4DIP	1.04E-04	2.91
MAB21L2	1.09E-03	-6.28	CLCA2	3.69E-04	2.92
EMCN	9.51E-04	-6.24	C1GALT1	5.78E-04	2.92
CDK5R2	5.38E-04	-6.24	TNIP1	7.96E-05	2.92
PRR6	7.23E-05	-6.24	EFNA4	1.83E-04	2.93
BRUNOL4	4.39E-04	-6.20	Pdzd2	7.12E-05	2.93
ANK2	4.68E-06	-6.19	NSUN5P1	3.52E-04	2.93
GAS7	6.75E-05	-6.19		1.17E-03	2.94
	1.05E-04	-6.18	HOXA7	3.65E-05	2.94
FAM89A	3.80E-07	-6.12	KIAA1217	4.07E-04	2.94
PAK3	5.13E-05	-6.10	LMF1	1.39E-04	2.94
RAB27A	3.68E-06	-6.02	GINS2	1.15E-03	2.94
CAMTA1	9.29E-04	-6.00		8.45E-04	2.94
PPP2R2B	1.69E-04	-5.98		8.77E-04	2.94
	7.86E-04	-5.97	SRGAP2	1.78E-04	2.95
GNG4	3.80E-04	-5.92		1.90E-05	2.95
ATCAY	8.01E-05	-5.90		6.35E-04	2.96
MYT1	5.54E-04	-5.86	CALR	4.08E-04	2.96
	5.89E-04	-5.85	ZNF608	1.28E-11	2.98
CHD5	3.31E-04	-5.85	PAPD4	3.16E-04	2.98
KIAA1107	4.93E-04	-5.81	GRAMD3	1.90E-04	2.98

ADORA2A /// CYTSA	2.24E-04	-5.79	IMMP2L	2.16E-04	2.98
SYT11	1.76E-04	-5.78	TECR	4.69E-04	2.99
C9orf125	2.28E-04	-5.74	TAF7L	1.37E-04	3.00
TRIM2	1.32E-04	-5.69	SGCD	9.30E-04	3.01
PTPRN2	5.25E-04	-5.67	NSUN5	4.88E-05	3.01
FLJ25076	4.23E-04	-5.62	RRBP1	8.42E-04	3.01
MLLT11	4.46E-05	-5.60	SC65	1.04E-03	3.01
GRIK2	2.54E-04	-5.57		8.25E-05	3.03
RUFY3	4.35E-04	-5.54	MOSC2	9.81E-04	3.04
GDAP1	2.14E-04	-5.51	PADI2	2.40E-04	3.04
UPK1B /// RGS5	9.00E-04	-5.47	PCK2	2.80E-05	3.04
TAGLN3	9.66E-04	-5.42	ADORA2B	5.25E-05	3.06
TMEM22	1.21E-04	-5.40	VAV3	7.45E-04	3.06
SPG3A	5.60E-05	-5.36		4.27E-04	3.07
PCDH17	6.44E-04	-5.33	MST1P9	3.09E-06	3.09
ST3GAL6	1.41E-04	-5.26	DLG1	1.17E-04	3.10
CYYR1	5.60E-04	-5.26	LOC284757	1.10E-03	3.10
SCRN1	2.71E-04	-5.26	CCDC8	8.57E-05	3.11
GAS7	4.21E-04	-5.23	ofd1	1.27E-04	3.11
NRG3	7.18E-04	-5.21		1.03E-03	3.11
SYNM	2.75E-04	-5.19	skap2	3.78E-05	3.12
SYBU	9.83E-04	-5.12	Atpif1	1.96E-04	3.13
PHYHIP	3.30E-05	-5.12	SMTNL2	5.24E-06	3.14
KIAA1946	3.46E-04	-5.11	PDIA4	1.13E-06	3.15
CRMP1	3.15E-04	-5.10	ROR1	5.88E-06	3.15
PCBP3	5.66E-05	-4.91	SLC22A18	4.16E-05	3.16
	6.20E-07	-4.83	HOXA1	1.29E-07	3.17
RSNL2	3.83E-04	-4.81	CENPK	1.11E-03	3.17
TRIM2	7.18E-05	-4.78		5.35E-04	3.19
NDN	5.13E-04	-4.78	PRKD1	5.83E-04	3.22
SYN1	3.62E-04	-4.69	SULT1C2	8.19E-06	3.22
SYNPO2	6.56E-04	-4.66	FLJ45482	9.00E-05	3.23
CPE	5.15E-05	-4.66	PLK2	3.35E-04	3.23
RUNDC3A	1.36E-05	-4.63	MGC23985	2.62E-04	3.23
EPB41L3	1.01E-04	-4.63	MACROD1	1.87E-04	3.24
KLF4	1.00E-03	-4.62	LMO4	1.48E-04	3.24
ADRBK2	9.11E-04	-4.62	LOC653562	1.43E-04	3.25
NAPB	2.06E-04	-4.61		8.63E-04	3.25
LOC133308	1.31E-06	-4.59	ALDH7A1	3.80E-05	3.26
HDGFRP3	1.63E-06	-4.57		1.19E-03	3.28
CELSR3	6.81E-04	-4.56	CENPF	1.14E-03	3.30
PCDH17	9.22E-04	-4.54	DKFZp761P0423	1.17E-03	3.32
IRS2	4.30E-05	-4.53	AURKA	1.01E-05	3.32
MANSC1	1.40E-04	-4.47	C5orf13	5.68E-05	3.34
HDGFRP3	6.76E-05	-4.37	PDGFC	6.97E-07	3.36
SLC8A2	6.45E-04	-4.37		6.45E-05	3.36
ASPHD2	1.12E-03	-4.35	LAMC3	7.84E-04	3.38
GOLM1	1.41E-05	-4.35	FREM2	2.51E-08	3.39
KLF4	8.38E-04	-4.32	TRIM6	9.62E-04	3.39
EPB41L3	6.14E-04	-4.31	FUS	9.19E-06	3.40
SPOCK2	4.46E-04	-4.30	OPN3	2.31E-05	3.41
CERK	1.92E-04	-4.28	DDAH1	4.20E-04	3.41

PTGER2	2.93E-04	-4.27	BMP1	5.73E-04	3.42
CELSR3	1.08E-03	-4.23	ALDH1L1	2.89E-05	3.43
NCOA7	5.91E-06	-4.23	TST	4.14E-04	3.44
LEF1	7.17E-04	-4.22	NID2	3.94E-04	3.46
IRS2	4.03E-05	-4.21	KLHDC8A	2.30E-04	3.47
	6.62E-04	-4.20	ACSF2	8.27E-04	3.50
DUSP26	1.17E-05	-4.06	TOB2	2.05E-04	3.50
RGS5	3.61E-04	-4.06	PPP1R1A	1.11E-03	3.51
ADCY1	1.15E-03	-4.06	GLS	2.67E-04	3.52
TRIM2	5.21E-05	-4.06		8.05E-04	3.53
LOC285550	1.06E-03	-4.03	DCI	1.26E-05	3.54
06-Sep	1.16E-04	-4.02	TPX2	4.09E-04	3.56
DNAJC12	6.50E-04	-3.99	FABP3	2.00E-07	3.56
INSM1	8.67E-04	-3.98	GALNT10	1.62E-04	3.59
C11orf70	9.34E-04	-3.97	AKR1C2	7.91E-04	3.59
LRRC49	4.35E-05	-3.97	CCDC8	4.52E-06	3.62
HDGFRP3	2.91E-04	-3.97	ALDH4A1	1.09E-05	3.62
03-Sep	7.58E-05	-3.94	ABCC3	1.51E-07	3.64
PPFIA2	9.39E-05	-3.92	GPC6	7.87E-06	3.64
RPH3AL	8.17E-04	-3.90		4.97E-04	3.65
MREG	1.12E-03	-3.81	SHMT1	3.84E-06	3.67
ETS2	8.84E-04	-3.73		4.86E-04	3.67
C9orf5	5.81E-04	-3.69	METTL7B	3.57E-04	3.69
TMEM204	7.64E-04	-3.67	---	1.78E-04	3.70
SGCE	2.66E-04	-3.65	NXT2	1.14E-04	3.72
EPAS1	5.51E-05	-3.63	OPLAH	3.82E-08	3.73
CACNA1C	4.01E-04	-3.62	KIF20A	1.40E-04	3.73
HAND2	3.71E-04	-3.61	RDH13	2.39E-04	3.73
KCNQ2	3.98E-04	-3.60	ZG16B	1.23E-04	3.77
CCND2	8.51E-04	-3.56	APOBEC3B	1.32E-05	3.77
C13orf21	1.69E-04	-3.51	EFCBP1	3.74E-04	3.78
ACOT7	9.29E-04	-3.50		1.01E-03	3.78
AKAP12	1.16E-03	-3.46	PTPRD	5.89E-05	3.83
	4.66E-04	-3.45	PDGFC	1.26E-04	3.84
AKT3	1.04E-05	-3.44	ADORA1	1.09E-03	3.84
UNC13A	1.87E-04	-3.43	ID2 /// ID2B	7.45E-04	3.85
CD55	5.44E-04	-3.36		8.55E-04	3.85
RGS5	1.11E-03	-3.34		7.86E-07	3.86
HDGFRP3	2.63E-06	-3.33		6.62E-04	3.86
C12orf34	3.20E-04	-3.30	LIFR	1.05E-03	3.88
CAMK2N2	1.14E-03	-3.29	NLN	2.83E-06	3.88
SNRPN	6.03E-04	-3.27	PPP1R3B	7.68E-05	3.89
WRB	8.09E-04	-3.26	TMEM132A	1.81E-04	3.90
TM2D1	5.75E-04	-3.25	SEC14L4	1.87E-05	3.90
GABARAPL1 /// GABARAPL3	1.06E-05	-3.23	SPAG4	6.82E-04	3.92
FGF2	6.42E-05	-3.20	COL5A3	1.04E-03	3.93
ICAIL	6.63E-04	-3.19	GPC6	3.73E-04	3.93
VWA5A	4.80E-04	-3.03	QPRT	8.05E-05	3.95
GNAO1	1.87E-04	-3.03		2.23E-04	3.96
BTG3	1.18E-04	-3.02	GPRC5C	2.20E-06	3.97
EPB41L3	9.21E-04	-3.02		4.31E-04	3.98

FXVD5	5.78E-05	-3.00		2.91E-04	3.98
NGRN	7.42E-04	-2.98	MCC	3.44E-04	3.98
TM6SF1	2.17E-05	-2.97	GRB14	5.18E-05	4.01
SCAMP5	1.14E-03	-2.95		1.20E-04	4.02
	4.72E-04	-2.92	HMMR	2.57E-04	4.03
NGRN	2.35E-04	-2.90	C6orf108	3.40E-04	4.08
RALGDS	8.01E-06	-2.90		3.35E-04	4.11
MAPK8IP2	6.67E-04	-2.89	HSD11B2	9.05E-04	4.12
GABARAPL1	1.36E-04	-2.88	RDH13	1.67E-04	4.17
CPE	7.08E-05	-2.88	HSD3B7	8.52E-07	4.22
CD44	4.16E-04	-2.87		5.27E-05	4.24
RALGDS	3.06E-05	-2.87	TRIP6	2.32E-04	4.24
KIAA0319	3.52E-04	-2.85	HOXA4	6.44E-06	4.24
NECAP1	5.39E-04	-2.84	LOC440331	3.46E-04	4.25
EIF1	1.22E-04	-2.82	GPC6	2.43E-04	4.27
TM6SF1	7.63E-04	-2.82	CXXC5	3.40E-05	4.28
	1.66E-05	-2.81	ABCC6	8.71E-08	4.29
CDC42EP3	3.87E-04	-2.78	ST8SIA5	5.97E-04	4.31
PSIP1	9.23E-04	-2.78	FABP3	1.64E-08	4.31
FXVD5	6.55E-05	-2.76		4.28E-04	4.32
WDR19	5.14E-04	-2.75	SLC6A8	1.03E-03	4.33
CD55	2.77E-04	-2.73	A2BP1	2.13E-04	4.35
NPDC1	6.12E-04	-2.65		5.29E-04	4.40
RGS5	2.31E-04	-2.63	SLC6A8	5.72E-04	4.42
IDS	1.96E-04	-2.62	SGCG	4.37E-04	4.42
BTG3	1.84E-04	-2.60	CDSN	7.88E-04	4.45
FAM60A	3.53E-04	-2.59	IGFBP5	3.81E-04	4.46
CHMP5	2.92E-05	-2.54	AKR1C1	1.19E-04	4.47
LOC283174	1.03E-04	-2.53	ASPM	9.58E-04	4.53
BRWD1	1.69E-04	-2.52	SLC6A8	4.46E-05	4.57
GNAS	4.91E-04	-2.52	ROR1	2.85E-05	4.57
ZNF10	4.49E-04	-2.52	EXPH5	8.96E-04	4.59
CD55	3.25E-04	-2.51	ENPEP	1.14E-03	4.61
ATP6V1G1	4.26E-05	-2.48	PTPRD	5.00E-04	4.62
TMEM59	4.00E-04	-2.48	ERGIC1	5.59E-05	4.62
DST	1.09E-03	-2.48	TMEM97	5.45E-05	4.66
GNAS	3.36E-04	-2.48	FAH	7.20E-05	4.66
H3F3B	4.62E-04	-2.47	CCNB1	5.72E-04	4.70
ISCU	2.81E-04	-2.46	TNNT2	8.18E-04	4.72
GNAS	3.25E-04	-2.45	TMEM97	1.08E-05	4.74
GNAS	3.30E-04	-2.43		5.51E-04	4.76
C10orf32	1.28E-04	-2.42	NHS	3.06E-05	4.79
GABARAPL1	8.63E-05	-2.41	EZH2	1.29E-05	4.80
IDS	2.98E-04	-2.40	LOC728061	1.26E-04	4.83
DNAJA1	1.90E-04	-2.37	ENO3	3.97E-04	4.85
FNDC3A	1.06E-03	-2.36	EGFR	2.90E-04	4.87
AGPAT4	8.44E-04	-2.34		3.49E-05	4.96
PARG	1.75E-04	-2.34	CXXC5	7.98E-06	4.97
DST	7.02E-04	-2.28	SLC9A3R1	2.30E-06	4.99
RFK	4.35E-04	-2.27	AKR1C1	2.47E-04	5.05
GRID1	6.38E-05	-2.27		2.45E-04	5.08
SLC25A32	1.96E-04	-2.26	PIK3R1	1.02E-03	5.15

SOCS2	1.09E-03	-2.26	RUNX1	6.29E-06	5.20
GNAS	8.00E-04	-2.25	---	3.61E-04	5.21
AKAP12	1.17E-03	-2.25	GIN51	3.53E-06	5.23
MAN2A2	9.42E-04	-2.25	Ap1s2	1.17E-04	5.24
EID1	5.71E-04	-2.24	CTTNBP2	2.95E-05	5.33
---	1.12E-03	-2.22	DEPDC7	2.66E-06	5.34
DPYD	5.11E-04	-2.22	TOP2A	2.07E-04	5.36
C2orf32	7.69E-06	-2.22	AKR1C3	5.54E-04	5.39
HSD17B11	7.12E-04	-2.19	Zeb2	2.18E-04	5.41
EIF1	3.42E-04	-2.16	PPARGC1A	2.81E-04	5.44
LYN	2.53E-04	-2.13	COL12A1	1.08E-03	5.47
EIF1B	2.29E-04	-2.09	C17orf27	3.91E-04	5.53
CDKN2AIP	6.19E-04	-2.07	SACS	2.73E-05	5.58
EIF1	2.35E-04	-2.06		5.11E-04	5.63
IQSEC3	5.57E-04	-2.05	CXXC5	2.20E-06	5.65
SERF2	9.58E-04	-2.05	CDK18	1.61E-05	5.79
WBP11	5.58E-04	-2.05	ABCC3	2.95E-07	5.80
C1orf108	7.85E-05	-2.05	PSCD1	2.95E-09	5.81
CAPN5	9.61E-04	-2.03	ACTR3C	1.38E-04	6.00
LRRFIP1	3.72E-05	-2.02	Thrsp	1.60E-04	6.06
GNB5	9.08E-04	-2.02	P2RY1	3.46E-04	6.08
H3F3B	1.79E-05	-2.01	MXRA5	1.15E-04	6.11
C19orf54	5.58E-04	2.00	VASH2	2.47E-04	6.11
	6.49E-04	2.00	TMEM72	1.74E-04	6.16
CASP2	3.57E-04	2.01	PIK3R1	4.86E-04	6.17
PTK2	3.31E-04	2.01	SDC4	3.41E-04	6.27
NFS1	1.09E-03	2.01	RHOBTB3	5.93E-05	6.29
APLP2	5.21E-04	2.02	RPS21	9.11E-05	6.32
FMO4	6.77E-04	2.03	CAPG	5.40E-04	6.39
ABCC1	8.60E-05	2.03	GREM2	9.24E-04	6.41
MST1	6.78E-05	2.04	TMEM97	1.56E-05	6.44
KIF14	1.57E-04	2.04		1.74E-04	6.45
---	8.15E-05	2.04		7.33E-04	6.53
NFE2L3	9.27E-04	2.04	GPD1	7.82E-06	6.65
	7.78E-04	2.04	IL32	5.91E-07	6.79
DECR1	2.54E-05	2.04	MYH3	1.17E-03	6.94
TXNL5	2.88E-04	2.04	Tmem37	3.30E-05	7.02
	7.42E-04	2.05	ENPP3	1.00E-04	7.13
	5.76E-04	2.05	PIK3R1	3.68E-06	7.18
	5.06E-04	2.05	TMEM46	9.32E-04	7.28
SLC25A10	1.47E-07	2.05	SULT1C2	3.15E-05	7.45
	7.80E-04	2.05	SLC2A5	3.17E-04	7.47
KIAA0391	5.92E-05	2.06	CYP21A2	1.63E-07	7.52
	2.95E-04	2.06	PIK3R1	2.68E-04	7.57
CDK16	4.26E-05	2.06	PYGM	3.63E-04	7.83
---	4.84E-04	2.07	HHATL	1.50E-04	7.83
CTPS2	3.35E-04	2.07	ENPP3	1.04E-03	7.89
	6.13E-04	2.08	SIX1	7.36E-05	8.03
	8.45E-04	2.08	LOC284757	1.05E-04	8.33
TTC38	8.40E-04	2.08	COL4A3	5.89E-05	8.34
	4.77E-04	2.08	Adamts15	5.10E-05	8.43
CENPF	8.46E-04	2.08	EGFR	2.68E-04	8.45

ABCB8	3.65E-05	2.08	---	9.35E-04	8.59
	7.48E-04	2.08	PAX1	1.04E-03	8.64
HMMR	1.01E-03	2.09	WNT5A	5.71E-04	8.66
LOC100170939	1.07E-04	2.09		5.20E-04	8.94
FH	4.90E-04	2.10	CLCA2	3.50E-04	8.95
	5.28E-04	2.10	C7orf29	3.56E-04	9.02
TMEM134	4.19E-04	2.10	CLCA2	9.58E-04	9.06
PDIA4	9.91E-04	2.10		6.92E-04	9.23
	4.21E-04	2.10	CELSR1	2.19E-08	9.25
	4.71E-05	2.12		3.70E-05	9.30
	4.93E-04	2.12		4.04E-04	9.34
	4.45E-04	2.12	CFB	1.57E-04	9.38
	4.35E-04	2.12		3.44E-04	9.54
PHF14	7.54E-05	2.13	CHRNA1	7.34E-04	9.56
NMRAL1	6.19E-05	2.13	SIX1	9.49E-04	9.69
APLP2	7.09E-04	2.13	OPCML	8.40E-09	9.80
FBXL17	2.79E-05	2.14	ATP1A2	8.73E-04	10.27
ARHGEF10L	1.57E-04	2.14	TMEM37	5.17E-06	10.31
UBA1	1.62E-04	2.14	ENC1	5.76E-05	10.92
mrps36	1.52E-04	2.14		4.25E-04	10.98
CALU	7.61E-04	2.14	PPP1R3C	3.73E-04	11.19
TFG	1.48E-04	2.14	WNT5A	2.50E-04	11.47
AURKA	7.70E-04	2.14	BBOX1	3.27E-04	11.61
MATR3	4.34E-08	2.15	DSG2	5.09E-06	11.92
C5orf33	2.41E-04	2.15	CKMT2	1.87E-07	12.24
GTF2IRD2	3.28E-05	2.16	WNT5A	5.50E-04	12.34
	6.88E-04	2.16	CDCA7L	2.09E-09	12.41
Tmem37	9.35E-05	2.16	ESRRG	2.35E-04	13.32
	6.30E-04	2.17	HOXA5	2.44E-09	14.11
	4.37E-04	2.17	RARRES2	1.69E-05	14.38
IDH2	8.69E-04	2.17	MAOB	7.16E-06	14.41
FOXN3	1.09E-03	2.17	IRX3	4.09E-09	15.80
	5.33E-04	2.17	HOXA3	8.48E-05	17.12
P4HB	8.07E-04	2.17	KCNJ16	1.15E-04	17.46
PDHA1	3.40E-04	2.18	OPCML	1.03E-06	18.73
RFC4	8.88E-04	2.18	CA12	2.59E-04	19.17
HPS3	1.14E-03	2.18	LRRN1	1.18E-03	20.78
	4.83E-04	2.18	LOC131873	2.77E-04	21.77
	8.75E-04	2.18	SLC47A1	1.15E-07	21.87
NAPEPLD	3.77E-05	2.18		5.19E-06	22.48
SEC24A	1.57E-04	2.18	CMBL	1.16E-06	22.69
EHD1	3.70E-04	2.19	CA12	2.63E-04	24.43
	6.51E-04	2.19	SALL1	8.15E-08	25.20
PLEKHA2	8.67E-05	2.19	CA12	2.33E-04	25.84
DBI	9.93E-04	2.19	CTXN3	2.06E-06	26.42
EHD1	7.04E-04	2.19	ENC1	6.94E-07	31.47
	5.51E-04	2.19		1.19E-06	32.20
RAB11FIP3	2.45E-05	2.19	PVALB	2.82E-04	32.65
SLIT3	2.16E-04	2.19	CA12	4.02E-04	34.09
CD9	3.37E-04	2.20	GPR64	3.87E-05	34.09
SLC4A2	2.68E-05	2.20	SALL1	1.09E-08	36.83
	5.18E-05	2.20	MYH8	2.62E-04	37.25

SLC35E1	3.68E-05	2.20	MYH8	1.42E-04	41.75
UBTD2	1.01E-03	2.20	CDH1	4.66E-04	45.74